Development of constructs for cardiac conduction system targeted gene therapy

A thesis submitted to the University of Manchester for the degree of Doctor of Philosophy in the faculty of Biology, Medicine and Health

2021

Luke Eoin Stuart

School of Medical Sciences

Table of Contents

List of abbreviations....5
Abstract....7
Declaration....8
Copyright statement....9
Acknowledgements....10
1.0 Chapter 1: General introduction....11
1.1 Introduction to the cardiac conduction system....11
1.1.1 Structure of the sinoatrial node (SAN)....11
1.1.2 Function of the SAN- pacemaking mechanisms and regulation....13
1.1.3 Structure and function of the atrioventricular node....18
1.1.4 Structure and function of the His-Purkinje system....19
1.2 Disorders of the cardiac conduction system- clinical implications....19
1.2.1 SAN- sinus node dysfunction....20
1.2.3 Atrioventricular node- heart block....20
1.2.4 His-Purkinje system- prolonged QRS and left bundle branch block....21
1.3 Mechanistic insights into CCS dysfunction in animal models....21
1.3.1 Sinus node dysfunction....21
1.3.2 AVN- Heart Block....25
1.3.3 His-Purkinje System- Long QRS complex and left bundle branch block....26
1.4 Gene therapy....30
1.4.1 Introduction and history of gene therapy....30
1.4.2 Retroviral and lentiviral vectors....31
1.4.3 Adenoviral vectors....32
1.4.4 Adeno associated virus (AAV)....33
1.5 Current approaches to treating CCS disease....47
1.5.1 Electronic pacemaker implantation- strengths and limitations....47
1.5.2 Biological pacing....48
1.6 Targeting the CCS via gene therapy....54
1.7 Cardiac conduction system specific promoter candidates....56
1.7.1 SAN- HCN4....56
1.7.2 CCS- KCNE1....59
1.8 Summary and conclusions....61
1.9 Hypothesis....61
1.10 Aims....61
2.0 Chapter 2: General methods....63
2.1 Boinformatic analysis of promoter constructs....63

2.2 Cloning of AAV and adenoviral plasmids 63
2.3 Adenoviral Production and purification 65
2.4 Primary neonatal rat cardiomyocyte (NRCM) isolation and culture 67
2.5 Cell culture 68
2.6 DNA transfection *in vitro* 68
2.7 Imaging cytometry 69
2.8 AAV9 production 70
2.9 *In vivo* administration of AAV9 70
2.10 Tissue collection and processing for immunohistochemistry and molecular analysis 71
2.11 Immunohistochemistry 72
3.0 Chapter 3: Results- Characterisation and generation of promoter constructs. 73
3.1 Introduction 73
3.2 Aims 74
3.3 Results 74
3.3.1 Identification and bioinformatic analysis of the HCN4 promoter 74
3.3.2 Identification and bioinformatic analysis of the mouse KCNE1 promoter 77
3.3.3 Cloning of promoter-GFP expression constructs 81
3.3.4 CMV enhancer cloning 81
3.3.5 Cloning of adenoviral plasmids 82
3.3.6 Adenoviral generation and titration 83
3.4 Discussion 99
3.4.1 Bioinformatic analysis of the HCN4 promoter 100
3.4.2 Bioinformatic analysis of the KCNE1 promoter 101
3.5 Summary and conclusions 103
4.0 Chapter 4: Results- in vitro characterisation of promoter constructs 104
4.1 Introduction 104
4.2 Hypotheses and aims 106
4.3 Results 107
4.3.1 Promoter specificity and transcriptional strength in vitro 107
4.3.2 Comparing promoter activity directly between cell lines 119
4.4 Discussion 121
4.5 Summary and conclusions 125
5.0 Chapter 5: Results- *In vivo* testing of promoter constructs using AAV9 126
5.1 Introduction 126
5.2 Hypotheses and aims 127
5.2.1 Aims 127
5.3 AAV9 CMV GFP 127

5.4 AAV9 cTnT GFP....132
5.5 AAV9 0.8 kb HCN4/ 1.2 kb HCN4/ 1.6 kb KCNE1....136
5.6 Discussion....138
5.7 Summary and conclusions....141
6.0 Chapter 6: General discussion....143
6.1 Introduction....143
6.2 CCS promoter candidates are active *in vitro* in ESC derived SAN cells....143
6.3 Effect of the CMV enhancer on promoter activity *in vitro*....145
6.4 CCS specific promoters are inactive *in vivo*....149
6.5 cTnT (or other cardiac specific promoters) for CCS gene delivery in a cardiac specific context....154
6.6 Improved CCS gene delivery may enable use of weaker promoters....156
6.7 Future directions for CCS specific gene delivery....157
6.7.1 Fine tuning AAV transgene expression using miR binding sites....160
6.8 Concluding remarks....162
7.0 References....165

Word count: 47,752

List of abbreviations

(r)AAV	(Recombinant) Adeno-associated virus
AAP	Assembly activating protein
AAV9	Adeno-associated virus serotype 9
AdV	Adenovirus
AF	Atrial fibrillation
Alpha-MHC	Alpha-myosin heavy chain
AVN	Atrioventricular node
CaMKII	Calcium/calmodulin-dependent protein kinase II
cAMP	Cyclic adenosine monophosphate
CBA	Chicken beta actin
CCS	Cardiac conduction system
CEA	Carcinoembryonic antigen
CMV	Cytomegalovirus
Cntn2	Contactin-2
CRT	Cardiac resynchronisation therapy
cTnT	Cardiac troponin T
DAD	Delayed afterdepolarisation
DDR	DNA damage response
DNA	Deoxyribonucleic acid
dsDNA	Dounle stranded deoxyribonucleic acid
ECG	Electrocardiogram
ESC	Embryonic stem cell
GFP	Green fluorescent protein
HCC	Hepatocellular carcinoma
HCN4	Hyperpolarization activated cyclic nucleotide gated potassium channel 4
HDAC4	Histone deacetylase 4
HF	Heart failure
HSC	Haematopoeitic stem cell
HSP	Heat shock protein
$I_{Ca,L}$	L-type calcium current
$I_{Ca,T}$	T-type calcium current
I_f	Funny current
$I_{K,1}$	Inwardly rectifying potassium current
$I_{K,s}$	Delayed rectifier potassium current
I_{NCX}	Sodium-calcium exchanger current
IP3R	Inositol type 3 receptor
iPSC	Induced pluripotent stem cell
ITR	Inverted terminal repeat
IVC	Inferior vena cava
KCNE1	Potassium voltage-gated channel subfamily E regulatory subunit 1
KCNE1	Potassium Voltage-Gated Channel Subfamily E Regulatory Subunit 1
LA	Left atrium

LBBB	Left bundle branch block
LV	Left Ventricle
MSC	Mesenchymal stem cell
MI	Myocardial infarction
miR	microRNA
MLC2V	Myosin light chain 2 ventricular
MRN	MRE11–RAD50–NBS1
mRNA	Messenger RNA
NCX1	Sodium-calcium exchanger
NHE1	Sodium-hydrogen exchanger isoform-1
PKA	Protein kinase A
PV	Pulmonary vein
qPCR	Quantitative polymerase chain reaction
RA	Right atrium
RCA	Replication competent adenovirus
RNA	Ribonucleic acid
ROS	Reactive oxygen species
RV	Right ventricle
RYR2	Ryanodine type 2 receptor
SAN	Sinoatrial node
scAAV	Self-complimentary adeno-associated virus
SCD	Sudden cardiac death
SCN5A	Sodium Voltage-Gated Channel Alpha Subunit 5
SND	Sinoatrial node dysfunction
SR	Sarcoplasmic reticulum
ssDNA	Single stranded deoxyribonucleic acid
STZ	Streptozotocin
SVC	Superior vena cava
TAC	Transverse aortic constriction
TF	Transcription factor
TFBS	Transcription factor binding site
TRX2	Thioredoxin-2
TSS	Transcriptional start site

Abstract

Introduction: Cardiac conduction system (CCS) dysfunction contributes significantly to morbidity and mortality associated with various pathologies, including heart failure. Evidence suggests that remodelling of CCS gene expression, particularly in ion channels regulating its function, are a leading cause of CCS dysfunction. Despite the emergence of these promising therapeutic targets, few methods are available to target the CCS for genetic modulation. Viral vectors offer a powerful method for gene delivery, and AAV9 has been shown to target the working myocardium efficiently. We aimed to utilise the cardiotropic AAV9 vector to modulate gene expression in the CCS from a single systemic intravenous dose, and spatially restrict transgene expression via tissue specific promoters. Doing so would provide a means of validating therapeutic targets of CCS disease, and offer a targeted means of correcting function.

Methods: Firstly, tissue specific promoter candidates for use in a CCS specific gene therapy vector were characterised. Two genes where expression is restricted to the CCS in the adult mouse heart were selected; HCN4, a key pacemaking ion channel responsible for I_f, and KCNE1, which in combination with KVLQT1 regulates $I_{K,s}$. We also selected the cardiac specific cTnT promoter and the ubiquitous CMV promoter as a positive control. Promoters were cloned upstream of GFP to provide quantitative information on their transcriptional activity. All promoters were first tested *in vitro* in a sinoatrial node-like ESC derived cell line (Shox2) to assess transcriptional strength, and in off-target cells including HEK293, HIH-3T3 to assess tissue specificity. To enhance transcriptional strength, the 380 bp CMV enhancer was appended upstream of each promoter. After *in vitro* validation, the most promising promoter constructs were packaged in AAV9 for *in vivo* testing.

Results: All CCS tissue specific promoter candidates showed relatively high activity in Shox2 cells, and low activity in all off target cells. The CMV enhancer increased transcriptional strength modestly in Shox2 cells, with only the CMVe 0.8 kb KCNE1 construct reaching significance. Some evidence of promiscuous activity in HEK293 and NIH-3T3 cells was also noted with CMVe. AAV9-CMV induced high level transgene expression in all tissues examined *in vivo*, particularly the heart and liver. The SAN was effectively targeted by AAV9, with a transduction efficiency of 65% using AAV9-CMV. CCS specific promoter candidates conferred no detectable transgene expression in any tissues examined. AAV9-cTnT was highly active in the cardiac ventricles and atria, and achieved a transduction efficiency of 7.23% in the SAN.

Conclusions: A single systemic intravenous injection of AAV9 is an effective means of targeting the SAN *in vivo*. Further work is required to elucidate the mechanisms surrounding fine patterning of gene expression in the CCS towards development of potent tissue specific promoter constructs.

Declaration

I declare that that no portion of the work referred to in the thesis has been submitted in support of an application for another degree or qualification of this or any other university or other institute of learning.

Copyright statement

Acknowledgements

The work covered by this thesis encompasses many challenges faced, including the Covid-19 pandemic, laboratory electrical fires and supervisory restructuring. During the navigation of these turbulent times however, I have gained the type of knowledge, skills and fortitude that can only be derived through perseverance. For these opportunities I am extremely grateful.

None of this would have been possible without the help and guidance of many people. Firstly, I would like to thank my supervisory team, particularly Dr. Delvac Oceandy and Professor Mark Boyett and Dr. Halina Dobrzynski for their guidance and support. I am fortunate to have had excellent mentors to guide my scientific pursuits. Thanks also to the members of the Oceandy and Boyett labs for their technical support throughout. Particular thanks is also due to Dr. Alicia D'Souza for providing valuable scientific support and expertise. Thanks also to Maria Petkova for her help and support which was invaluable during the Covid-19 pandemic and otherwise.

I have also come to appreciate the value of collaboration, and the importance of seeking out help and expertise when needed. To this end, I am indebted to collaborators in Trieste, Italy for their key role in making this project possible and for their hospitality during my visit to Trieste. Thanks in particular to Lorena Zentilin, Marina Dapas, Michaela Zotti and Professor Mauro Giacca for accepting the invitation to collaborate, and providing important expertise and resources.

I would also like to extend profound gratitude towards my family for their ongoing support and encouragement, which was particularly valuable in the latter stages where working a full time job and preparing the thesis was particularly challenging. Extending from this, it is thanks to their unwavering support and gentle guidance that I am where I am today. I would like to dedicate this thesis to my mother Isobel Stuart, father Charles Stuart, and brother Dr. Charles Stuart Jr. Particular thanks to Charles Jr. for always providing a high benchmark to reach for!

1.0 Chapter 1: General introduction

1.1 Introduction to the cardiac conduction system

The cardiac conduction system (CCS) comprises the sinoatrial node (SAN), atrioventricular node (AVN) and the His-Purkinje network. These tissues comprise specialized cells involved in either generation or propagation of action potentials, and their molecular and structural architecture is directly related to their precise function[1,2]. Synchronous function of these tissues is required for efficient heart function. Dysfunction of the CCS is a significant cause of morbidity and mortality in cardiovascular disease including heart failure (HF)[2,1], hypertension[3] and diabetes[4].

1.1.1 Structure of the sinoatrial node (SAN)

The SAN was first identified and described by Keith and Flack in 1907[5]. The SAN is located at the junction of the superior vena cava within the right atrium[6] (figure 1.1). In humans, the SAN is more extensive than initially thought, and comprises also a transitional paranodal region[7]. This region, situated inferiorly to the main SAN structure, is comprised of intermediate tissue with both atrial and SAN characteristics[7] (figure 1.1). Pacemaking from inferior regions of the SAN is known to be slower, and thus shift of the leading pacemaker site to the inferior paranodal region could be a mechanism underlying bradycardia in sinus node dysfunction (SND)[8–10] (see figure 1.2 for structure).

The cellular makeup of the SAN heterogeneous, and characteristics vary depending on the anatomical location within the node. In the centre, typical nodal cells are found, thought to be primarily responsible for pacemaker activity, with distinctive characteristics including a spindle shape, small size, few poorly organised myofilaments and low mitochondrial density[11]. Moving out from the centre of the node towards surrounding atrial muscle, cellular characteristics gradually change towards a more atrial myocyte-like appearance[11]. Compared to the central nodal myocytes, peripheral nodal myocytes have a more organised myofilament network, contain more mitochondria and are larger[11–13]. These peripheral transitional cells act to conduct the pacemaker action potential to surrounding atrial muscle[12,14].

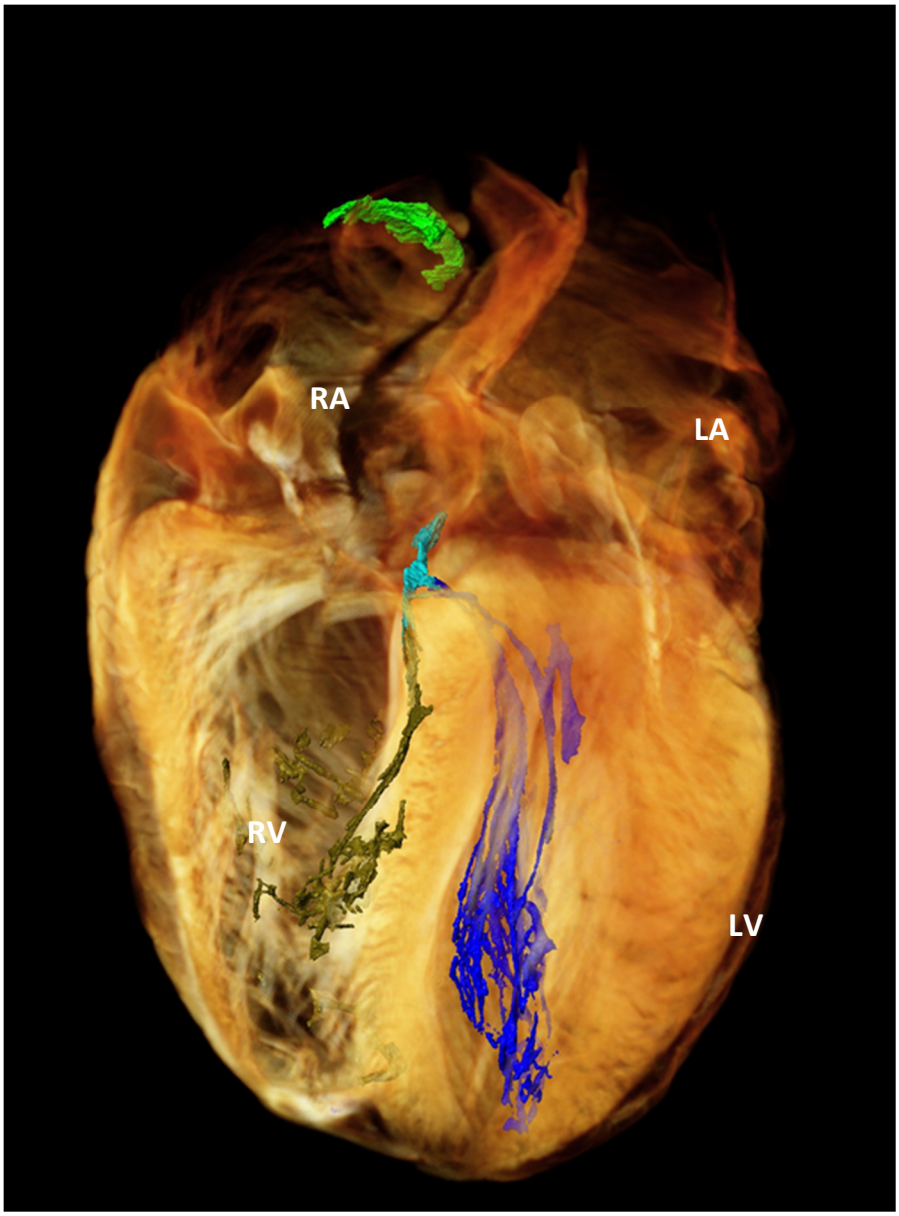

Figure 1.1: Gross anatomy of the human CCS, visualized by microCT scanning. Conduction tissues are superimposed within the working myocardium. Primary structures include the sinoatrial node (SAN) (green) located at the junction of the RA and SVC, atrioventricular node (AVN) (turquoise), left and right Purkinje fibres (blue and dark green respectively). From Stephenson et al., 2013[497]. RA- right atrium; LA- left atrium; RV- right ventricle; LV- left ventricle.

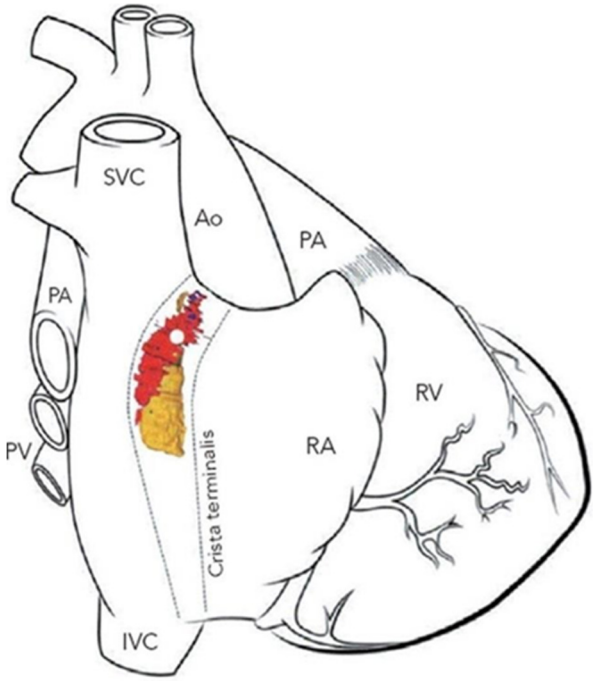

Figure 1.2: computer generated 3D map determined by immunohistochemical and histological data showing structure and location of the SAN within the human heart**.** Red represents the SAN with white circle denoting the leading pacemaker site, yellow depicts a transitional region known as the paranodal tissue. Ao= aorta; IVC= inferior vena cava; PA= pulmonary artery; PV= pulmonary vein; RA=right atrium; RV=right ventricle; SVC= superior vena cava. From Chandler et al., (2011) .

1.1.2 Function of the SAN- pacemaking mechanisms and regulation

The SAN is the pacemaker of the heart, and spontaneously generates action potentials. A key characteristic of SAN electrical activity is the lack of a steady state resting potential due to the absence of $K_{ir}2.1$ channels and their corresponding ionic current $I_{K,1}$[15]. In the working myocardium, depolarisation occurs when an action potential is conducted from one cell to the next via connexin containing gap junctions[16]. In the SAN, action potentials are spontaneously generated. A key aspect of SAN automaticity is the diastolic depolarisation phase (figure 3). A gradual depolarisation derived from multiple ionic currents is initiated until threshold potential (approximately -40 to -30mV) is reached, at which point the next action potential is triggered[17]. A key mediator of the diastolic depolarisation is I_f, or the 'funny current' brought about by hyperpolarisation activated cyclic nucleotide gated channels (HCN), among which the key player is the HCN4 isoform[18]. HCN channels possess a high conductance for Na^+ and K^+ but are also somewhat permeable to Ca^{2+}[19]. I_f is initiated at hyperpolarised potentials, usually below -40/-45mV, which are achieved at the end of an action

potential[20]. The resultant inward mixed K^+ and Na^+ current contributes to depolarisation necessary to achieve threshold potential.

HCN channels possess a cAMP binding domain in the C-terminal region, and modulation of I_f by cAMP represents an important mechanism through which the heart responds to autonomic input; a key aspect of the chonotropic response to emotion and exercise[21]. For example, sympathetic stimulation would elevate cAMP levels and thus heart rate, whereas vagal stimulation would decrease cAMP and heart rate[22]. This is achieved via a shift in the activation kinetics of I_f towards a more depolarised potential, increasing the number of open HCN channels and thus increasing the rate of diastolic depolarisation and shortening time between successive spontaneous action potentials[23].

Although undoubtedly a key player, I_f is not the only mechanism of involved in pacemaker activity. To this end, pharmacological blockade of I_f using ivabradine causes only a modest decrease in pacemaker firing rate[24], and genetic knockout of I_f does not abolish spontaneous pacemaker action potential firing, albeit animals suffer arrhythmia and sinus bradycardia[25,26]. Notably however, HCN4 loss of function mutations in humans have been linked to familial sinus bradycardia[27,28], and gain of function mutations increasing cAMP sensitivity have been linked to familial inappropriate sinus tachycardia[29]. As well as induction of I_f, a net increase in other inward ionic currents including L and T type calcium currents ($I_{Ca,L}$, $I_{Ca,T}$)[30] and the calcium dependent sodium-calcium exchange current (I_{NCX})[31], as well as a net reduction in outward currents including the rapid and slow delayed rectifier potassium currents ($I_{K,r}$ and $I_{K,s}$ respectively)[32,33] contributes to depolarisation towards threshold potential (figure 1.3). The combined activity of these plasmalemmal voltage sensitive ion channels and their corresponding currents comprise the membrane clock mechanism of pacemaking (figure 1.3).

Another key aspect of SAN pacemaking and automaticity referred to as the calcium clock mechanism, identifies localised ryanodine receptor type 2 (RYR2) mediated sarcolemmal calcium transients as key mediators of diastolic depolarisation[34]. Calcium release through inositol triphosphate receptors (IP3Rs) is also involved in modulating RYR2 activity, via regulating local Ca^{2+} concentration[35]. Released Ca^{2+} activates the sodium-calcium exchanger NCX1[31,36]. NCX1 which extrudes 1 Ca^{2+} and internalises 3 Na^+ ions per cycle, generating an net depolarising current which brings about membrane depolarisation[31]. Although much controversy exists over which of these pacemaking mechanisms is dominant, the accepted view is that of a 'coupled clock' mechanism, where the calcium and membrane clocks act synergistically to regulate pacemaker activity[37] (figure 1.3). A multitude of complex crosstalk mechanisms are thought to exist- for example, membrane

clock L-type calcium channels determine the intracellular Ca^{2+} concentration, and thus influence localised calcium induced calcium release from RYR2s[37]. Refinements to this paradigm include a role for calcium calmodulin kinase II (CaMKII) in modulating L-type calcium channel activity[38]. Furthermore, cardiac knockout of I_f causes altered calcium handling and aberrant calcium release from the sarcoplasmic reticulum (SR) in SAN cells, suggesting a mechanistic link between these two signalling units[26]. Ablation of Cav3.1 and Cav1.3 also perturbs late diastolic intracellular calcium release, suggesting that Cav1.3 and Cav3.1 support the correct function of calcium clock signalling pathways[39].

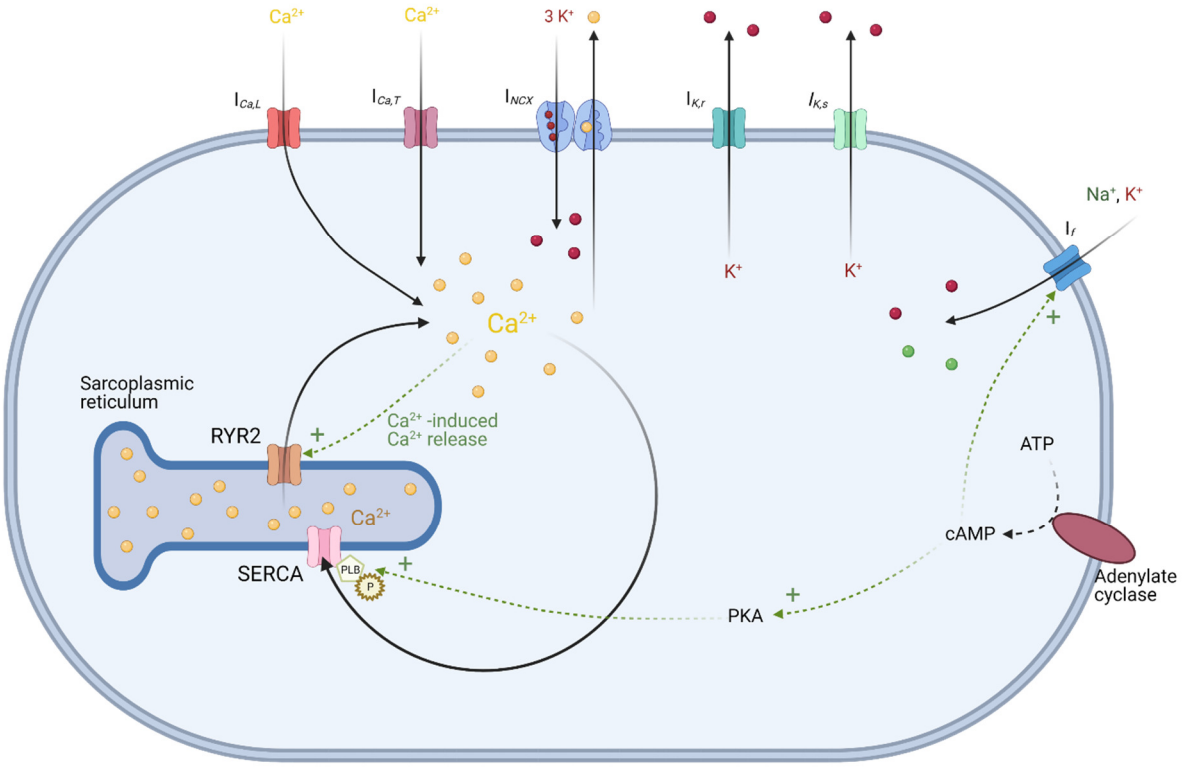

Figure 1.3: Mechanisms of membrane clock and calcium clock in pacemaking, and interactions. Activation of outward plasmalemmal cation currents (such as HCN/ funny channels, $I_{Ca,L}$, $I_{Ca,L}$) and reduction of outward cation currents (e.g. $I_{K,r}$, $I_{K,s}$) results in depolarisation to threshold potential and action potential generation (see figure 3 for temporal activation timing during AP generation). Local Ca2+ releases occur spontaneously in SAN cells under basal conditions in the form of calcium sparks from RYR2s in the SR. SR Ca^{2+} flux increases during diastolic depolarization, peaking when RYRs are activated by cytosolic Ca^{2+} derived from influx through L-type Ca^{2+} channels. This interaction is known as calcium induced calcium release. Released Ca^{2+} activates the sodium-calcium exchanger NCX1, which generates a net intracellular charge of +2 per cycle that contributes to depolarisation[31,36]. The figure represents baseline physiological conditions. Here, constitutively active Ca^{2+}-activated adenylate cyclases create high intracellular cAMP levels. As well as directly activating HCN channels, cAMP activates protein kinase A (PKA), which subsequently phosphorylates multiple membrane ($I_{Ca,L}$, $I_{K,r}$, $I_{K,s}$) and Ca^{2+} clock (RyR, PKA) components, leading to increased intracellular calcium concentration. Elevated calcium provides a substrate for further activation of adenylate cyclases in a positive feedback loop. PKA also phosphorylates phospholamban, relieving it's inhibition upon SERCA, exerting dynamic control over SR Ca^{2+} cycling. (Figure created using BioRender).

The SAN action potential has distinctive characteristics from that of the working myocardium, including a slower upstroke and longer duration[40,41]. Differences in ion channels responsible for each action potential phase explain these varying characteristics- for example, slow L type calcium channels, which also generate a smaller amplitude, are primarily responsible for the upstroke in the SAN as opposed to the working myocardium which utilises fast sodium channels [40] (figure 1.4).

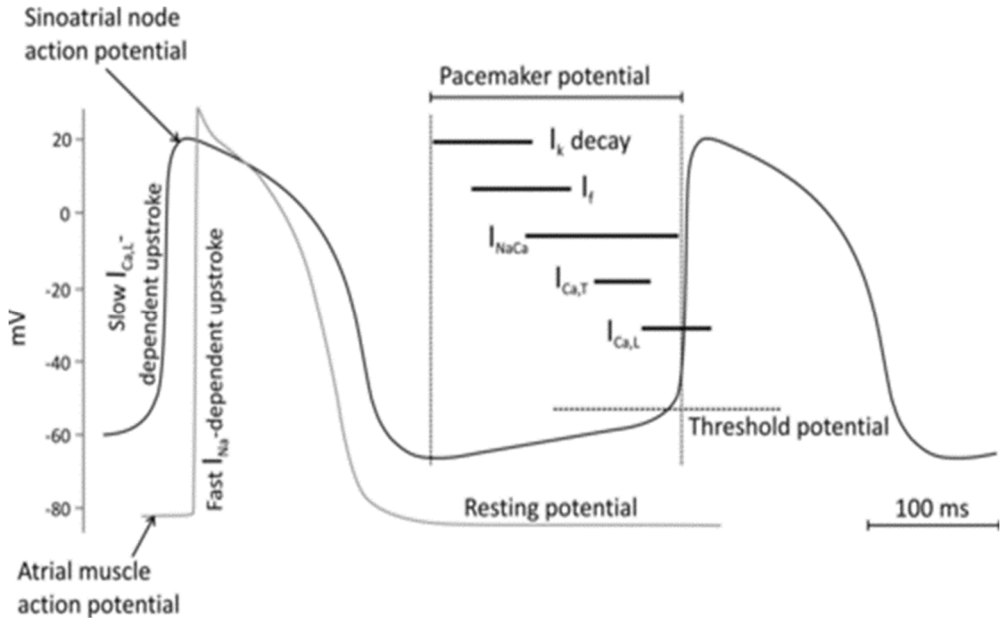

Figure 1.4: Comparison of SAN pacemaker action potential characteristics, including contribution of ions channels, with those of atrial muscle. Upstroke is rapid in atrial muscle due to the action of Na^+ channels, contrasting with the slow activation kinetics of L-type calcium channels in the SAN. Action potential duration is longer in the SAN and of smaller amplitude compared to atrial muscle. Whereas the atrial muscle returns to a stable resting potential (approximately -80 mV) after repolarisation, diastolic depolarization is initiated in the SAN, generating the pacemaker potential. Decay of the outward I_K current, as well as induction of inward currents I_f, $I_{Na,Ca}$ (sodium-calcium exchange current), and L- and T-type calcium currents ($I_{Ca,L}$ and $I_{Ca,T}$ respectively) bring about depolarisation up to threshold potential, at which point the next action potential is generated. From Monfredi et al. (2010).

1.1.3 Structure and function of the atrioventricular node

The atrioventricular node (AVN), located at the base of the atrial septum (figure 1.1), is a key component of the atrioventricular conduction axis, through which action potentials generated in the SAN are propagated to the ventricles. Conduction velocity is important at the AVN- action potential propagation is delayed in order to allow ventricular filling following atrial systole. The conduction delay and extended refractory period also protect the ventricles from tachyarrhythmias[42]. The AVN can act as a subsidiary pacemaker in the event that the SAN is dysfunctional, although pacing is slower and less robust than that of the SAN is thus suppressed under physiological conditions[42]. Two conduction pathways have been characterised via the AVN; the anterior 'fast' pathway and the posterior 'slow' pathway. The fast pathway travels in the anterior portion of the triangle of Koch adjacent to the compact AVN, whereas the slow pathway extends in the direction of the coronary sinus along the boundary demarcating the tricuspid valve[43]. This 'dual pathway' electrophysiology is thought to be an important determinant of conduction delay at the AVN, and is implicated in AV nodal re-entry[44,45]. It is the physical separation of these two pathways (estimated at 15 mm) that facilitates safe ablation of the slow pathway for treatment of AV nodal re-entrant tachycardia with minimal risk of inducing heart block[43].

As with the SAN, the AVN is comprised of a heterogeneous cell population. Nodal myocytes are found towards the centre of the compact node, along with atrio-nodal and nodo-His cells, in the atrial transitional zone and the pre-His bundle respectively[46]. Nodal myocytes are capable of diastolic depolarisation, albeit less robust than that of the SAN, with evidence for the contribution of both membrane and calcium clock mechanisms[42,47]. As with the SAN, ion channel expression can explain variations in electrophysiological characteristics of the AVN; for example, action potential upstroke (depolarisation) is more rapid in transitional atrio-nodal and nodo-His myocytes of the AVN compared to nodal myocytes, as a greater proportion of these cells express depolarising I_{Na}[48].

Slow conduction through the AVN may be partially explained by the expression connexins which form gap junctions. The intermediate conductance isoform connexin 43, the abundant isoform expressed in ventricular myocardium, is poorly expressed in the AVN where the small conductance connexin 45 is predominant[46,49,50]. Furthermore, connexins are poorly expressed and gap junctions relatively sparse and are smaller in the AVN compared to working myocardium[51]. In addition, low expression of $Na_v1.5$ channels and corresponding I_{Na} gives rise to slow action potential upstroke velocity which relies on slow inward Ca^{2+}, and thus slow conduction[52]. AVN myocytes are also small in diameter, and physically separated by interspersed connective tissue, further slowing and limiting impulse conduction velocity[51]. These factors contribute to the conduction decrement that

protects rapidly generated supraventricular impulses reaching the ventricles and causing ventricular tachycardia. It is also noteworthy that the fast conduction pathway has a longer refractory period as compared with the slow pathway, again limiting the number of impulses that can be conducted to the ventricles[43].

1.1.4 Structure and function of the His-Purkinje system

The His-Purkinje network is responsible for propagating the action potential to the ventricles, promoting a highly ordered excitation and thus enabling efficient pump function. The bundle of His extends from the AV conduction axis, and is distinguished histologically by its insulation from the surrounding myocardium by a fibrous sheath. This singular bundle branches asymmetrically at the top of the ventricular septum to form the left and right bundle branches which progressively branch further downstream, eventually terminating at the Purkinje fibres. The bundle branches are electrically insulated from the myocardium in order to prevent abnormal activation of the ventricles, whereas at the Purkinje fibres, insulation is lost at specific sites in order to allow ventricular activation[53,54]. Conduction velocity via the Purkinje fibres is much more rapid than that through the working myocardium, occurring at rates of 2-3m/s and 0.2-0.4m/s respectively[55]. Abundant expression of high conductance connexin isoforms 43 and 40, as well as the specialised architecture of Purkinje cells within free running fibres is thought to facilitate high conduction velocity[56,57]. In addition, the characteristics of the Purkinje fibre action potential facilitate rapid conduction; a steep, rapid upstroke velocity, high amplitude, rapid repolarisation and longer duration compared to that of ventricular muscle has been noted[58,59]. These characteristics are related to ion channel expression, as described by Atkinson et al. (2011)[60]. Depolarisation during the action potential upstroke is primarily mediated by the inward Na^+ current, I_{Na}[61]. Nav1.5 and Nav1.1 channels are highly expressed in the rabbit Purkinje fibres, concurrent with high I_{Na} density, providing a robust depolarising current and facilitating the fast action potential upstroke[60]. Robust expression of the fast recovering K^+ ion channel Kv.4.3, contributing to the transient outward potassium current I_{to} is thought to be responsible for rapid phase 1 repolarisation[40,60,62].

1.2 Disorders of the cardiac conduction system- clinical implications

CCS dysfunction, which may be attributable to congenital or acquired factors, results in arrhythmias. Acquired CCS dysfunction is a hallmark of heart failure (HF) for example, where dysfunction of the entire CCS has been noted[45,46]. From a congenital or inherited viewpoint,

mutations in the HCN4 gene cause familial sinus bradycardia, and pathogenic variants in various ion channel genes including SCN5A, HCN4 and KCNE3 have been linked to Brugada syndrome, characterized by ventricular fibrillation and high risk of sudden cardiac death[27,63].

1.2.1 SAN- sinus node dysfunction

Sick sinus syndrome, also known as sinus node dysfunction (SND), is characterised by abnormal action potential generation and propagation by the SAN, which ultimately compromises the ability of the heart to meet physiological demands. Arrhythmias including sinus bradycardia, sinus pauses or arrest, atrial tachyarrhythmias among others are associated with SND[47,48]. SND accounts up to half of all electronic pacemaker implantations in the United States and Europe[49]. Ageing is a primary risk factor for SND, with a median age of 74 reported in patients aged over 21 years[50,51]. Studies using Holter monitoring in end stage HF patients revealed that between 28 and 62% were bradycardic at the point of death, suggesting SND as a contributing factor[52–55]. Endurance athletes also exhibit sinus bradycardia and dysfunction[64]. Although initially a physiological adaptation to the high workload placed on the heart during training, professional endurance athletes suffer increased susceptibility to arrhythmias and SND with ageing, with a pacemaker implantation frequency greater than in the general population[56]. More than half of all patients with SND also develop atrial tachycardia, often atrial fibrillation (AF), giving rise to tachy-brady syndrome. The interactions between tachycardia and bradycardia are bi-directional, where AF induces SAN electrophysiological remodeling leading to dysfunction[65]. Widespread remodeling of key pacemaking ion channels in the SAN, including HCN2 and HCN4, concurrent with SND has been documented in response to AF in animal models[66,67]. Tachy-brady syndrome is associated with greater risk of embolic stroke and AV block, which manifests in up to 50% of SND patients[68].

1.2.3 Atrioventricular node- heart block

Dysfunction of the AVN commonly manifests as heart block, of which there are 3 types with varying severity: 1st degree block involves a slowing of impulse conduction from atria to ventricles. 1st degree heart block is common in HF, presenting in between 10 and 50% of cases[69–71]. Clinically, 1st degree heart block is associated with poor prognosis in HF patients, and intermittent high degree block in patients suffering from advanced stage HF is associated with a higher risk of sudden cardiac death (SCD)[58,61]. 2nd degree block involves a more severe slowing of AV conduction, and occasional failure of atrial to ventricular impulse propagation. 2nd degree block can be further divided into Mobitz type 1 (Wenckebach phenomenon) and Mobitz type 2. Wenckebach, a generally benign and reversible phenomenon, is characterised by a gradual prolongation of the PR interval, resulting in

non-conducted P waves. Conduction block is usually situated at the AVN. This may be caused by reversible ischemia, myocarditis, or medications that result in slowed conduction through the AVN, e.g. beta blockers[72]. Mobitz type 2 is characterised by erratic non-conducted P waves. Unlike Wenckebach, the conduction block is situated below the level of the AVN at the His bundle or bundle branches[72]. Block is often caused by structural damage for example resulting from myocardial infarction. In 3rd degree or complete heart block, there is a complete absence of AV conduction, resulting in uncoordinated and inefficient pump function and uncoupling of P and QRS complexes on ECG[73]. 3rd degree heart block is an independent risk factor for increased mortality risk in patients with acute myocardial infarction (MI)[74]. AV block is also associated with Lyme carditis, a systemic complication of Lyme disease, where cardiac inflammation and fibrosis occurs as a result of microbial invasion[75]. In these cases, severity of AV conduction block progresses quickly, resulting in aberrant and slowed ventricular rhythm and potential development of critical arrhythmias including ventricular fibrillation. Although potentially fatal in the acute setting, the condition is usually reversible with intravenous antibiotics, and permanent pacing is not usually indicated[75].

1.2.4 His-Purkinje system- prolonged QRS and left bundle branch block

Approximately 26% of HF patients present with left bundle branch block (LBBB), characterised by a prolonged QRS duration >120ms[76]. SCD underlies approximately 40% of HF related deaths, and evidence suggests a primary mediator of SCD is ventricular fibrillation arising from the His-Purkinje network[56,77,78]. QRS prolongation is associated with poor prognosis, in terms of generalised mortality and risk of SCD, in HF[79–81] and non ischemic cardiomyopathy[82]. As well as contributing to SCD via fatal arrhythmia, dysfunction of the His-Purkinje network also mechanistically contributes to death via pump failure[83]. Purkinje dysfunction causes dys-synchronous activation of the ventricles, a common hallmark of LBBB, and reduced left ventricular ejection fraction[84]. To this end, a positive correlation between interventricular conduction delay, a hallmark of dys-synchrony, and mortality has been demonstrated[85].

1.3 Mechanistic insights into CCS dysfunction in animal models

1.3.1 Sinus node dysfunction

The primary pathophysiological mechanisms underlying SND are debated and likely context specific. Degenerative fibrosis of the SAN is thought by some to be a key contributor, and has been documented in the SAN[86–88] as well as the working myocardium with age[89]. Fibrosis may be

associated with SAN cell death, causing a shift in the leading pacemaker site to peripheral nodal myocytes. Peripheral myocytes show a differing ion channel expression profile, including lower HCN4 levels, which results in slower action potential generation and thus bradycardia[90]. However, conflicting evidence exists, such as a lack of evidence for either fibrosis or SAN cell remodelling with ageing, SND in the absence of fibrosis and stark fibrosis in the absence of SND[87,91,92]. Elevated SAN fibrosis induced by Calsequestrin 2 (CASQ2) knockout disrupted electrical coupling between SAN myocytes and caused slowed impulse propagation and sinus pauses, providing a potential mechanism explaining how CASQ2 mutation predisposes to SND[93].

1.3.1.1 Ion channel remodelling in health

Ion channel remodelling linked to altered CCS function has been documented during the physiological processes of ageing, athletic training and pregnancy. In the ageing rat, decreased action potential upstroke velocity was observed in the SAN periphery, most likely due to a decrease in $Na_v1.5$ and corresponding I_{Na}[94]. To this end, mutations in the SCN5A gene which encodes $Na_v1.5$ are known to cause familial SND[95]. Recently, it was also demonstrated that age related remodelling of Cav1.2 and Cav1.3 contributed to decreased instrinsic pacemaker rate and SND[96]. Ageing rats also exhibited widespread changes in calcium clock associated genes including decreased RYR2, and ion channels including Nav1.5, Cav1.2 and HCN1[97].

Veteran athletes exhibit elevated rates of CCS dysfunction, exemplified by higher rates of pacemaker implantation[98–100]. Sinus bradycardia similar to that in observed in human athletes was induced in mice via swim-training, where SND was caused by decreased expression of HCN4 at transcript and protein levels in the SAN, concurrent with reduced I_f density[101]. Importantly, a causative role was also established for I_f remodelling in training induced bradycardia observed in human athletes. Bradycardia persisted in the presence of complete autonomic blockade, ruling out a significant mechanistic role for varying autonomic tone, and athletes showed a blunted response to the I_f blocking drug ivabradine, suggesting lower expression of the HCN4 channel upon which it acts[102].

Heart rate is typically elevated during pregnancy as a physiological adaptation to raise cardiac output[103]. Elevated levels of HCN2 in the SAN of pregnant mice was found to contribute to accelerated heart rate via upregulation of I_f density, again highlighting the importance of HCN channel expression in modulation of heart rate[104].

1.3.1.2 Ion channel remodelling in disease

A vast body of literature supports a role for dysregulated ion channel expression as a primary mechanism of SND associated with comorbidities such as AF[66] and HF[105]. For example, HF induced by myocardial infarction in rats caused decreased intrinsic heart rate concurrent with widespread changes in ion channel expression in the SAN[106]. Increased expression of K^+ subunits ERG (mediating $I_{K,r}$), KvLQT1 (mediating $I_{K,s}$), Kir2.4, TASK1, TWIK1, and TWIK2, increased HCN2 and HCN4, and increased Cav1.2 and Cav3.1 were observed[106]. Increased $I_{K,r}$ and $I_{K,s}$ could slow pacemaking via opposing diastolic depolarization and thus depressing automaticity. Particularly intriguing in this model was increased expression of HCN4, which would usually be associated with an increase in pacemaker activity and intrinsic heart rate. This could be explained as an adaptive response to increased K^+ channel expression, as transcription factors (TFs) regulating it's expression were also elevated[106]. In the HF mouse, downregulated SAN HCN4, HCN1 and HCN2 and corresponding I_f was a key mechanism of SND via depressed SAN automaticity[107]. Interestingly, no changes in calcium clock associated transcripts were observed, and rescuing HCN4 expression improved SAN and heart function, and survival[108]. These evidence point towards I_f reduction as the dominant mechanism in SAN dysfunction in this model, although some fibrosis was also noted[107]

Mutations in the HCN4 gene often underlie familial sinus bradycardia, providing further evidence of dysfunctional ion channel expression or activity as a mechanism of SND[28,109]. SND associated with certain HCN4 mutations has also been linked to AF and early onset of symptoms[110]. Furthermore, in a rabbit model of HF utilising combined pressure and volume overload, depressed intrinsic pacemaker activity was observed[111]. Later studies utilising the same model reported a 40% reduction in density of I_f in SAN pacemaker cells concurrent with this phenotype. Downregulation of the HCN4 gene was also reported in unison with decreased I_f density in a canine HF model[105,112].

Diabetes is also associated with increased risk of arrhythmia, particularly AF, associated with structural and molecular remodelling of heart (reviewed by Grisanti, 2018[4]). Remodelling of the SAN has also been demonstrated in diabetic animal models. In a streptozotocin (STZ) induced diabetic rat model, SAN conduction time was slowed, with elevated low conductance connexin 45 mRNA expression whilst no connexin remodelling was observed the atria and ventricles[113]. In the same model, decreased connexin 45 protein levels in the SAN were seen[114]. It is possible that aberrant post transcriptional modifications underlie these seemingly disparate results, perhaps involving microRNAs (miRs), elevated expression of which would cause decreased protein levels. Elevated connexin 45 mRNA was also observed in the SAN of rats in heart failure[106]. Connexin

expression naturally varies throughout the SAN due to varying electrophysiological demands. Low conductance connexin isoforms 45 and 30.2 are highly expressed in the central region, with low expression of connexin 43. In peripheral regions, connexin 43 is robustly expressed in order to allow efficient driving of the atrial muscle that surrounds the node[115]. To this end, it would be interesting to evaluate if connexin distribution is altered across different regions of the SAN in response to disease. Altered expression of key pacemaking ion channels including membrane clock (HCN4 and I_f, Cav1.3, Cav3.1) and calcium clock proponents (NCX1) were also observed in the SAN of STZ diabetic rats, presenting a mechanistic insight into cardiac electrophysiological disturbances associated with this disease model[114].

1.3.1.3 Mechanisms underlying SND associated ion channel remodeling

Mechanisms underlying the modification of ion channel expression in SND remain largely unknown, although recent studies have pointed towards particular signal transduction pathways and miRs. Transient activation of the embryonic CCS development-associated notch signalling pathway induced long term alteration in the expression of genes such as SCN5A, resulting in reduced atrial action potential upstroke velocity and slowed atrial conduction rate, manifesting as sinus bradycardia with intermittent pauses[116]. Thioredoxin 2 (Trx2), a molecule involved in counteraction of oxidative stress and reactive oxygen species (ROS) scavenging, was also linked to modulating HCN4 expression[117]. Induction of oxidative stress via CCS specific knockout of Trx2 resulted in drastically reduced HCN4 expression in the SAN, with severe sinus bradycardia and AV block[117]. Elevated ROS led to increased transcription of histone deacetylase HDAC4 in the CCS, which bound to a MEF2 site within the HCN4 enhancer, causing transcriptional repression of HCN4. Previous studies have shown the important role of MEF2 TF binding to an intronic HCN4 enhancer, where mutation of this binding site drastically reduced transcriptional activity in vitro[118]. Interestingly, Trx2 CCS deletion had no effect on fibrosis in the SAN, and so phenotypic observations could be predominantly attributed to altered HCN4 expression[117]. Indeed, increased oxidative stress is a hallmark of many disorders strongly associated with SND, including ageing[119], AF[120,121], HF and hypertension[122].

Calcium-calmodulin dependent protein kinase II (CaMKII) functions as an oxidation sensor in the heart[123]. Oxidation of CaMKII leads to SAN cell apoptosis and fibrosis, culminating in SND after chronic angiotensin II infusion[124]. Furthermore, CaMKII is involved in activation of TFs including MEF2 via direct signalling with HDACs, suggesting interplay between pro fibrotic and ion channel remodelling mechanisms in the pathogenesis of SND[125]. Inhibiting oxidation of CaMKII also

protected the SAN from dysfunction in an angiotensin II induced hypertension SND model[126]. Further supporting the notion of a multi-factorial mechanism for SND, decreased levels of SCN5A (encoding Nav1.5) in SCN5A$^{+/-}$ mice potentiated fibrosis via upregulation of pro fibrotic gene TGF-β1 in ageing, as well as widespread ion channel remodeling[127]. These changes resulted in decreased SAN automaticity and slowed conduction through the SAN[127].

Studies in swim-trained mice identified miR-423-5p upregulation in the SAN and concurrent HCN4 and I_f downregulation as a key factor driving training induced SND[128]. Inhibiting miR-423-5p *in vivo* via systemic administration of an antimiR restored HCN4 expression and function to the SAN, abolishing the training induced bradycardia[128]. MiR-370-3p, a repressor of HCN4, was upregulated in the SAN in chronic HF mice, concurrent with decreased HCN4 expression[108]. Decreasing MiR-370-3p levels using an antagomiR rescued HCN4 expression and improved heart function and survival[108]. Furthermore, it is known that remodelling of calcium clock related ion channels can lead to SND in the context of ageing[129,130,97,96]. Recently, it was demonstrated that age related remodelling of Cav1.2 and Cav1.3, which contributed to decreased instrinsic rate and depressed pacemaker activity, was related to elevated miR-1976 in the SAN[96]. Interestingly, this miR was also upregulated in the plasma of both aged rabbits and humans, suggesting this could be a prospective therapeutic target and biomarker for age related SND[96].

1.3.2 AVN- Heart Block

Animal models of cardiovascular dysfunction including HF[131,132] and pulmonary hypertension[133] develop AVN dysfunction, manifesting as heart block with prolonged PR interval. In the chronic pulmonary hypertension rat, qPCR on the AVN revealed widespread ion channel remodelling including a greater than 50% reduction of HCN1/2/4, as well as Ca_v1.2/1.3, and biophysical *in silico* modelling predicted these changes to result in heart block[133]. In a rabbit model of congestive heart failure induced by pressure and volume overload, downregulation of HCN1 and connexins 40/43 was observed, likely contributing to slowed AV conduction, along with Ca_v1.3, a key mediator of the action potential upstroke phase[131]. Ca_v1.3 knockout models exhibit heart block and depressed automaticity, and thus downregulation of this channel in HF likely contributes to heart block[134]. Furthermore, in rats with HF post MI, widespread structural and molecular AVN remodelling has been demonstrated, including hypertrophy and apoptosis of AVN myocytes, elevated fibrosis and downregulation of HCN4 at protein and mRNA levels[132]. Finally, athletes are also prone to AVN dysfunction[135]. Recent studies conducted in racehorses and in mice trained by swimming demonstrated a central role for I_f and $I_{Ca,L}$ reduction in the trained AVN, underscored by miR

mediated transcriptional remodelling[135,128]. Targeting miRs partially restored first degree AV block to pre-training levels in mice[128]. Thus, ion channel remodelling is central to AVN dysfunction in animal models, as is the case with SAN dysfunction (table 1.1)

1.3.3 His-Purkinje System- Long QRS complex and left bundle branch block

Studies in animal models, particularly of HF, suggest a key role for remodelling of ion channels and their corresponding currents in the pathogenesis of His-Purkinje dysfunction[136–138]. In a canine ventricular tachypacing HF model, widespread ionic remodelling was observed in Purkinje cells, including downregulation of ion channels responsible for action potential propagation (connexin 40/43) and repolarisation ($K_v3.4$ and $K_v4.3$)[136]. Commensurate with these changes, slowed impulse conduction velocity along Purkinje fibres was observed in *ex vivo* and *in vivo* preparations, causing dys-synchronous ventricular activation[136]. As discussed, this could have important prognostic implications in HF patients, specifically those with LBBB. In the same model, remodelling of ionic currents in Purkinje cells was observed[137]. Decreased density of K^+ currents I_{to} (outward repolarising current), and the inward rectifier $I_{K,1}$ were evident, in addition to delayed L-type calcium current inactivation causing prolongation of the action potential[137]. HF Purkinje cells showed an altered response to K^+ channel blocking agents, commonly used antiarrhythmic drugs, including an exaggerated action potential prolongation[137]. This could partially explain the increased propensity of chronic HF patients for developing Torsades de Pointes, a potentially lethal ventricular tachyarrhythmia precipitated by QT prolongation via drugs such as K^+ channel blockers[139].

Structural and molecular remodelling of Purkinje fibres has also been demonstrated in the mouse in response to pressure overload via transverse aortic constriction (TAC)[138]. Purkinje cells were hypertrophic, and showed a shift in connexin isoform expression with elevated connexin 40 and decreased connexin 43[138]. HCN4 was significantly upregulated at mRNA level but showed no difference in protein expression[138]. This could suggest aberrant post-transcriptional modification of gene expression in the TAC animals. In a pressure and volume overload induced rabbit HF model, widespread ionic remodelling of the Purkinje fibres, particularly on the left side, was documented[140]. Of 36 transcripts central to Purkine fibre electrical function, 78% of these, including HCN4, CaV1.2, RYR2, NCX1 and connexins 40 and 43 were significantly downregulated in left Purkinje fibres within the failing heart[140]. Structural remodelling including rupture of the nuclear membrane and infiltrating intranuclear mitochondria were also observed in Purkinje fibres isolated from the failing rabbit heart[140]. HCN4 expression showed no significant change in right Purkinje fibres. To this end, the authors of the former mouse study isolated Purkinje fibres from both right

and left sides for qPCR data, as well as pooling from 3 individual hearts, likely owing to the small size of mouse Purkinje fibres. This could partially explain disparate results for HCN4 mRNA in HF between the two studies. See table 1.1 for summary of proposed mechanisms for His-Purkinje dysfunction in heart failure.

	Causes	Proposed aetiology	Effect on function
Sinus node dysfunction/ altered SAN function*	Heart failure	↑miR-370-3p, NRSF, ↓Tbx18, Isl1 leading to ↓ HCN4[108]. ↑K+ channel expression (KVLQT1, ERG)[106].	Elevated negative regulators of HCN4, decreased positive regulators of HCN4 expression, I_f reduction and depressed automaticity. Opposition of diastolic depolarisation via increased $I_{K,r}$, $I_{K,s}$ density.
	Athletic training	↑miR-423-5p, ↑miR-1, ↓Tbx3 leading to↓HCN4[101,128].	Depressed pacemaker automaticity via decreased HCN4 and I_f.
	Ageing	↓NaV1.5, TBX3[127]. SAN degenerative fibrosis commensurate with↑TGF-beta[127]. ↓ SAN Connexin 43 expression[141].	↓AP upstroke velocity, widespread ion channel remodelling leading to impaired pacemaking. Physical separation of SAN cells, impaired conduction. Slow SAN impulse conduction, prolonged conduction time.
	Diabetes	↑connexin 45. ↓HCN4, Cav1.3, Cav3.1, NCX1[114].	Increased low conductance connexin expression, slowed conduction. ↓ key membrane and calcium clock pacemaking ion channels causing depressed automaticity.
	Oxidative stress (applicable to all above)	Induced by TRX2 knockout[117].	Transcriptional repression of HCN4 via HDAC-MEF2 pathway, thus depressed automaticity via decreased I_f.
	Pregnancy	↑HCN2[104].	Elevated pacemaker activity via increased I_f density, increased cardiac output to meet physiological demands.
Heart block (AV nodal dysfunction)	Heart failure	↓HCN1, Connexin 40, 43, Cav1.3[131]. AVN Myocyte hypertrophy and apoptosis, elevated fibrosis[132].	Slowed and impaired AV nodal impulse conduction, reduced AP upstroke velocity.
	Athletic training	↑miR-211-5p, miR-432. ↓ Connexin30.2. ↓Cav1.2, RYR2, HCN4[135].	Elevated negative regulators of ion channels responsible for

			I_f and $I_{Ca,L}$, aberrant Ca^{2+} handling, impulse conduction.
	Ageing	↓Connexin 43, HCN4, Nav1.5, Ryr2; ↑ Connexin 40, serca2A[142].	Shift in connexin isoform expression, aberrant AV nodal calcium handling and thus impulse conduction.
	Pulmonary hypertension	↓HCN1/2/4, Cav1.2, Cav1.3, TWIK1, Cx30.2, Ryr2[133].	Slowed AV nodal impulse conduction.
His-Purknje dysfunction	Heart failure	↓Connexin 43, connexin 40, ↓Kv3.4, Kv4.3[136]. Purkinje myocyte hypertrophy[138]. ↓HCN4, Cav1.2, RYR2, NCX1, connexin 40, connexin 43[140].	Decreased connexin expression (and shift towards low conductance isoform expression) resulting in slowed impulse conduction; delayed repolarisation; culminating of abnormal ventricular activation.

Table 1.1: summary of experimental evidence relating to the causes of SND, heart block/ AVN dysfunction, and His-Purkinje dysfunction.

Mechanisms underlying aberrant miR expression are not well understood. As can be seen in table 1.1, different miRs and genes are dysregulated in different disease states. Many miRs lie within the non-coding region between genes, so called 'intergenic' miRs. miRs may also exist in the intronic regions of coding transcripts, known as intronic miRs, and thus upregulation of transcription of their host gene can lead to upregulation of the respective miR expression. To this end, it has been shown that intronic miRs often share promoters with their host genes, and thus the miR and host gene are co-expressed[143]. miR-423-5p expression was elevated in exercise training and caused repression of HCN4 in the SAN[128]. It was also found that the miR host gene, NSRP1, was also significantly upregulated, in line with upregulation of transcription factors regulating it's expression[128]. Thus, different disease models and pathological stimuli produce aberrant expression of different transcription factors and genes containing diverse miR elements, and thus dysregulated expression of different miRs. The unique stressors of each pathophysiological state and associated adaptive responses involve distinct signaling pathways and molecules. For example, myocardial infarction and associated extensive cardiomyocyte death due to ischemia leads to high levels of inflammation and activation of myofibroblasts[144]. Expression of intergenic miRs is commonly controlled by their own specific promoters, which may be activated or inactivated by epigenetic changes such as methylation[145].

1.4 Gene therapy

Gene therapy can be described as the transfer of genes to target cells and organs in order to prevent or treat disease. It can be considered that the ideal gene therapy 'would be administered by a noninvasive route, would target only the desired cells within the target tissue, and would express a therapeutic amount of transgene products with desired regulation for a defined length of time[146].' Each of these criteria presents inherent challenges. Perhaps one of the most significant challenges is achieving transgene expression at therapeutic levels only within the desired target cell type. Each of these points is considered in detail below.

1.4.1 Introduction and history of gene therapy

In early stages of gene therapy research, the main focus for treatment was inherited single gene disorders, where replacement of a single defective gene could be curative[147]. Furthermore, viral gene delivery, especially to post-mitotic cells such as in the heart or central nervous system, could achieve a long term therapeutic benefit, in contrast to many agents that require repeated administration. Clinical studies began in the early 1990s, but were plagued by toxic effects, such as insertional mutagenesis from integrating viral vectors used at the time and severe host immune responses against the vectors[148]. Nonviral methods of gene delivery have also been explored, which typically involves using naked DNA or encapsulating the DNA in lipid-based nanoparticles. These have the advantage of being relatively non-immunogenic, as opposed to viral proteins, and onset of gene expression is rapid, however transfection efficiency is significantly lower compared to many viral vectors[149]. Although lipid-based nanoparticles in standard form typically do not have tissue / cell tropism or specificity, methods of functionalizing the surface of the particles have been developed so as to confer and /or improve gene delivery to certain tissues. For example in cancer therapy, nanoparticles can be modified to express tumor specific proteins to preferentially target cancer cells[150]. Despite efforts, gene delivery to many non-proliferative cells such as cardiomyocytes is ineffective using these methods. For example, the best lipid based method (lipofectamine 2000) tested by Djurovic et al. resulted in only 8.1% transfection efficiency in primary neonatal rat cardiomyocytes, whereas AAV2 achieved 88.1% transduction in the absence of toxicity[151]. Furthermore, such cationic lipid-based nanoparticles suffer from rapid clearance, toxicity and induction of inflammatory responses when administered systemically in vivo partially due to their positive charge[152]. Neutral lipid nanoparticles are superior for systemic gene delivery, and induced cardiac regeneration via overexpression of pro-proliferative miRs via systemic venous delivery[153]. Notably, repeated daily injections were required since induced transgene expression lasted only for

24 hours from a single injection.

1.4.2 Retroviral and lentiviral vectors

There are a number of considerations when selecting any gene therapy vector; the target cells, intended administration route, and therapeutic gene target all require careful and rational consideration in order to maximize chances of success. Some early studies in gene therapy aimed to augment or replace defective genes by *ex vivo* transfer into stem cells, following on from prior success of bone marrow transplantation in the treatment of primary immunodeficiencies[154]. Bone marrow transplantation however requires a human leukocyte antigen (HLA) identical donor, which is often unavailable. The prospect of harvesting haematopoeitic stem cells from the patient, genetically modifying the cells using gene therapy approaches, and transplanting back into the same patient (autologous) was thus attractive. In these circumstances, it is essential that integrating viral vectors are used for gene transfer in order to retain the transgene in light of multiple rounds of cell division. However, oncogenic activation is a constant risk with these vectors and was documented widely in early clinical trials using gamma-retroviral vectors[155,156]. Later, lentiviral vectors came into use, derived from the HIV-1 virus. These vectors were less genotoxic compared to early retroviral vectors. This is thought to be due to differences in integration preferences. Gamma retroviral vectors tend to integrate near transcriptional start sites (TSS) (upstream or downstream) whereas lentiviral vectors integrate anywhere along the transcriptional unit, but not upstream of the TSS[157]. In addition, for clinical use, it is possible to use engineered lentiviruses with deleted viral regulatory elements, further lowering pathogenicity. Despite these characteristics, the persisting risk of insertional oncogenesis makes these vectors unfavourable in terms of safety profile. Some tissues are inefficiently transduced *in vivo* despite efforts of pseudotyping capsids with proteins / receptors to enhance specific tissue tropism[158]. For example, hepatocytes are inefficiently transduced after systemic lentiviral administration due to rapid interferon based immune response and clearance of transduced cells[159]. Lentiviral transduction of the heart is also relatively inefficient, especially when compared with AAV and adenoviral vectors[160]. After direct intramyocardial injection, lentiviral transgene delivery was shown to peak between 3 and 7 days post injection and subsequently decline[161]. Studies have also shown that transduction of the adult mouse heart is inefficient after systemic IV administration of lentivirus, whereas the neonatal heart showed better transduction[162]. In addition, studies have shown that VSV-G pseudotyped lentiviral vectors (the most commonly used and studied) are highly sensitive to serum based inactivation by complement, presenting a significant challenge to their for systemic administration and gene delivery[163]. There is also an unmet need for a method to produce lentivirus at sufficient

concentrations to be effective after systemic administration. Characteristics and primary advantages and disadvantages associated with lentiviral vectors are laid out in table 1.2.

1.4.3 Adenoviral vectors

Adenoviruses were among the first used vectors in clinical gene therapy trials. Adenoviruses are non-integrating DNA viruses commonly isolated from many species including humans, with a generally low pathogenicity and high capacity for transgene cargo (around 7.5 kb). Adenoviruses can also confer a very high transduction efficiency with rapid onset of gene expression across a broad range of cell types, including non-dividing cells[146]. However, their endemic nature within the human population presents challenges. An estimated 80% of humans carry neutralizing antibodies against the most commonly used adenoviral serotype (Ad5), severely reducing the efficacy of the vector and raising the possibility of severe inflammatory reactions upon administration[164]. This is thought to have contributed to the high profile death of a patient in 1999 undergoing adenoviral gene therapy for congenital ornithine transcarbamylase deficiency[165]. Since then, next generation adenoviral vectors have been developed, where all viral regulatory gene elements aside from inverted terminal repeat (ITR) sequences and a packaging signal are deleted, thus also increasing gene cargo capacity to around 36 kb[166]. These so called 'gutless' vectors are capable of longer term transgene expression compared to early adenoviruses, where strong immune responses limited transgene expression to around 2 weeks[167,168]. Long term expression of transgenes from gutless adenoviral vectors has been demonstrated, for example intramuscular injection of Ad5-lacZ resulted in persistent expression over 84 days[169]. Promising results led to the trial of gutless adenovirus in baboons, where expression of the alpha 1 antitrypsin gene in the liver persisted for over a year, albeit gradually decreasing throughout this time[170]. Thus, adenoviruses are still best suited towards applications where transient gene expression is applicable as transgene expression stability over extended periods is still challenging, and re-administration is met by rapid immune response preventing subsequent viral gene expression**.** Marked inflammatory responses mediated by the innate immune system recognizing the adenoviral capsid are also still a concern with gutless vectors[171].

The deletion of viral gene elements necessitates the use of helper viruses for adenoviral production, commonly replication competent adenoviruses (RCAs). These could induce fatal immune reactions if delivered to patients, and the complete exclusion of these contaminating viruses in final preparations still presents a challenge[168]. However, a recent proof of concept study detailed a novel system in which a helper plasmid substitutes place of helper viruses, designed to preclude

conversion to RCA and eliminate production of RCA byproducts[172]. Using this system, no replication competent adenovirus contaminants were detected in the final vector product[172]. Characteristics and primary advantages and disadvantages associated with adenoviral vectors are laid out in table 1.2.

1.4.4 Adeno associated virus (AAV)

AAV is a non-pathogenic virus endemic to human and non-human primates[173]. AAV contains a 4.7 kb single stranded genome, which can be either sense or antisense, flanked by two ITRs which serve as origins of replication and priming sites for host cell DNA polymerase to synthesise a second complementary strand during infection (pathway summarized in figure 1.5)[174]. The wild type genome comprises rep genes, encoding proteins required for viral replication, and cap genes which encode capsid components. A third gene, assembly activating protein (AAP), contained within the cap coding sequence has been shown to promote viral assembly[175]. For use in gene therapy, recombinant adeno associated virus (rAAV, henceforth referred to as AAV) was developed, in which all viral coding genes are deleted and replaced with synthetic transgene cassettes, aside from the ITRs which are necessary for viral production. Although wild type AAV can integrate into the AAVS1 locus in humans to establish latency, this is significantly ameliorated by deletion of the rep gene in recombinant AAV[176,177,178]. Very small degrees of genomic insertion have been reported using recombinant AAV, at 0.05% in mouse liver[179] and at a frequency between 10^{-4} and 10^{-5} in the skeletal muscle and liver of non-human primates after clinically relevant dosages[180]. One report associated AAV genomic insertion with tumorigenesis, identifying inserted AAV2 genomes in 11/193 hepatocellular carcinoma samples derived from human patients[181]. Importantly, a follow up to the aforementioned primate study demonstrated no genomic integration at gene loci implicated in AAV mediated driving of hepatocellular carcinoma[182]. Further evidence supporting AAV induced neoplasia is extremely rare, and none of the 1000's of ongoing AAV clinical trials have reported oncogenesis[183]. It is also important to consider that the study indicating AAV in driving HCC referred to infection by the wild type AAV2 virus, and as previously discussed, AAVs used in gene therapy have considerably less potential for genomic integration due to deletion of viral genes.

Despite its non-integrating nature, AAV is capable of conferring long term stable transgene expression in terminally differentiated non dividing cells, where viral DNA is stablisied in episomes within the nucleus[184,185] (figure 1.5). Highlighting the promise and clinical utility of AAV, the first approved gene therapies in both Europe and the USA are both AAV based. Glybera, an AAV1 vector designed to overexpress lipoprotein lipase in deficient individuals received approval and

recommendation by the European Medcines Agency in 2012[186]. In 2017, the FDA approved the use of Luxturna in those with retinal dystrophy associated with mutations in the RPE65 gene. AAV2 vectors are injected directly into the sub-retinal space and deliver functional copies of the RPE65 gene, driven by a hybrid CMV enhancer/ chicken beta actin promoter, to restore production of critical retinal proteins, halting visual degeneration in individuals who would otherwise progress to complete blindness[187]. The eye is considered an ideal gene therapy owing to its immunoprivileged nature and relative ease of access[188]. Mechanisms behind ocular immunoprivilege are debated, but it is hypothesized the lack of lymphatic circulation, effective blood-retinal barrier, and existence of immunosuppressive substances all limit inflammatory responses in a physiological mechanism (reviewed by[189].) Characteristics and primary advantages and disadvantages associated with AAV vectors are laid out in table 1.2.

1.4.4.1 Distinct AAV capsid properties allow preferential tissue targeting

Another attractive feature of AAV is the ability to target tissues with a degree of selectivity owing to differing tissue tropisms across serotype capsids. AAV gains access to cells via initial interactions with specific receptors on the surface of target cells, including sialic acid, galactose, integrins and laminins[190]. Each serotype preferentially interacts with different subsets of receptors, which determines tissue tropism. For example, AAV2 utilises heparan sulphate proteoglycan as a primary receptor mediating transduction[190]. This receptor is widely expressed across many cell types, and thus AAV2 has a broad tissue tropism. However, it is recognised that interaction with primary receptors is insufficient to mediate viral attachment and entry, and further interactions with other secondary receptors such as laminin receptors and integrins is necessary. AAV9's primary cell surface receptors are terminal B-galactose residues of glycans[191]. The Laminin receptor has also been shown to play a key role in AAV9 transduction[192]. AAV9 is cleared from the blood slowly, a characteristic that has been associated with specific structures within the capsid. Low blood clearance is associated with the ability of this serotype to confer high cardiac transduction and lends to its use as a systemic gene delivery vector[193]. After interaction with target cell surface receptors, the virion enters the cell via endocytosis and is trafficked to the nucleus where gene expression is induced. Detailed transduction pathway events are depicted in figure 1.5.

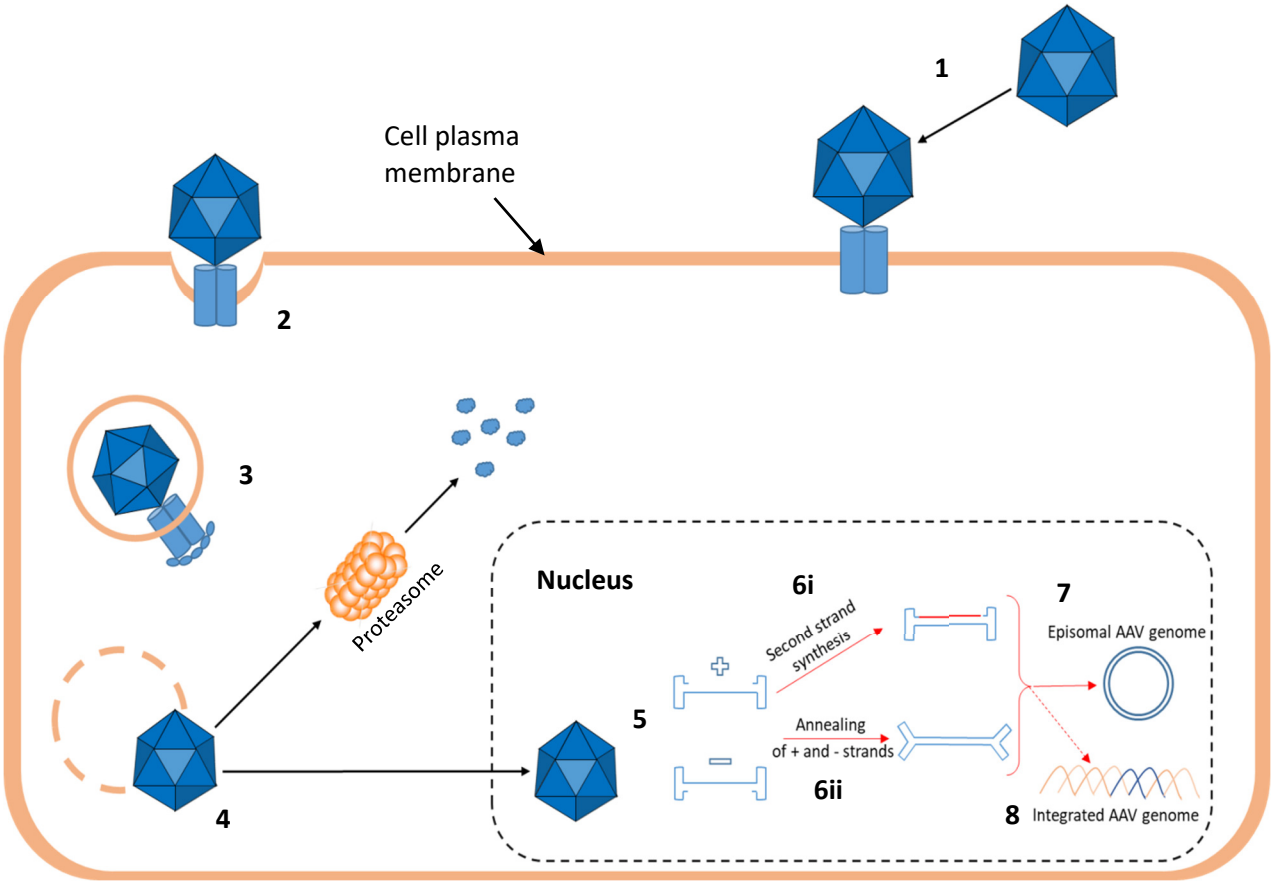

Figure 1.5: Mechanism of AAV transduction and transgene expression. 1. AAV binds to cell surface receptors, the preference for which depends upon the capsid serotype. 2. Following initial receptor interactions, the virus is internalized via clathrin mediated endocytosis and enters the cytosol. 3. The virus is trafficked within the cytosol via anchoring to the microtubules of the cytoskeleton. Studies have estimated this transportation to occur at approximately 1.8 – 3.7 µm/s[498]. 4. Acidic pH within the endosome induces conformational changes in the capsid, including externalization of nuclear localization signals and phospholipase domains which facilitate nuclear transport and endosomal escape. Vectors may be degraded before reaching the nucleus, most likely via the proteasome, evidenced by the finding that inhibition of the proteasome enhances AAV mediated transduction[499]. 5. Virions that reach the nucleus undergo uncoating, freeing the DNA cargo from the capsid protein shell. ssAAV contains either sense or antisense single stranded DNA, which must be converted to doubled stranded form in order to become transcriptionally active. This can be achieved by second strand synthesis using host cell polymerases (6i), or annealing of sense and antisense strands that may co-exist within the same cell as a result of transduction by multiple virions (6ii). ITRs in the DNA structure prime the DNA for inter or intra molecular recombination generating circular episomes that persist in the nucleus (7). At very low frequency, AAV can also integrate into the host chromosome (8).

Viral vector	Adenovirus	rAAV	Lentivirus
Transgene expression profile	Transient	Transient, long term in post mitotic tissues	Transient or stable
Immunogenicity	High	Very low	Low
Transduction profile	Broad	Broad, serotype dependent	Moderate
Insertional mutagenesis potential	Very low (non integrating)	Low (very low frequency of genomic integration)	Moderate (integrating vectors; although integrase deficient variants available)
Maximum insert size	3.0 - 8.0 kb/ 35 kb in gutless vectors	<5 kb	<9 kb
Transduction efficiency	Very high	High	Moderate
Infect dividing cells?	Yes	Yes	Yes
Infect non dividing cells?	Yes	Yes	Yes
Genomic content	dsDNA	ssDNA	ssRNA
Primary drawbacks	Transient gene expression only, high immunogenicity	Limited packaging capacity, requires helper viruses for production, delayed peak transgene expression-up to 100 DPI using AAV9[194]	Potential for insertional mutagenesis, transgene expression and transduction efficiency lower than AAV, adenovirus, low transduction efficiency
Primary strengths	High transgene expression and transduction efficiency with rapid onset	Low immunogenicity, broad transduction efficiency (tailored via serotype selection), high transgene expression	Capable of transient or stable transgene expression, sustained transgene expression in rapidly dividing tissues

Table 1.2: comparison of commonly used viral vectors for gene therapy applications

1.4.4.2 Safety profile of AAV vectors

AAV vectors are generally considered to have a highly favorable safety profile, due to minimal genomic integration and low level immunogenicity. Despite this, some reports linking AAV integration to genotoxicity have been documented, although this remains controversial and the precise link unclear. One study in dogs undergoing AAV mediated gene therapy for haemophilia identified clonal expansion of transduced liver cells, with evidence of genomic integration proximal to genes regulating cell growth[195]. Consensus is generally divided in terms of the true role, or lack thereof, of AAV integration in driving hepatocellular carcinoma. Integration of vector gnomes is inherently difficult to study, and it is difficult to parse out potential roles of the transgene, promoter, mouse strain used, all of which commonly vary between studies (Russell, 2007). In the context of the multitude of ongoing AAV clinical trials, and multiple FDA approved medicines, no instances of oncogenesis have been observed to date[196]. Analysis of AAV clinical trials encompassing 101 studies with 3328 enrolled patients revealed no cancer incidence, and an overwhelmingly positive overall safety profile of the vectors[196]. Given the inherent shortcomings and risks of complications arising from electronic pacemaker implantation including lead breakage, infection and battery depletion, the safety profile of a prospective AAV based therapy, which would in turn offer vast benefits such as complete chonotropic response and physiological function, lends toward this being a favourable strategy to treat CCS dysfunction. Furthermore, whilst electronic pacing is relatively effective for some conditions such as SND, many other arrhythmic conditions such as LBBB, where an estimated 20-40% of patients do not derive any benefit from current CRT approaches[197].

The apparently extremely low risk of vector toxicity appears at an acceptable level when weighing against the vast array of benefits of the propose therapeutic approach for those suffering from arrhythmias. Rates of complications arising from electronic pacemaker implantation must also be considered. To this end, the novel therapy should offer an improvement over the existing approach. Major complications were observed in up to 15% of procedures involving implantation or modification of implantable cardioverter defibrillator devices, presenting a significant healthcare burden and negative impact on patient quality of life[198]. In a review encompassing 3328 patients enrolled in AAV clinical trials, no studies were terminated on safety grounds at the time of publication, and all completed studies attained safety end points[196].

1.4.4.3 AAV9 is an effective vehicle for cardiac gene delivery

AAV9 is regarded as the most cardiotropic serotype and transduces the heart with excellent

efficiency after systemic administration in mice and rats[194,199,200]. After intravenous injection of 1 x 10^{11} AAV9 particles carrying the ubiquitous CMV promoter driven LacZ transgene in adult mice, over 80% cardiac transduction was observed, whilst the liver was only transduced at a very low rate of just over 5%[200]. This suggests that at low doses, AAV9 targets the heart with high selectivity, even without the use of tissue specific promoters. To this end, AAV transduces post-mitotic cells of the cardiac and skeletal muscle extremely efficiently, whereas tissues undergoing higher turn-over and thus cell cycling are less efficiently transduced[201]. Upon terminal differentiation, cardiac and skeletal muscle cells downregulate proteins involved in DNA damage response (DDRs) in response to the cessation of DNA replication[202]. Specifically, DDR proteins of the MRN complex physically bind to internalized rAAV genomes and may induce transcriptional silencing or block their conversion to transcriptionally active dsDNA[203]. Supporting this mechanism, delivery of shRNA targeting MRN complex members markedly increased transduction efficiency in hepatocytes in vivo[203]. Further, treatment of cells with DNA damaging agents increases AAV transduction efficiency by effectively baiting the DDR machinery away from infecting AAV genomes[204].

At a higher dose of 1 x 10^{12} vg/ mouse, the heart was transduced with 100% efficiency, but liver transduction was increased to over 50%[200]. This suggests that intrinsic tissue tropism can be partially overridden at high doses, and that the viral dosage is important when considering tissue specific targeting. Indeed, due to the signal stranded nature of AAV, higher vector genome copies per cell, correlating with higher dosage, would increase the likelihood of plus and minus strand coinfection and annealing within target cells. To this end, single stranded AAV genomes must be converted to double stranded DNA within mammalian cells to become transcriptionally active. As discussed later, this mechanism is an important limiting factor in AAV transduction efficiency. Furthermore, reporter gene expression driven by a cardiac specific cardiac troponin T (cTnT) promoter was highest using AAV9 as a delivery vector after intravenous injection in neonatal mice, closely followed by AAV8[205]. Another study demonstrated that after intravenous injection of 1 x 10^{11} AAV9 vector particles in adult mice, GFP expression was 92% higher in the heart compared to liver using the CMV promoter, whilst expression was 40% higher in the liver compared to the heart using the chicken beta actin (CBA) promoter, and expression in other organs such as lung and kidney was negligible[206]. Another study compared the ability of AAV5, AAV6 and AAV9 to transduce the heart after intracoronary perfusion or intravenous injection via the jugular vein. It was found that AAV9 provided the best cardiac transduction regardless of administration route, and that intracoronary perfusion was superior to intravenous injection. Interestingly, intracoronary perfusion dramatically improved cardiac gene transfer in AAV serotypes 5 and 6 by 238 and 24 fold

respectively, whilst AAV9 only saw a 2.5 fold higher in transgene expression[207]. This highlights the distinct behavior of AAV serotypes, the need for characterization of all experimental variables when selecting which serotype to use, and the potent efficacy of AAV9 after systemic administration in mice. This was perhaps seen as AAV9 is known to be one of the least immunogenic AAV serotypes, attributable to unique physical properties of the AAV9 capsid[208]. Thus its ability to escape immune clearance could result in higher concentrations reaching the heart after systemic intravenous injection. Interestingly, it was found that in the context of intra cardiac injection in pigs, AAV6 out-performed AAV9, again highlighting the context and species specific tropism disparities exhibited by AAV vectors[209].

1.4.4.4 Second strand synthesis / annealing is a rate limiting factor in AAV mediated transgene expression

One limiting factor intrinsic to AAV is the time taken to achieve maximal transgene expression. Figures vary depending upon factors such age and species of animals used, administration route (systemic vs localized) and capsid serotype. It has been demonstrated that onset of gene expression varies greatly between serotypes. AAV9 and AAV7 are capable of rapid onset of gene expression, whereas AAV3 and 4 are much slower[194]. After intravenous systemic administration of 1 x 10^{11} viral particles containing the luciferase transgene under control of the CMV promoter, luciferase expression was recorded from AAV9 and AAV7 7 days after administration, whereas expression from AAV2 and AAV3 did not reach levels above background until 29 days after injection[194]. Although onset of expression from AAV9 was relatively fast, it did not peak until 100 days post injection, where it recorded the highest expression of all serotypes[194]. This referred to total luciferase bioluminescence from mice and did not address onset and kinetics of expression across specific organs. A later study using the same age of mice and administration route studied onset of GFP transgene expression in the heart and liver conferred by AAV9 using CMV and CMV enhancer/ chicken beta actin promoters. Transgene expression peaked at 5 weeks post injection in the heart (with transduction efficiency over 80% using the CMV promoter) and liver, with a small decline observed at the next time point (week 8)[206].

It is thought that one of the main rate-limiting factor during AAV transduction and transgene expression is host cell synthesis of the second complementary strand from the template single stranded AAV genome[210,211]. AAV DNA is packaged in single stranded linear form, and upon reaching the host cell nucleus, the genome must be converted to double stranded form in order to become transcriptionally active. Double stranded genomes can also be derived from annealing of sense and

antisense strands derived from separate virons infecting one cell[212]. As well as being a rate limiting step for transgene expression, failure to undergo second strand synthesis can also present a barrier to achieving high transgene expression efficiency[213]. For example, it has been shown that the inability of AAV to successfully transduce trabecular meshwork cells of the eye is due to an instrinsic failure of these cells to convert viral ssDNA to dsDNA[214]. In order to circumvent this rate-limiting step, self-complementary AAV vectors (scAAV) were developed, in which both strands are packaged as a dimeric single molecule[215]. Upon nuclear entry, sense and antisense strands spontaneously anneal and form a transcriptionally active unit, bypassing second strand synthesis[215]. The main drawback of scAAV is that the packaging capacity is halved compared with the already limited conventional AAV (2.2 kb vs 4.7 kb)[215]. However, this can still prove useful for applications where the expression cassette is small, such as in RNA overexpression or interference. It has been shown that scAAV1 vectors can confer cardiac transgene expression within 4 days post injection, whereas expression was not evident until 11 days using ssAAV1[216]. Evidence suggests that scAAV enhances muscle transduction 11-15 fold over ssAAV vectors, and confers more rapid onset of gene expression in many tissues in vivo[217].

1.4.4.5 Overcoming limited packaging capacity of AAV vectors

AAV can only accommodate relatively small transgenes (up to 4.7 kb, corresponding to the wild type genome size)[218]. Attempts to generate AAV containing larger transgenes results in truncation of the transgene and vastly reduced expression in vivo[219]. Innovative strategies have been employed to circumvent this limited packaging capacity. Large transgene cassettes can be split between multiple vectors, and after co-infection within the same cell, the entire transgene can be reconstituted by a number of mechanisms:

1.4.4.5.1 Trans-splicing AAV vectors

These vectors harness the natural tendency for AAV genomes to undergo concatemerisation via ITR mediated intermolecular recombination. Typically, the cassette is split between two vectors. Dual vectors increase packaging capacity from ~5 kb to ~9 kb. One vector contains the promoter and 5' portion of the coding sequence and a splicing donor sequence, and the other contains the splice acceptor, remaining coding sequence and terminal polyadenylation signal. Upon co transfection and subsequent head to tail concatemerisation, intervening sequences are spliced out and the transgene reconstituted in full[220] (figure 1.6 A) Transgene expression is typically lower than that achieved using a single vector, owing to dependence of cotransfection of multiple vector products

within the same cell and the necessity for concatemerisation in a specific (head to tail) orientation. Efficiencies of between 4.3 and 7% compared to single vectors were observed, depending on the tissues examined[221]. Refinements in the technique allowed successful delivery of a 6 kb Dystophin gene fragment to the muscles of Duchenne muscular Dystophy mice, resulting in an improved phenotype[222]. Triple AAV vectors have been used to even further increase the deliverable gene size from AAV vectors to up to 15 kb. In the context of CCS gene therapy, HCN4, a key target of interest has a coding sequence length of 6.9 kb. Thus, triple vectors would allow provision of the full coding sequence plus a minimal promoter and necessary regulatory elements. Triple trans splicing AAV vectors have successfully delivered the full length dystrophin gene to muscles in mice[223]. In the mouse retina, only 4% transduction efficiency was achieved using triple AAV vectors, however transduction efficiency was 40% of that achieved using single vectors in the pig[224]. Despite generation of aberrant transcripts, only the full intact reconstituted versions were capable of being translated, addressing an important translational safety concern[224]. In this case, the enclosed retinal space is an ideal substrate for co-infection with numerous viruses, however, it is yet to be determined how effective this system could be in the context of systemic administration. Indeed, one of the key translational hurdles for systemic AAV gene therapy is the necessity for high doses and thus viral concentrations in large animal models and humans[201]. Thus, the need for administration of two or three separate vectors could exacerbate this issue.

1.4.4.5.2 Overlapping AAV vectors

This approach involves homologous recombination between two vectors which contain two portions of an expression cassette that share an overlapping homologous region within the coding sequence (figure 1.6 B). As a result of this mechanism, genes that possess highly recombinogenic regions are ideal candidates. This strategy has been used to deliver a variety of transgenes successfully in vivo, reviewed by[225].

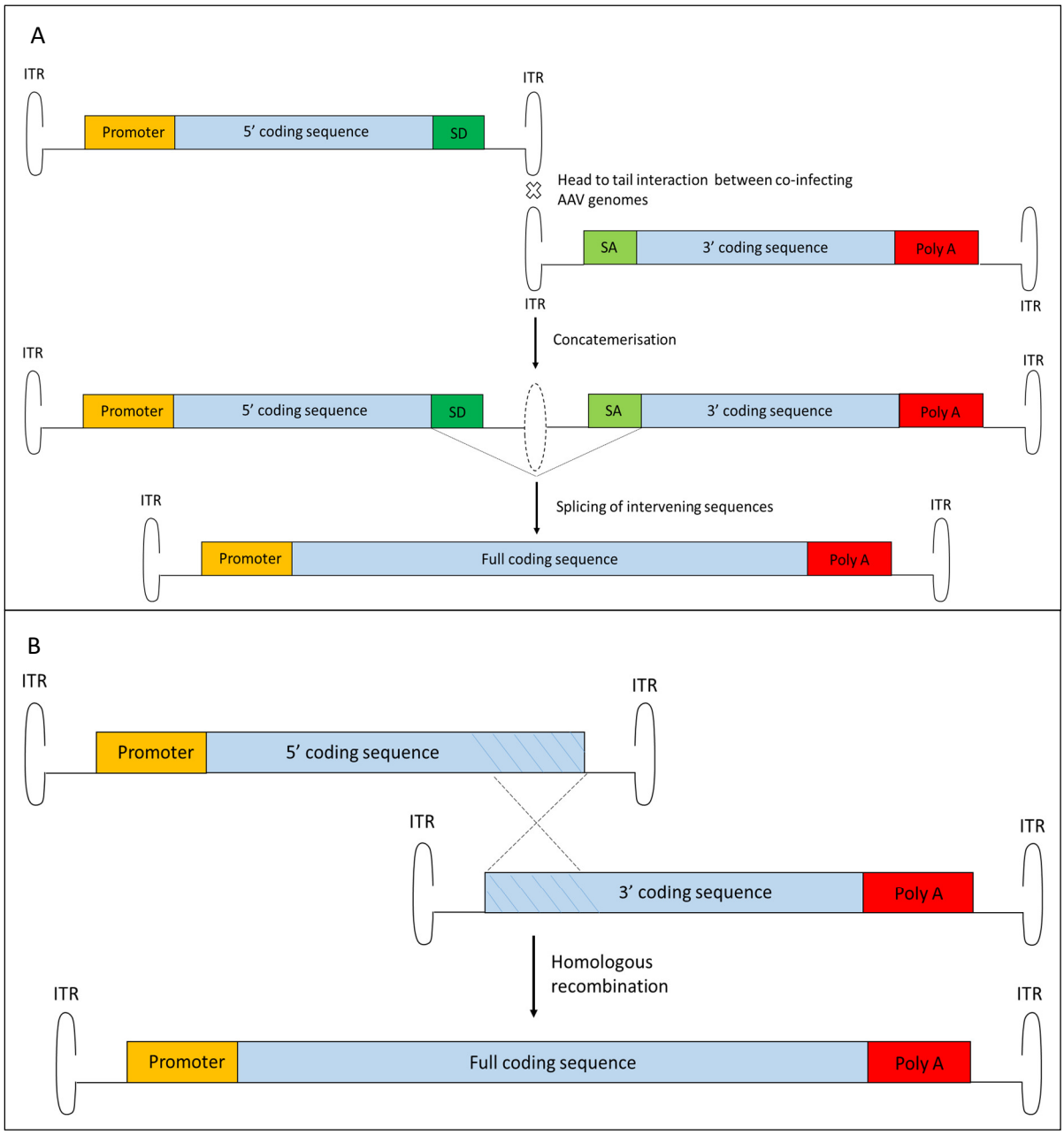

Figure 1.6: mechanisms for increasing AAV transgene capacity. A) dual trans splicing AAV vectors. The first vector comprises the promoter, 5' portion of the transgene and splice donor (SD) signal. The second vector comprises the splice acceptor (SA) sequence, 3' portion of the transgene and polyadenylation (PolyA) sequence. Co-infection of the same cell with both vectors leads to concatemerisation via interaction of vector inverted terminal repeats (ITRs) as shown, reconstituting he full length transgene. The intervening ITR structure is then spliced out utilizing the splice donor and acceptor sites, reconstituting the full length RNA of the transgene. B) Overlapping dual AAV vector approach. The first vector contains the promoter and 5' portion of the transgene coding sequence, whilst the second vector contains the 3' portion of the coding sequence and PolyA signal. A portion of the coding sequence is repeated in both vectors (represented by the blue hatched region in B), at the 3' end of the first vector, and 5' end of the second vector. This repeated sequence may be a sequence contained by both portions of the coding sequence, or a designated recombinogenic sequence. The full length transgene coding sequence is reconstituted upon homologous recombination between the two overlapping sequences upon coinfection of the same cell by the respective vectors.

1.4.4.6 'Designer' AAVs- circumventing immunity and tissue specificity

Although AAV tissue tropism and infection preference varies between serotypes, it is often not possible to achieve true tissue specific transduction and transgene expression using naturally discovered AAV serotypes alone. Most often, a constitutively active strong promoter is used to drive high transgene expression, such as human cytomegalovirus (CMV), Simian Virus 40 (SV40) and hybrid CMV enhancer/chicken beta actin (CAG)[226] promoters. Thus, tissue specific expression could be achieved by modifying the viral capsid and / or tissue substrate to manipulate transduction, and/ or using a tissue specific promoter to drive transgene expression.

1.4.4.6.1 Customised AAV capsids

One of the most limiting factors to AAV use in a clinical setting the prevalence of pre-existing neutralizing antibodies (NAbs) in the population[227]. It is estimated that between 40 and 80% of people possess such antibodies, depending upon the serotype and age of the individual[228]. AAV2 antibodies are thought to be the most frequently present in humans[229]. One study examining sera from 226 healthy adults found a 59% seroprevelence of AAV2 NAbs, whereas those directed against AAV8 and AAV9 were significantly less prevalent, at frequencies of 19 and 33.5% respectively[230]. The presence of NAbs drastically reduces transduction efficiency of systemically administered AAV[231,232,233]. Indeed, the first clinical trial for Haemophilia B involving intra-arterial administration of AAV2-FactorIX demonstrated that low concentrations (up to 1:17) of NAbs were sufficient to block transgene expression even in high dosage groups[234]**.** As immune responses are directed against the viral capsid, a number of strategies have been employed in attempts to modify the capsid to decrease it's immunogenicity. As AAV attachment and entry to target cells is also mediated by capsid proteins, capsid engineering can also be employed to modify and / or enhance tissue tropism and transduction efficiency.

AAV capsid modification by rational design involves mutating and modifying specific structural elements involved in immunological recognition and / or tissue tropism. It is known that the 3 fold protrusion structures of the capsid play key roles in tissue tropism and immunogenciity, and so represent an ideal site for modification[235]. Modifying specific proteins within this region yielded a novel AAV2 variant that showed heightened ability to evade Nabs, without affecting other characteristics such as tropism or infectivity[236]. High throughput DNA shuffling may also be employed, where genetic sequences from multiple capsid serotypes be combined and replaced to yield novel variants (strategy and technique reviewed by[237]). Using serum from rabbits with prior

exposure to AAV2, a variant was evolved via error prone PCR and mutagenesis combined with high-throughput selection methods which showed a 96 fold resistance to neutralization by NAbs compared to wild type AAV2[238].

For some tissue targets such as the heart, transduction efficiency from naturally occurring AAV serotypes (such as AAV9) is extremely efficient, and capsid engineering strategies are aimed towards de-targeting vectors from other tissues, particularly the liver, in order to achieve tissue specific transduction. Either decreasing the expression of glycans in target organs, or decreasing the glycan binding affinity of AAV9, resulted in liver de-targeting without compromising cardiac transduction[239]. Mutations introduced at positions P504A/G505A and Q590A in the AAV9 capsid also achieved liver de-targeting whilst efficient cardiac transduction was preserved in mice[240]. Using directed evolution of the AAV9 capsid, a novel variant (M41) was developed which showed attenuated liver transduction by approximately 20 fold, whereas cardiac transduction was only reduced by 2 fold after tail vein injection in mice[241]. Indeed, many different approaches have been successfully employed to achieve liver de-targeting and other tropic modifications of AAV vectors, as reviewed by[242,243,244,].

1.4.4.6.2 Spatial restriction of transgene expression by tissue specific promoters

Despite efforts discussed above, an AAV capsid capable of complete tissue specific transduction is yet to be developed. However, using the natural tropism of AAV serotypes synergistically with tissue specific promoters has proven capable of tissue specific transgene expression. Many such promoters have been characterized, whilst the main challenge with AAV therapeutics is again the limited (4.7 kb) packaging capacity to include the promoter, transgene and all regulatory elements including ITRs.

Strong, ubiquitous promoters confer high transgene expression, at the expense of tissue specificity. One of the most commonly used strong promoters is the human immediate / early cytomegalovirus enhancer/ promoter (CMV)[245], which is active in most cells and tissues including heart, liver lung, skeletal muscle and brain, and is capable of driving high transgene expression[246,247]. Notably, the first clinically approved AAV gene therapy (Glybera, as previously mentioned) utilizes the CMV promoter for therapeutic transgene (lipoprotein lipase) expression[186]. Despite its high transcriptional strength, the CMV promoter is prone to transcriptional silencing in vivo, associated with extensive promoter methylation[248,249]. This phenomenon has been markedly shown in tissues of the CNS[250], liver[251], and skeletal muscle[249]. In agreement with this finding, inhibition of DNA

methylation resulted in reactivation of silenced CMV promoter driven transgenes *in vitro*[252]. Methylation can induce transcriptional silencing via the recruitment of proteins involved in transcriptional repression, such as histone deacetylases, or physical inhibition of TF binding[253]. Furthermore, toxicity and inflammatory responses have been associated with supraphysiological levels of transgene expression from constitutive promoters, for example in the case of hepatic delivery of factor VIII in the context of haemophilia[254], and dystrophin to skeletal muscles[255]. Furthermore, delivery of cell cycle inducing micoRNAs (miRs) via AAV under control of the CMV promoter was shown to induce uncontrolled cell cycle activity in the heart over time, inducing fatal arrhythmias, pointing to a need for temporal control of transgene expression in this context[209].

Endogenous promoters are less prone to silencing than strong viral promoters and present the opportunity to spatially regulate transgene expression to one specific tissue, thus minimizing off target effects. Several potent cardiac specific promoters have been characterized. A 363 bp fragment of the human alpha-MHC promoter was shown to drive high and specific transgene expression in the heart after systemic delivery of AAV9, whereas the desmin promoter was efficient in heart, skeletal muscle and brain, though neither was as potent as the CMV promoter[247]. MHC is a major structural protein in cardiomyocytes, important for contractile function[256]. In humans, it is noteworthy that the alpha MHC subunit expression is restricted to the atria, whereas in mice it is also expressed in the ventricles[257]. One of the most effective cardiac specific promoters suitable for AAV gene therapy applications is a 418 bp fragment of the cardiac troponin T (cTnT) promoter[205]. Coupled with AAV9 using a systemic intravenous administration route, the cTnT promoter drove luciferase reporter gene expression at over 640 fold higher levels compared to the next highest organ (liver), and close to 100% cardiac transduction efficiency could be achieved using a relatively low dose of 3.15×10^{10} vector genomes per 1 week old mouse[205]. Despite an abundance of potent and relatively specific minimal cardiac promoters, few validated CCS specific candidates exist. The entire KCNE1 and HCN4 regulatory elements are capable of recapitulating endogenous CCS specific gene expression in transgenic mice, although extensive regulatory elements are not appropriate for use in AAV vectors due to restrictions on packaging capacity[258,259]. Inter-species disparities must also be considered- for example, KCNE1, a beta subunit to KCNQ1 and mediator of $I_{K,s}$ is more highly expressed in the working myocardium of many large animals, commensurate with higher $I_{K,s}$ density[260]. Thus, a KCNE1 promoter may be less CCS specific in large animals than in mice.

Furthermore, whilst cardiac contractile proteins, which represent most characterized cardiac specific promoters, are highly expressed across the entire working myocardium, plasmalemmal

pacemaking ion channels are confined to minute regions, and their expression may also be relatively low, even compared to intracellular ion channels. For context, HCN4 ion channel copy number per SAN myocyte was estimated to be 1000 fold lower than SERCA2[261]. Thus, plasmalemmal pacemaking ion channel promoters may have low transcriptional strength compared to other established cardiac specific promoters.

Despite the existence of some potent tissue specific promoters, one of the main drawbacks limiting their utility is their relatively low transcriptional strength, especially when compared to strong ubiquitous promoters such as CMV. One approach to counteract this is to engineer synthetic promoter variants to include exogenous enhancer elements. It must also be considered that for AAV applications, the promoter size must be minimized in order to also accommodate the transgene and other regulatory elements within the 4.7 kb packaging limit. One promising strategy to enhance transcriptional strength is to append the human immediate early CMV enhancer (CMVe) upstream of tissue specific promoters[262]. After systemic administration of AAV2 in mice, a hybrid promoter comprising the CMV enhancer upstream of the cardiac specific myosin light chain (MLC) promoter was shown to induce 50 fold higher transgene expression in the left ventricle compared to the CMV promoter, whilst maintaining only low level expression in the liver and kidneys[263]. Later studies showed the promise of the promoter construct in preclinical (porcine) model of heart failure using AAV9 as a delivery vector via coronary venous infusion[264]. Cardiomyocyte restricted expression of S100A1, a calcium sensor protein implicated in heart failure pathogenesis, driven by CMVe-MLC, resulted in improved calcium handling and enhanced cardiac function in heart failure pigs[264]. Gruh et al.[262] investigated the effect of the CMV enhancer on the performance of a variety of promoters in vitro. Performance of the atrial specific atrial naturietic factor (ANF) promoter was enhanced 40-fold in the murine atrial cell line HL-1 by inclusion of the CMVe[262]. Aside from a 7-fold induction in fibroblasts, no other off target cell lines showed reporter gene expression, indicating that the ANF promoter maintains a high degree of tissue specificity despite a significant induction in transcriptional strength[262]. Importantly, this also shows that endogenous promoters can act synergistically with synthetic enhancer elements. In the same study, the lung specific SP-2 promoter showed significantly enhanced transcriptional strength without loss of tissue specificity[262]. However, the interactions with such enhancer elements appear to vary between promoters. Introduction of the CMV enhancer caused the alpha MHC promoter to lose a high degree of tissue specificity[262]. Moreover, Jia et al.[265] reported that tumor specific carcinoembryonic antigen (CEA) and alpha-fetoprotein (AFP) promoters did not maintain tumor specific transgene expression upon introduction of the CMV enhancer, raising concerns about this approach in the context of cancer

gene therapy[265]. Importantly, it must be considered that cell lines typically do not recapitulate the *in vivo* environment, such as TF expression, and thus performance of promoters *in vitro* performance may not necessarily reflect *in vivo*. Notably, in vivo the CMV enhancer boosted neuron specific expression from the PDGF-beta promoter whilst maintaining a high degree of specificity[266].

In summary, AAV is an ideal vector for gene therapy due to its low immunogenicity and ability to effectively transduce a variety of cell types. Pertaining to cardiac gene therapy, the ability of AAV serotypes (particularly AAV9) to confer high level and selective cardiac gene transfer after systemic administration is particularly appealing. In mice, AAV9 is the ideal vector for targeting the heart, and perhaps the CCS, after systemic administration.

1.5 Current approaches to treating CCS disease

Despite its prevalence and significant contributions to morbidity and mortality, treatments for CCS dysfunction are mainly limited to palliative device implantation. Pacemaker implantation and pharmacological modulation of heart rate are currently front line therapies in the treatment of most arrhythmias, including SND. For example, cardiac resynchronization therapy (CRT) is used to treat LBBB and Purkinje dysfunction, and electronic pacemaker implantation is used to treat symptomatic SND[267]. However, these strategies have inherent shortcomings as discussed below.

1.5.1 Electronic pacemaker implantation- strengths and limitations

Currently, the gold standard treatment for symptomatic SND is pacemaker implantation, where SND accounts for approximately half of all pacemaker implantations[268]. Electronic pacing is currently the only effective treatment for SND, which is caused predominantly by ageing, HF or inherited genetic variants in pacemaking ion channels[269]. Although pacing has proven effective in partially alleviating symptoms of SND, such as chonotropic incompetence, no significant effect on mortality is conferred[270,271]. Pacing may be induced via the atria, ventricles, or via both atria and ventricles. Dual chamber pacing may offer improved atrioventricular synchrony and thus improved cardiac output and patient longevity[272], although this method is more complicated to implant, more expensive and more prone to complications compared to single chamber pacing methods[273]. Each pacing method has indications and contraindications, and so the precise clinical picture must be considered when selecting a pacing protocol. For example, single lead atrial pacing is contraindicated in those with SND due to the risk of developing total heart block[274]. CRT, or dual

ventricular pacing has proven effective in decreasing mortality and pathogenic remodeling in those with HF and His-Purkinje dysfunction[275–277]. However, an estimated 20-40% of patients do not derive any benefit from CRT[197].

Pacing from the RV apex requires access through the tricuspid valve, which can disrupt its closed conformation and cause regurgitation[278]. Pacing from the RV apex also fails to recapitulate the physiological activation pattern of the ventricles[279]. This abnormal activation sequence exacerbates left ventricular dysfunction, reduces coronary perfusion and impairs systolic and diastolic performance[280–282]. Left ventricular dysfunction attributed to right ventricular pacing is known as pacing induced cardiomyopathy (PICM), and has a prevalence of between 5 and 20%[283]. Alternative lead implantation sites have been tested, including the His-bundle, atrial septum and AV septum (reviewed by Kaye, 2018[283]). Pacing from the His bundle achieves a more physiological cardiac activation sequence. A 10% reduction in PICM using His-bindle pacing vs right ventricular pacing has been demonstrated[284]. However, implantation procedures associated with His-bundle pacing are technically challenging, with longer surgical times and widely varying success rates reported between 44% and 95%[285]. Furthermore, His pacing necessitates the use of higher energies to achieve His bundle capture, which compromises battery life[286].

In order to circumvent shortcomings such as the possibility of infection at the lead implantation site, lead damage and valvular regurgitation, leadless pacing technology has been explored. This typically involves implantation of sensing electrodes and their stimulation by extra-cardiac ultrasound or magnetic waves[287]. The first two approved leadless systems (Abbot Nanostim and Medtronic Micra) performed favourably in trials, however a 4 - 6.5% rate of severe complications was observed after implantation, including cardiac perforation in 1.3% of cases[288,289]. Due to the design, implantation procedures and implantation site, leadless devices are difficult to retrieve in the event of complication or battery depletion..

1.5.2 Biological pacing

Electronic pacemakers also suffer from battery depletion over time, and replacement requires additional surgical procedures. In young patients, battery longevity is a particularly relevant issue, given patients frequently require life-long pacing. Furthermore, leads are prone to damage mainly by breakage or erosion of the outer insulation. Approximately 5% of pacemaker implantations have serious adverse complications[290]. Electronic pacemakers also confer little chronotropic response to emotion or physical stimulation, since they are not responsive to autonomic stimulation[291]. For

these reasons, engineering a biological pacemaker has received considerable interest.

1.5.2.1 Engineering a biological pacemaker via gene therapy

One approach to biopacemaking is to induce pacemaker activity in non-pacemaker cells. This can be achieved by disrupting the stable resting potential by either inhibiting outward hyperpolarising currents, or enhancing inward depolarising currents, thus facilitating spontaneous depolarisation. Automaticity of SAN cells is related to low expression of $I_{K,1}$ and high expression of depolarising currents such as I_f, and modifying the expression of these currents formed the early attempts at biological pacemaker gene therapy.

1.5.2.1.1 Inhibition of the inward rectifier ($I_{K,1}$) current

$I_{K,1}$, mediated by Kir2.1 channels, plays a key role in the maintenance of the stable negative resting potential, where upregulation of outward $I_{K,1}$ reduces cellular excitability and inhibits spontaneous diastolic depolarisation[292]. A dominant negative Kir2.1 isoform with attenuated function was generated and overexpressed via adenoviral vectors in the guinea pig left ventricle[293]. Effective transient knockdown of $I_{K,1}$ was achieved, and transduced cardiomyocytes exhibited spontaneous depolarisation[293]. A later study combined the same dominant negative Kir2.1 with HCN2 overexpression and thus I_f induction, and achieved physiologically relevant pacing in a porcine model of total heart block after adenoviral gene delivery to the AV junction[294]. Inhibition of repolarising currents, however, is not without safety concerns. Prolongation of the action potential predisposes to Torsades de Pointes, a potentially fatal ventricular tachyarrhythmia[295]. To this end, loss of function mutations in Kir2.1 manifest clinically as Long-QT Syndrome, where patients frequently suffer from arrhythmias precipitated by prolonged repolarisation.

1.5.2.1.2 Manipulation of HCN (I_f) channel expression

As discussed, HCN channels mediate I_f, which contributes to the diastolic depolarisation and thus automaticity of the SAN.. Overexpression of I_f could thus induce spontaneous depolarisation in quiescent tissues or cells. Since I_f only activates selectively at hyperpolarised potentials during the diastolic depolarisation phase of the action potential, this approach would avoid prolonging the action potential and thus reduce predisposition to induced arrhythmia[296]. HCN2 overexpression in the left atrium generated spontaneous action potentials during experimentally induced sinus arrest, albeit pacing was less robust compared to physiological sinus rhythm[297]. Adenoviral HCN2 overexpression in the canine left bundle branch upregulated I_f, and enhanced automaticity[298].

However, injury at the injection site resulted in tachycardias soon after injection, and again pacing was bradycardic compared to the native SAN[298].

HCN channels have been modified in efforts to achieve higher pacing rates and improve autonomic response. A mutant HCN2 (E324A missense substitution) elicits a more rapid diastolic depolarisation with a more positive activation threshold and enhanced autonomic responsiveness to catecholamines compared to wild type HCN2[299]. This construct was injected into the left bundle branch of dogs carrying an implanted electrical pacemaker device, which served as a backup when rate from the biopacemaker dropped below a set threshold of 45 bpm. Low reliance on backup pacing was observed, with approximately 70% of beats originating from the biopacemaker[299]. To this end, electrical pacemakers are likely to play a continuing role in future clinical trials of biopacemakers, providing a safety net in case of failure or inefficiency.

A chimeric HCN construct, 'HCN212' was also created[300]. The included portion of the HCN1 channel conferred a more positive diastolic threshold potential compared with HCN2, and the C and N termini of HCN2 contributed enhanced autonomic responsiveness compared to HCN1 alone[300]. However, this approach resulted in ventricular tachycardia when transfected to the canine left bundle branch, which was responsive to I_f block with ivabradine[300].

Evidence supports the existence of backup pacemaker activity in the parandodal (or subsidiary atrial pacemaker SAP) region of the SAN in goats, which becomes active upon SAN ablation[301]. A similar paranodal area exists in the human SAN, and a shift in the leading pacemaker site to this region has been postulated as a mechanism surrounding SND. Due to differences in molecular makeup, particularly in pacemaking ion channel expression, pacemaking from the SAP is bradycardic and inefficient[302]. Since the molecular and structural makeup of the paranodal area is similar to the SAN, fine tuning gene expression in this region could generate a more robust pacemaker in the event of SAN failure. Morris et al. (2013)[90] transfected this region with adenoviral constructs encoding HCN2 or chimeric HCN212, and observed an accelerated pacing rate. This is an attractive approach since the SAP more closely resembles the complex and distinct molecular and structural architecture of the SAN compared to other ectopic sites, such as the ventricular myocardium or His- bundle[90]. For example, $I_{K,1}$ and conexin43 are poorly expressed in the SAP similarly to the SAN[303,304]. To this end, the level of intercellular coupling in the SAN is low compared to working myocardium, due to specific connexin isoform expression and abundance[302]. Computer simulation studies showed that a gradually increasing level of electrical coupling from the SAN towards the periphery which

interfaces with the atrium is necessary for the SAN to drive the atrial muscle[305]. The precise molecular and physical architecture of the SAN- atrial boundary helps shield the SAN from hyperpolarising influence of the atrium. Thus, effective biological pacemaker activity likely necessitates the accurate recapitulation of many complex factors unique to the SAN microenvironment.

1.5.2.1.3 Adenylate Cyclase and Skeletal Muscle Sodium Channels

Adenylate cyclase (AC) produces cAMP, which enhances pacemaking by shifting the activation of I_f towards a more positive voltage threshold[306]. Adenoviral overexpression of AC1 and HCN2 in the canine left bundle branch resulted in robust pacemaking with favourable autonomic responsivity[307]. However, the HCN2/AC1 combination also induced tachycardias which responded to ivabradine[307]. Concerns also exist over elevating intracellular cAMP levels, which could alter calcium handling. To this end, cAMP regulates the activity of PKA, which in turn modulates L- type calcium channels and RYR2[308].

A hybrid approach utilising HCN2 and skeletal muscle Na+ channel (SKM1) overexpression was also trialled via adenoviral vectors[309]. In this system, HCN4 provided the depolarising current towards activation threshold of the rapid Na+ current, and thus action potential generation. SKM1 channels are favourable compared to cardiac Nav1.5 channels since their threshold potential is more negative, and thus less depolarisation is needed for the triggering of the action potential, enhancing automaticity[310]. The HCN2/ SKM1 construct exhibited robust pacing after injection into the left bundle branch of dogs, with average basal and maximal rates of 80 bpm and 130 bpm achieved[309]. Rate was responsive to autonomic and circadian stimuli, highlighting it's potential physiological applicability and advantageous behaviour over electronic pacemakers. Long term pacing by this method has not been investigated, and could be achieved using alternative viral vectors for gene delivery such as lentivirus or AAV.

1.5.2.1.4 Transcription factors and reprogramming

Overexpression of certain TFs (Myc, Oct3/4, Sox2 and Klf4) can be used to reprogram somatic cells into stem cells (induced pluripotent stem cells (iPSCs))[311]. These stem cells could then be directed along specific lineages, such as cardiomyocytes or SAN cells, providing a rich and potentially autologous source of transplantable cells for regenerative medicine. As well as this, direct reprogramming facilitates conversion between cell types, bypassing the pluripotent step and thus achieve reprogramming in situ[312]. One of the first applications of this technology in regenerative

medicine was towards regeneration of cardiomyocytes lost to ischemia. Overexpression of reprogramming factors in the post-MI mouse heart successfully reprogrammed fibroblasts into functional cardiomyocytes *in situ*, with ameliorated remodelling and enhanced cardiac function[313].

These principles are can also be applied to biopacemaking, where biological pacemakers could be generated by reprogramming cells towards the cardiac pacemaker lineage at ectopic sites such as the atrial myocardium or His bundle. TBX3 is a CCS specific TF responsible for maintenance of the pacemaker phenotype through repressing the working myocardial gene expression[314]. Overexpression of TBX3 in the adult atrial myocardium downregulated some working myocardial genes including inward rectifier K^+ channels and connexin 43, but ultimately failed to induce ectopic pacemaker activity[315]. A later study showed that adenoviral overexpression TBX3 and HCN2 in iPSC derived cardiomyocytes resulted in spontaneous diastolic depolarization, suggested a combinatorial approach could be appropriate[316].

TBX18 controls SAN development, with a precise role in regulating SAN conduction velocity via connexin 43 transcriptional repression[317,318]. Overexpression of TBX18 in the apex of the guinea pig heart induced automaticity with contributions from both calcium and voltage clock pacemaking mechanisms, and conferred a SAN cell-like phenotype[319]. Reprogrammed cells were also sensitive to autonomic stimulation, suggesting that biopacemakers could address a key shortcoming of electronic pacemakers[319]. Adenoviral overexpression of TBX18 in the porcine AV junction reprogrammed cardiomyocytes *in situ*, inducing a SAN-like gene expression profile, including reduced Kir2.1 and elevated HCN4 levels[320]. Robust pacemaker activity and autonomic responsiveness was achieved without incurring heightened risk of arrhythmia[320]. Long term studies are necessary to determine if this strategy is appropriate for life-long pacing, since a loss of pacemaker phenotype and activity was seen after approximately 1 week, which was ameliorated by inhibition of epithelial-to-mesenchymal transition. Efforts to improve efficiency of reprogramming and thus yield and quality of induced SAN cells are ongoing.

1.5.2.2 Cell therapy for biopacemaker development

Implantation of cells with intrinsic automaticity, or cells engineered to express depolarising currents (such as I_f), may be employed to generate a biological pacemaker. Both these strategies rely on strong electromechanical integration of the graft in order to form a functional syncytium with host cells. Notably, this aspect has been a key stumbling block in the progress of cell therapy for other cardiac regenerative applications (reviewed by Segers and Lee, 2008[321]).

Engraftment of HCN2 expressing human mesenchymal stem cells (hMSCs) to primary neonatal rat cardiomyocytes resulted in propagation of I_f in co-culture, and elevated beating rate[322]. *In vivo* proof of concept was also demonstrated, with evidence of electrical coupling between HCN2-hMSCs and host cardiomyocytes when engrafted into the canine left ventricle with complete heart block, with sinus rhythm of 60bpm achieved originating from the injection site[322]. A later, longer term study using the same HCN2-hMSC system demonstrated robust pacemaker activity from transplanted cells up to 6 weeks, with no evidence of apoptosis, inflammation or immune rejection in the absence of immune suppression[323]. Although no asystole was observed when backup pacing was ceased, bradycardic episodes were recorded, indicating a need for optimisation[323]. Similarly, HCN4-MSC autograft also showed promise in a porcine model of heart block[324]. However, some concerns exits when considering use of MSCs, including their propensity to migrate from the site of transplantation[325]. To this end, biomaterial based scaffolds have shown potential in culturing and containing HCN2-hMSCs, without affecting their ability to electrically couple and transduce depolarising current to neighbouring cells[326]. Cardiac progenitor cells (CPCs) isolated from foetal hearts possess favourable characteristics including strong electromechanical integration, minimal migration from the injection site, and absence of proliferation and differentiation outside the cardiac lineage[327]. These cells are being investigated for the delivery of HCN2 and SKM1 for long term biopacemaking applications[328].

Pluripotent stem cells can be differentiated along the cardiomyocyte lineage temporal application of TFs and activation or repression of certain gene programmes[329]. Early in their development along the cardiomyocyte lineage, cells show a pacemaker phenotype, and continuing efforts are underway to enhance differentiation into pacemaker cells. Overexpression of SHOX2 upregulates the pacemaker gene programme and enhances automaticity in early caridomyocytes[330]. Spontaneously beating cells may be isolated from 3D hESC cultures[331]. Injection of these cells into the myocardium of pigs with complete heart block achieved electromechanical integration and robust pacing, evidenced by the formation of connexin 43 positive gap junctions with resting rates of 59 bpm[332]. Retrospective analysis of graft cells revealed some evidence of differentiation, and so it remains to be seen whether transplanted cells maintain a naïve phenotype or form mature cardiomyocytes, at which point automaticity would be lost. Temporal induction of bone morphogenic (BMP) and retinoic acid, and inhibition of fibroblast growth factor (FGF) signalling pathways was found to support the differentiation of $Nkx2.5^-$ SAN like cells from human pluripotent stem cells[333]. These cells were capable of pacing the rat heart when transplanted into the ventricular apex, although pacing ranged from isolated ectopic beats to sustained pacemaker

activity.

iPSC technology has also been applied to biopacemaking. Advantages include a plentiful source of cells (adult somatic cells such as fibroblasts may be used) and negation of the requirement for immune suppression in autologous grafts[334]. Pacemaker activity in engrafted iPSC-CMs persisted up to 3 months, at which time the experiment was terminated due to magnitude of the immune response against the graft[335]. iPSCs were derived from xenograft cells, and thus issues surrounding immune response would be ameliorated using autologous somatic cells to generate iPSCs.

Thus, despite some promising proof of concept studies, it seems that biopacemakers are some distance away from clinical application. One might reason that correcting the underlying dysfunction of the native pacemaker or wider CCS would be advantageous, and circumvent many of the difficulties encountered with the strategies discussed above. Although a wide body of experimental evidence now points towards molecular remodelling of the CCS as an important mechanism in SND[94,108,101,128], AV block[135,142,336] and His-Purkinje dysfunction[114,137,138], there is a paucity of studies that aim to develop systems to harness such promising therapeutic targets. A targeted method for the modulation of CCS gene expression may provide a means for reversal or prevention of CCS functional decline in disease. Via a systemic gene therapy based approach, multiple CCS components could also be targeted simultaneously utilising the broad tropism of viral vectors such as AAV. This may be important in light of the demonstrated interplay between SND and AV block[337].

1.6 Targeting the CCS via gene therapy

Many intensively investigated gene therapy approaches to treat CCS dysfunction are aimed at creating de novo pacemakers via the methods discussed previously, including reprogramming cardiomyocytes to pacemaker myocytes, inducing automaticity in quiescent cells, and engraftment of cells that possess automaticity. In a practical sense, these methods are typically invasive and, most importantly do not address the underlying dysfunction of the physiological pacemaker or conduction tissue. It has also been shown that the unique pacemaker substrate is a vital factor in its function, and recreating this in ectopic sites is challenging[338]. Few current approaches aim to repair the endogenous pacemaker / CCS tissue itself via targeting it's intrinsic remodeling. As discussed previously, remodeling of ion channels and fibrosis within the CCS are both promising therapeutic targets that could be exploited in order to restore function to the failing CCS.

It has been shown that AAV vectors can be used to modulate gene expression in the working myocardium towards ameliorating disease. For example, cardiac overexpression of miR-148a using AAV9 preserved systolic function in a transverse aortic constriction (TAC) mouse model of heart failure[339]. In a similar model, AAV9 mediated cardiac delivery of a miR-25 inhibitor resulted in preservation of cardiac function via increasing SERCA2A, a knowns target of miR-25 and critical regulator of calcium homeostasis implicated in heart failure pathogenesis[340]. AAV9 in combination with the cardiac specific promoter cTnT mediates extremely efficient and cardiac specific transgene expression after systemic intravenous dleivery[205]. Thus far, studies demonstrating successful translation of these principles to the SAN / CCS are limited.

In order to target the atrioventricular node, selective intracoronary perfusion has been employed via catheterization of the AV nodal branch of the right coronary artery in pigs[341]. Using this approach, 45% of AV nodal myocytes were successfully transduced via adenoviral infusion combined with VEGF and nitroglycerin. Transgene expression was also seen in peripheral tissues including liver, kidney and ovaries[341]. The authors also demonstrated successful modification of AVN electrophysiology using this method to overexpress an inhibitory protein to the β-adrenergic signaling pathway[341]. Of note, adenovirus is only capable of conferring short term gene expression, as previously discussed. Adaptation of this method using AAV vectors could lead to long term transgene expression coupled with relatively rapid onset of gene expression.

In HF, elevated heart rate is often associated with poor prognosis, indicating to the widespread use of bradycardic agents such as the I_f blocker, Ivabridine[342,343]. A proof of concept study in pigs showed that downregulation of a B-adrenergic signaling pathway activator resulted in decreased heart rate, conferred via injection of adenovirus directly into the SAN followed by electroporation[344]. Using this gene delivery method, transgene expression was detected in 48% of cells in the SAN region. Transgene delivery was also observed in the right atrium and left ventricle at frequencies of 20% and 5% respectively[344]. This technique is limited by its invasive nature, the possibility of inflammation and tissue damage at the injection site, and the risk of inducing arrhythmia during electroporation, as well as expression in off-target cardiac cells.

Specific and complete transmural gene delivery has been achieved in the atria, using an epicaridal gene painting method. Adenoviral vectors are applied directly to the atrial surface, in combination with a poloxamer gel to increase virus-tissue contact time and mild trypsinisation to enhance vector

penetration[345]. Noteably, without the addition of trypsin, only superficial epicardial transgene expression was achieved due to lack of penetration of the virus into the atrial tissue. Mechanical disruption of atrial tissue by trypsinisation did not significantly affect the physio-mechanical state of the tissue, although a transient decrease in atrial function was observed[345]. This technique is yet to be applied in the context of SAN gene delivery and electrophysiological modification, and so it remains to be seen whether factors such as trypsinisation could negatively affect SAN function. Furthermore, the miniscule size and relatively inaccessible location of the SAN could limit the applicability of the approach, as well as the inherent invasiveness of the procedure.

Thus, there is an unmet need for a minimally invasive, specific, and efficient method for targeted gene delivery to the CCS. Thus far, the closest method to meeting these criteria is selective coronary arterial perfusion as discussed for the AVN above. We aim to target the SAN and CCS via a single systemic injection of AAV9 to address this unmet need. To restrict transgene expression to the CCS, we aim to identify novel CCS tissue specific promoters to drive transgene expression.

1.7 Cardiac conduction system specific promoter candidates

1.7.1 SAN- HCN4

HCN4 is the primary HCN isoform expressed in the SAN, and is highly enriched in this tissue[346]. In the adult mouse SAN, HCN4 was highly abundant at protein level determined by immunohistochemistry and absent in the atria, whilst labelling of HCN1,2 and 3 were absent in the SAN[269,347] (see figure 1.7). In the dog and rabbit, HCN4 constitutes ~80% of all HCN isoforms in the SAN[105,348]. Furthermore, in the rabbit SAN, HCN4 mRNA is highly abundant and scarce in the atrial muscle[349]. The importance of HCN4 in SAN pacemaking is highlighted by the multitude of loss of function mutations in the HCN4 gene that underlie congenital SND (reviewed by Verkerk and wilders, 2015[346]). Furthermore, bradycardia as a result of both athletic training, heart failure and ageing has been attributed to downregulation of HCN4 and I_f[101,105,350]. HCN4 is required for proper function and development of the cardiac conduction system, and is expressed highly in the region of the developing SAN, where the superior vena cava enters the right atrium[351].

As HCN4 is a highly enriched and specific marker of the SAN, as well as being indispensable for SAN function, this promoter will be used to direct transgene expression to the SAN. Kuratomi et al. (2007)[118] characterised the mouse HCN4 promoter and analysed the transcriptional activity of a variety of 5' truncations of the promoter via transfection of promoter-luciferase constructs into

NRCMs in vitro (figure 1.8). The core promoter sequence (~0.8 kb) and a longer ~1.2 kb sequence with slightly lower transcriptional activity are suitable for AAV based studies, owing to their relatively short length.

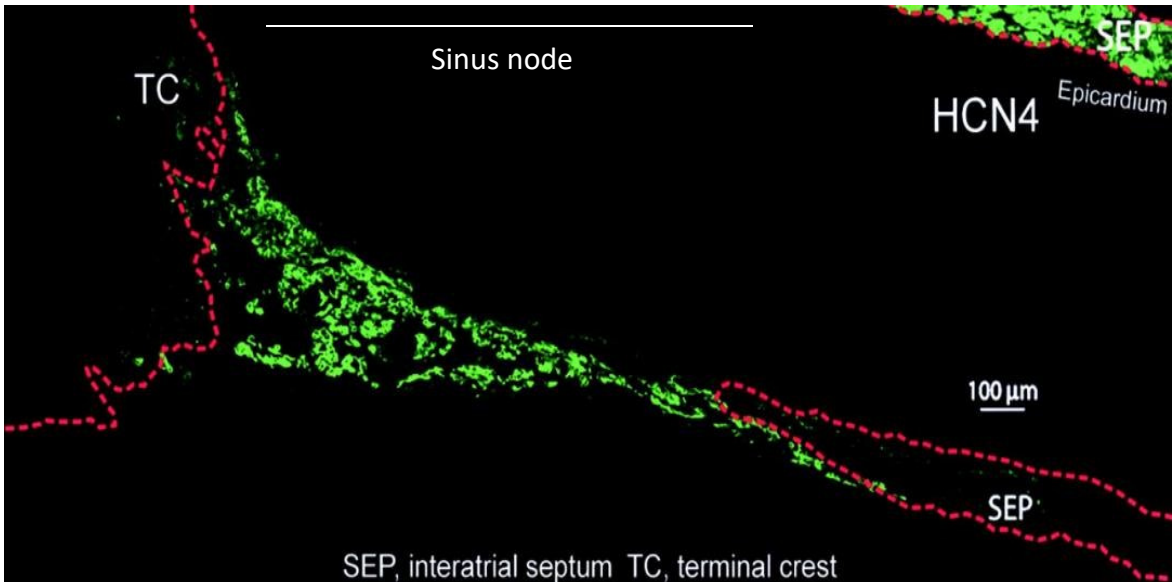

Figure 1.7: HCN4 immunohistochemistry in the SAN, crista terminalis and atrial septum. Strong HCN4 staining (green signal) is seen in the SAN, but is absent from the atrial tissue and crista terminalis. From Dobrzynski et al. (2007)

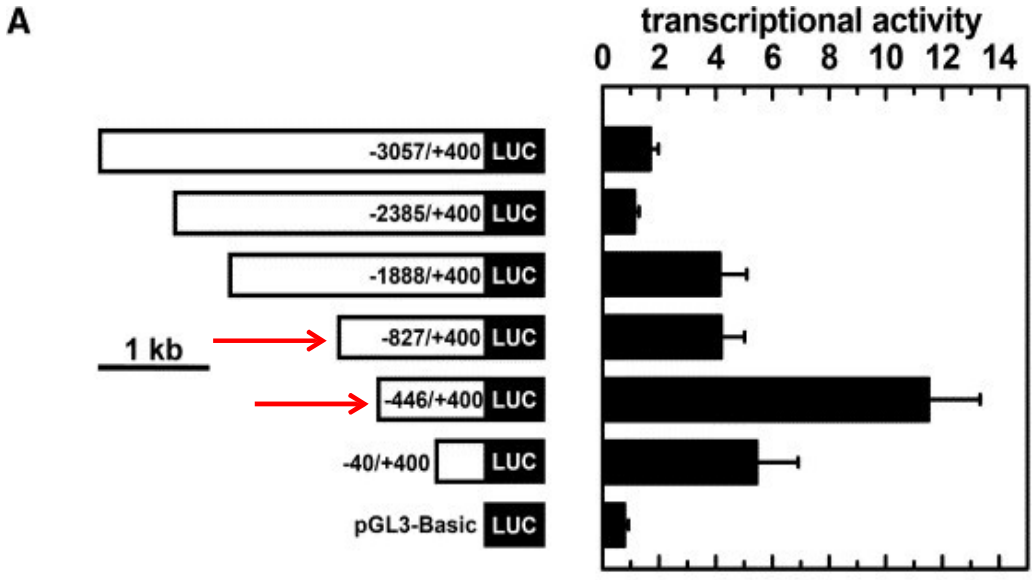

Figure 1.8: transcriptional activity of various mouse HCN4 promoter constructs in NRCMs. The luciferase gene was placed under transcriptional control of each promoter fragment, and the transcriptional activity measured corresponding to luciferase activity. Arrows indicate promoter fragments selected for driving CCS specific expression. From Kuratomi et al. (2007).

1.7.2 CCS- KCNE1

KCNE1 is a beta subunit for the voltage gated potassium channel KCNQ1, and when co-assembled the KCNQ1-KCNE1 complex generates a slow delayed rectifier potassium current $I_{k,s}$ responsible for repolarisation during the cardiac action potential[352]. Loss of function mutations in KCNE1 are associated with long-QT syndrome due a delay in potassium channel mediated repolarisation, leading to torsades de pointes, ventricular fibrillation and sudden cardiac death[353]. A key area for focal activity in triggering torsades de pointes is derived from re-entry in the cardiac Purkinje network[354]. KCNE1 knockout mice suffer from long-QT syndrome and are also deaf, corresponding with clinical links to deafness and sudden cardiac death risk[355]. KCNE1 is also expressed in the inner ear, where dysregulated K+ homeostasis and endolypmh production in knockout animals leads to the death of sensory hair cells[356].

Some studies have shown significant enrichment of the KCNE1 gene in canine Purkinje fibres compared to ventricular tissue, although at protein level, KCNE1 was more strongly expressed in the ventricular myocardium[357]. In the mouse, replacement via homologous recombination of the KCNE1 gene with LacZ, thus driven by the KCNE1 promoter, resulted in LacZ expression in the SAN, AVN and ventricular conduction tissue, whereas expression was absent from the working myocardium[258] (figure 1.9). In the ventricles, the LacZ substrate beta galactosidase co-localised with connexin 40 expression which is exclusively expressed in the ventricular conduction system[258]. To this end, connexin 40-GFP mice have been used successfully to mark and visualise the ventricular conduction system, comprised of the His bundle, bundle branches and Purkinje fibres[358]. However connexin 40 is also expressed robustly in the atria and in the coronary vessels, and connexin 40-GFP mice showed significant reporter gene expression in these regions[359]. Thus, in the mouse, KCNE1 expression appears confined to the CCS and the KCNE1 promoter is capable of driving transgene expression in the CCS specifically.

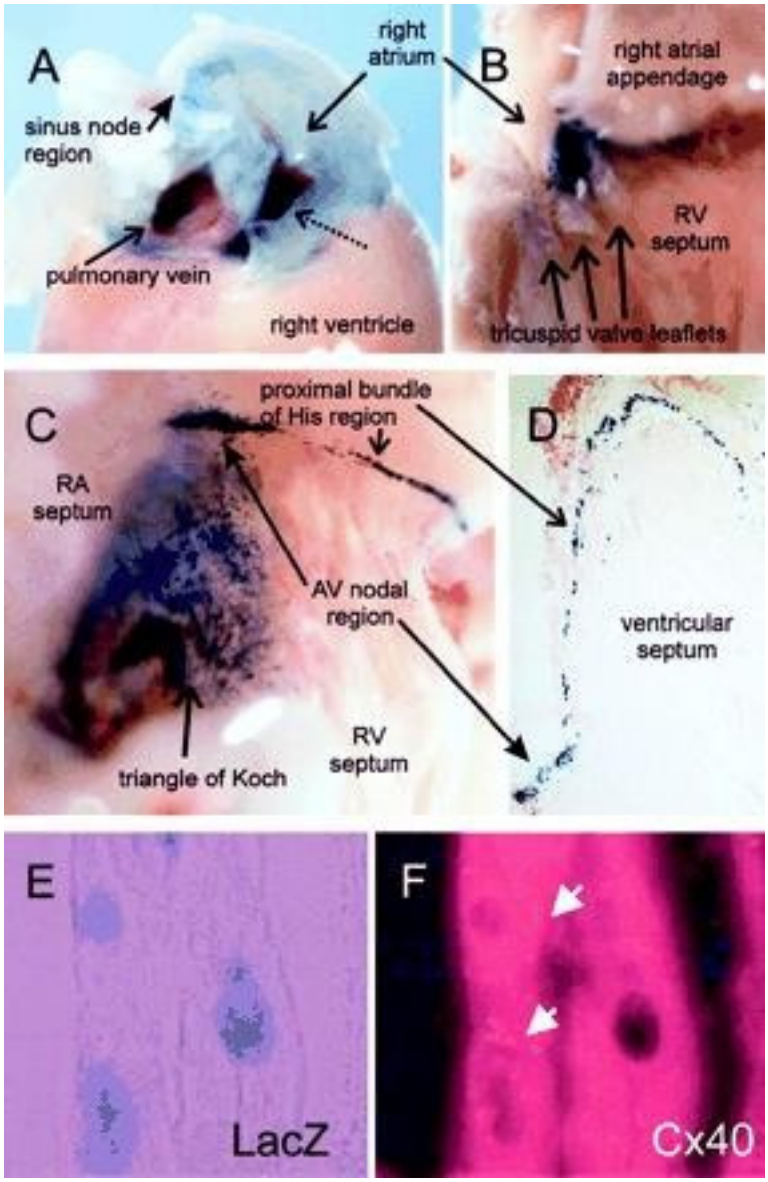

Figure 1.9: expression of beta galactosidase in the heart of KCNE1/lacZ mice. A) Posterior view of the right atrium showing beta galactosidase staining of the SAN. Dashed arrow indicates a region of intense staining on the atrial septum. B) View of the right ventricular septum. As in panel A, intense staining is seen on the right atrial septum, in close proximity to the tricuspid valve. C) Zoomed in view of the area of intense staining shown in panels A and B. The staining is confined to the triangle of Koch and to the region of the AV node and proximal His bundle. D) Microscopic section of the staining shown in panel C. Staining is confined to the CCS tissue comprising the AV node and His bundle. E) Higher-magnification view of panel D showing nuclear β-galactosidase staining in endocardial cells. F) Cx40 immunostaining of the same section as in panel E. Connexin 40 is clearly present at junctions between β-galactosidase expressing cells. No β-galactosidase or Cx40 staining was observed in myocardial cells. (From Kuperschmidt et al. (1999)).

1.8 Summary and conclusions

Dysfunction of the cardiac conduction system is a significant cause of morbidity and mortality not only in congenital contexts such as familial SND, but also in a range of acquired common pathological states including HF, diabetes, ageing, and chronic exercise training. Thus far, engineering a biological pacemaker has proved challenging, likely owing to highly specialized cellular architecture, molecular makeup and substrate of the native SAN, AVN and Purkinje fibres. Animal models of disease have provided key insights into the molecular mechanisms underlying dysfunction of the CCS, with aberrant ion channel expression and subsequent electrical remodeling emerging as a key factor leading to dysfunction. Despite the emergence of these promising therapeutic targets, there is a stark lack of studies addressing how to target the CCS in a tissue specific manner, with the aim of restoring physiological gene expression and thus function to the failing tissues.

AAV9 is a highly cardiotropic, lowly immunogenic vector capable of highly effective gene delivery to the heart. Placing AAV9- delivered transgenes under the control of tissue specific promoters has shown great promise in tissue specific gene expression in the heart (cTnT, ANF promoters) and other organs. While it is clear that AAV9 is effective in delivering genes to the working myocardium, it is not known whether, or indeed to what extent, gene delivery is possible in the minute, structurally and molecularly distinct CCS tissues, particularly from systemic administration of viral vectors. Thus, we aim to address these fundamental questions, and identify tissue specific promoter candidates capable of driving transgene expression in the CCS specifically. This would create a versatile biological tool for the investigation of restorative therapies for CCS dysfunction across various pathological contexts.

1.9 Hypothesis

AAV9 vectors with tissue specific promoters can be used to specifically modulate the expression of key miR/ gene targets implicated in CCS dysfunction.

1.10 Aims

The primary objective is to develop a CCS specific system for *in vivo* gene delivery, targeting the SAN and CCS/ Purkinje fibres. Achieving this goal consists of a number of secondary aims:

i) Select and characterize tissue specific promoter candidates for targeting SAN and wider CCS.

ii) Clone promoters into both adenoviral and adeno-associated viral (AAV) plasmids driving reporter gene (green fluorescent protein, GFP) expression for in vitro validation.

iii) Test promoter activity in vitro in target (Shox2) and off target (NIH 3T3 fibroblasts, HEK 293) cell lines using flow cytometry and fluorescence microscopy, allowing selection of the most promising candidates for in vivo validation in terms of tissue specificity and transcriptional strength.

iv) Package the best performing promoter/ reporter constructs into AAV9 vectors for in vivo testing.

v) Optimise in vivo testing conditions in terms of viral dose, incubation time, tissue processing protocols for transgene detection.

vi) Assess promoter performance in vivo in directing CCS specific transgene expression using fluorescence microscopy based detection of GFP reporter expression, and detection of AAV9 vector genomes in multiple tissues (SAN, AVN, Purkinje fibres, ventricle, atria, liver, lung, skeletal muscle, kidney, brain).

2.0 Chapter 2: General methods

2.1 Boinformatic analysis of promoter constructs

Sequences of interest were input into Ciiider[360] software in FASTA format to interrogate transcription factor binding sites (TFBS) that contribute to promoter regulation. Ciiider implements a MATCH[361] algorithm to predict potential TFBS in regions of interest. Ciiider was used with the position frequency matrix (PFM) in JASPAR[362] format. The mapping of each putative TFBS was carried out with a deficit value of 0.15, which determines the stringency of the scan. The deficit value of 0.15 means the scan will log any TFBS with a MATCH score of 0.85 or greater, of a maximum possible score of 1 indicating a perfect match. The MATCH threshold specified is the same for both core and matrix scores. The core region in the PFMs corresponds to a highly conserved core binding region, typically flanked by areas of higher variability. Candidate sequences are split into overlapping five-base segments, which are compared with the core PFM. If the similarity score meets a defined threshold, the full length of the putative TFBS is computed and the similarity score with the full PFM is calculated.

2.2 Cloning of AAV and adenoviral plasmids

HCN4 and KCNE1 promoters were synthesised by Dundee Biosciences, and cloned into a pBluescript vector backbone. Restriction sites were incorporated for cloning into the desired expression vectors. The 1.2 kb HCN4 promoter fragment was designed to incorporate flanking EcoRI and HindIII sites for convenient cloning into PZac 2.1 and pAAV backbone vectors with compatible restriction sites. PZac 2.1 was obtained from the Vector Core Facility, Medical Genetics Division, Department of Medicine, University of Pennsylvania, Philadelphia, PA, USA. A BglII site was also placed at the 0.8 kb core promoter boundary to enable testing of this fragment in isolation. The KCNE1 promoter was synthesised in a similar method, with the same restriction sites, enabling convenient cloning using the same set of enzymes with compatible destination vectors.

Restriction enzymes used were all from New England Biolabs (NEB) unless otherwise stated. For the 1.2kb HCN4 / GFP construct, the construct (figure 2.1 A) was cloned into the pAAV cTnT luciferase plasmid[363] backbone using EcoRI and NotI restriction sites, excising the cTnT ptomoter and luciferase sequences and replacing with 1.2 kb HCN4 promoter driving GFP. Ligation was carried out using T4 ligase (Promega) at 16^{o}C overnight at ratios of vector:insert ranging from 1:1 to 1:3, according to the following formula:

$$\frac{\text{ng of vector} \times \text{kb size of insert}}{\text{kb size of vector}} \times \text{molar ratio of} \frac{\text{insert}}{\text{vector}} = \text{ng of insert}$$

Cloning of 0.8 HCN4 kb GFP (figure 2.1 A) was carried out using BglII and NotI restriction sites, using the PZac2.1 plasmid backbone (figure in chapter 3, section 3.3.3).

A 1.6 kb truncation of the mouse KCNE1 promoter sequence was cloned into a pbluescript vector, synthesised by DC Biosciences (figure in chapter 3, section 3.3.3). The 1.2 kb HCN4 promoter was excised from pAAV 1.2 kb HCN4 / GFP using EcoRI and HindIII restriction sites, and replaced with the 1.6 kb KCNE1 promoter (figure 2.1 B) using the same restriction sites. The same procedure was used for cloning the 0.8 kb KCNE1 variant into PZac 0.8 kb HCN4 / GFP, using BglII and HindIII sites. After ligation, plasmids were transformed into competent DH5α E. coli (Thermo Fisher Scientific) via heat shock and grown on 100 mg/ml Ampicillin or Kanamycin (pEntr plasmids only) plates overnight at 37^{o}C for negative selection. Plasmid DNA containing bacterial colonies were then grown in LB broth containing ampicillin or kanamycin at 1:1000 dilution overnight at 37^{o}C under agitation. Plasmid DNA was then amplified using the QIAprep Spin Miniprep Kit (Qiagen) as per the manufacturer's instructions, and again digested with the appropriate restriction enzymes to verify the bacterial colony selected for contained the successfully cloned plasmid of interest. Following this, the bacterial culture was amplified using the PureLink HiPure Plasmid Filter Maxiprep Kit (Thermo fisher Scientific) and again restriction digested for verification. Final plasmid stocks were finally confirmed by Sanger sequencing via dideoxynucleotide chain termination method[364]. CMV enhancer constructs were generated as described and depicted in chapter 3, section 3.3.4.

Adenoviral expression vectors were generated using Gateway cloning technology (Thermo Fisher Scientific). HCN4 and KCNE1 promoter constructs driving GFP, as previously generated in AAV plasmids, were first cloned into an entry vector, pEntr11 (Invitrogen) between ATTL1 and ATTL2 sites. Bacteriophage lambda site specific recombination was then carried out between ATTL sites of the entry clone and ATTR sites within the destination vector using LR clonase II (Thermofisher scientific) as per manufacturer's instructions[365]. The pAd/CMV/V5 expression vector was used for creating a positive control plasmid driving GFP from the ubiquitous cytomegalovirus (CMV) promoter, and the pAd/PL/Dest expression vector used to generate plasmids in which the promoter of choice drove GFP expression (HCN4 or KCNE1). All plasmids were propagated using the DH5α E. coli strain (Invitrogen), aside from pAd destination vectors for which One Shot™ ccdB Survival™ 2 T1R Competent Cells (Thermo Fisher Scientific) were used.

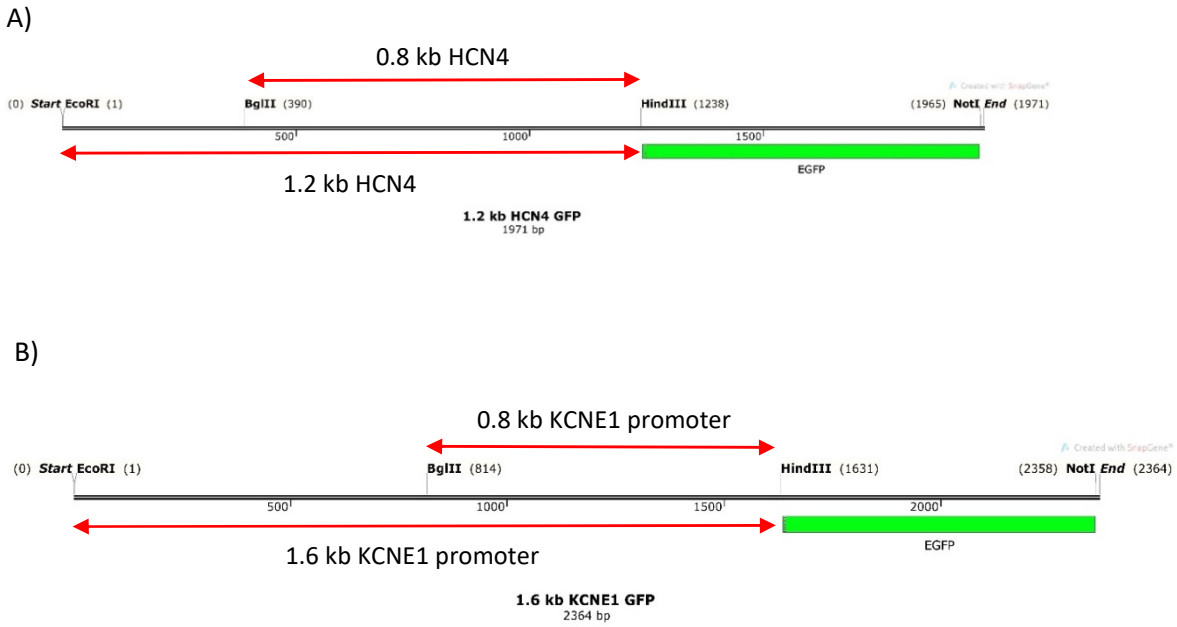

Figure 2.1: (A) HCN4 promoter construct driving GFP and (B) KCNE1 promoter construct with main restriction sites used for cloning (constructs utilized same restriction sites).

2.3 Adenoviral Production and purification

Recombinant adenovirus was generated by infecting 293A cells with the expression plasmids generated. 2 x 10^6 293A cells were seeded into a T25 cell culture plate containing 5 ml complete culture media (10% Dulbecco's modified Eagle's medium (DMEM), 100 µg Penicillin, 100 µg Streptomycin (Life Technologies)) and allowed to attach overnight. 10 µg of each adenoviral expression vector was digested with PACI enzyme (New England Biolabs) overnight. The next day, 1 µl of the restriction digest was run on a 0.8% agarose gel at 100 mV for 40 minutes to confirm the digestion. Cells seeded the previous day were inspected to confirm >90% confluence had been reached. Two sterile 1.5 ml Eppendorf tubes were used to prepare the transfection mixture. In one tube, Optimem was mixed with Lipofectamine 2000 at a 6% dilution, and in the other, PACI digested plasmid DNA was mixed with Optimem at a 2% dilution. Tubes were incubated at room temperature for 15 minutes, mixed together at a 1:1 ratio and incubated for a further 20 minutes at room temperature. Cell culture media was replenished and the transfection mixture applied dropwise to the 293A cells. Cells were inspected periodically to monitor the extent of adenoviral infection. After approximately 2 days, cells were transferred to a T75 flask and left for a further ~10 days until

approximately 80-90% cytopathic effect was seen (figure 2.2). Cells were harvested by pipetting up and down the culture media on the bottom surface of the tissue culture flask. The mixture was centrifuged at 1200 RPM for 5 minutes, the supernatant removed, and the pellet resuspended in 500 µl PBS. This constituted the primary adenoviral stock, which was stored at -80^{o}C. For amplification, 20 µl of the primary viral stock was used to infect each of two confluent T175 flasks containing 293A cells (Thermo Fisher Scientific), and the resultant viral pellet resuspended in 1 ml PBS. For the final tertiary viral prep, the same process was repeated using 6 T175 flasks for each virus to be generated, and the viral pellet resuspended in 3 ml PBS. To purify the virus, it was subjected to 3 freeze thaw cycles (-80^{o}C to 37^{o}C cycles), and 1 volume of chloroform was added and mixed vigorously. The sample was centrifuged at 1000 RPM for 5 minutes and the top layer of supernatant containing the purified virus removed. This was then aliquoted at 500 µl and stored at -80^{o}C. Titration was carried out using the Adenoviral QuickTiter immunoassay (Cell Biolabs) as per manufacturer's instructions.

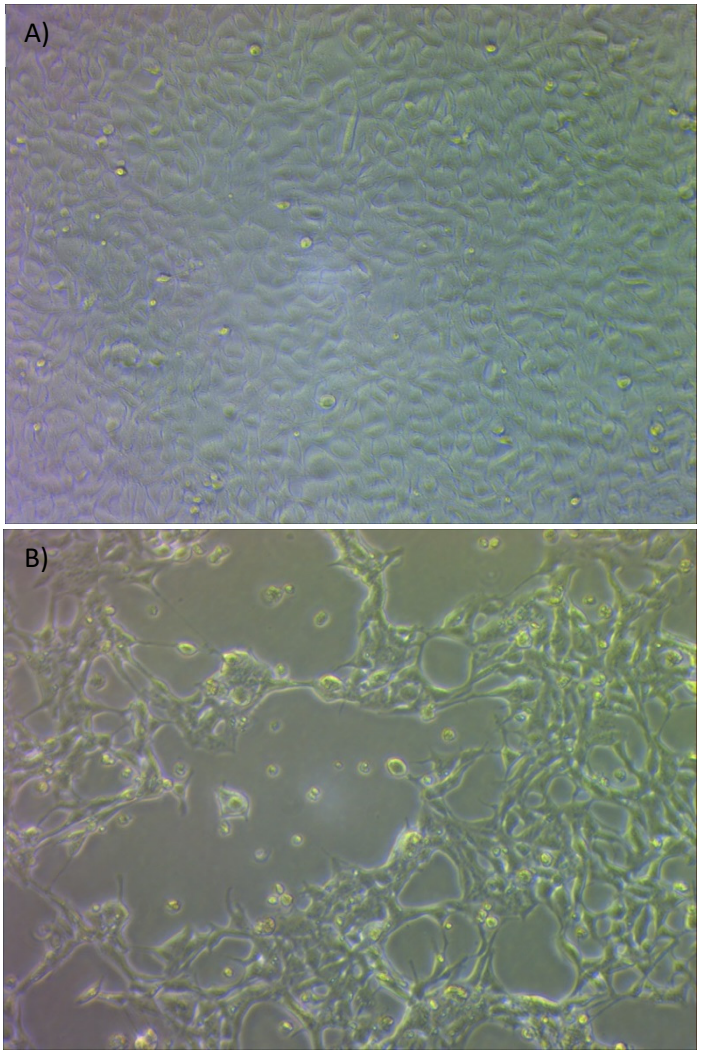

Figure 2.2: Cytopathic effect in adenovirus infected 293A cells. Cells were 90-100% confluent prior to infection (panel A). Approximately 10 days post infection, cells had progressed to advanced infection, characterised by widespread cell death and detachment (panel B)

2.4 Primary neonatal rat cardiomyocyte (NRCM) isolation and culture

Cardiomyocytes were isolated from the hearts of 2-3 day old Sprague-Dawley rats (Charles River Laboratories). Pups were euthanised via cervical dislocation, and the hearts removed via anterior chest incision. Hearts were transferred to ice-cold, sterile artificial digestion solution (ADS)(116 mMNaCl, 20 mM HEPES, 1mM NaH2PO4, 6 mM glucose, 5 mMKCl, 0.8 mM MgSO4, pH 7.4). Inside a class II tissue culture hood, the hearts were cut longitudinally and dissociated in a serial enzymatic digestion in 7 ml ADS supplemented with collagenase A (0.33 U/mL) and pancreatin (100 mg/mL). Dissociation was carried out at 37^{o}C for 10 – 15 cycles of 5 minutes digestion under agitation. Between each cycle, hearts were triturated to assist the digestion mechanically. The resulting

suspension was then passed through a cell strainer and 3 ml Fetal Bovine Serum was added to halt the digestion. The collected cells were centrifuged at 1,200 rpm for 5 minutes, and the resulting pellets resuspended in 40 ml of pre-plating media (67% DMEM, 17% Medium 199, 10% Horse Serum, 5% Fetal Bovine Serum, 1% Penicillin-Streptomycin, 1% Fungizone). The cell suspension was seeded onto uncoated 10 cm tissue culture dishes and incubated at 37°C, 5% CO2 for 1 hour, facilitating the attachment of fibroblasts and thus allowing their separation from cardiomyocytes. The supernatant comprising mostly cardiomyocytes was collected, and the cells were counted. Cardiomyocytes were plated at the appropriate density in plating media (67% DMEM, 17% Medium 199, 10% Horse Serum, 5% Fetal Bovine Serum, 1% Penicillin-Streptomycin, 1% Fungizone, and 1 µM Bromodeoxyuridine (BrdU) and further 23 incubated at 37°C 5% CO2. After 24 hours, the cells were washed several times with PBS, and transferred to maintenance medium (80% DMEM, 20% Medium 199, 10% Fetal Bovine Serum, 1% Penicillin-Streptomycin, 1% Fungizone, and 1% BrdU).

2.5 Cell culture

Mouse embryonic stem derived nodal cardiomyocytes (Shox2 cells, (ATCC)) were maintained in sterile culture media comprised of mouse embryonic stem cell basal medium (ATCC), 15% FBS, 0.05 mM 2-mercaptoethanol (Sigma Aldrich) and 0.1% penicillin / streptomycin. NIH-3T3 fibroblasts (ATCC) and HEK 293A cells (Invitrogen) were maintained in Dulbecco's Modified Eagle's Medium (Gibco) supplemented with 10% FBS and 1% penicillin / streptomycin. All cell cultures were maintained in an environment of 95% air/ 5% CO_2 at 37°C. Cells were subcultured upon reaching 70-80% confluence. Shox2 cells were passed through a 70 um nylon cell strainer prior to re-seeding in order to exclude aggregates.

2.6 DNA transfection *in vitro*

In order to test the efficacy of the promoters in driving GFP expression in different tissues, AAV promoter / reporter plasmids were transfected into Shox2, NIH3T3 and HEK 293A cells. Cells were seeded at a density of 80,000 cells per well in a 24 well plate and left overnight under normal conditions to attach. Prior to transfection, cells were washed with PBS and the culture media replaced with 0.5 ml fresh media. Using lipofectamine 3000 (Thermo Fisher Scienctific), 500 ng of plasmid DNA was transfected per well in 24 well plates, with each plasmid transfected in triplicate per experimental replicate. 1 µl lipofectamine and P3000 reagent was added per well, as per manufacturer's recommendations. Cells were incubated for 48 hours at 37°C, 95% air / 5% CO_2.

For adenoviral testing *in vitro*, NRCMs were washed with PBS. Adenoviral supernatant was then added into each well at a ratio of 1:100 with fresh maintenance culture media, mixed gently by agitation and the plates transferred to an incubator at 37°C, 5% CO_2 for 48 hours. Cells were imaged using an EVOS digital inverted microscope (Life technologies).

2.7 Imaging cytometry

48 hours after transfection, cells were washed with PBS and dislodged from culture plates by adding 0.3 ml TrypLE Express (Thermo Fisher Scientific) per well and incubated at room temperature. An equal volume of complete culture media was added to neutralise the dissociation agent, and the cells transferred into siliconized 1.5 ml centrifuge tubes. Cells were pelleted by centrifuging at 1000 RPM for 5 minutes. Cells were resuspended in 200 µl resuspension solution (PBS / 2% FBS). To identify dead cells, 5 µl TO-PRO-3 stain (Thermo Fisher Scientific) was added to the solution as a cellular viability stain, mixed, and incubated at room temperature for 10 minutes shielded from light. Tubes were placed on ice and transported to the flow cytometry core facility, University of Manchester.

Fluorescence intensity and percentage GFP positive cells were analysed using the ImageStream®X Mk II Imaging Flow Cytometer (Amnis). Laser power settings were consistent between samples for each cell line: 488 channel (GFP) 30 mW (Shox2), 0.5 mW (NIH 3T3 and HEK 293A), and TO-PRO-3 100 mW. Cells were analysed a maximum of 30 minutes after dissociation from culture vessels, and in triplicate for each plasmid transfected. A minimum of 3000 cells per transfection in triplicate, or 9000 cells per construct, were analysed in each experimental replicate. Data analysis was carried out using Image Data Exploration and Analysis software (IDEAS, Amnis). GFP positive threshold was set using untransfected cells from each experimental replicate. GFP positive cells deemed those brighter than 99% of the untransfected cells in the 488 channel. Experiments were carried out in HEK 293A, NIH 3T3 and Shox2 cells. Fluorescence was quantified by calculating the change in fluorescence over negative control using the following formula: (Average intensity of GFP positive cells x percentage GFP positive cells) – background fluorescence[262]. Transfection efficiency was determined for each experimental replicate using the CMV construct, and the percentage GFP positive cells for all other constructs normalised to this value. For example, a 25% transfection efficiency assumed successful transgene delivery to 25% of cells in that given experimental replicate. Dead cells were excluded from analyses via retrospective gating using TO-PRO-3 dye, which is impermeant to live, viable cells.

2.8 AAV9 production

Recombinant AAV9 vectors used in this study were generated by vector core unit at the International Centre for Genetic engineering and Biotechnology (ICGEB), Trieste, Italy (http://www.icgeb.org/avu-core-facility.html) as previously described[366]. Vectors were prepared in HEK293T cells using a calcium phosphate based triple plasmid transfection method for packaging, where plasmids were transfected in a 1:1:1 ratio. Cells were verified free of mycoplasma contamination. Viral stocks were obtained by polyethylene glycol (PEG) precipitation and purified using a double cesium chloride gradient centrifugation. Purified vector stocks were dialyzed in sterile PBS. In order to determine final viral titer, a fraction of each viral stock was subjected to DNAse digestion in order to digest residual DNA, and proteinase K mediated digestion of the viral capsid. Viral titer was measured using real time PCR, measured as viral SV40 Polyadenylation sequence copy number/ ml. Final titers are detailed in table 2.1. Vectors were aliquoted into single use shots and stored at -80C until use.

2.9 *In vivo* administration of AAV9

8 week old male C57BL6/J mice were injected with 1.5 x 10^{12} (AAV9-CMV, 0.8 kb HCN4, 1.2 kb HCN4, cTnT GFP) or 2.5 x 10^{11} (AAV9-1.6 kb KCNE1 GFP) vector genomes of AAV9 suspended in up to 167 µl PBS via the lateral tail vein using a 0.5 ml insulin syringe. Prior to injection, mice were placed in a warming chamber (37^{o}C) for 10 minutes in order to dilate the vein. Mice were maintained for 5 weeks post-injection before sacrifice, corresponding to the expected peak of transgene expression[206]. N.B. vector genome dose for AAV9 1.6 kb KCNE1 GFP was lower due to the low viral titer and restrictions on maximum safe intravenous injection volume[367].

Virus	**Titer (vector genomes / ml)**	**Volume injected**	**Final dose**
AAV9 CMV GFP	1.5 x 10^{13}	100 µl	1.5 x 10^{12} vg
AAV9 1.2 kb HCN4 GFP	1.0 x 10^{13}	150 µl	1.5 x 10^{12} vg
AAV9 0.8 kb HCN4 GFP	9.4 x 10^{12}	159 µl	1.5 x 10^{12} vg
AAV9 1.6 kb KCNE1 GFP	1.5 x 10^{12}	167 µl	2.5 x 10^{11} vg
AAV9 cTnT GFP	9.5 x 10^{12}	157.9 µl	1.5 x 10^{12} vg

Table 2.1: Viral titers for AAV9 generated by ICGEB for use in in vivo studies, final volume injected per mouse for each vector, and final dose equivalent.

2.10 Tissue collection and processing for immunohistochemistry and molecular analysis

After 5 weeks, mice were sacrificed via cervical dislocation (figure 2.3). The heart, liver, lungs, skeletal muscle, kidney and brain were rapidly removed. A portion of each tissue was snap frozen in liquid nitrogen for molecular analysis. For the heart, the ventricular apex and left atrial tissue was frozen for these purposes, and the right quadricep was selected as representative skeletal muscle. The remaining tissues were rinsed in PBS to remove residual blood and debris, and immersed in freshly prepared 4% paraformaldehyde (PFA) solution in PBS, pH 7.4 and incubated at room temperature for 1.5 hours under agitation. Tissues were then rinsed with PBS in order to remove PFA. Tissues were placed into 30% sucrose solution in PBS, pH 7.0, and left overnight at 4°C for cryoprotection. In order to examine the sinoatrial node in detail, it was dissected from the heart and frozen in OCT after overnight cryoprotection of the whole heart. The remaining ventricular tissue was returned promptly to 30% sucrose solution. Tissues were removed from sucrose and passed through a solution comprising of 30% sucrose and OCT at a 1:1 ratio. Finally, the tissues were passed through a bath containing 100% OCT, and rapidly frozen in OCT within plastic tissue moulds using cooled (-80C) isopentane. Samples were transferred to -80°C for long term storage. For sectioning, tissues were first allowed to equilibrate to cryostat internal temperature (-21°C) for 30 minutes. Tissues were sectioned at 10 µm and sections collected onto Superfrost Plus glass slides (VWR). Slides were transferred to -80°C for long term storage.

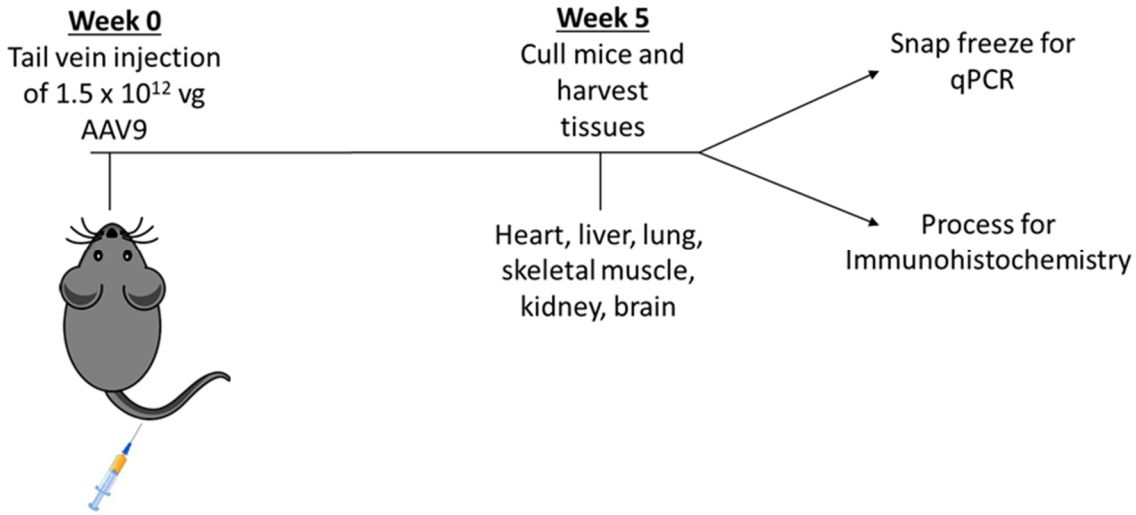

Figure 2.3: Experimental workflow for in vivo studies comprising injection of AAV9 vectors and reporter transgene expression.

2.11 Immunohistochemistry

Select slides were allowed 10 minutes at room temperature to thaw, before being washed in PBS. Sections were then permeablised in 0.5% Triton X-100 in PBS for 10 minutes at room temperature, and washed 2x in PBS. Sections were then blocked in 1% BSA /10% goat serum / 0.1% triton X in PBS for 1 hour at room temperature. Primary antibodies were diluted in blocking buffer, applied to sections, and incubated overnight at 4C protected from light in a humidified chamber. For GFP staining, chicken polyclonal primary antibody was used (Abcam, ab13970), diluted at 1:1000. For HCN4 staining, a rabbit polyclonal primary antibody was used (Alomone labs, APC-052) at 1:50 dilution. The next day, sections were washed in PBS and secondary antibody staining carried out. Alexa Fluor 647 conjugated goat anti chicken (Abcam, ab150171) and Alexa Fluor 555 conjugated goat anti rabbit (Fisher Scientific, A27039) were used to detect GFP and HCN4 bound primary antibodies respectively. Secondary antibodies were diluted 1:200 in blocking buffer, and sections incubated for 1 hour at room temperature. Sections were washed in PBS and incubated with 4',6-diamidino-2-phenylindole (DAPI (Sigma-Aldrich) diluted 1:5000 in PBS. Sections were again washed and subsequently coverslipped with ProLong Gold antifade mountant mounting medium (Thermo Fisher). Images were acquired using a Zeiss Axioimager upright fluorescence microscope running µManager acquisition software[368].

3.0 Chapter 3: Results- Characterisation and generation of promoter constructs.

3.1 Introduction

Having identified suitable promoter candidates via review of the published literature, (HCN4 and KCNE1 for CCS specificity, cTnT for cardiac specificity, and CMV as a positive control/ ubiquitous promoter), I next set out to evaluate mechanisms surrounding the transcriptional regulation of these promoters and generating the tools with which to test their activity in vitro. The CMV and gallus cTnT promoters are already well characterised, and thus the promoter fragments used were the same as in the published literature where their efficacy in vivo is well demonstrated[363,369]. In silico analysis of these promoters was thus not carried out.

The HCN4 promoter has been characterised in vitro, although it's in vivo performance is unclear. I selected previously characterised regulatory regions comprising the 0.8 kb core promoter and longer 1.2 kb truncation[118,370]. As part of this workflow, I also aimed to gain further insights into specific regulatory elements involved in transcriptional regulation of the HCN4 promoter using in silico bioinformatic approaches. Such information may provide a basis for further optimising promoters and identifying motifs important in the regulation of cell type specific activation and/ or repression. Of note, NRCMs express low levels of HCN4 and I_f; I sought to assess the value of promoter candidates in driving transgene expression restricted to SAN tissue, where HCN4 expression is endogenously high. To this end, ventricular HCN4 transcription is highest at E9.5 and gradually declines until birth, after which levels are barely detectable in the mouse[371].

The KCNE1 promoter has been previously characterised in humans, but the murine promoter has not been studied in detail[372,373]. I aligned the human core promoter region[372,373] to the mouse KCNE1 regulatory region and selected a highly conserved region for further analysis. I also aimed to examine TFBS to gain further insight into potential regulatory mechanisms. Identification of regions important for transcriptional and tissue specific KCNE1 expression would also aid in selecting minimal elements that could be capable of inducing tissue specific transcription *in vivo*, a key factor given the length restriction placed on the promoter for AAV use. To this end, it is known that the full length mouse KCNE1 and HCN4 regions produce robust transgene expression in the CCS in vivo[258,259,374].

After selecting appropriate promoters based on literature studies and TFBS expression, I next sought to develop tools to assess key characteristics of promoter performance; transcriptional

strength and tissue specificity. Each promoter of interest was cloned upstream of the GFP reporter gene and the resultant constructs inserted into plasmid vectors. In order to ensure robust transduction of a variety of in vitro cell types, including primary cells where transfection is challenging, constructs were also cloned into adenoviral vectors and adenovirus produced carrying each promoter- reporter construct.

Finally, since tissue specific promoters are often plagued by weak transcriptional activity, and preliminary experiments suggested low activity compared to the CMV promoter, we aimed to enhance transcriptional strength of CCS specific candidates by addition of the strong 380 bp CMV enhancer element. This approach has been successfully used to enhance many promoters, including cardiac specific ANF, MLC, neuron specific PDGF-beta and chicken beta actin[262,266,375,376]. The effect of the CMV enhancer upon both transcriptional strength induction and on tissue specificity appears context and promoter specific[262]. Thus, the intention was to generate strong hybrid enhancer-promoters capable of high-level CCS transgene expression.

3.2 Aims

I. Characterise and select CCS tissue specific promoter candidates (HCN4, KCNE1) using pre-existing literature and bioinformatics assessment of transcriptional regulatory motifs.
II. Generate promoter-reporter constructs for in vitro testing of promoter activity, to include specificity and transcriptional strength.
III. Generate hybrid enhancer- promoters designed for high level CCS tissue specific transgene expression.
IV. Generate adenoviral vectors capable of delivering promoter- reporter constructs effectively to a variety of cells, to include primary cells (neonatal ventricular rat cardiomyocytes).

3.3 Results

3.3.1 Identification and bioinformatic analysis of the HCN4 promoter

I selected the ~0.8 kb HCN4 core promoter region in accordance with previously published work by Kuratomi et al.[118], occupies positions -446 to + 401 relative to the transcription start site (TSS) (illustrated in figure 3.1). The second construct was designed by adding ~0.4 kb fragment upstream of the 0.8 kb core promoter resulting in ~1.2 kb variant extending from positions -827 to + 400 relative to the TSS (figure 3.1). Many transcription factor binding sites (TFBS) were predicted using Ciiider, however only those of specific interest and with previously demonstrated roles in regulation

of the HCN4 promoter are shown. Figure 3.2 shows the distribution of TBFS of interest along the full 1.2 kb and truncated 0.8 kb HCN4 promoter fragments. The 0.8 kb core promoter contains two SP1 binding sites, whilst the full 1.2 kb fragment contains 3 (figure 3.2, table 3.1). SP1 has been shown to play key roles in transactivation of the HCN4 promoter[377]. Other TFs of interest including ISL1[259], TBX3[378], Nkx2.5[379], Hand2[380] and Nkx2.5[379] were predicted to bind to the HCN4 promoter, as shown in figure 3.2. Table 3.1 show matrix and core similarity scores for each putative TF binding site of interest.

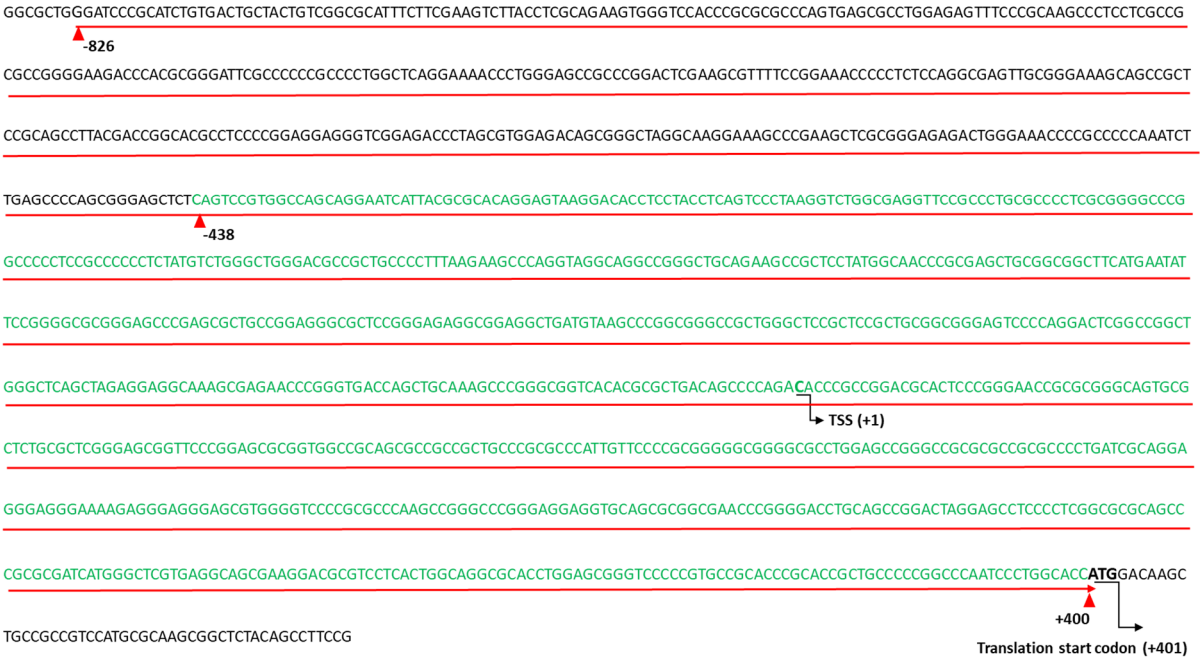

Figure 3.1: Characterisation of the HCN4 promoter. The 0.8 kb promoter variant is highlighted in green, comprising positions -438/ +400 relative to the transcriptional start site (TSS). The longer 1.2 kb variant is underlined by the red arrow, occupying positions -826 / +400 relative to the TSS.

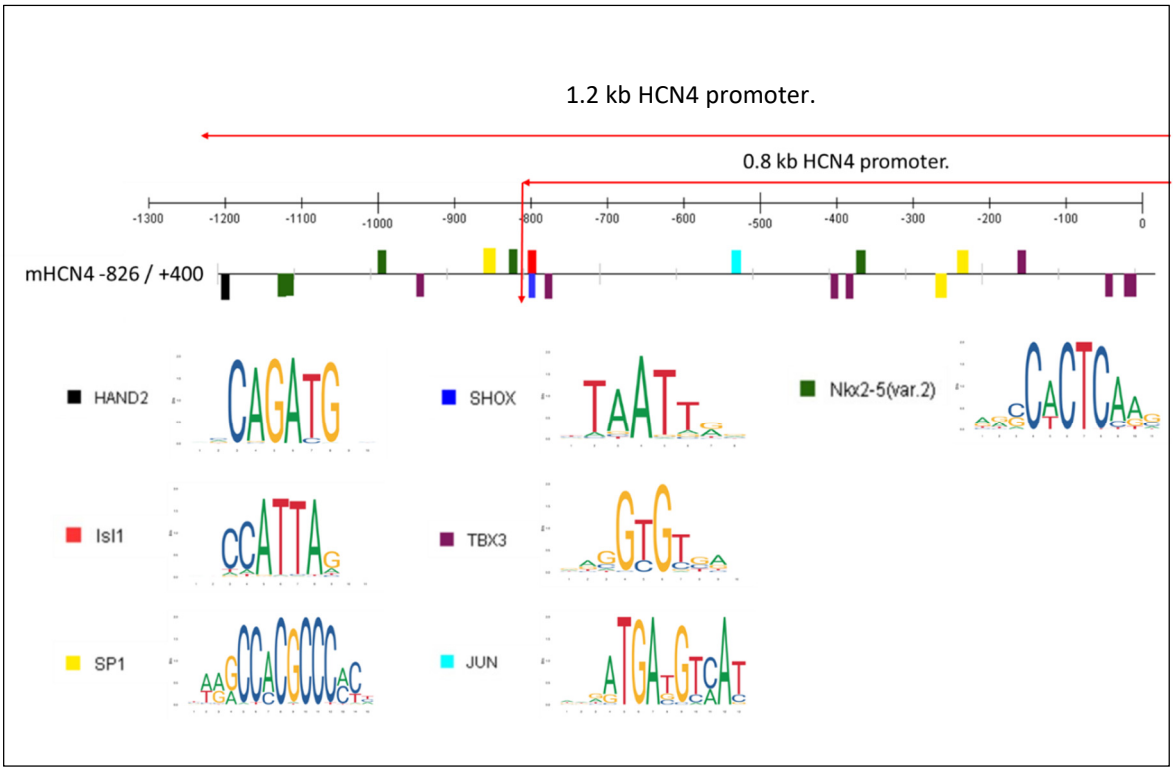

Figure 3.2: In silico prediction of TFBS on the mouse -826/ +400 mHCN4 promoter region. Positions -838 - 0 correspond to the 0.8 kb core promoter. A) Select transcription factors with particular relevance to HCN4 expression in the CCS are shown, with a matrix similarity of >= 85%, assessed using Ciiider. TF sequence logo is presented alongside each TF. Each logo is based upon the position weight matrix (PFM). Individual base heights are in proportion to their frequencies. Logos were obtained from JASPAR.

Transcription Factor Name	Transcription factor ID	Start Position	End Position	Strand	Core Match Score	Matrix Match Score	Sequence
HAND2	MA1638.1	6	15	-1	1	0.998	CACAGATGCG
Isl1	MA1608.1	407	417	1	1	0.869	AATCATTACGC
SP1	MA0079.4	349	363	1	1	0.928	GAAACCCCGCCCCCA
SP1	MA0079.4	968	982	1	1	0.861	CGCGCCGCGCCCCTG
SP1	MA0079.4	940	954	-1	1	0.909	GGCGCCCCGCCCCCG
SHOX	MA0630.1	408	415	-1	0.904	0.899	GTAATGAT
TBX3	MA1566.1	1048	1057	1	0.915	0.872	GAGGTGCAGC
TBX3	MA1566.1	1193	1202	-1	0.915	0.879	GCGGTGCGGG
TBX3	MA1566.1	1187	1196	-1	0.915	0.882	CGGGTGCGGC
TBX3	MA1566.1	1162	1171	-1	0.915	0.886	CAGGTGCGCC
TBX3	MA1566.1	823	832	-1	1	0.942	CGGGTGTCTG
TBX3	MA1566.1	803	812	-1	0.965	0.952	CGCGTGTGAC
TBX3	MA1566.1	429	438	-1	1	0.957	GAGGTGTCCT
TBX3	MA1566.1	261	270	-1	0.883	0.861	GAGGCGTGCC
JUN	MA0488.1	673	685	1	1	0.857	AGGCTGATGTAAG
Nkx2-5(var.2)	MA0503.1	210	220	1	0.943	0.854	CCCCTCTCCAG
Nkx2-5(var.2)	MA0503.1	382	392	1	0.943	0.892	GAGCTCTCAGT
Nkx2-5(var.2)	MA0503.1	837	847	1	1	0.856	ACGCACTCCCG
Nkx2-5(var.2)	MA0503.1	89	99	-1	0.943	0.851	AAACTCTCCAG
Nkx2-5(var.2)	MA0503.1	80	90	-1	0.907	0.855	AGGCGCTCACT

Table 3.1: Ciiider predicted TFBS output, detailing each putative TFBS predicted within the entire 1.2 kb mHCN4 promoter sequence (including 0.8 kb fragment). Binding site co-ordinates, strand location, core and matrix match scores (out of a possible 1), and motif sequence are detailed. Matrix and core scores explained in chapter 2.

3.3.2 Identification and bioinformatic analysis of the mouse KCNE1 promoter

Previously published work identified the human KCNE1 isoforms 1 and 2 core promoter region at position -311 / +16 relative to the TSS and confers high cardiac specificity, although another fragment comprising -1609 / +16 confers the highest absolute cardiac expression in cultured primary ventricular cardiomyocytes[373]. These studies formed the basis for the identification and selection of the mouse KCNE1 promoter fragment. The 5' regulatory region of mKCNE1 was found to share approximately 50% sequence homology with hKCNE1 isoforms 1 and 2. I thus selected a highly conserved region of the mKCNE1 regulatory region comprising regions -1289 / +333 relative to the TSS for further analysis, along with a truncated -479 / +333 region based on human promoter sequence homology and potentially important regulatory motifs identified by in silico bioinformatics studies (figure 3.3).

In silico analysis predicted multiple regulatory motifs of relevance for KCNE1 transcriptional regulation. Tbx20 was predicted to bind to mKCNE1 -1278 / +333, with one site in the shortened -479/ +333 region, and a total of 2 in the full -1278/ +333 region (figure 3.4 A). Cardiac K^+ channel promoters often contain multiple SP1 binding sites[381,373], and SP1 is a validated transactivator of the hKCNE1a promoter[382,383]. I observed one putative SP1 binding site in mKCNE1 lying within the shortened -479/ +33 segment (figure 3.4 A). Other relevant TFBs identified included ETV1[384] for which 3 putative binding sites were identified, notably all lying within the shorter -479/ +333 region (figure 3.4 A). One GATA binding site was also predicted in the putative mKCNE1 core promoter region, whereas notably the human core promoter contains three according to previously published work[373] (figure 3.4 A). I also identified 4 predicted MYOD1 binding sites, 1 of which lies within the -479/ +333 promoter variant (figure 3.4 A). Many Tbx3 binding sites were predicted in the mKCNE1 fragment (n= 31) (figure 3.4 B). Table 3.2 shows matrix and core similarity scores for each putative TFBS of interest. The relevance of these and other TFBS of interest are discussed further in section 3.4.2.

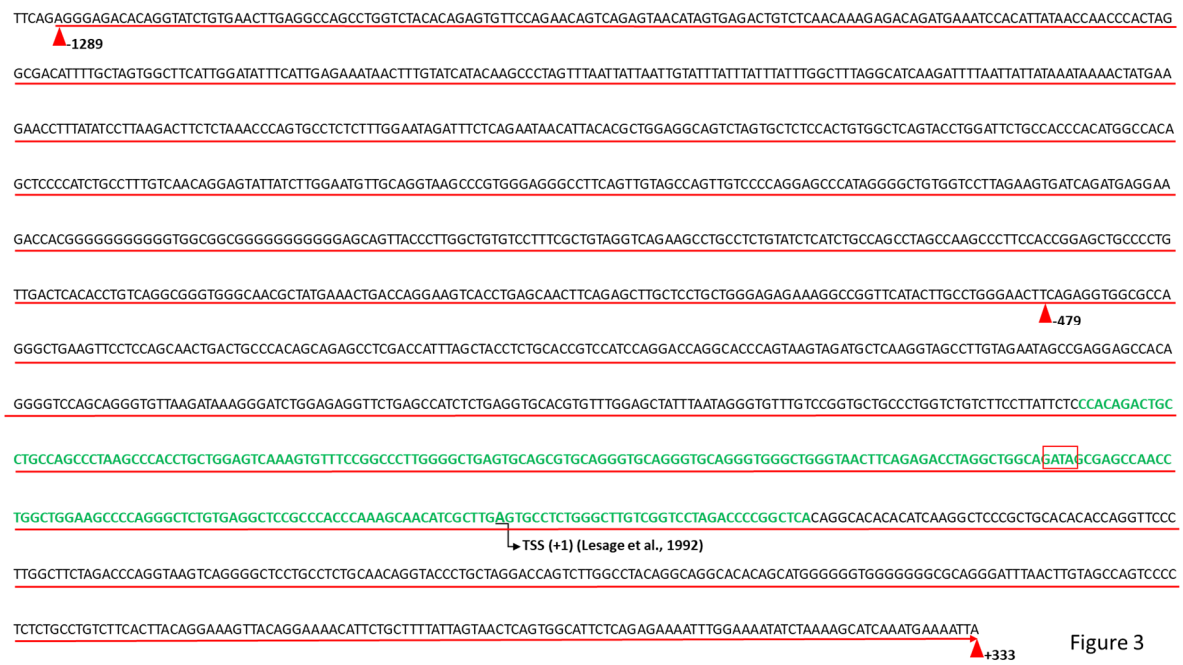

Figure 3.3: Characterisation of the KCNE1 promoter. The chosen 0.8 kb promoter variant occupies positions -479/ +433 relative to the transcriptional start site (TSS). The longer 1.6 kb variant is demarcated by red underline, occupying positions -1289 / +333. Promoter coo-ordinates are indicated by red arrows. Green font denotes the human KCNE1 core promoter region, as described by Lesage et al., (1992).

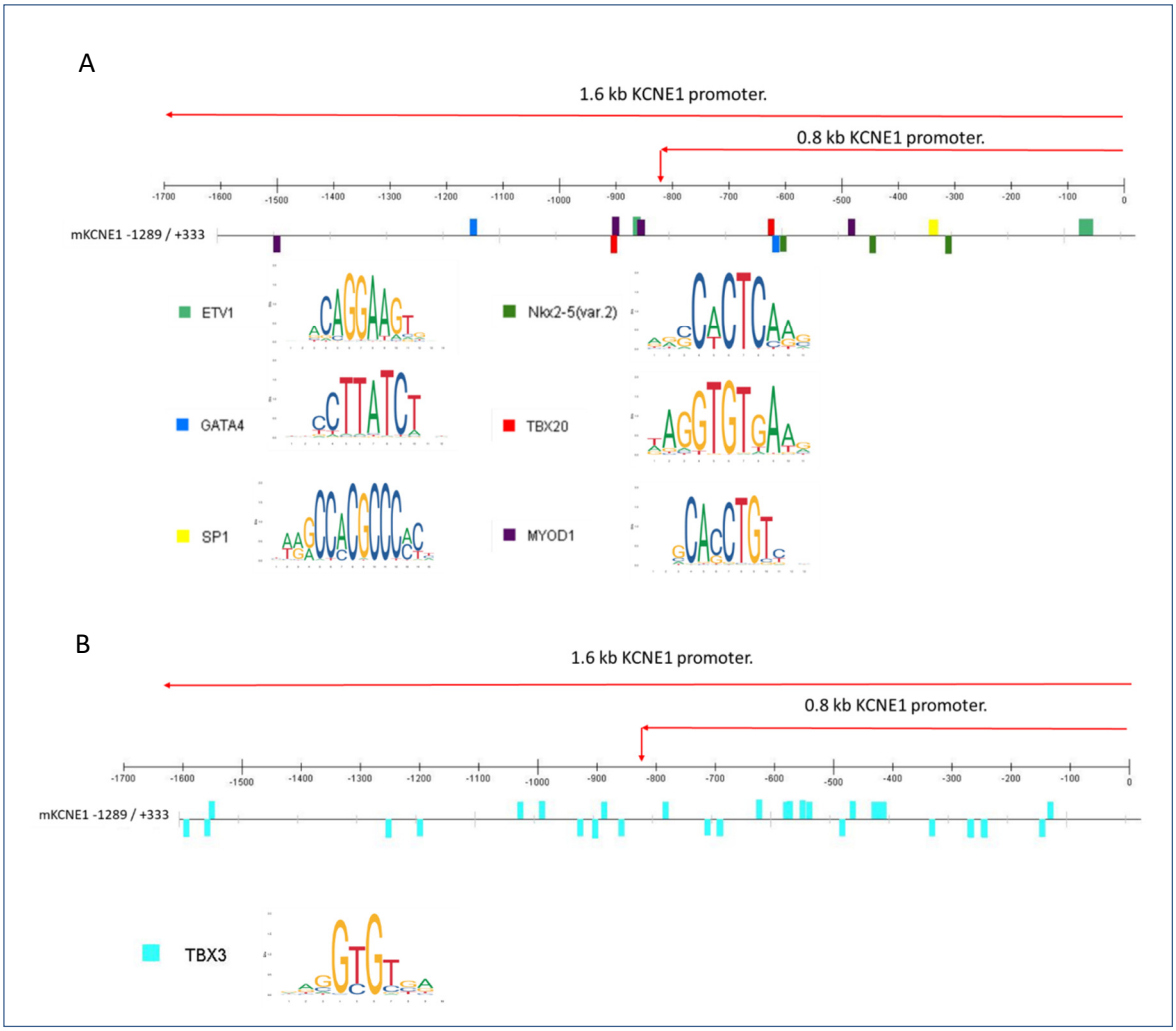

Figure 3.4: bioinformatic analysis of the mouse -1289 / +333 KCNE1 promoter region. Positions 0 / -812 correspond to the 0.8 kb core promoter. A) Select TFs with key relevance to KCNE1 expression in the CCS are shown, with a matrix similarity of >= 85%, assessed using Ciiider. TF sequence logo is presented alongside each TF. Each logo is based upon the position weight matrix (PFM). Individual base heights are in proportion to their frequencies. Logos were obtained from JASPAR. B) Location and distribution of predicted TBX3 binding sites in the KCNE1 promoter.

Transcription Factor Name	Transcription Factor ID	Start Position	End Position	Strand	Core Match Score	Matrix Match Score	Sequence
ETV1	MA0761.2	737	750	1	1	0.971	GACCAGGAAGTCAC
ETV1	MA0761.2	1527	1540	1	1	0.864	TTACAGGAAAGTTA
ETV1	MA0761.2	1538	1551	1	1	0.865	TTACAGGAAAACAT
GATA4	MA0482.2	449	460	1	1	0.875	AGTATTATCTTG
GATA4	MA0482.2	984	995	-1	1	0.905	CCCTTTATCTTA
SP1	MA0079.4	1262	1276	1	1	0.851	GAGGCTCCGCCCACC
Nkx2-5(var.2)	MA0503.1	1290	1300	-1	1	0.992	AGGCACTCAAG
Nkx2-5(var.2)	MA0503.1	1156	1166	-1	1	0.935	CTGCACTCAGC
Nkx2-5(var.2)	MA0503.1	998	1008	-1	0.943	0.874	AACCTCTCCAG
TBX20	MA0689.1	977	987	1	0.91	0.865	AGGGTGTTAAG
TBX20	MA0689.1	698	708	-1	1	0.932	CAGGTGTGAGT
MYOD1	MA0499.2	700	712	1	1	0.974	TCACACCTGTCAG
MYOD1	MA0499.2	745	757	1	1	0.851	AGTCACCTGAGCA
MYOD1	MA0499.2	1118	1130	1	1	0.868	GCCCACCTGCTGG
MYOD1	MA0499.2	100	112	-1	0.907	0.907	TTTCATCTGTCTC
TBX3	MA1566.1	51	60	1	0.956	0.898	AGAGTGTTCC
TBX3	MA1566.1	573	582	1	0.893	0.855	GGGGTGGCGG
TBX3	MA1566.1	609	618	1	0.953	0.895	GCTGTGTCCT
TBX3	MA1566.1	714	723	1	0.893	0.855	CGGGTGGGCA
TBX3	MA1566.1	818	827	1	0.893	0.866	GAGGTGGCGC
TBX3	MA1566.1	977	986	1	1	0.971	AGGGTGTTAA
TBX3	MA1566.1	1022	1031	1	0.915	0.864	GAGGTGCACG
TBX3	MA1566.1	1028	1037	1	0.965	0.918	CACGTGTTTG
TBX3	MA1566.1	1050	1059	1	1	0.94	AGGGTGTTTG
TBX3	MA1566.1	1061	1070	1	0.915	0.86	CCGGTGCTGC
TBX3	MA1566.1	1135	1144	1	0.956	0.911	AAAGTGTTTC
TBX3	MA1566.1	1172	1181	1	0.915	0.858	AGGGTGCAGG
TBX3	MA1566.1	1179	1188	1	0.915	0.858	AGGGTGCAGG
TBX3	MA1566.1	1186	1195	1	0.893	0.856	AGGGTGGGCT
TBX3	MA1566.1	1469	1478	1	0.893	0.866	GGGGTGGGGG
TBX3	MA1566.1	1455	1464	-1	0.953	0.907	GCTGTGTGCC
TBX3	MA1566.1	1358	1367	-1	1	0.95	CTGGTGTGTG
TBX3	MA1566.1	1356	1365	-1	0.953	0.913	GGTGTGTGCA
TBX3	MA1566.1	1335	1344	-1	0.953	0.926	GATGTGTGTG
TBX3	MA1566.1	1333	1342	-1	0.953	0.91	TGTGTGTGCC
TBX3	MA1566.1	1269	1278	-1	0.893	0.855	TGGGTGGGCG
TBX3	MA1566.1	1117	1126	-1	0.893	0.867	CAGGTGGGCT
TBX3	MA1566.1	910	919	-1	0.915	0.864	TGGGTGCCTG
TBX3	MA1566.1	889	898	-1	0.915	0.852	ACGGTGCAGA
TBX3	MA1566.1	744	753	-1	0.892	0.854	CAGGTGACTT
TBX3	MA1566.1	699	708	-1	1	0.996	CAGGTGTGAG
TBX3	MA1566.1	674	683	-1	0.893	0.854	CCGGTGGAAG
TBX3	MA1566.1	403	412	-1	0.893	0.875	TGGGTGGCAG
TBX3	MA1566.1	350	359	-1	0.965	0.928	AGCGTGTAAT
TBX3	MA1566.1	44	53	-1	0.953	0.886	TCTGTGTAGA
TBX3	MA1566.1	8	17	-1	0.953	0.893	CCTGTGTCTC

Table 3.2: Ciiider predicted TFBS output, detailing each putative TFBS predicted within the 1.6 kb KCNE1 promoter (including 0.8 kb fragment). Binding site co-ordinates, strand location, core and matrix match scores (out of a possible 1), and motif sequence are detailed. Matrix and core scores explained in chapter 2, section 2.1

3.3.3 Cloning of promoter-GFP expression constructs

Promoter/ GFP reporter constructs were into an AAV expression construct to enable testing in vitro, and if appropriate, packaging into AAV for in vivo testing. Using EcoRI and NotI restriction sites, the cardiac troponin promoter was excised from the pAAV cTnT luciferase plasmid backbone (figure 3.5 A) and replaced with the 1.2 HCN4 promoter driving GFP flanked by the same restriction sites. Successful cloning was verified by digesting the final pAAV 1.2 HCN4 GFP plasmid with EcoRI and NotI to excise the promoter plus GFP. Expected bands were seen when visualised via DNA gel electrophoresis, at 1.9kb and 3.6kb corresponding to the plasmid backbone (figure 3.5 C). A similar workflow was used in cloning the 0.8 HCN4 promoter driving GFP into the PZac 2.1 backbone using BglII and NotI restriction sites, with expected DNA bands at 1.5kb and 3.5kb (figure 3.6).

From these plasmids, the KCNE1 promoter was then cloned in to drive GFP expression, replacing the HCN4 promoters to generate KCNE1 promoter / reporter constructs. The 1.2 kb HCN4 promoter was excised from pAAV 1.2 kb HCN4 GFP using EcoRI and HindIII restriction sites, and the 1.6 KCNE1 promoter ligated in using the same sites to yield pAAV 1.6 kb KCNE1 GFP. Expected bands at 1.6kb (corresponding to the promoter) and 4.3kb (corresponding to the plasmid backbone) were observed upon restriction digest (figure 3.7). The 0.8 kb HCN4 promoter was excised from PZac 2.1 0.8 kb HCN4 GFP using BglII and HindIII restriction sites, and the truncated 0.8 kb KCNE1 promoter ligated in its place using the same complementary sites. Expected bands were observed after gel electrophoresis of the resultant plasmid DNA after digestion with BglII and HindIII to liberate the promoter from the backbone plus GFP, at 0.8kb and 4.2kb (see figure 3.8). All plasmids were verified by Sanger sequencing.

3.3.4 CMV enhancer cloning

In order to enhance transcriptional strength of tissue specific promoters, the human immediate early CMV enhancer was incorporated upstream of 0.8 kb HCN4, 1.2 kb HCN4, and 0.8 kb KCNE1 promoters. A 380 bp region of the CMV enhancer was synthesised by Aruru Molecular, corresponding to the region previously used to enhance transcription from the neuron specific PDGF-beta promoter[266], and corresponding to the CMV enhancer sequence used in the pAd CMV V5 Dest vector (Life Technologies). The synthesised fragment included a 5' XbaI and 3' EcoRI restriction sites in order to facilitate cloning upstream of the 1.2 kb HCN4 promoter in pAAV 1.2 kb HCN4 GFP, in addition to a 5' NcoI site to facilitate cloning the CMVe 1.2 kb HCN4 GFP fragment into pENTR11 (figure 3.9 A-B). In order to generate CMVe 0.8 kb HCN4 GFP, the 380 bp CMV enhancer sequence plus the first 68 bp of the 0.8 kb HCN4 promoter, up to the Bsu36I site, was synthesised to include 5' BglII and NcoI sites (figure 3.9.1 A-B). This fragment was cloned into PZac

0.8 kb HCN4 GFP upstream of GFP using BglII and Bsu36I sites (figure 3.9.1 C). To generate CMVe 0.8 kb KCNE1 GFP, the 380 bp CMV enhancer sequence plus the first 14 bp of the 0.8 kb KCNE1 promoter up to and including KasI, was synthesised to include 5' BglII and NcoI sites (figure 3.9.2 A-B). This fragment was cloned into PZac 0.8 kb KCNE1 GFP using BglII and KasI sites (figure 3.9.2 C). All plasmids were verified by sanger sequencing.

3.3.5 Cloning of adenoviral plasmids

The 1.2 kb HCN4 GFP construct was cloned using EcoRI and NotI sites, creating pEntr 1.2 kb HCN4 GFP, verified by digestion with the same enzymes (figure 3.9.3). 1.6 kb KCNE1 was also cloned using EcoRI and NotI (figure 3.9.5). For 0.8 kb HCN4 and KCNE1 promoter variants, pEntr11 was cut with BamHI and NotI, as the entry vector did not contain a BglII site. BamHI was used as it generates compatible ends with BglII. Cloning was verified using SalI and NotI, where expected bands were seen after gel electrophoresis (figures 3.9.4 and 3.9.6). A control entry vector, containing only the GFP gene, was generated by excising the 1.2 HCN4 promoter from 1.2 kb HCN4 pEntr using XCMI. The control vector pEntr GFP, was verified by digestion with XMCI and NotI, excising the GFP gene, and expected bands were again viewed via gel electrophoresis (figure 3.9.7). Sanger sequencing of the plasmids again confirmed the correct sequence and directionality of the inserts.

After generation of the entry vectors, these were recombined with pAd destination vectors using bacteriophage lambda site-specific recombination to generate final adenoviral expression constructs. For all expression vectors other than CMV GFP, the pAd PL Destination vector (Life Technologies) was used, which enables incorporation of the promoter of choice (figures 3.9.8 – 3.9.9.2). The pAd CMV V5 plasmid (Life Technologies) was used to generate the positive control expression vector, where the ubiquitous strong CMV enhancer-promoter drives expression of GFP (figure 3.9.9.3). These plasmids were again verified by restriction digest using PACI and subsequently Sanger sequencing.

3.3.6 Adenoviral generation and titration

Recombinant adenovirus was successfully generated via the methods outlined in chapter 2, section 2.3.

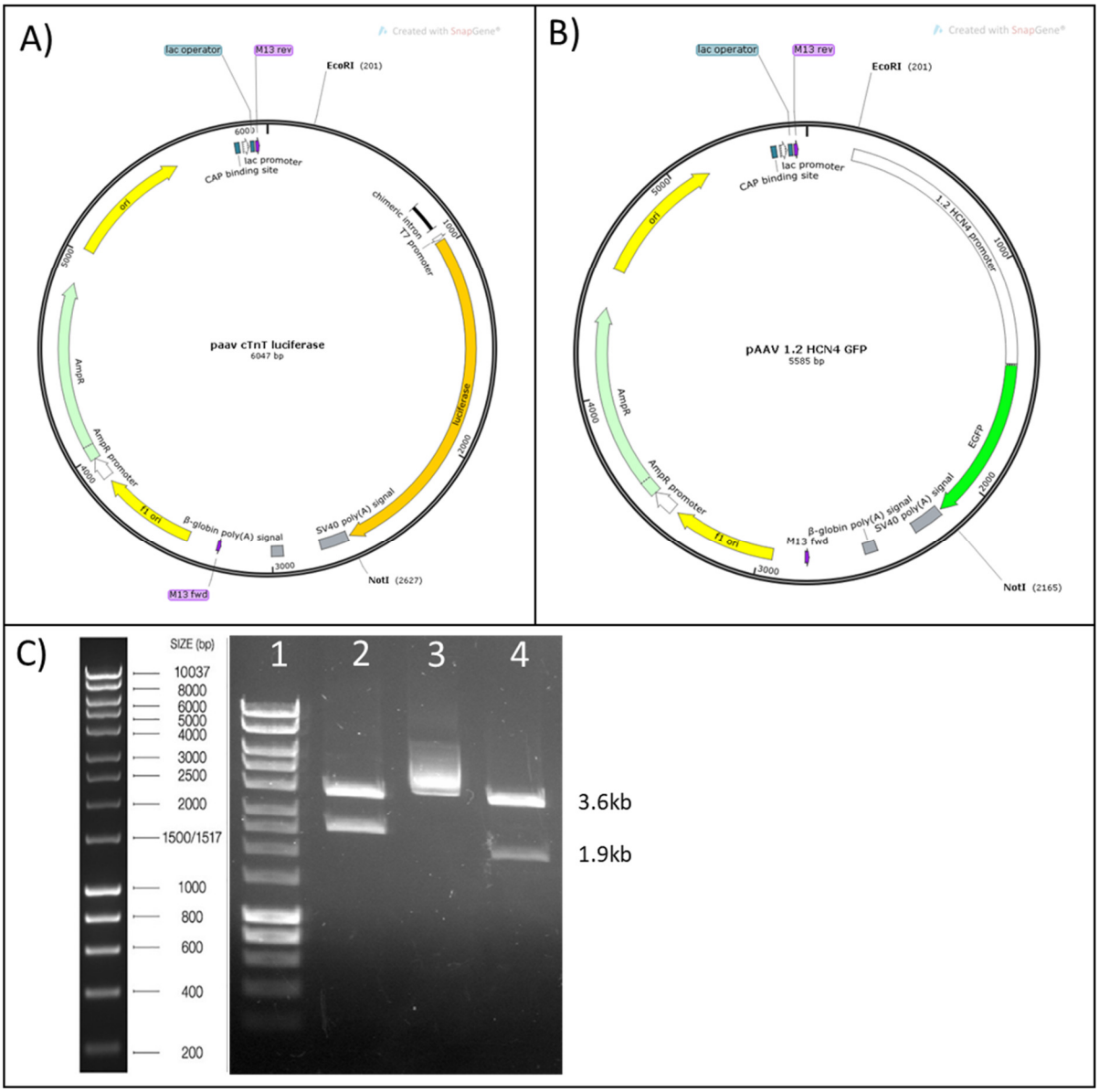

Figure 3.5. pAAV 1.2 HCN GFP plasmid cloning. A) pAAV cTnT luciferase backbone plasmid. B) Cloned pAAV 1.2 HCN4 GFP plasmid. C) Corresponding DNA gel electrophoresis: 1) DNA Ladder. 2) backbone pAAV cTnT luciferase plasmid cut with EcoRI, NotI to excise insert. 3) final pAAV 1.2 HCN GFP plasmid uncut. 4) final pAAV 1.2 HCN4 GFP cut with EcoRI, NotI for verification of successful cloning.

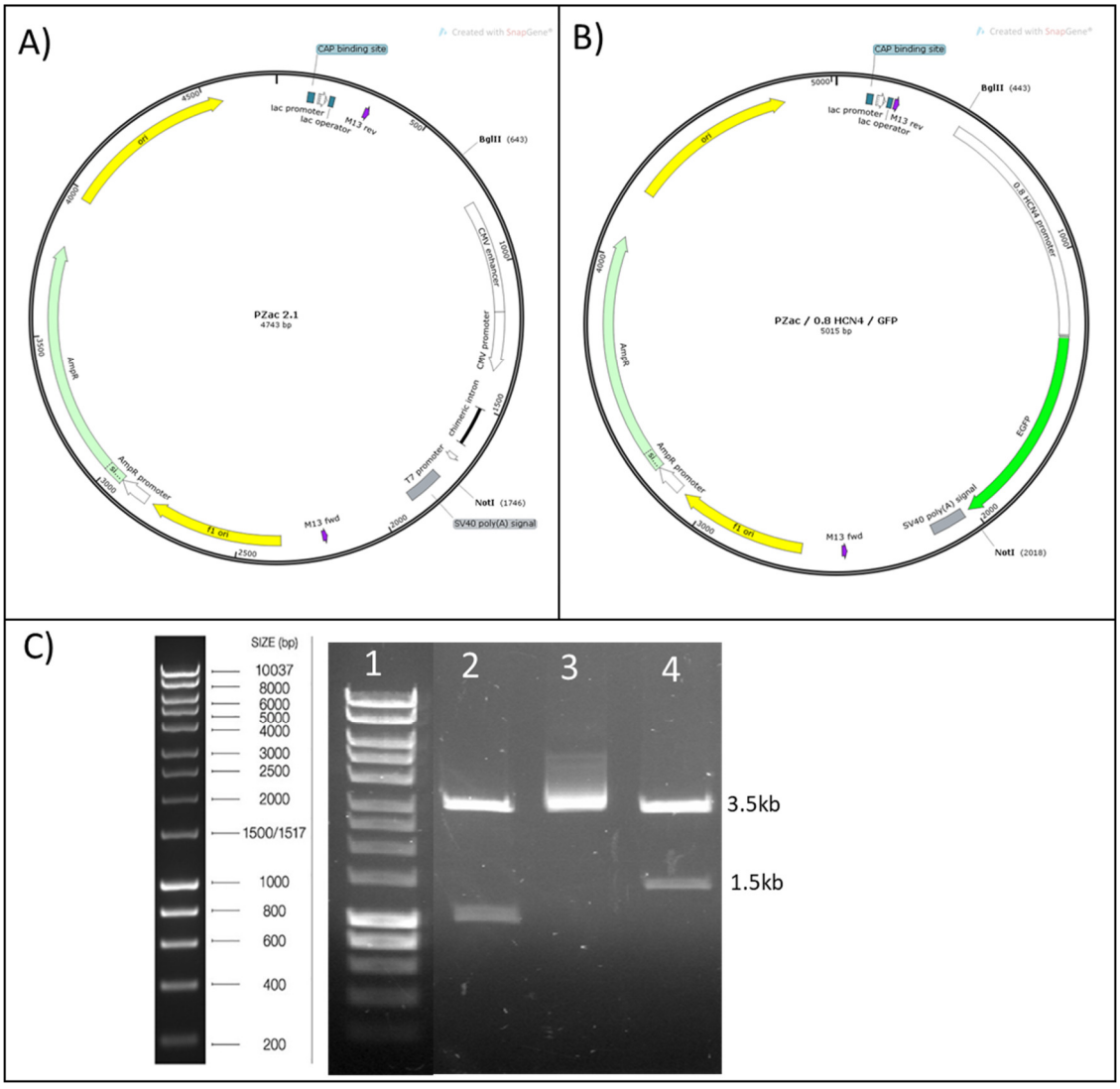

Figure 3.6. pZac 2.1 0.8 HCN4 GFP plasmid cloning. A) PZac 2.1 backbone plasmid. B) Cloned pZac 2.1 0.8 HCN4 GFP plasmid. C) Corresponding DNA gel electrophoresis: 1) DNA Ladder. 2) backbone PZac 2.1 plasmid cut with BglII, NotI to excise insert. 3) final pZac 2.1 0.8 HCN4 GFP plasmid uncut. 4) final pZac 2.1 0.8 HCN4 GFP cut with BglII, NotI for verification of successful cloning.

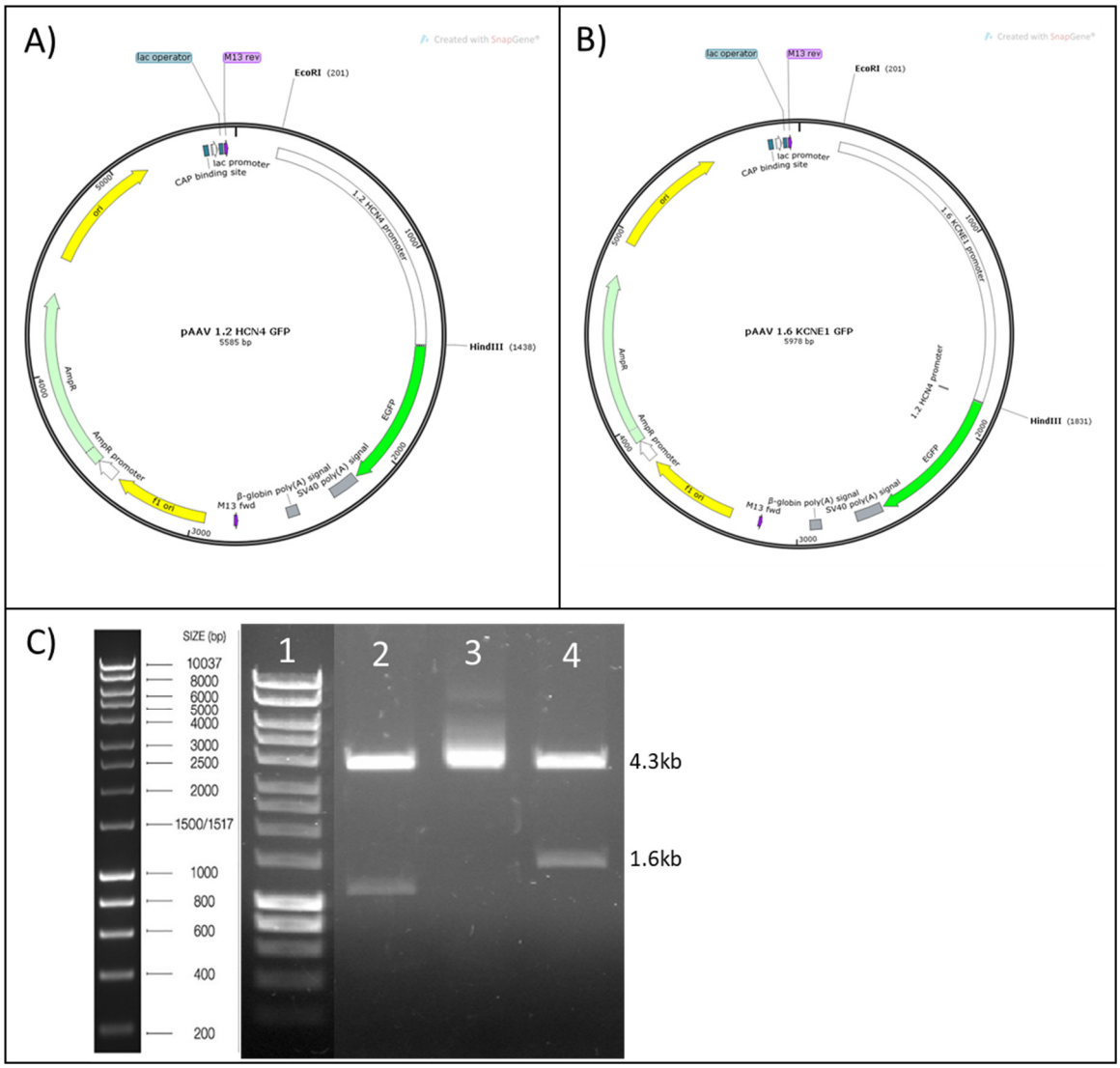

Figure 3.7. pAAV 1.6 KCNE1 GFP plasmid cloning. A) pAAV 1.2 HCN4 GFP backbone plasmid. B) Cloned pAAV 1.6 KCNE1 GFP plasmid. C) Corresponding DNA gel electrophoresis: 1) DNA Ladder. 2) backbone pAAV 1.2 HCN4 GFP plasmid cut with EcoRI, HindIII to 1.2 HCN4 promoter. 3) final pAAV 1.6 KCNE1 GFP plasmid uncut. 4) final pAAV 1.6 KCNE1 GFP cut with EcoRI, HindIII for verification of successful cloning.

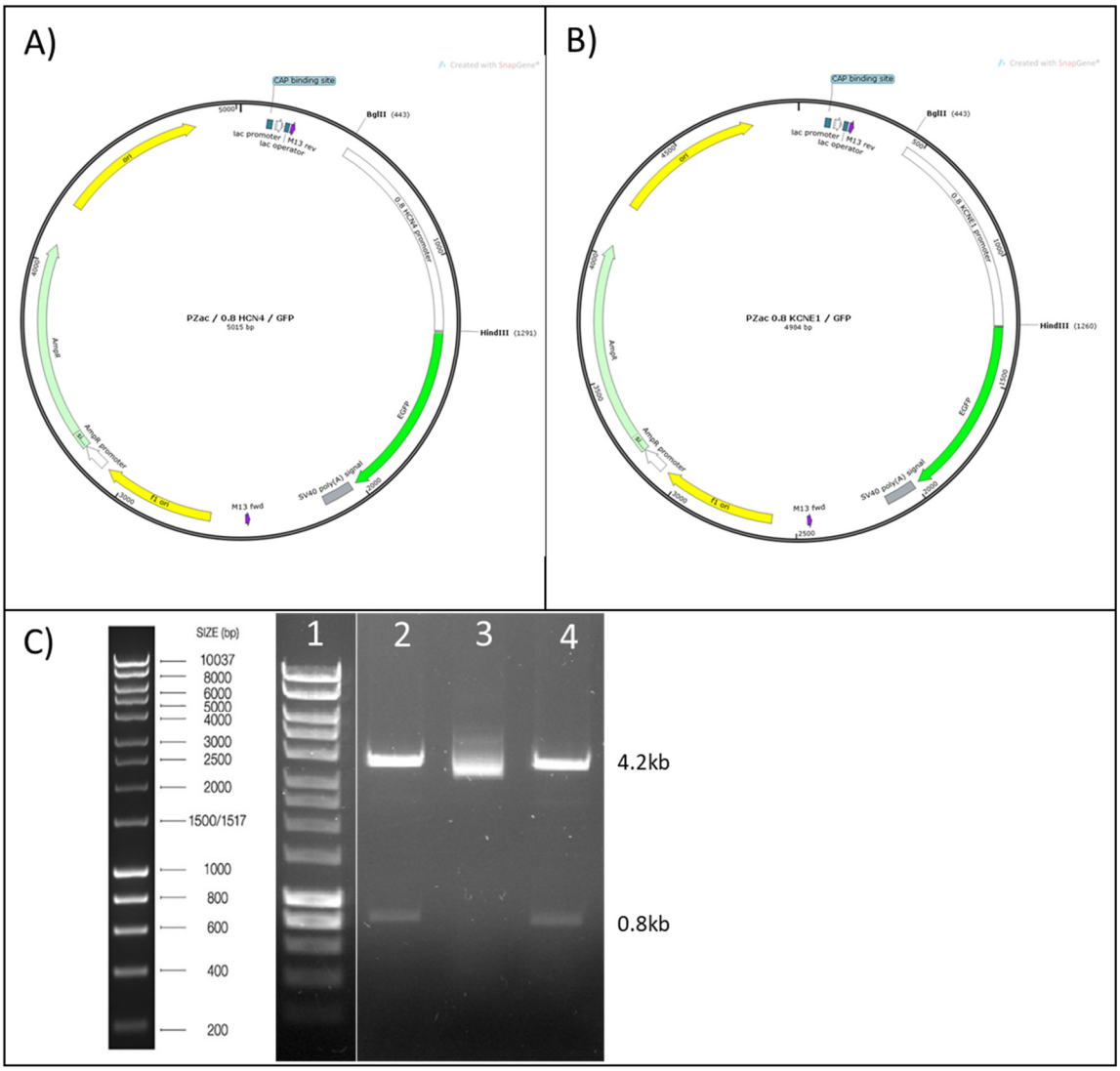

Figure 3.8. PZac 2.1 0.8 KCNE1 GFP plasmid cloning. A) PZac 2.1 0.8 HCN4 GFP backbone plasmid. B) Cloned pZac 2.1 0.8 KCNE1 GFP plasmid. C) Corresponding DNA gel electrophoresis: 1) DNA Ladder. 2) backbone PZac 2.1 0.8 HCN4 GFP plasmid cut with BglII, HindIII to excise insert. 3) Final pZac 2.1 0.8 HCN4 GFP plasmid uncut. 4) Final pZac 2.1 0.8 KCNE1 GFP cut with BglII, HindIII for verification of successful cloning.

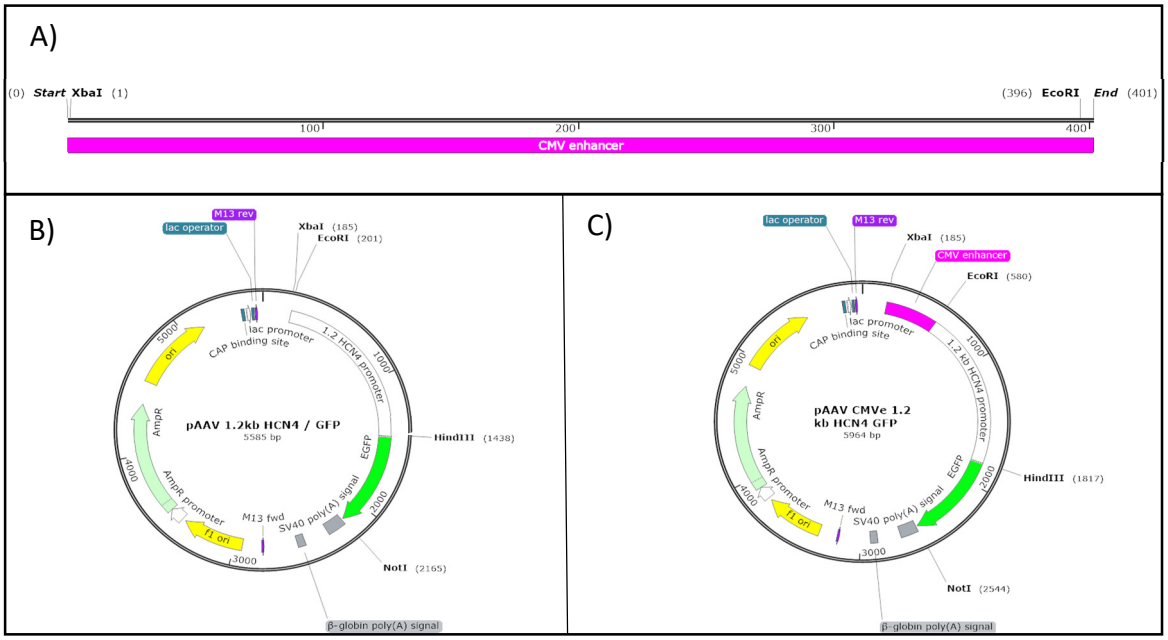

Figure 3.9. pAAV CMVe 1.2 kb HCN4 GFP cloning. A) CMVe construct deigned for cloning upstream of 1.2 kb HCN4 promoter in pAAV 1.2 kb HCN4 GFP plasmid, flanked by XbaI and EcoRI restriction sites. B) pAAV 1.2 kb HCN4 GFP backbone plasmid, showing upstream XbaI and EcoRI sites used for insertion of CMVe. C) Final cloned pAAV CMVe 1.2 kb HCN4 GFP, completed using XbaI and EcoRI sites for insertion of CMVe upstream of 1.2 kb HCN4 promoter.

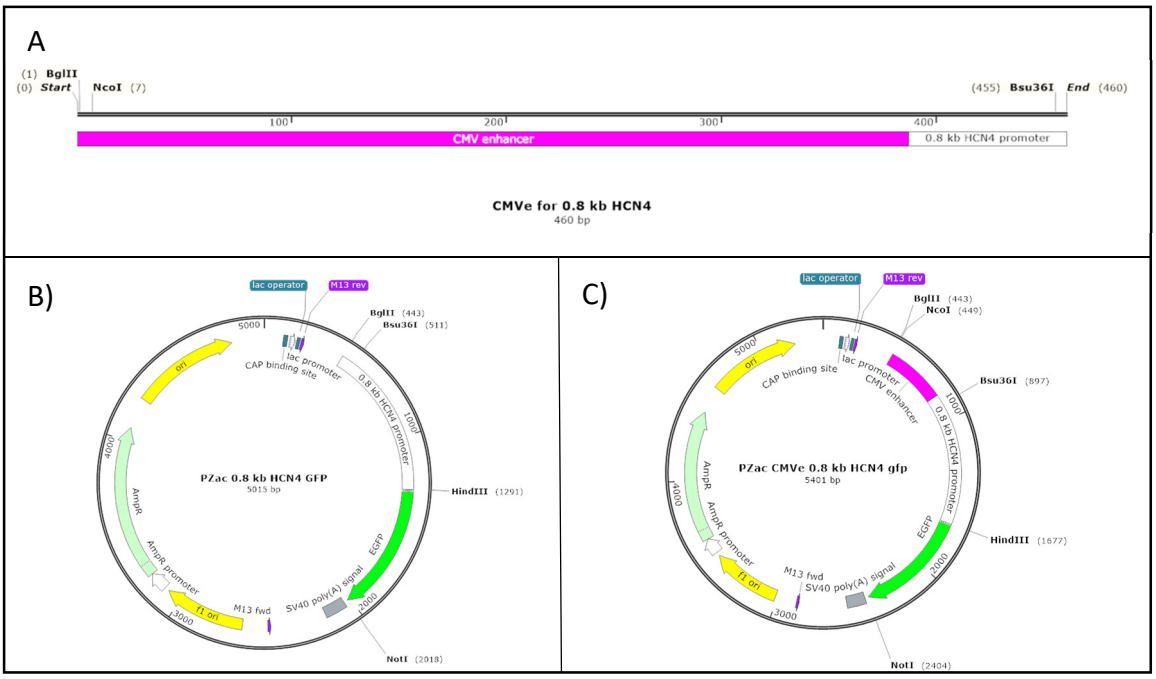

Figure 3.9.1 pZac CMVe 0.8 kb HCN4 GFP cloning. A) CMVe construct designed for cloning upstream of 0.8 kb HCN4 promoter in PZac 0.8 kb HCN4 GFP plasmid. The CMVe sequence was synthesised with an upstream flanking BglII site for cloning upstream of the 0.8 kb HCN4 promoter. A portion of the 0.8 kb HCN4 promoter, up to and including the Bsu361 site, was synthesised immediately downstream of the CMVe sequence to allow insertion of the construct and reconstitution of the full 0.8 kb HCN4 sequence after cutting with Bsu36I. B) PZac 0.8 kb HCN4 GFP backbone plasmid, showing the positions of BglII and Bsu36I restriction sites for insertion of the CMV enhancer. C) Final cloned PZac CMVe 0.8 kb HCN4 GFP plasmid. The CMV enhancer is present directly upstream of the 0.8 kb HCN4 promoter driving GFP.

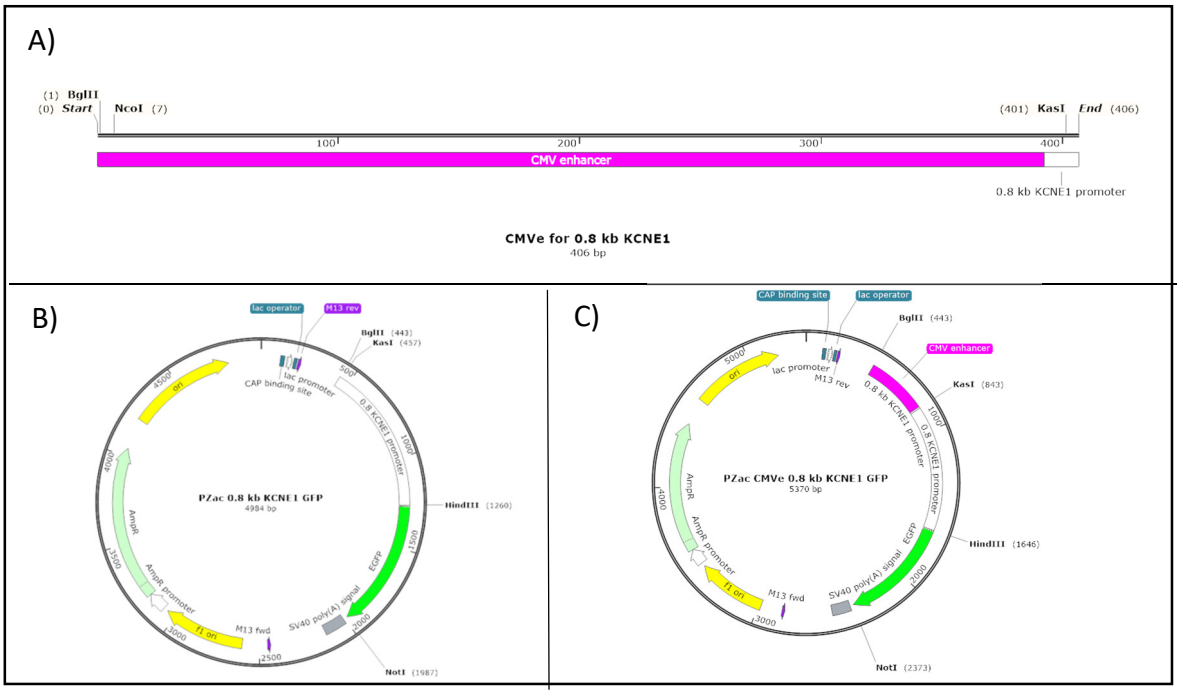

Figure 3.9.2 pZac CMVe 0.8 kb KCNE1 GFP cloning. A) CMVe construct designed for cloning upstream of 0.8 kb KCNE1 promoter in PZac 0.8 kb KCNE1 GFP plasmid. The CMVe sequence was synthesized with upstream flanking BglII and KasI restriction sites for cloning upstream of the 0.8 kb KCNE1 promoter. B) PZac 0.8 kb HCN4 GFP backbone plasmid, showing the positions of BglII and KasI restriction sites for upstream insertion of the CMV enhancer. C) Final cloned PZac CMVe 0.8 kb KCNE1 GFP plasmid. The CMV enhancer is present directly upstream of the 0.8 kb KCNE1 promoter driving GFP.

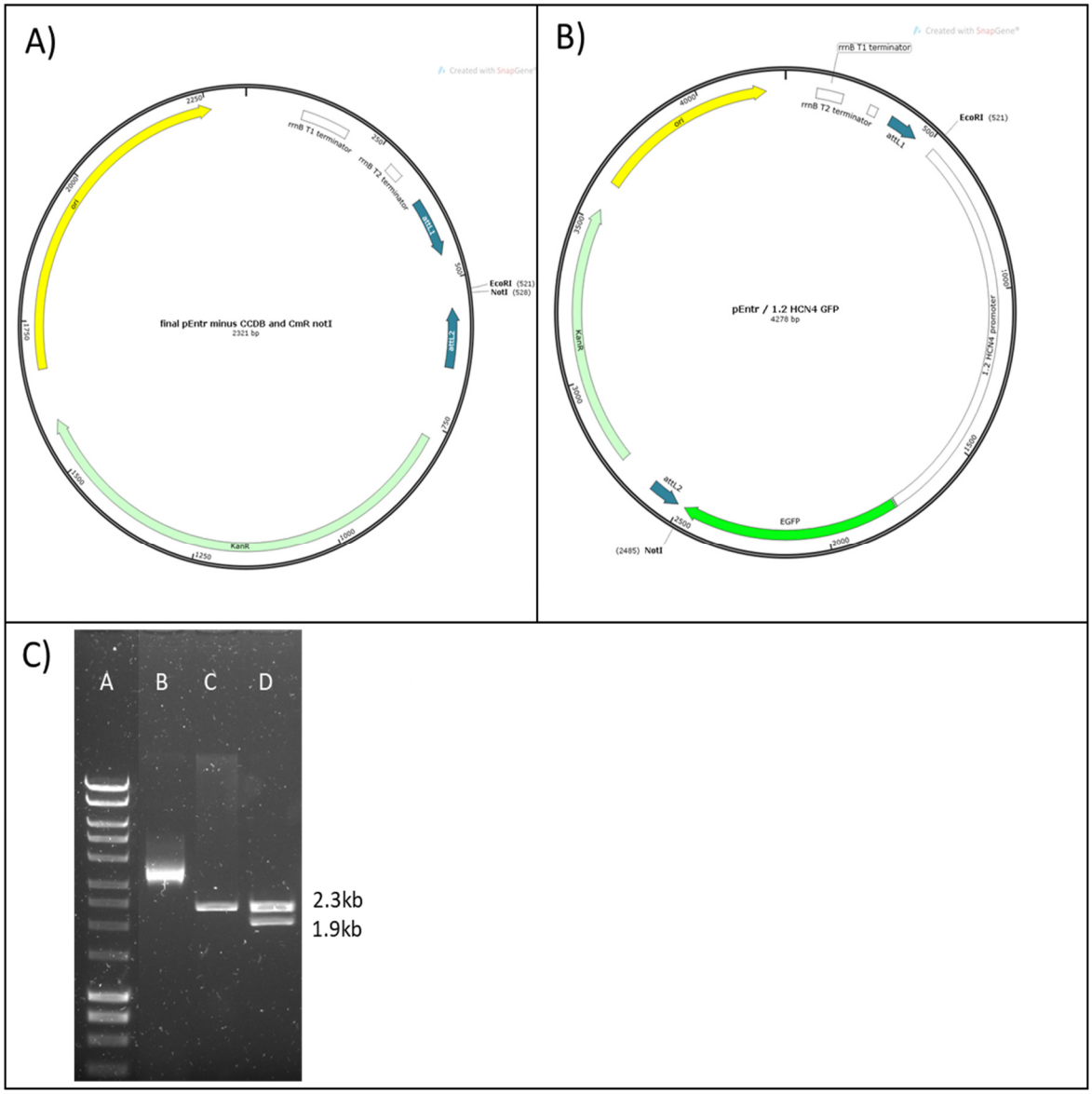

Figure 3.9.3. pEntr 1.2 HCN4 GFP plasmid cloning. A) pEntr11 backbone plasmid. B) Cloned pEntr 1.2 HCN4 GFP plasmid. C) Corresponding DNA gel electrophoresis: 1) DNA Ladder. 2) Final pEntr 1.2 HCN4 GFP plasmid uncut. 3) backbone pEntr11 plasmid cut with EcoRI, NotI. 4) Final pEntr 1.2 HCN4 GFP cut with EcoRI, NotI for verification of successful cloning.

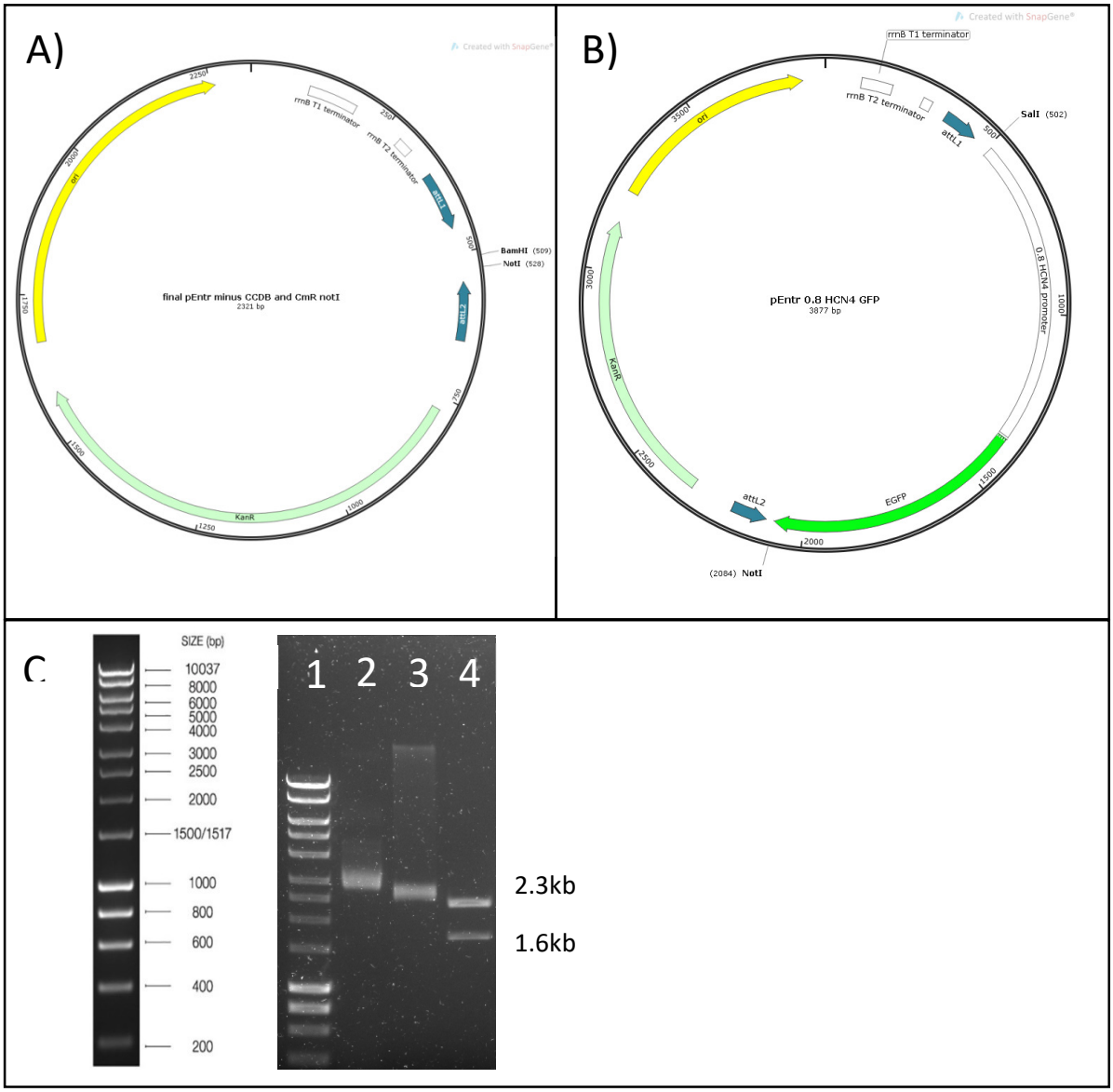

Figure 3.9.4. pEntr 0.8 HCN4 GFP plasmid cloning. A) pEntr11 backbone plasmid. B) Cloned pEntr 0.8 HCN4 GFP plasmid. C) Corresponding DNA gel electrophoresis: 1) DNA Ladder. 2) backbone pEntr11 plasmid cut with BamHI, NotI. 3) Final pEntr 0.8 HCN4 GFP plasmid uncut. 4) Final pEntr 0.8 HCN4 GFP cut with SalI, NotI for verification of successful cloning.

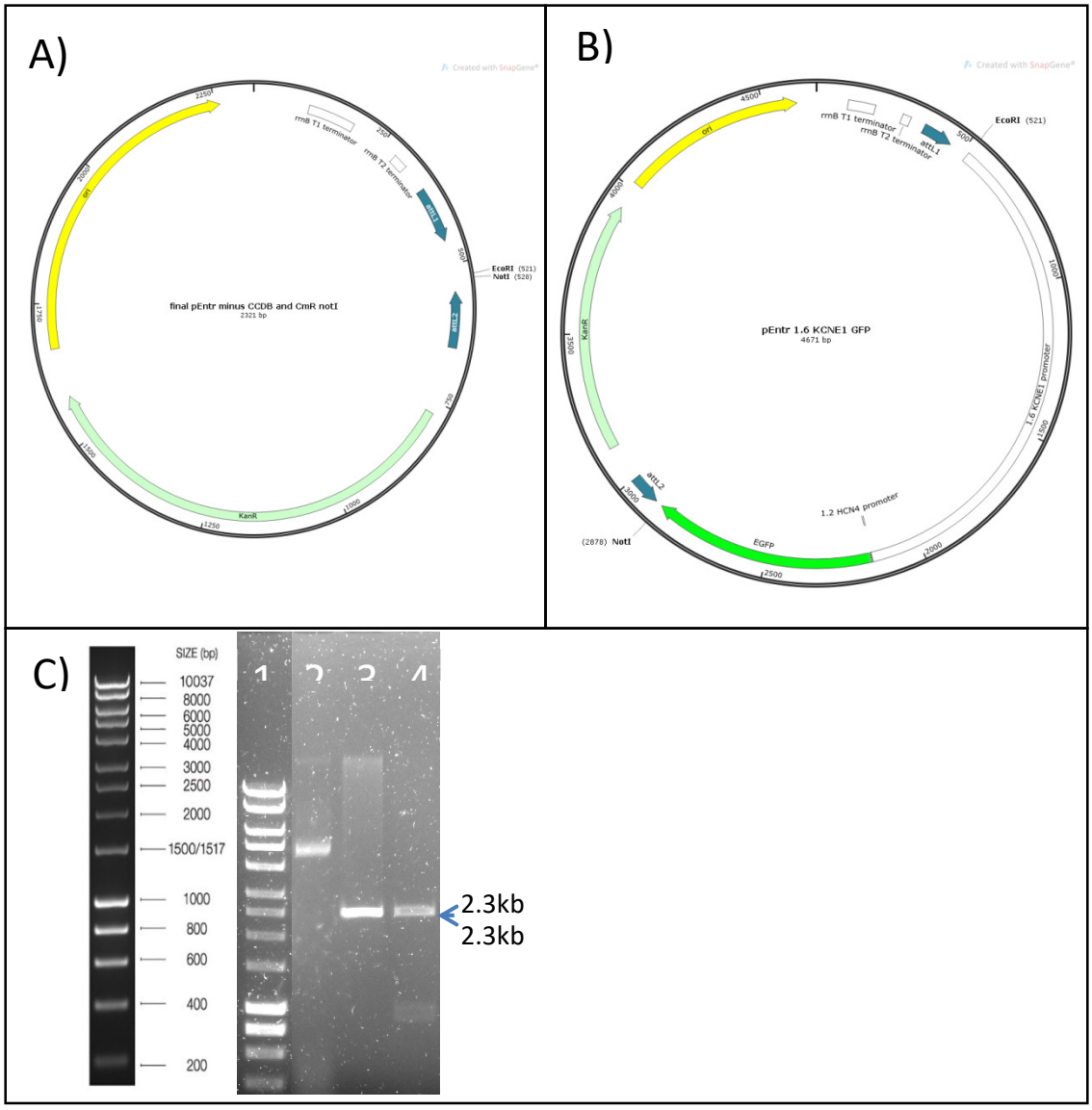

Figure 3.9.5. pEntr 1.6 KCNE1 GFP plasmid cloning. A) pEntr11 backbone plasmid. B) Cloned pEntr 1.6 KCNE1 GFP plasmid. C) Corresponding DNA gel electrophoresis: 1) DNA Ladder. 2) Final pEntr 1.6 KCNE1 GFP plasmid uncut. 3) backbone pEntr11 plasmid cut with EcoRI, NotI. 4) Final pEntr 1.6 KCNE1 GFP cut with EcoRI, NotI for verification of successful cloning.

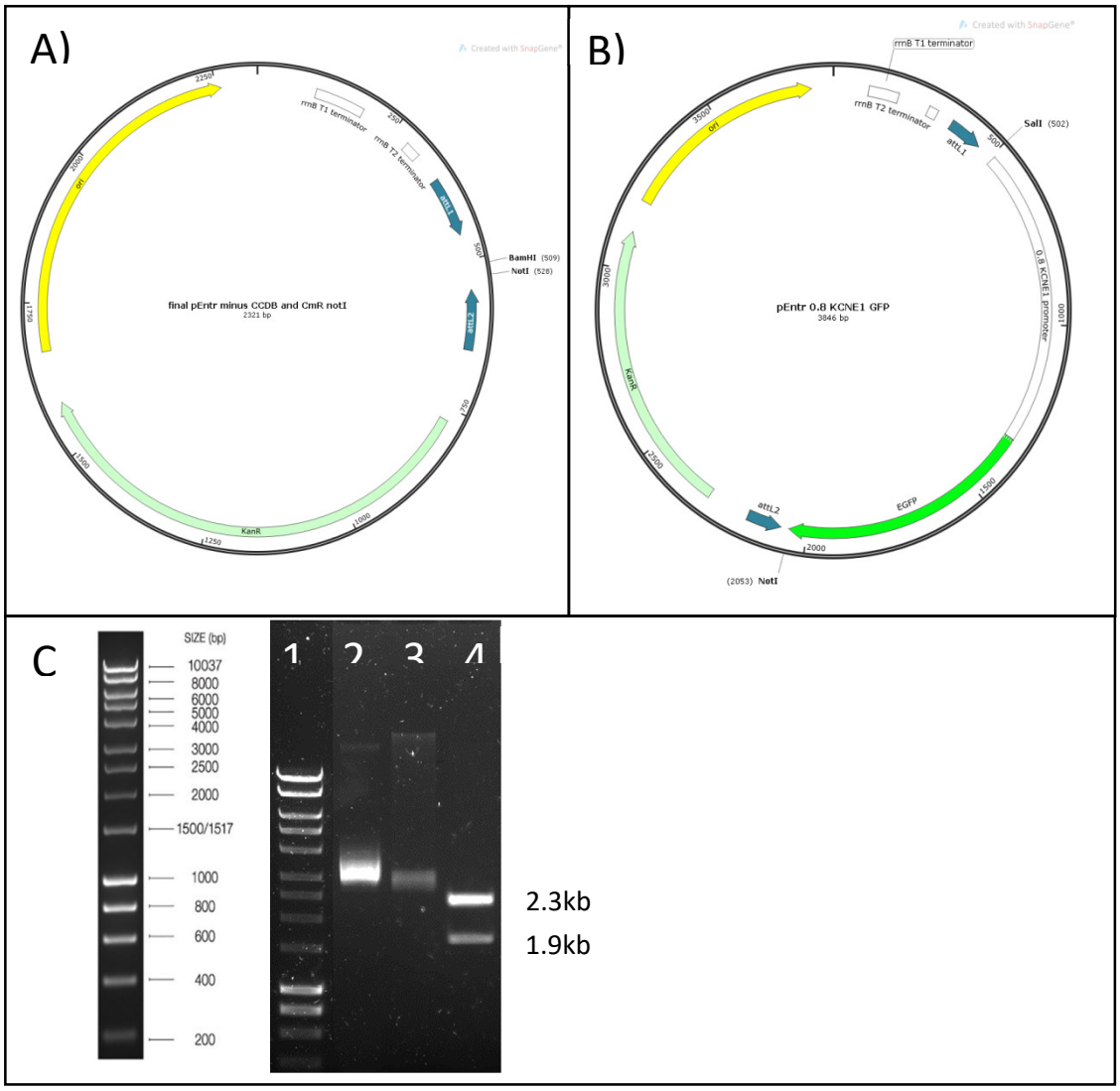

Figure 3.9.6. pEntr 0.8 KCNE1 GFP plasmid cloning. A) pEntr11 backbone plasmid. B) Cloned pEntr 0.8 KCNE1 GFP plasmid. C) Corresponding DNA gel electrophoresis: 1) DNA Ladder. 2) Final pEntr 0.8 KCNE1 GFP plasmid uncut. 3) backbone pEntr11 plasmid cut with BamHI, NotI.4) Final pEntr 0.8 KCNE1 GFP cut with SalI, NotI for verification of successful cloning.

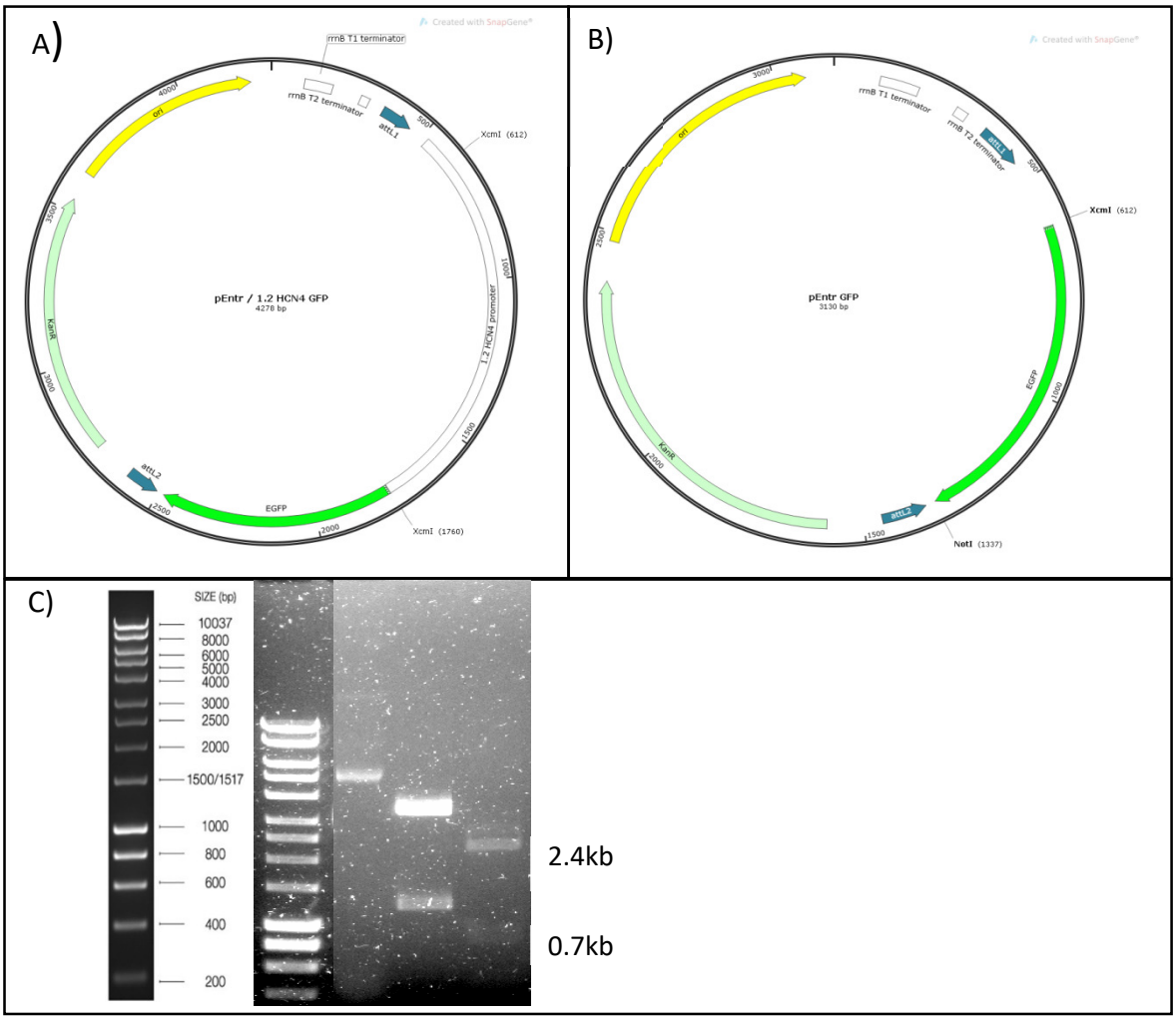

Figure 3.9.7. pEntr GFP plasmid cloning. A) pEntr 1.2 HCN4 GFP backbone plasmid. B) Cloned pEntr GFP plasmid uncut. C) Corresponding DNA gel electrophoresis: 1) DNA Ladder. 2) Final pEntr GFP plasmid uncut. 3) Backbone pEntr 1.2 HCN4 GFP cut with XCM1. 4) Final pEntr GFP cut with XCMI, NotI for verification of successful cloning.

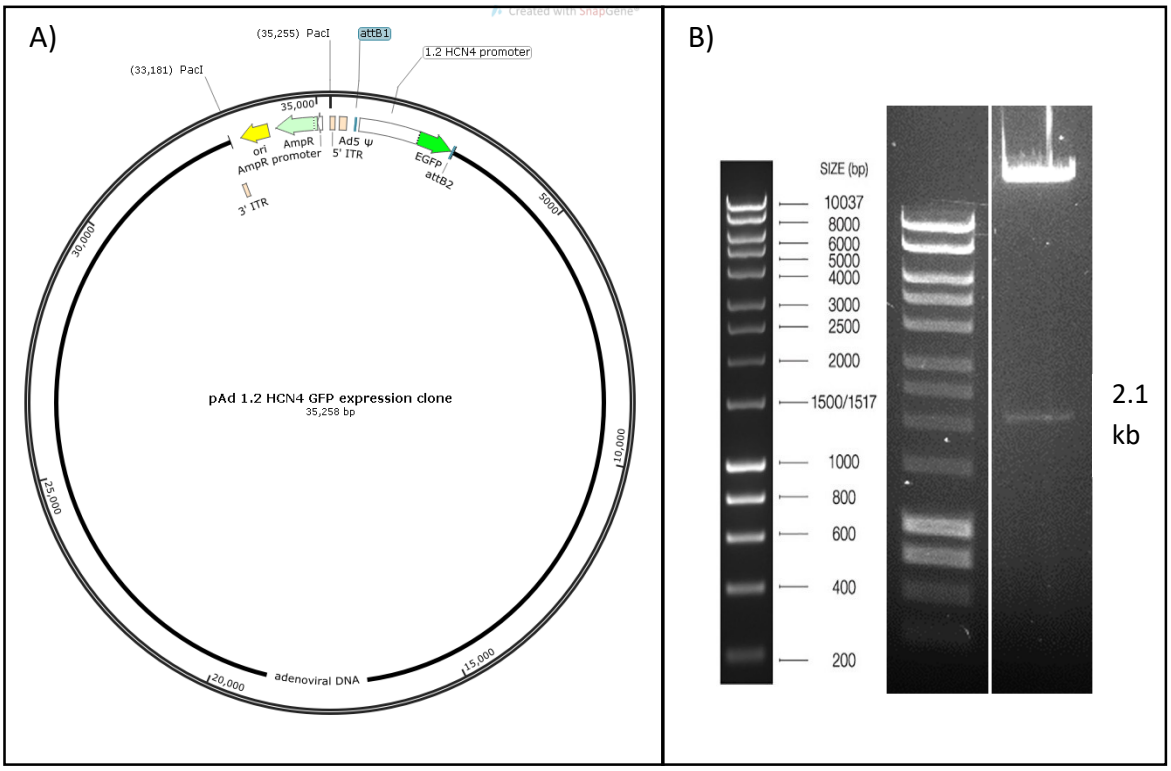

Figure 3.9.8. A) 1.2 HCN4 GFP expression clone map. Promoter / GFP construct is flanked by ATTB recombination and PACI restriction sites are labelled. B) DNA gel electrophoresis after PACI digestion, showing expected bands

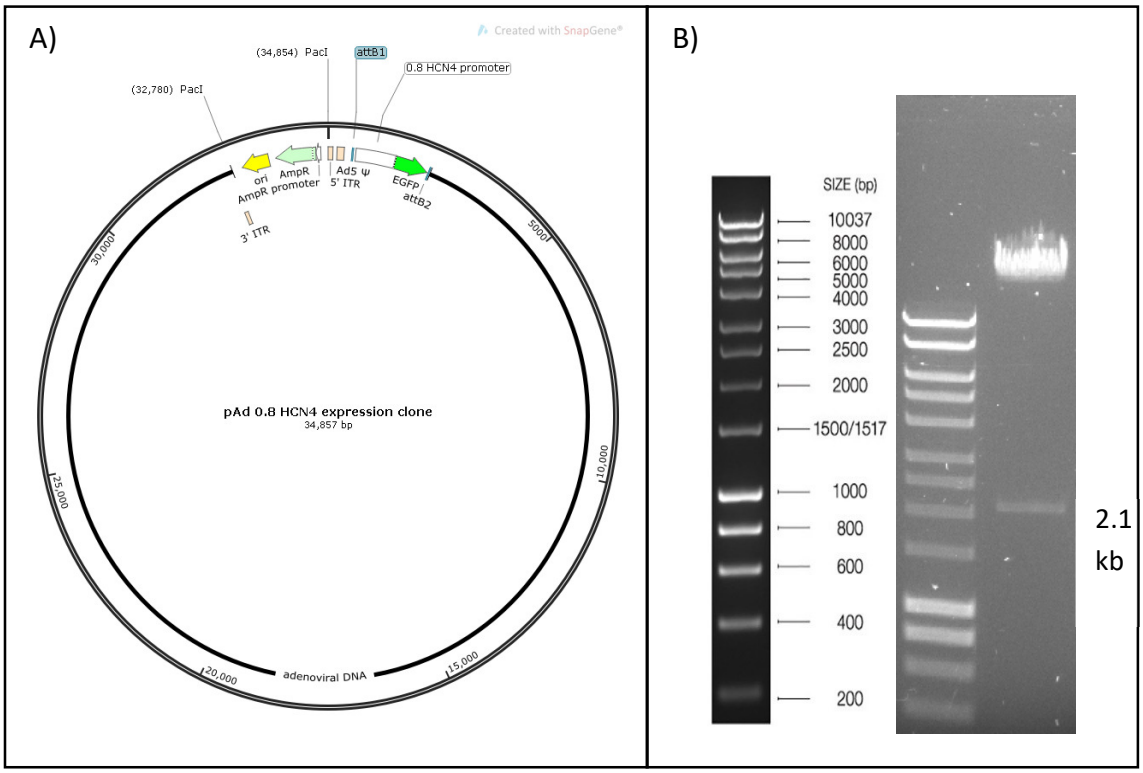

Figure 3.9.9. A) 0.8 HCN4 GFP expression clone map. Promoter / GFP construct is flanked by ATTB recombination and PACI restriction sites are labelled. B) DNA gel electrophoresis after PACI digestion, showing expected bands

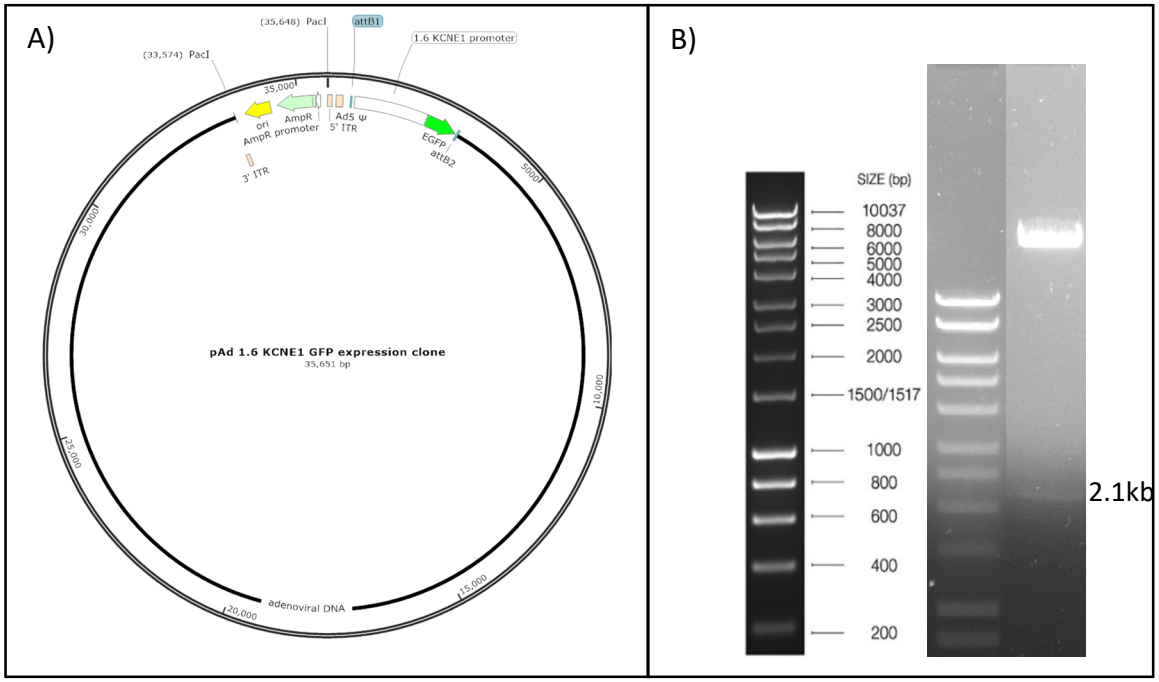

Figure 3.9.9.1 A) 1.6 KCNE1 GFP expression clone map. Promoter / GFP construct is flanked by ATTB recombination and PACI restriction sites are labelled. B) DNA gel electrophoresis after PACI digestion, showing expected bands

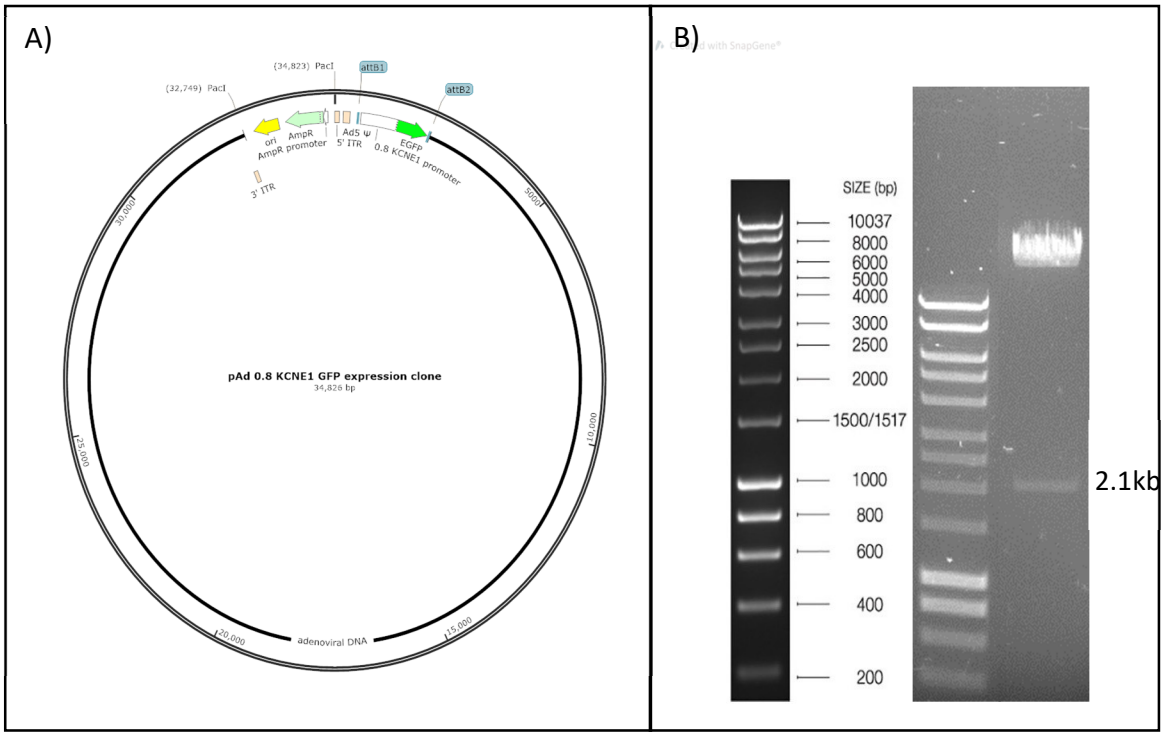

Figure 3.9.9.2. A) 0.8 KCNE1 GFP expression clone map. Promoter / GFP construct is flanked by ATTB recombination and PACI restriction sites are labelled. B) DNA gel electrophoresis after PACI digestion, showing expected bands

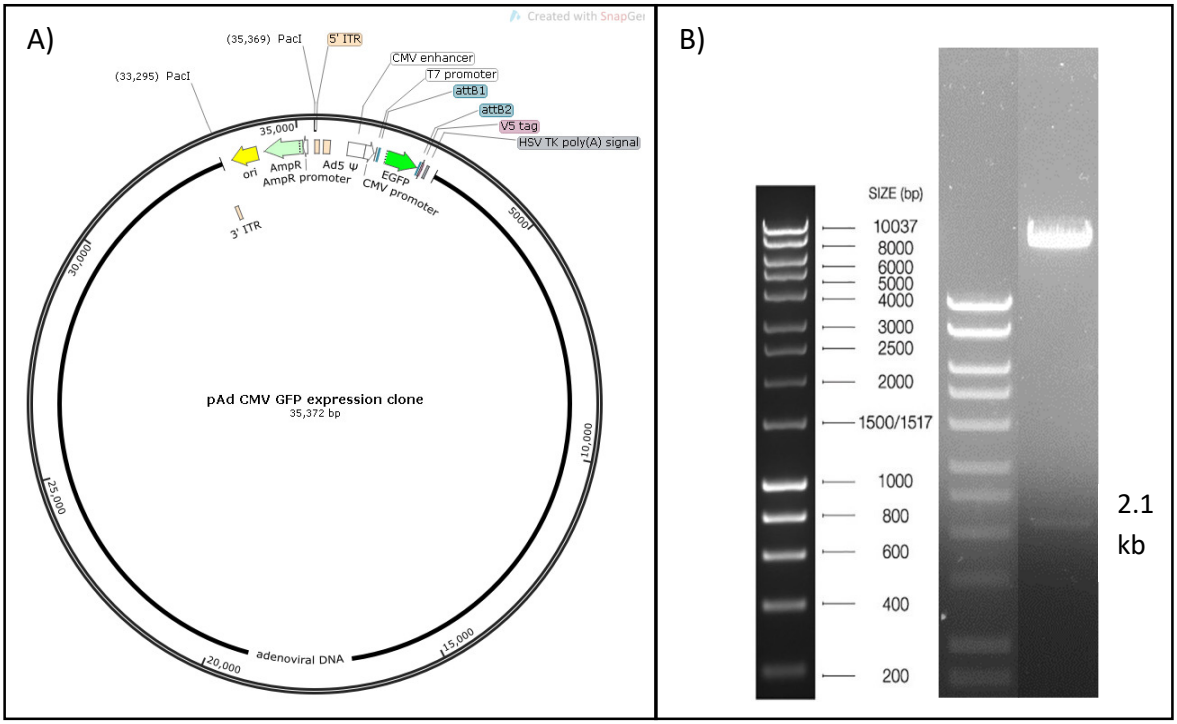

Figure 3.9.9.3. A) pAd CMV GFP expression clone map. Promoter / GFP construct is flanked by ATTB recombination and PACI restriction sites are labelled. B) DNA gel electrophoresis after PACI digestion, showing expected bands.

3.4 Discussion

The results described in this chapter summaries the development of tools to test the activity of tissue specific promoter candidates of HCN4 and KCNE1, comparing to known benchmarks of the ubiquitous CMV and strong cardiac specific cTnT promoters. This involved generating numerous plasmids comprising the promoter of choice upstream of the GFP transgene and relevant regulatory elements. Since the ultimate aim is to test the most promising candidates *in vivo* using AAV9, plasmids with the necessary regulatory elements for AAV production were selected for the plasmid backbone (PZac 2.1 for 0.8 kb promoter variants, and pAAV for the 1.2 kb HCN4 and 1.6 kb KCNE1 variants). In vitro testing would also benefit from high efficiency of transgene delivery, and so promoter constructs were also cloned into adenoviral vectors and adenovirus produced for these purposes. Unfortunately, later analysis of adenoviral constructs uncovered erroneous placement of restriction sites, resulting in exclusion of the polyadenylation signal from the final constructs. In the absence of polyadenylation signals, mRNA is not stabilized and suffers high levels of degradation, precluding translation to protein[385]. Thus, since promoter activity was to be measured by GFP protein fluorescence, the constructs were deemed unsuitable for use. The PZac 2.1 and pAAV based

plasmids were intact and correct, and thus lipofection of these plasmids into target cells was ultimately considered the best method for in vitro assessment of promoter performance going forward. This also precluded analysis on NRCMs, as plasmid lipofection efficiency was low in these cells as expected (not shown).

Insight into the regulation of promoter candidates was also gained through bioinformatics analyses, using sequences derived from the literature which detailed the human KCNE1 promoter region, and mouse HCN4 promoter region. Since bioinformatic tools merely offer predictions on TF binding activity, it must be considered that a predicted binding may not always reflect true binding of TFs to the promoter in the native context. Nevertheless, these assessments provided insight into the potential regulation of these promoters, and assisted in the process of rational design of minimal constructs applicable to AAV9 based strategies, in which promoter size must be minimized in light of limited viral packaging capacity. This was particularly relevant for KCNE1, where only the human and not the mouse promoter had been characterized and identified.

3.4.1 Bioinformatic analysis of the HCN4 promoter

The mHCN4 promoter region selected was subjected to bioinformatics analysis to identify putative TFBS of particular relevance to transcriptional regulation of HCN4 expression. SP1 is a key transcriptional activator of the human HCN4 promoter, and elevated expression of SP1 was found to drive overexpression of HCN4 under hypertrophic stimuli[377]. Our studies identified 3 putative SP1 binding sites were identified via bioinformatic analysis of the full 1.2 kb mouse HCN4 promoter, 2 of which lie within the 0.8 kb core promoter region (figure 3.2). SP1 is likely to contribute to transcriptional activation of the HCN4 promoter, and is a ubiquitously expressed TF found in most mammalian tissues[386]. SP1 is robustly expressed in liver, lung, kidney and brain among others, although there was more than a 100 fold variation in expression levels between different organs, suggesting it may play tissue specific roles beyond its established role in activation of housekeeper genes[387]. To this end, it has been demonstrated that SP1 Interacts with and transactivates the SERCA promoter in the working myocardium[388]. Of note, SP1 mRNA is more highly expressed in the SAN compared to right atrial tissue[101] and it has been demonstrated that SP1 can act synergistically with tissue specific TFs[389]. For example, SP1 interacts with an NFKB site in the NR1 promoter, controlling transcription of a glutamate receptor important for maintaining neuronal plasticity, resulting in its transcriptional transactivation[390].

ISL1 was also predicted to bind within the 0.8 kb HCN4 core promoter region (figure 3.2). SAN specific ablation of ISL1 in mouse embryos resulted in hypoplasia of the SAN, bradycardia, and

significantly decreased HCN4 and TBX3 expression in remaining SAN cells, suggesting regulation of these genes by ISL1[391]. Another study validated the role of ISL1 in establishing the SAN transcriptional programme, where RNA sequencing of SAN tissue lacking ISL1 also demonstrated decreased levels of HCN4, and high enrichment of ISL1 binding sites in those genes downregulated in response to ISL1 ablation[259]. Thus ISL1 is likely an important regulator of HCN4 expression.

SHOX is also predicted to bind to the 0.8 kb HCN4 core promoter region (figure 3.2). SHOX, and its murine orthologue shox2 were found to function similarly in regulating SAN formation, and functional redundancy between the two was demonstrated where mice expressing SHOX in place of Shox2 exhibited normal pacemaker function[392]. Ablation of Shox2 in the mouse heart results in decreased levels of HCN4 in the SAN from E10.5 and ectopic expression of Nkx2.5, concurrent with decreased rate of spontaneous automaticity[393]. However, it is not clear whether Shox2 directly regulates HCN4 transcription, as SAN HCN4 expression is reduced in Nkx2.5 overexpressing hearts in the absence of altered Shox2 expression, and ectopic Shox2 expression fails to significantly induce HCN4 expression and pacemaker activity[379]. In this context, Shox2 is thought to repress Nkx2.5 and thus resist induction of a working myocardium gene expression profile[379].

Other TFs that play key roles in development and maintenance of the SAN gene expression programme including TBX3[378], Nkx2.5[379] and Hand2[380] were predicted to bind to the HCN4 promoter region (figure 3.2). Hand2 promotes activation of pacemaker genes, including HCN4, via modifying chromatin assembly during reprogramming of fibroblasts cells to induced SAN cells[380].

3.4.2 Bioinformatic analysis of the KCNE1 promoter

After alignment of the mKCNE1 promoter to the previously characterized and published hKCNE1 core promoter region, similar bioinformatics analyses were carried out to identify putative regulatory motifs that could be important for activation and tissue specific activity of the mKCNE1 promoter. This information was also used to identify and select the final fragment to be used in vitro studies going forward.

The KCNE1 promoter was chosen to drive CCS specific transgene expression, based on the observation that KCNE1-LacZ knock-in mice express lacZ confined to the CCS[258]. The human KCNE1 promoter is well characterised[372,373], whereas the mouse KCNE1 promoter region lacks detailed characterisation[352]. Lundquist et al.[372] identified 2 KCNE1 variants in the human heart, designated KCNE1a and KCNE1b. The putative KCNE1a -1278 / +257 promoter drove higher levels of transgene expression in atrial HL1 cells compared to the corresponding KCNE1b region[372]. Multiple KCNE1 isoforms exist in the human heart, where two isoforms (designated isoforms 1 and 2[373]) make up 80% of those present in the heart and share a common promoter, as identified

in a later study.

Our in silico analysis predicted Tbx20 to bind to mKCNE1 -1278 / +333, with one site in the shortened -479/ +333 region, and a total of 2 in the full -1278/ +333 region (figure 3.4 A). Human and mouse KCNE1 promoters share consensus Tbx20 binding sites. Overexpression of Tbx20 increased KCNE1 levels in HL1 Cells, as well as transcriptional activity from the human KCNE1 promoter[394]. Cardiac K^+ channel promoters often contain multiple SP1 binding sites[381,373], and SP1 is a validated transactivator of the hKCNE1a promoter[382,383]. We observed one putative SP1 binding site in mKCNE1 lying within the shortened -479/ +33 segment (figure 3.4 A).

ETV1 is a transcriptional activator with functions relating to cellular proliferation, differentiation and maturation[384]. ETV1 Is highly expressed in the His-Purkinje network, and mutations are associated with bundle branch and AV block in humans[384]. ETV1 plays a key role in the regulation of genes enabling fast conduction, a hallmark of Purkinje fibres, and ETV1 deficient mice showed prolonged QRS duration and aberrant development of the ventricular conduction system[384]. Overexpression of ETV1 in neonatal ventricular rat cardiomyocytes induced a Purkinje-like gene expression profile, including elevated expression of KCNE1[395]. mKCNE1 -1278 / +333 contained 3 putative ETV1 binding sites, notably all lying within the shorter -479/ +333 region (figure 3.4 A).

Bioinformatic analysis identified one GATA binding site the putative mKCNE1 core promoter region, whereas the human core promoter contains three[373] (figure 3.4 A). GATA binding sites are critical to the function of the hKCNE1 promoter[373]. Mutation of all three GATA elements halved promoter activity and compromised cardiac specificity, also leading to an aberrant transcriptional response to hypertrophic stimuli[373]. Knockdown of GATA4 in NRCMs resulted in a 40% reduction in hKCNE1 promoter activity, indicating GATA4 in particular is a key determinant of hKCNE1 promoter activity in cardiomyocytes[373]. The -1278 / +333 mKCNE1 fragment contains 2 putative GATA4 binding sites (1 of which lies within the -479/ +333 region), which likely contribute to transcriptional activity and specificity in the heart (figure 3.4). Interactions between GATA4 and the KCNE1 promoter are further modulated by FOG2, where knockout of FOG2 or generation of a GATA4 mutant that blocks interactions with FOG2 results in significantly upregulated KCNE1 expression in the mouse heart[396].

MYOD binding sites are highly conserved between mouse and human KCNE1 promoter sequences, suggesting a key functional role in regultion[372]. We identified 4 predicted MYOD1 binding sites, 1 of which lies within the -479/ +333 promoter variant (figure 3.4 A).

mKCNE1 -1278 / +333 contained many predicted Tbx3 binding sites (n= 31) (figure 3.4 B). Tbx3 is a critical regulator of the SAN gene expression profile, activating expression of SAN markers including

HCN4, whilst actively repressing the chamber myocardial gene profile[397]. Tbx3 acts to suppress genes relating to fast conduction in the developing AVN, and Tbx3+/- mice exhibit increased KCNE1 expression, indicating the Tbx3 acts as a repressor of KCNE1 in the AVN[398]. Thus, the high density of Tbx3 sites may contribute to specific fine patterning of KCNE1 expression in the CCS.

Thus, the promoter fragments selected contain many TFBS relating to their transcriptional control and tissue specific expression. Further *in vitro* and *in vivo* testing is required to assess whether these fragments are, in reality, capable of driving transgene expression at therapeutically relevant levels in the CCS, and in a tissue specific manner. In order to address this, promoter/ reporter constructs were cloned into AAV and adenoviral plasmids for *in vitro* characterisation of transcriptional activity.

3.5 Summary and conclusions

In conclusion, constructs comprising 0.8 kb HCN4, 1.2 kb HCN4, 0.8 kb KCNE1, 1.6 kb KCNE1, cTnT and CMV promoters were successfully characterized and generated. These constructs form the basis for initial *in vitro* testing and validation of CCS tissue specific promoter constructs.

4.0 Chapter 4: Results- in vitro characterisation of promoter constructs

4.1 Introduction

In vitro studies were designed to test two primary characteristics of promoter candidate performance; specificity, pertaining to the ability of the promoter to drive transgene expression only in target (SAN / CCS) cells, and transcriptional strength, relating to the ability of the promoter to induce transcription of the transgene at therapeutically relevant levels. For example, for miR competitive inhibition applications, typically strong promoters such as CMV are used, as high levels of miR decoy transgenes are necessary in order to achieve effective miR inhibition[399]. Equally, it must be considered that constitutively active strong viral promoters such as CMV may not be appropriate in certain applications. One study demonstrated that overexpression of pro-regenerative miRs in the heart via AAV6-CMV resulted in fatal arrhythmia due to uncontrolled cardiomyocyte proliferation[209]. To this end, endogenous promoters, such as cTnT, are more likely to express genes at physiologically relevant and appropriate levels.

The CMV promoter is one of the most well characterised strong ubiquitous promoters, shown to be highly active across most cell types[400]. Furthermore, CMV driven reporter gene expression is extensive in most tissues *in vivo* when delivered via AAV vectors[401,206]. With these factors considered, the CMV promoter represents an appropriate positive control and benchmark for assessing transcriptional strength of CCS tissue specific promoter candidates. The well-known and characterised cardiac specific promoter cTnT was used as another benchmark[363]. The cTnT promoter has proved capable of driving high levels of cardiac specific transgene expression[363]. Although cardiac troponin T is expressed in the SAN[261], it is currently unknown whether the promoter construct under observation is active in SAN tissue. Thus, I reasoned that it could be a promising candidate for SAN gene delivery in a cardiac specific context. I also designed HCN4 and KNCE1 promoters to achieve SAN/ CCS specific gene expression (described in detail in chapter 3). HCN4 is a highly specific and enriched SAN gene and a significant contributor to membrane clock pacemaking via generating I_f[20,347]. KCNE1 interacts with KCNQ1 to mediate $I_{K,s}$, and was shown to be expressed exclusively in the CCS of adult mice[258]. Thus, I reasoned these promoters, which drive expression of their respective genes in a CCS restricted manner, would be appropriate for driving exogenous transgenes in a similarly spatially restricted manner.

In order to assess promoter specificity, promoters I aimed to test constructs in cells corresponding to the SAN and some off target tissues that are known to be transduced by AAV9[401,206]. Plasmids comprising the promoter of choice upstream of the GFP reporter gene were transfected into each cell line using lipofectamine 3000 (Invitrogen). Cells were collected 48 hours thereafter and GFP fluorescence in live cells quantified via imaging cytometry, using the Amnis ImageStream system (Amnis Corporation, Seattle, WA) and IDEAS software. SAN cells were represented by the mESC derived sinoatrial node-like Shox2 cell line[402] (ATCC® CRL-3256), and off target tissues of the fibroblasts, and kidney were represented by NIH-3T3 (ATCC® CRL-1658), and HEK 293A (Invitrogen R70507) cells respectively. Shox2 cells endogenously express high levels of HCN4[402], (as shown in figure 4.1), and thus can be considered an appropriate model for assessing activity of the HCN4 promoter constructs tested. Expression of KCNE1 was not measured, though Shox2 cells have a transcriptional profile largely similar to primary SAN cells and so their applicability for testing other CCS specific promoter constructs remains well founded[402]. In addition to high HCN4 expression, Shox2 cells have a gene expression similar to bona fide SAN cells including Cx45, Cx30.2, Tbx2, and Tbx3[402]. Although these cells also express some cardiac genes including Tbx5, GATA4, and MLC2V, the native SAN is also known to express some working myocardial associated genes including cardiac troponin I (cTnI) and MLC2V[403]. Critical repressors of the SAN gene expression profile such as Nkx2.5, and atrial specific ANF are very lowly expressed in Shox2 cells[402].

In order to effectively assess promoter strength, incorporating both the percentage of GFP positive cells and their mean fluorescence intensity, the mean fluorescence of GFP positive cells was multiplied by the percentage of GFP positive cells and background fluorescence subtracted to give the fluorescence change over negative control (untransfected) conditions[262]. In order to account for differing transfection efficiencies across the cell lines, and between experimental replicates using the same cell line, the transfection efficiency for each promoter construct within a given experiment was normalised to that of the ubiquitous CMV promoter. Raw transfection efficiencies of 25.14%, 18.03% and 59.03% were achieved for Shox2, NIH 3T3 and HEK 293A cells respectively.

Thus, the studies described herein pertain to assessing the utility of the candidate promoter constructs generated in chapter 3 to drive tissue specific transgene expression within an in vitro context.

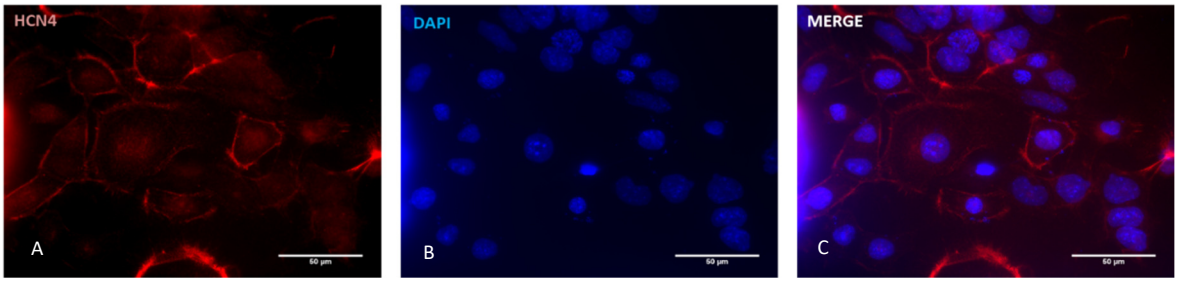

Figure 4.1: HCN4 expression in Shox2 cells visualised via immunocytochemistry. A) HCN4 protein expression pseudocoloured red. B) DAPI stain of the same field as in A showing cell nuclei (blue). C) Overlay of panels A and B. Scale bar denotes 50 µm.

4.2 Hypotheses and aims

I. The ubiquitous CMV promoter is highly active across all cell lines tested, whilst HCN4 and KCNE1 promoter constructs should confer specific transgene expression in SAN-like Shox2 cells *in vitro*, without measureable activity in off target cells.

II. Hybrid CCS specific promoter/ CMV enhancer constructs possess more potent transcriptional activity whilst maintaining tissue specificity of the endogenous promoters.

Aims:

I. Assess the transcriptional strength of CCS specific promoter candidates in SAN-like Shox2 cells, compared to characterised benchmarks of the CMV and cTnT promoters.

II. Assess tissue specificity of CCS specific promoter candidates by testing constructs in cell lines corresponding to off target cell types, HEK 293A and NIH 3T3, representing kidney and fibroblasts respectively.

III. Assess the effect of the CMV enhancer on CCS specific promoter candidates, in terms of transcriptional strength enhancement and tissue specificity.

IV. Select promising promoter constructs for AAV9 production and *in vivo* testing in mice.

4.3 Results

4.3.1 Promoter specificity and transcriptional strength in vitro

4.3.1.1 Shox2 cells

Relative transcriptional strength of promoters was first measured in Shox2 cells in order to assess their ability to drive transgene expression in SAN / CCS tissue. Fluorescence was quantified as the change in fluorescence compared to negative control, taking into account both percentage GFP positive cells, fluorescence intensity, and background fluorescence. This metric is henceforth referred to as 'fluorescence.' Firstly, both HCN4 promoter variants were active in Shox2 cells as shown by the significant change in fluorescence over negative control (figure 4.2A) and GFP fluorescence observed via fluorescence microscopy (figure 4.2 B). Fluorescence conferred by the 0.8 kb HCN4 promoter appeared moderately higher at 4155.24 compared with 1459.63 with the 1.2 kb promoter, equating to a 96.02% difference (p= 0.49) (figure 4.2 A, table 4.1). Both KCNE1 promoter variants (0.8 kb and 1.6 kb) outperformed the HCN4 promoters in Shox2 cells (figure 4.2 a, table 4.1). 0.8 kb KCNE1 appeared to have slightly albeit statistically non-significantly higher transcriptional strength compared to 1.6 kb KCNE1, with fluorescence quantified at 13669.41 compared with 9839.16 using the 1.6 kb variant, corresponding to a 32.6% difference (figure 4.2 A, table 4.1). The cTnT promoter significantly out-performed both the 0.8 kb and 1.2 kb HCN4 promoters ($p \leq 0.05$, $p \leq 0.01$ respectively) (figure 4.2 A, table 1). There was no statistically significant difference between the performance of cTnT and 0.8 kb or 1.6 kb KCNE1 promoters (figure 4.2 a, table 4.1). Robust fluorescence conferred by all promoter candidates in shox2 cells could be visualised via fluorescence microscopy (figure 4.2 B).

The highest performing promoter candidate (0.8 kb KCNE1) achieved a fluorescence value 10% of that of the positive control (CMV), whilst fluorescence conferred by the 0.8 kb and 1.2 kb HCN4 promoters was 3% and 1.07% respectively of CMV (table 4.1). Due to the necessity for high levels of transgene expression in many gene therapy applications, I aimed to enhance transcriptional strength of CCS specific promoter candidates using the CMV enhancer. This approach has been successfully used to enhance transcriptional strength of multiple tissue specific promoters, including cardiac muscle specific promoters, *in vitro* and *in vivo* whilst minimally affecting tissue specificity in many contexts[262,266]. The 380 bp human immediate early CMV enhancer was cloned upstream of 0.8 kb HCN4, 1.2 kb HCN4 and 0.8 kb KCNE1 promoters using cloning techniques outlined in chapter 3, section 3.3.4. The 1.6 kb KCNE1 promoter was excluded from these studies due to the strict constraints on promoter size for use in AAV vectors.

In Shox2 cells, the CMV enhancer had a modest effect on the 0.8 kb HCN4 and 1.2 kb HCN4 promoters, generating increased fluorescence levels compared with the native promoters, albeit the difference was not statistically significant (figure 4.3 A, table 4.1). Addition of the CMV enhancer increased fluorescence by 90.2% and 138.6% for the 0.8 kb and 1.2 kb HCN4 promoters respectively (figure 4.3 A) ($p= 0.2$ and 0.6 respectively). Fluorescence distribution histograms from imaging cytometry data revealed only a small deviation of the CMVe trace from that without CMVe for 0.8 kb (figure 4.3 B i) and 1.2 kb HCN4 (not shown). Notably, significantly higher area under the curve was seen for 0.8 kb HCN4 and 1.2 kb HCN4 promoters in the GFP positive fluorescence range vs negative control, again confirming their activity in the Shox2 cell line (figure 4.3 B i). Significantly increased fluorescence was seen with the incorporation of CMVe into the 0.8 kb KCNE1 promoter construct, resulting in a 73.1% fluorescence increase ($p\leq 0.0001$) (figure 4.3 A, table 4.1). Increased fluorescence was evident from fluorescence distribution histograms, with a slight rightward shift in the curve, and higher area under the curve in the GFP positive fluorescence range (figure 4.3 B). Indeed, the CMVe 0.8 kb KCNE1 promoter was the most potent of all tissue specific promoter candidates ($p\leq 0.0001$) (figure 4.3 A). Fluorescence conferred by CMVe 0.8 kb KCNE1 was 17.4% of that conferred by the positive control promoter CMV (table 4.1). CMVe 0.8 kb KCNE1 also out-performed the well-characterised strong cardiac specific cTnT promoter ($p\leq 0.0001$). Apparently higher fluorescence levels from CMVe constructs, particularly CMVe 0.8 kb KCNE1, were also evident using fluorescence microscopy (figure 4.3 C).

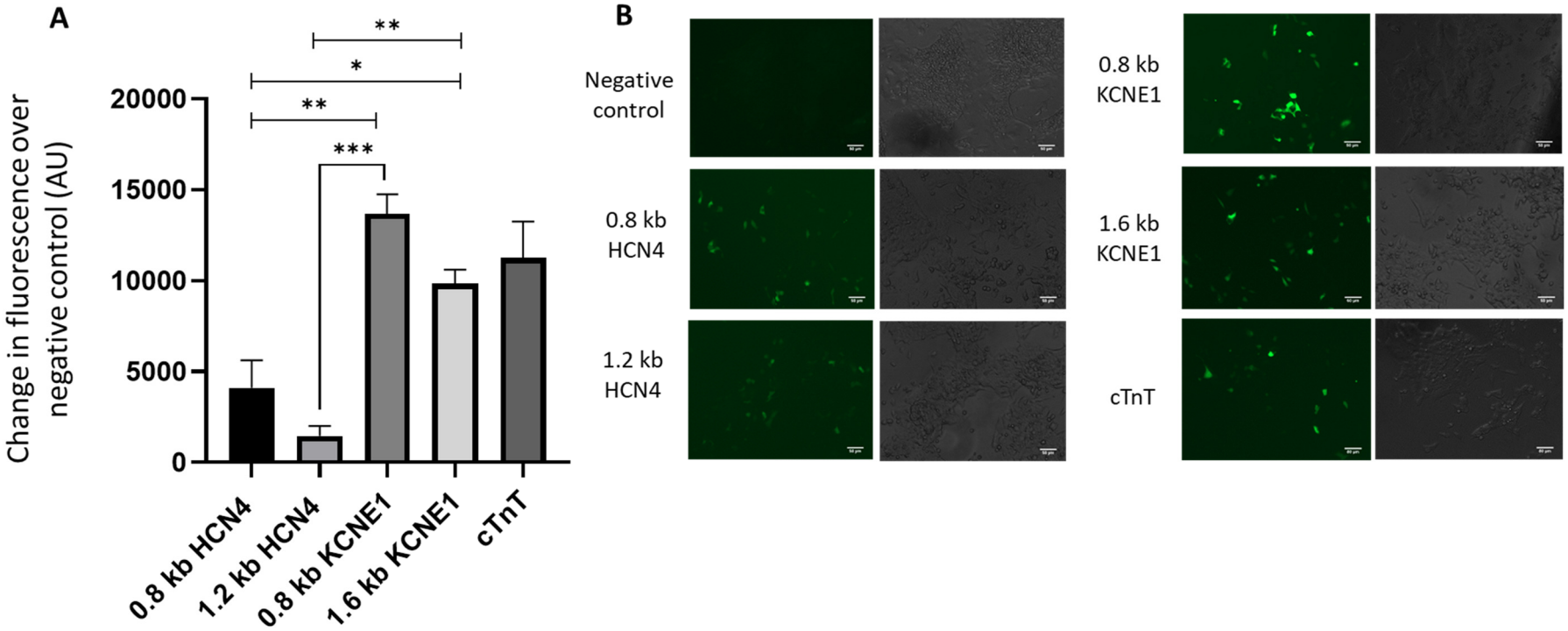

Figure 4.2: Promoter activity in Shox2 cells. (A) change in fluorescence over negative control for each promoter construct in Shox2 cells measured by flow cytometry. Data pooled from 3 independent experiments, each comprising 3 technical replicates for each construct. Error bars denote SEM. *p ≤ 0.05, **p ≤0.01. ***p ≤0.001, ****p ≤0.0001. One way ANOVA used to determine significance. B) Representative images for each promoter construct 48 hours after transfection into the Shox2 cell line, collected via fluorescence microscopy. Brightfield images depict the same field as fluorescence images, showing cellular distribution within the field. Scale bar denotes 50 µm

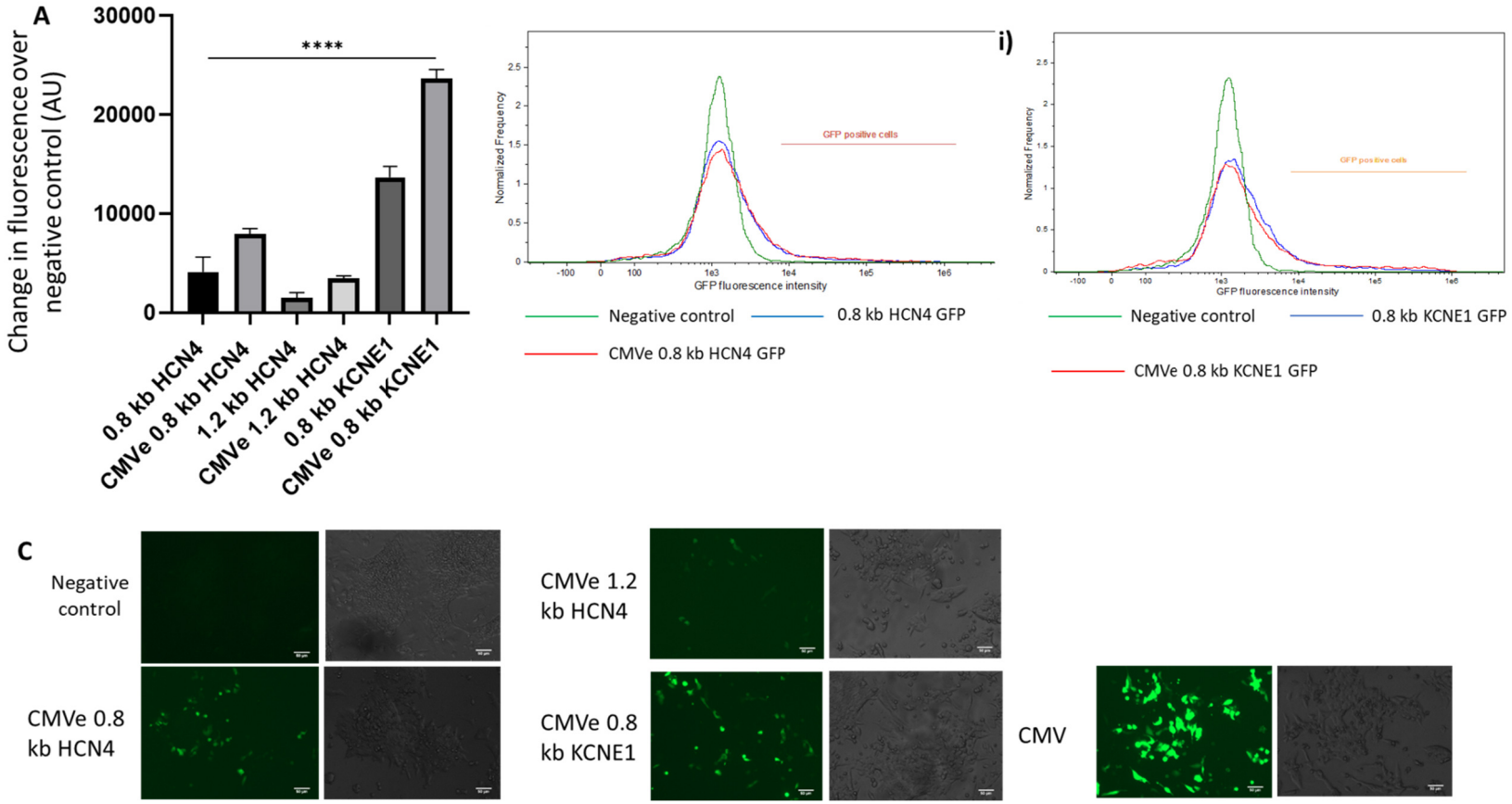

Figure 4.3: Effect of the CMV enhancer on CCS specific promoter candidate activity in Shox2 cells. A) change in fluorescence over negative control for each promoter construct in Shox2 cells measured by flow cytometry. Data pooled from 3 independent experiments, each comprising 3 technical replicates for each construct. Error bars denote SEM. Ns $p>0.05$.*$p \leq 0.05$, **$p \leq 0.01$. ***$p \leq 0.001$, ****$p \leq 0.0001$. One way ANOVA used to determine significance. B) Representative fluorescence histograms for 0.8 kb HCN4 and CMVe 0.8 kb HCN4 GFP (B i) and 0.8 kb KCNE1 and CMVe 0.8 kb KCNE1 GFP (B ii) contrasted with negative control (untransfected). GFP positive cells were deemed those with fluorescence higher than 99.5% of cells in the negative (untransfected) control. C) Representative images for each CMVe coupled CCS specific promoter construct 48 hours after transfection into the Shox2 cell line, collected via fluorescence microscopy. Brightfield images depict the same field as fluorescence images, showing cellular distribution within the field. Positive control (CMV) is shown for reference, illustrating transfection efficiency. Scale bar denotes 50 µm.

Promoter construct	Fluorescence change over negative control	Fluorescence change over negative control as % of CMV
CMV	135988 ± 2651	100%
0.8 kb HCN4	4115 ± 1507	3.03%
CMVe 0.8 kb HCN4	7902 ± 591	5.81%
1.2 kb HCN4	1460 ± 549	1.07%
CMVe kb 1.2 HCN4	3484 ± 240	2.56%
0.8 kb KCNE1	13669 ± 1085	10.05%
CMVe 0.8 kb KCNE1	23662 ± 908	17.40%
1.6 kb KCNE1	9839 ± 766	7.24%
cTnT	11264 ± 1999	8.28%

Table 4.1: Shox2 data summary for each promoter construct. Average values displayed for fluorescence change over negative control, ± SEM derived from 3 distinct experiments each comprising 3 technical replicates for each construct. Fluorescence values as a percentage of those conferred by the positive control CMV promoter are shown in the right column.

4.3.1.2 NIH 3T3 cells

The positive control CMV promoter again drove robust GFP transgene expression In NIH 3T3 cells, despite lower transfection efficiency achieved in this cell line (figure 4.5 C, table 4.2). It is noteworthy that illumination power for GFP detection was set lower than in Shox2 cells due to higher activity of the CMV promoter in this cell line, necessary to avoid oversaturation of the fluorescence detector from the brightest cells (see methods, chapter 2 section 2.7). This contributed to the lower overall fluorescence values compared with Shox2 cells. Fluorescence was not detected above background for any CCS or cardiac specific promoter candidates or cTnT in NIH 3T3 cells, with negative values reported (figure 4.4 A, table 4.2). The lack of fluorescence conferred from these promoters is also evidenced by lack of fluorescence observed using fluorescence microscopy (figure 4.4 B).

The effect of the CMV enhancer on promoter specificity was also assessed. CMVe 1.2 kb HCN4 maintained fluorescence levels below background (figure 4.5 A, table 4.2), resulting in negative fluorescence values (figure 4.5 A). Fluorescence microscopy also revealed only very low numbers of cells expressing weak GFP fluorescence (figure 4.5 C), and representative fluorescence distribution histograms did not deviate significantly from the negative control (not shown). Conversely, the CMVe 0.8 kb HCN4 and CMVe 0.8 kb KCNE1 promoters significantly increased fluorescence compared to the corresponding native promoters ($p \leq 0.01$, $p \leq 0.001$ respectively) (figure 4.5 A, table 4.2). Fluorescence distribution traces showed some deviation from the

enhancer-less constructs, particularly evident in CMVe 0.8 kb KCNE1, with higher area under the curve in the GFP positive fluorescence range (figure 4.5 B i-ii). Notably, traces for the native 0.8 kb HCN4 and 0.8 kb KCNE1 did not deviate from the negative control , confirming their lack of activity in this cell line (figure 4.5 B i-ii). Moderately increased fluorescence from CMVe 0.8 kb KCNE1 and HCN4 promoters was also evident from fluorescence micrographs from (figure 4.5 C) when compared against the native promoters and negative control (figure 4.4 B). However, compared to the native CMV enhancer/ promoter used as positive control, these hybrid CMVe/ CCS specific promoter candidates still produce minimal transgene expression in NIH 3T3 cells. CMVe 0.8 kb HCN4 and CMVe 0.8 kb KCNE1 produced fluorescence levels of 1.48% and 4.2% of the positive control CMV promoter respectively, indicating that coupling the CMV enhancer to CCS specific promoters confers a degree of CCS selectivity (table 4.2).

In conclusion, it appeared that all native CCS specific promoter candidates were inactive in NIH 3T3 cells. Addition of the CMV enhancer appeared to somewhat sacrifice promoter specificity for transcriptional strength as measured in this cell line, particularly the strongest candidate CMVe 0.8 kb KCNE1. Of note, all CMVe coupled promoters maintained activity well below that of the native CMV enhancer/ promoter construct in this cell line.

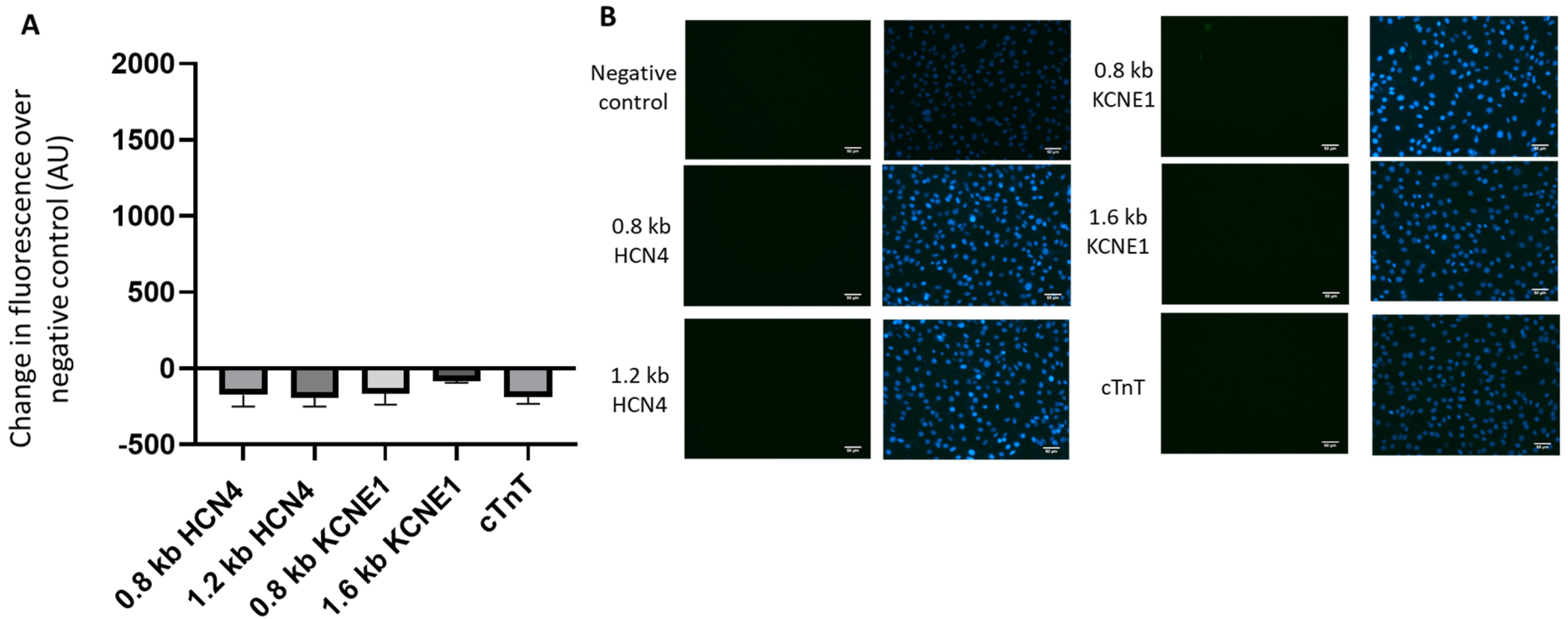

Figure 4.4: Promoter activity in NIH 3T3 cells. (A) change in fluorescence over negative control for each promoter construct in Shox2 cells measured by flow cytometry. Data pooled from 2 independent experiments, each comprising 3 technical replicates for each construct. Error bars denote SEM. **p ≤0.01. One way ANOVA used to determine significance. B) Representative images for each promoter construct 48 hours after transfection into the NIH 3T3 cell line, collected via fluorescence microscopy. Left panel for each construct depicts GFP fluorescence imaging, left panel depicts merge between GFP and DAPI signals, where DAPI represents cell nuclei. Scale bar represents 50 µm.

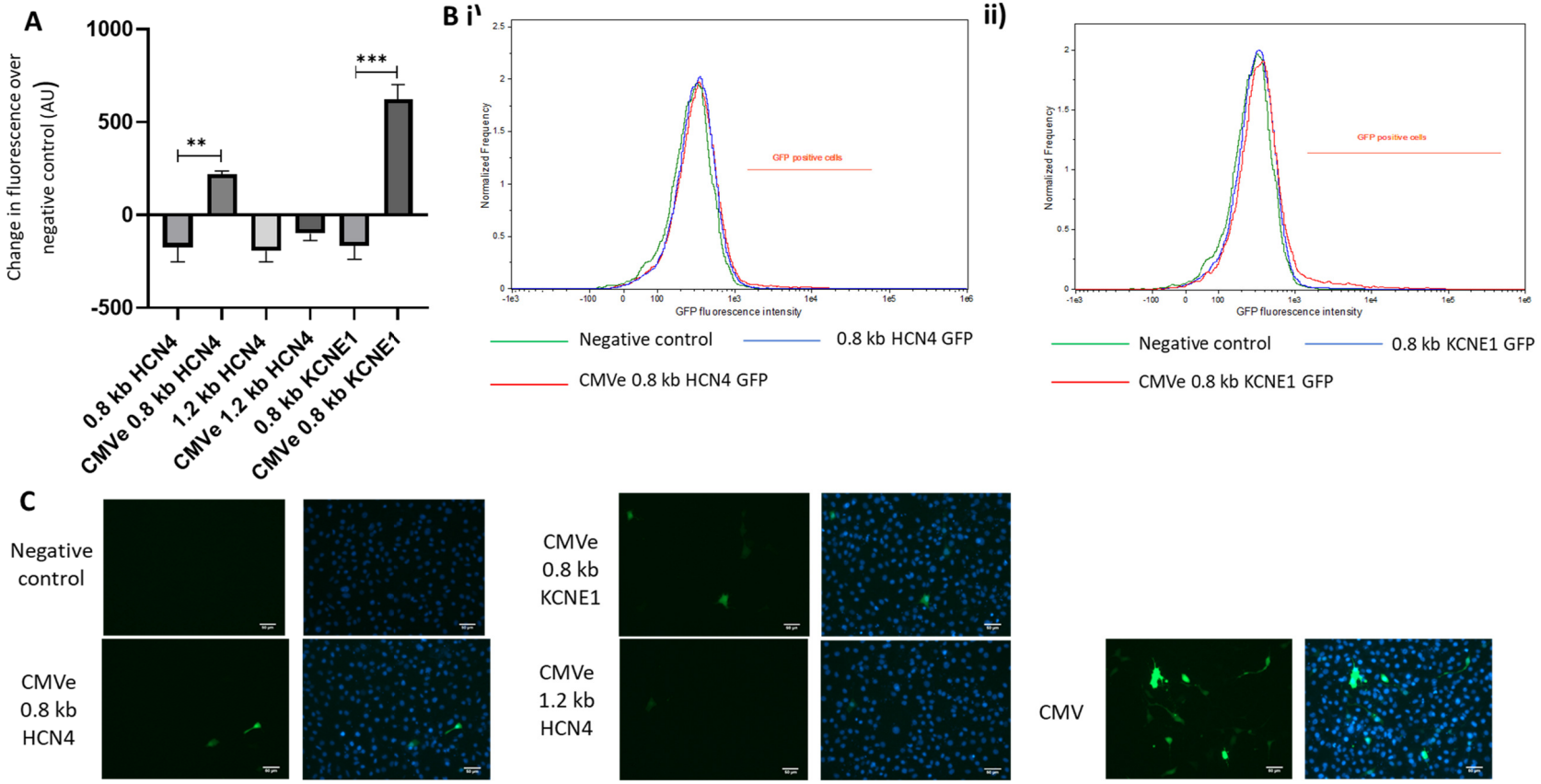

Figure 4.5: Effect of the CMV enhancer on CCS specific promoter candidate activity in NIH 3T3 cells. A) change in fluorescence over negative control for each promoter construct in NIH 3T3 cells measured by flow cytometry. Data pooled from 2 independent experiments, each comprising 3 technical replicates for each construct. Error bars denote SEM. *p ≤ 0.05, **p ≤0.01. ***p ≤0.001, ****p ≤0.0001. One way ANOVA used to determine significance. B) Representative fluorescence histograms for 0.8 kb HCN4 and CMVe 0.8 kb HCN4 GFP (B i) and 0.8 kb KCNE1 and CMVe 0.8 kb KCNE1 GFP (B ii) contrasted with negative, denoting the distribution of cellular fluorescence after transfection with each promoter construct. GFP positive cells were deemed those with fluorescence higher than 99.5% of cells in the negative (untransfected) control. C) Representative images for each CMVe coupled CCS specific promoter construct 48 hours after transfection into the NIH 3T3 cell line, collected via fluorescence microscopy. Left panel for each construct depicts GFP fluorescence imaging, left panel depicts merge between GFP and DAPI signals, where DAPI represents all cell nuclei. Positive control (CMV) is included for reference and illustrates transfection efficiency. Scale bar denotes 50 µm.

Promoter construct	Fluorescence change over negative control	Fluorescence change over negative control as % of CMV
CMV	14857 ± 2788	100%
0.8 kb HCN4	-173 ± 78	-
CMVe kb 0.8 HCN4	220 ± 17	1.48%
1.2 kb HCN4	-193 ± 59	-
CMVe 1.2 kb HCN4	-99 ± 38	-
0.8 kb KCNE1	-165 ± 72	-
CMVe 0.8 kb KCNE1	623 ± 79	4.19%
1.6 kb KCNE1	-85 ± 10	-
cTnT	-188 ± 44	-

Table 4.2: NIH 3T3 data summary. Average values displayed for fluorescence change over negative control, ± SEM derived from 2 distinct experiments each comprising 3 technical replicates for each construct. Fluorescence values as a percentage of those conferred by the positive control CMV promoter are shown in the right column.

4.3.1.3 HEK 293A cells

The CMV promoter was highly active in In HEK 293A cells, with high transfection efficiency (figure 4.7 B, table 4.3). Fluorescence excitation power was kept constant with the level of 0.5 mW used for the NIH 3T3 cell line, which maintained the brightest cells just below detector saturation levels. 0.8 kb and 1.2 kb HCN4 promoters conferred minimal GFP reporter fluorescence, with negative fluorescence values reported (figure 4.6 A, table 4.3). Fluorescence microscopy also showed low numbers of weakly GFP positive cells for both HCN4 promoter constructs (figure 4.6 B). Both the 0.8 kb and 1.6 kb KCNE1 promoters conferred detectable GFP reporter fluorescence albeit only at very low levels, with fluorescence values of 149.08 and 34.55 respectively (figure 4.6 A, table 4.3). To contextualise these figures, they represent proportions of 0.38% and 0.09% compared to the positive control CMV construct respectively (table 4.3). Fluorescence values reported for cTnT, 0.8 kb KCNE1 and 1.6 kb KCNE1 constructs were positive albeit very low, suggesting a small degree of promoter activity in these HEK 293A cells (figure 4.6 A, table 4.3). In agreement with the imaging cytometry data, some weakly GFP positive cells could be seen with 0.8 kb and 1.6 kb KCNE1 and cTnT promoters using fluorescence microscopy (figure 4.6 B).

In HEK 293A cells, the CMV enhancer appeared to confer increased activity of all CCS specific promoter candidates (figure 4.7 A). Fluorescence from the 0.8 kb HCN4 promoter was not significantly detected in HEK 293 cells, with a negative value of -117 reported (figure 4.6 A, table 4.3). Inclusion of the CMV enhancer increased fluorescence to a value of 427.33 ($p \leq 0.05$) (figure

4.7 A, table 4.3). Representative fluorescence distribution traces show a significant increase in GFP positive cells from CMVe 0.8 kb HCN4 compared to 0.8 kb HCN4, with a higher area under the curve in the GFP positive fluorescence range (figure 4.7 B i). The same was observed for CMVe 0.8 kb KCNE1 (figure 4.7 B ii), particularly within the range of 1000 to 10,000 fluorescence units. Increased GFP fluorescence in HEK 293A cells using the CMVe 0.8 kb HCN4 and CMVe 0.8 kb KCNE1 constructs was also evident in fluorescence micrographs (figure 4.7 C). The CMV enhancer did not significantly increase activity of the 1.2 kb HCN4 promoter in HEK 293A cells (figure 4.7 A, table 4.3). However, some increase in GFP positive cells was observed using fluorescence microscopy (figure 4.7 C). It is important to note that before inclusion of the enhancer, 0.8 kb HCN4 promoter conferred no detectable fluorescence, and fluorescence from 0.8 kb KCNE1 was barely detectable (figure 4.6 A, table 4.3). Thus, in the context of HEK 293A cells, it appears that the CMV enhancer induces some promiscuous activity of CCS specific promoter candidates.

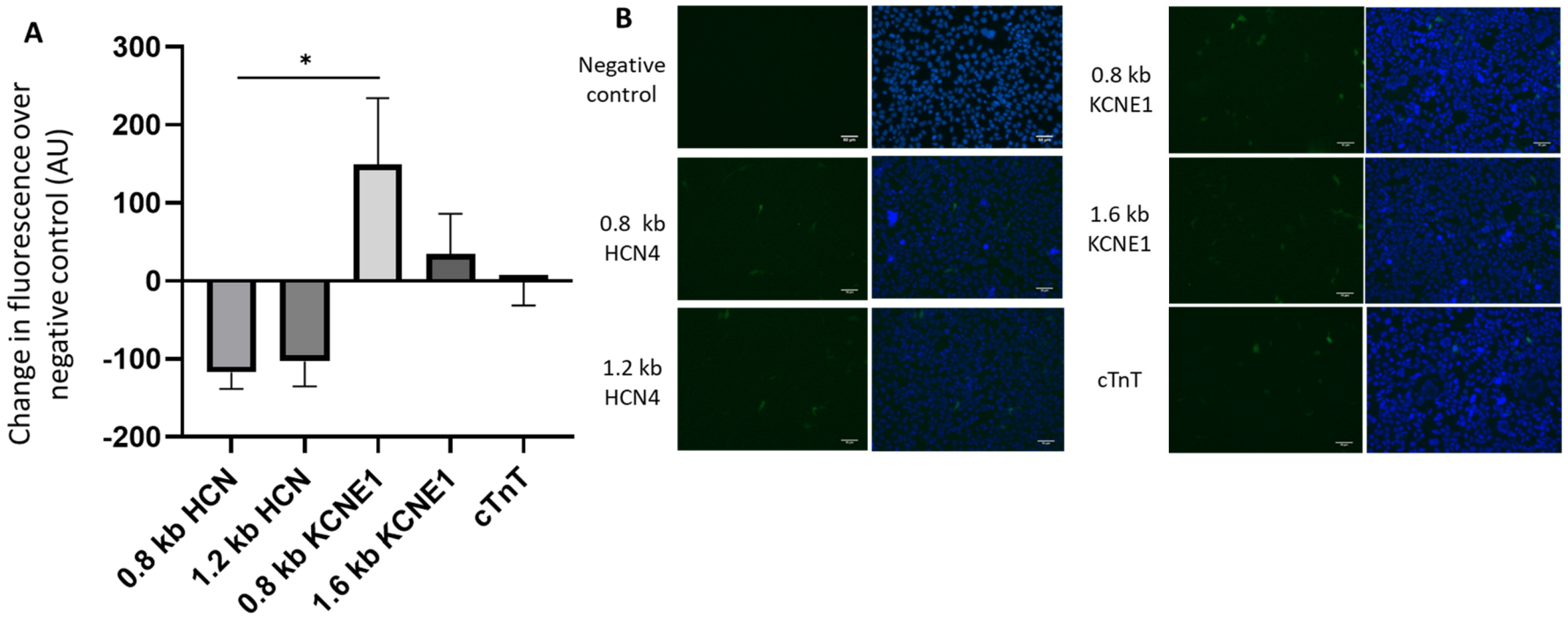

Figure 4.6: Promoter activity in HEK 293A cells. (A) change in fluorescence over negative control for each promoter construct in HEK 293A cells measured by flow cytometry. Data pooled from 3 independent experiments, each comprising 3 technical replicates for each construct. Error bars denote SEM. *p ≤ 0.05, **p ≤0.01. ***p ≤0.001, ****p ≤0.0001. One way ANOVA used to determine significance. B) Representative images for each promoter construct 48 hours after transfection into the HEK 293A cell line, collected via fluorescence microscopy. Left panel for each construct depicts GFP fluorescence imaging, left panel depicts merge between GFP and DAPI signals, where DAPI represents cell nuclei. Scale bar represents 50 µm.

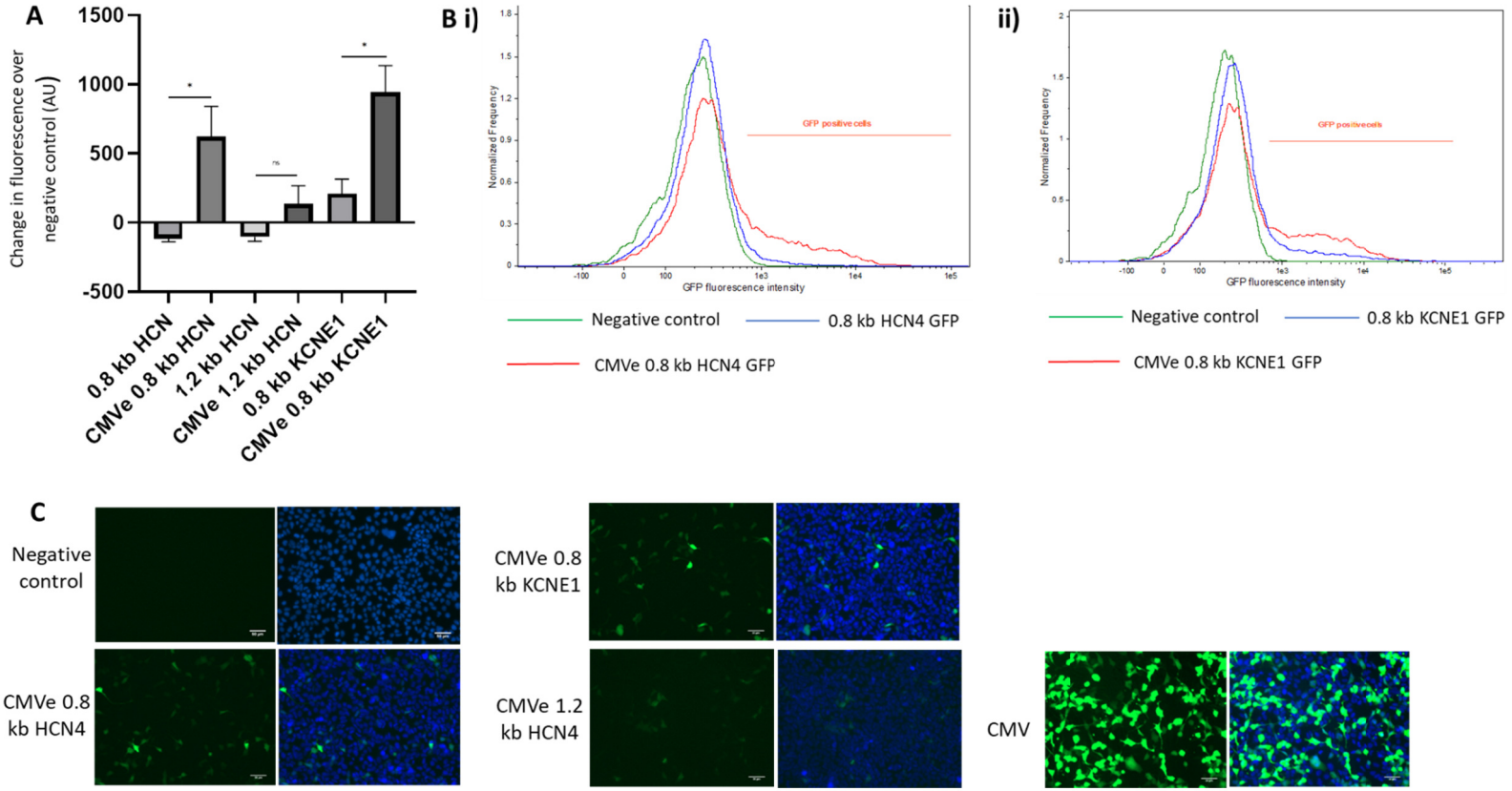

Figure 4.7: Effect of the CMV enhancer on CCS specific promoter candidate activity in HEK 293A cells. A) change in fluorescence over negative control for each promoter construct in NIH 3T3 cells measured by flow cytometry. Data pooled from 3 independent experiments, each comprising 3 technical replicates for each construct. Error bars denote SEM. ns $p>0.05$; *$p \leq 0.05$, **$p \leq 0.01$. ***$p \leq 0.001$, ****$p \leq 0.0001$. One way ANOVA used to determine significance. B) Representative fluorescence histograms for 0.8 kb HCN4 and CMVe 0.8 kb HCN4 GFP (B i) and 0.8 kb KCNE1 and CMVe 0.8 kb KCNE1 GFP (B ii) contrasted with negative control, denoting the distribution of cellular fluorescence after transfection with each promoter construct. GFP positive cells were deemed those with fluorescence higher than 99.5% of cells in the negative (untransfected) control. C) Representative images for each CMVe coupled CCS specific promoter construct 48 hours after transfection into the HEK 293A cell line, collected via fluorescence microscopy. Left panel for each construct depicts GFP fluorescence imaging, left panel depicts merge between GFP and DAPI signals, where DAPI represents all cell nuclei. Scale bar denotes 50 µm.

Promoter construct	Fluorescence change over negative control	Fluorescence change over negative control as % of CMV
CMV	38628 ± 4422	100%
0.8 kb HCN	-117 ± 21	-
CMVe 0.8 kb HCN	427 ± 231	1.11%
1.2 kb HCN	-103 ± 32	-
CMVe 1.2 kb HCN	134 ± 132	0.35%
0.8 kb KCNE1	149 ± 85	0.39%
CMVe 0.8 kb KCNE1	683 ± 283	1.77%
1.6 kb KCNE1	35 ± 51	0.09%
cTnT	0 ± 31	-

Table 4.3: HEK 293A data summary for each promoter construct. Average values displayed for fluorescence change over negative control, ± SEM derived from 3 distinct experiments each comprising 3 technical replicates for each construct.

4.3.2 Comparing promoter activity directly between cell lines

Excitation laser power used for flow cytometry varied across cell lines (see methods, chapter 2 section 2.7). This was due to the fact that the laser power was set using the brightest sample for each cell line (CMV promoter-driven GFP), the activity of which varied across the cell lines used. Some variation in strength of the CMV promoter across various cell lines has been reported previously in the literature[400]. Therefore, in order to compare the activity of each promoter between the various cell lines directly, fluorescence values within each cell line were normalised to an internal control, the CMV GFP construct. Excitation laser power was kept constant for all constructs within each cell line. As previously mentioned, the CMV promoter is highly active across most cell lines and tissues, and is one of the most well characterised strong constitutive promoters[400]. Therefore, normalisation to this construct provides an indicator of promoter activity against a well-known standard, and as previously mentioned, controls for many variables between cell lines (discussed further in discussion section). Fluorescence values normalised to CMV in each cell line are summarised in figure 4.8. It can be seen that in Shox2 cells, GFP fluorescence conferred by most tissue specific promoter candidates was significantly higher compared to both NIH 3T3 and HEK 293A cells, in which GFP signal was minimal compared with CMV. The 1.2 kb HCN4 promoter, the weakest candidate promoter, conferred no significantly higher transgene expression in Shox2 cells compared to HEK 293A cells (figure 4.8). Despite increased activity in NIH 3T3 and HEK 293A cells, CMVe 0.8 kb HCN4 and CMVe 0.8 kb KCNE1 remained highly significantly more active in Shox2 cells as compared with off-target cell lines of HEK-293A and NIH-3T3 ($p \leq 0.0001$) (figure 4.8).

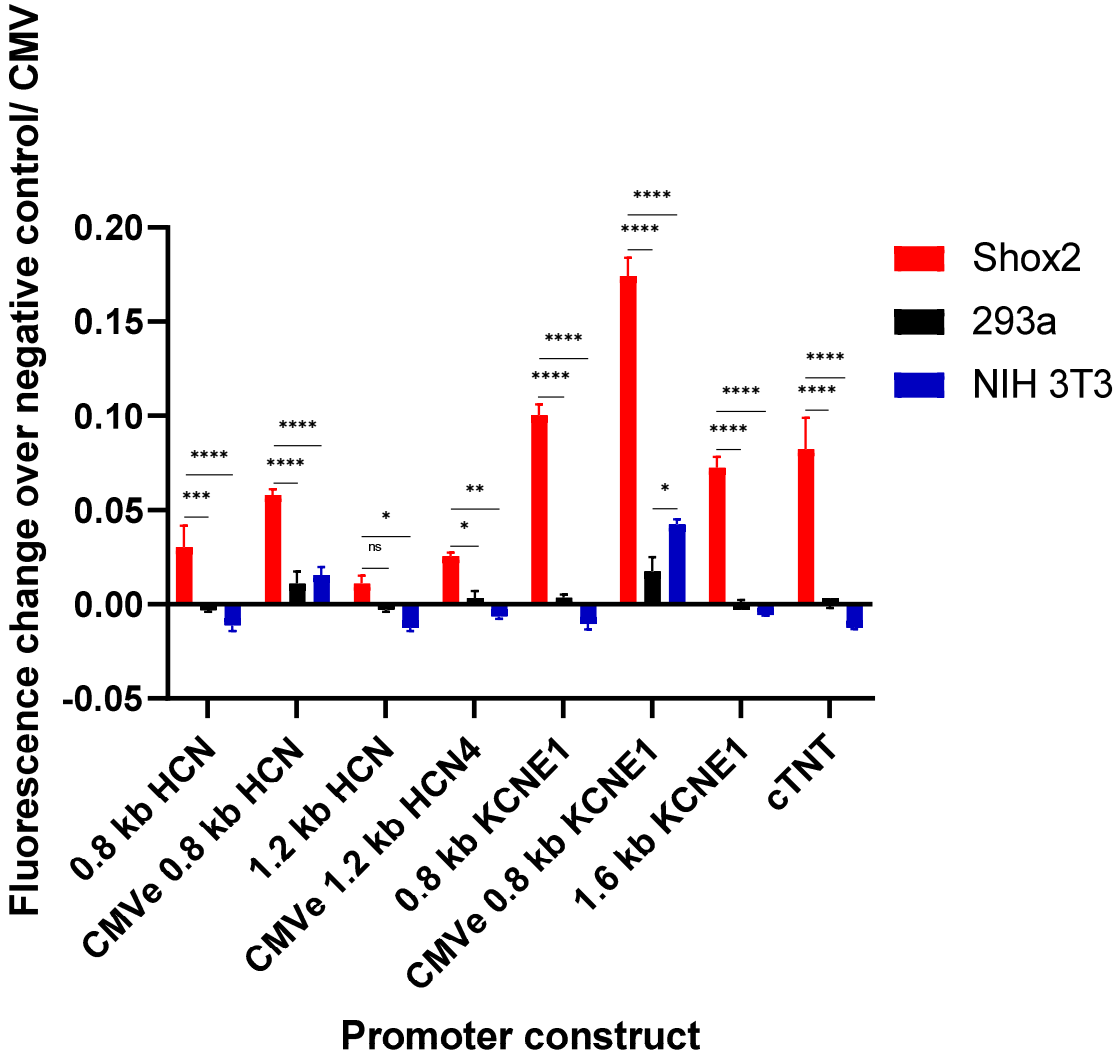

Figure 4.8: Direct comparison of promoter activity across 3 cells lines (Shox2, NIH 3T3 and HEK 293A). Promoter performance quantified as change in fluorescence over negative control normalised to CMV. Ratio of 1 corresponds to no change vs CMV. Error bars denote SEM, derived from 3 (Shox2 and HEK 293A) or 2 (NIH 3T3) experimental replicates. Two way ANOVA used to determine significance. *p ≤ 0.05, **p ≤0.01. ***p ≤0.001, ****p ≤0.0001.

4.4 Discussion

Here we have shown multiple CCS specific promoter candidates with robust transcriptional activity in SAN-like Shox2 cells, and minimal activity in off target cells. Interestingly, shorter HCN4 and KCNE1 promoters appeared more active than their longer counterparts, agreeing with the initial study of the HCN4 core promoter in vitro[118]. This could be due to the presence of additional repressor elements in the extended sequences. To this end, the Kruppel-like Factors (KLF) TFs, hailing from the same family as the SP factors (SP/ KLF family), can act as transcriptional repressors or activators[404]. Group 1 (KLFs 3, 8, and 12) are repressors that interact with carboy-terminal binding protein, Group 2 (KLFs 1, 2, 4, 5, 6) are predominately transcriptional activators, and Group 3 (KLFs 9, 10, 11, 13, 14, and 16) repress transcriptional activity via interaction with a common transcriptional repressor Sin3A[404]. Sin3A contributes to histone deacetylation via the recruitment of HDACs, thus shifting chromatin state towards it's transcriptionally silent form[405]. KLF and SP1 activities and interactions are complex and cell, tissue and context specific[406]. KLFs may compete with SP1 for DNA binding and elicit potent transcriptional repression, for example KLF11 represses the caveolin gene promoter in this way via antagonising SP1[407]. KLF15 is a critical regulator of cardiac electrophysiology via regulating circadian oscillations in KCHIP2[408]. Thus, interactions between SP1 and KLF factors in the extended promoter fragments could act to repress transcription from the promoter. Although the 1.2 kb HCN4 fragment contains 1 additional SP1 site compared to 0.8 kb HCN4, it also contains 3 additional KLF15 and 2 additional KLF11 sites (data not shown). Given the key role documented for SP1 in HCN4 promoter activity[377] it is possible that these additional sites interfere with SP1 mediated transcriptional activation. In addition, Nkx2.5 is a negative regulator of the SAN gene expression profile. In Shox2 -/- mice, ectopic Nkx2.5 expression in the SAN was associated with downregulation of SAN genes including HCN4[393]. The 0.8 kb HCN4 promoter contains only one predicted Nkx2.5 binding site, whilst the 1.2 kb fragment contains an additional 4 (chapter 3, section 3.3.1). Binding of Nkx2.5 to these sites could also present a mechanism by which the activity of the HCN4 promoter is repressed.

Sp1 is also suggested to be a key activator of the KCNE1 promoter[372]. Analysis of the extended 1.6 kb KCNE1 promoter revealed presence of multiple KLF16 binding sites, which could mediate transcriptional repression (data not shown). GATA4 was also found to be a potent activator of the KCNE1 promoter[373]. However, distribution of GATA4 sites cannot explain the higher activity of the 0.8 kb promoter, since it contains only one predicted GATA4 site, whilst the full length 1.6 kb promoter contains two (chapter 3, section 3.3.2, figure 3.4). Thus it is unclear why the shorter promoter fragments appeared more active, though it is possible that the longer fragments contain additional transcriptional repressor elements.

Whilst CCS specific promoters had relatively low activity in Shox2 cells compared with the positive control CMV promoter, this does not mean that their activity is not robust. It could be seen clearly in fluorescence micrographs that all the CCS specific promoter candidates conferred relatively high levels of fluorescence, particularly the KCNE1 promoter variants and CMVe coupled promoters. Imaging cytometry data also confirmed robust increases in fluorescence compared to negative control (untransfected) conditions using all CCS specific candidates, particularly KCNE1 promoters. Ultimately, comparing to CMV sets a high benchmark. In a similar study, activity of the strong cardiac specific promoter cTnT was only 7.03% relative to CMV in the HL-1 cardiac cell line *in vitro*[409]. It is known that *in vivo*, the cTnT promoter confers highly potent cardiac specific transgene expression when delivered via AAV9[205]. In our experiments, cTnT activity was 8.28% of CMV in Shox2 cells, and was outperformed by 0.8 kb KCNE1 (10.05%), CMVe 0.8 kb KCNE1 (17.4%), and virtually the same as 1.6 kb KCNE1 (7.24%). Thus, it is plausible that CCS specific promoter candidates, and cTnT, may be capable of inducing high-level transgene expression in the SAN/ CCS *in vivo.* Validation of these constructs *in vivo* is therefore warranted.

Technically, comparing promoter activity across multiple cell lines is challenging. Several confounding factors vary between cell lines including different proliferative rates of each cell type and differing transfection efficiency. To this end, plasmids introduced to cells by lipofection are not stably integrated into the cellular DNA and thus the expressed transgene will be diluted upon each round of cell division. It is also important to consider in this context that DNA-lipid nanoparticles are stable for approximately 6 hours, and thus after this stage no further transgene will be delivered to cells. From seeding to cell collection, corresponding to 48 h of growth, confluence levels among HEK 293A, NIH 3T3 and Shox2 cells were markedly different, with HEK 293A generally being the most confluent and thus fastest proliferating (data not shown). 48 h incubation was used under recommendation from Invitrogen with lipofectamine 3000, corresponding to the expected peak of transgene expression. This time point should also reduce the impact of varying incubation time upon transgene expression, as the expression should have reached approximately steady state levels. This was important, as flow cytometry experiments were quite lengthy, and thus the last batch of cells analysed would have been incubated for slightly longer than the first.

The method of calculating change in fluorescence over negative control was adapted from another study, in which the effect of the CMV enhancer on various tissue specific promoter candidates was being assessed via flow cytometry[262]. The authors of this study used lentivirus to introduce transgenes to the cells and thus achieved highly efficient transduction, with at least 7 integrated viral genome per cell in the lowest transduced line (fibroblasts)[262]. I intended to use adenovirus for similarly high efficiency transgene delivery to cells. However, as discussed previously, viral

constructs erroneously lacked polyadenylation signals, and thus the true extent of promoter efficacy would have been difficult to assess in light of high level-mRNA degradation. Efficiency of polyadenylation has been shown to dramatically influence transgene expression. Inefficient or absent polyadenylation results in severely impaired transgene expression attributable to decreased steady state mRNA levels after plasmid transfection[385]. This discovery necessitated a change in approach, to lipofection of AAV plasmid constructs into target cell lines. Lipofection proved less efficient in terms of transfection efficiency compared to viral approaches, ranging from 18% in NIH 3T3 cells to 69% in HEK 293A cells. Since change in fluorescence over negative control was calculated by multiplying average fluorescence intensity of GFP by the normalised percentage of GFP positive cells and subtracting background fluorescence, this occasionally led to a negative fluorescence value, particularly when fluorescence intensity was low and background fluorescence relatively high. To this end, the GFP/FITC channel is known to produce high levels of autofluorescence. Nevertheless, the values obtained represented the fluorescence level of the samples effectively. Any negative value or near zero value obtained via flow cytometry analysis also showed little or no fluorescence under fluorescence microscopy.

Transfection efficiencies varied widely according to the cell line used, and were less efficient compared to that expected from viral vectors. HEK 293A cells were the most permissive to lipofection with an average transfection efficiency of 59%, whilst lower efficiencies of 25% and 18% were achieved for Shox2 and NIH 3T3 respectively. Thus, differences in the percentage of GFP positive cells between cell lines represents both differences in transfection efficiency as well as cell type dependent differences in promoter transcriptional activity. Given the percentage GFP positive cells was used in calculating the change in fluorescence over negative control, the main metric for assessing promoter activity, it was important to normalise and account for varying transfection efficiency to generate comparable and meaningful figures. For these reasons, the percentage GFP positive cells for each construct was normalised to the transfection efficiency, which was determined using the CMV GFP construct. As discussed, the ubiquitous CMV promoter typically shows strong transcriptional activity in most cell lines and thus serves as an effective standard. For example, if the transfection efficiency in given experiment was deemed to be 25% using the CMV construct, it was assumed that the transgene was effectively delivered to 25% of cells. Within one individual experiment, this transfection efficiency was then extrapolated to the rest of the constructs. This normalisation also provided a method of accounting for differing transfection efficiencies between individual experiments using the same cell line. These differences may arise from varying cell seeding densities and small methodological deviations such as incubation time between experiments. Reproducibly seeding cells between experimental replicates was particularly

challenging for Shox2 cells, since they grow in aggregated clumps which are difficult to separate and count. Albeit minimal, these inter-experiment disparities could significantly impact the change in fluorescence over negative control values. It must be considered that the transfection efficiency applied remained an approximation, and thus may not completely accurately reflect the true transfection efficiency for each individual plasmid transfection. Importantly however, within one given experiment, transfection efficiencies were highly reproducible between technical replicates, and so this method of normalisation for transfection efficiency in this context was well founded.

For comparing the activity of CCS specific promoter candidates between different cell lines, the change in fluorescence over negative control was normalised to that of the positive control, CMV. I.e. values for each construct were divided by that for the CMV construct in the corresponding experimental replicate to yield a ratio. Normalising the change in fluorescence for each promoter construct to the CMV construct in each cell line provided a means of accounting for inter-cell line confounders such as varying proliferative rates and differing illumination power used in GFP detection. In this way, CMV acted as an internal control and benchmark against which to assess the activity of other constructs under the same experimental conditions. Importantly, GFP illumination power settings used in imaging cytometry were always kept constant for all constructs using the same cell line. CMV provided an effective benchmark as a widely used strong constitutive promoter that is highly active across most cell lines and tissues *in vivo*. Despite its warranted use as a benchmark for such normalisation, it must be considered that the CMV promoter does show moderately differing activity across different cell lines. Thus, in a cell line where the CMV promoter is less active, other promoters may appear more active in comparison. Nevertheless, I believe it a worthy comparison and an effective means of accounting for the inter-cell line variables discussed.

CMV promoter activity was particularly high in HEK 293A cells. Illumination power on the flow cytometer was set using the brightest sample (CMV in all cases) to avoid saturation of the detector and thus skewing of data. Inter-cell line variability in CMV activity necessitated using different laser powers between different cell lines (see chapter 2, section 2.7). Significant range in GFP brightness was observed in the CMV group for all cell lines. Imaging cytometry fluorescence distribution histograms demonstrated some cells had fluorescence levels approaching the upper end of the scale before saturation, whilst many were also at the lower end of brightness above background. Thus, the illumination power was set relatively low for the detection of less bright cells, although this was necessary to avoid saturation at the upper end of the scale. Again, the use of different illumination powers makes direct comparison of promoter activity between cell lines difficult. This provided further basis for normalising the fluorescence conferred by tissue specific constructs relative to CMV for inter-cell line promoter performance comparisons.

ESC derived Shox2 cells may not perfectly replicate native SAN/ CCS tissue in terms of their molecular expression profile, and the *in vitro* environment is of course markedly different from the *in vivo* context. This is discussed further in chapter 6, general discussion. However, given their SAN-like gene expression profile and characteristics, these cells are likely an adequate model for SAN tissue at least, and the promising performance of CCS tissue specific promoter candidates in this system warrant further testing *in vivo*.

4.5 Summary and conclusions

In summary, 0.8 kb and 1.2 kb HCN4 promoters, in addition to 0.8 kb and 1.6 kb KCNE1 promoters appear to be capable of conferring transgene expression in SAN- like cells whilst maintaining specificity for SAN / CCS tissue. To this end, the strongest CCS specific candidate, 0.8 kb KCNE1, achieved fluorescence levels 10.05% of those achieved by CMV, whilst the weakest, 1.2 kb HCN4, conferred fluorescence levels of 1.07% as a proportion of CMV (table 4.1). Importantly, all these promoters also showed high cell- type specificity. Although addition of the CMV enhancer element to these promoters modestly increases their transcriptional strength in Shox2 cells, this appears to compromise their tissue specificity at least to some extent *in vitro*. To this end, GFP fluorescence levels conferred by the strongest hybrid promoter in Shox2 cells, CMVe 0.8 kb KCNE1, were 17.40% of those achieved by the CMV enhancer/ promoter construct. However, increases in fluorescence were also seen in NIH 3T3 and HEK 293A cells, albeit still significantly lower than those conferred by the native CMV enhancer/ promoter construct. Thus, it would be interesting to see if the hybrid promoter can perform comparably to CMV in terms of promoter strength, and how the addition of the CMVe element may influence tissue specificity *in vivo.*

For *in vivo* testing, AAV9 was chosen as a gene delivery vector. AAV9, whilst being a highly cardiotropic gene delivery vector, also delivers transgenes effectively to many tissues when administered systemically[199,200,401]. Thus, a strong tissue specific promoter with high specificity for SAN / CCS tissue is necessary in order to spatially restrict transgene expression and minimise off target effects. Further testing of these candidate constructs *in vivo* using AAV9 vectors is necessary to validate their utility for specific transgene expression in native tissues.

5.0 Chapter 5: Results- *In vivo* testing of promoter constructs using AAV9

5.1 Introduction

Vorburger and Hunt[146] eloquently set out the key characteristics for consideration in gene therapy vector development, stating that "the perfect vector system for use in gene therapy would be administered by a non-invasive route, would target only the desired cells within the target tissue, and would express a therapeutic amount of transgene products with desired regulation for a defined duration." As detailed in chapter 4, all CCS specific promoter constructs showed promising transcriptional profiles *in vitro*, inducing robust GFP transgene expression in Shox2 sinoatrial node-like cells and minimal expression in non-SAN cell lines cell lines (HEK 293A and NIH 3T3). This suggested that the criteria for tissue specific expression and therapeutic levels of transgene expression could be within reach using our candidate promoters. In order to assess the potential of these promoters to drive therapeutically relevant transgene expression restricted to the CCS *in vivo*, I aimed to test the constructs via packaging into AAV9 vectors and administering to adult mice. Addressing the criterion for non-invasive administration, I opted for tail vein injection of the vectors. The systemic venous route is a widely used administration method for AAV vectors, and AAV9 injected in this way targets the heart and other tissues extremely effectively[199,410].

All studies of AAV mediated gene delivery to the heart examine the working myocardium of the atria or ventricles, and so I first sought to assess whether the distinct, specialised tissues comprising the cardiac conduction system could be transduced effectively by AAV9 after systemic intravenous delivery. To this end, numerous studies have demonstrated the distinct structural and molecular makeup of the SAN[347], AVN and Purkinje fibres[60] in comparison to working myocardial cells[1,411] and thus it remains to be seen whether these tissues can be targeted systemically by AAV9 vectors. This could be assessed using the constitutively active CMV promoter, which has been shown to be highly active in most tissues[206,410]. After optimising gene delivery conditions for CCS targeting using the CMV construct, (in terms of viral dose, incubation time, tissue processing for GFP detection), I aimed to test CCS specific promoter candidates in the same way. In addition, I aimed to test another well characterised minimal cardiac specific promoter, cTnT, which induces high level transgene expression in the working myocardium. cTnT is also highly expressed in the SAN, and so cTnT could provide a means of delivering transgenes to the SAN in a cardiac specific context[261]. *In vitro* studies also confirmed robust activity of the cTnT promoter in Shox2 cells. This could prove useful where therapeutic targets of interest are not expressed outside the heart or in the working myocardium, such as CCS specific miRs. For example, when aiming to inhibit miRs only expressed in the CCS and

not in the working myocardium, cardiac specific expression of miR inhibitor transgenes would be appropriate as long as the promoter is active in the CCS as well as working myocardium.

5.2 Hypotheses and aims

I. AAV9 can effectively target the CCS via a single systemic intravenous dose of vector.

II. Transgene expression can be restricted to the CCS using minimal KCNE1 and HCN4 tissue specific promoters.

III. AAV9 cTnT GFP is capable of conferring transgene expression in the CCS in a cardiac specific context (pan-cardiac expression including CCS).

5.2.1 Aims

I. Assess the capacity for CCS genetic targeting using systemic intravenous administration of AAV9.

II. Assess the performance of CCS specific promoter candidates *in vivo*, in terms of transcriptional strength and tissue specificity using detection of the GFP reporter.

5.3 AAV9 CMV GFP

As detailed in methods, 5 weeks after administration of AAV9 vectors, GFP, and HCN4 for SAN sections, were detected via immunohistochemistry to track reporter transgene delivery throughout multiple organs. In 4 chamber heart sections, the SAN appeared as a small, discrete HCN4 positive region at the junction of the SVC and RA, as expected (figure 5.1).

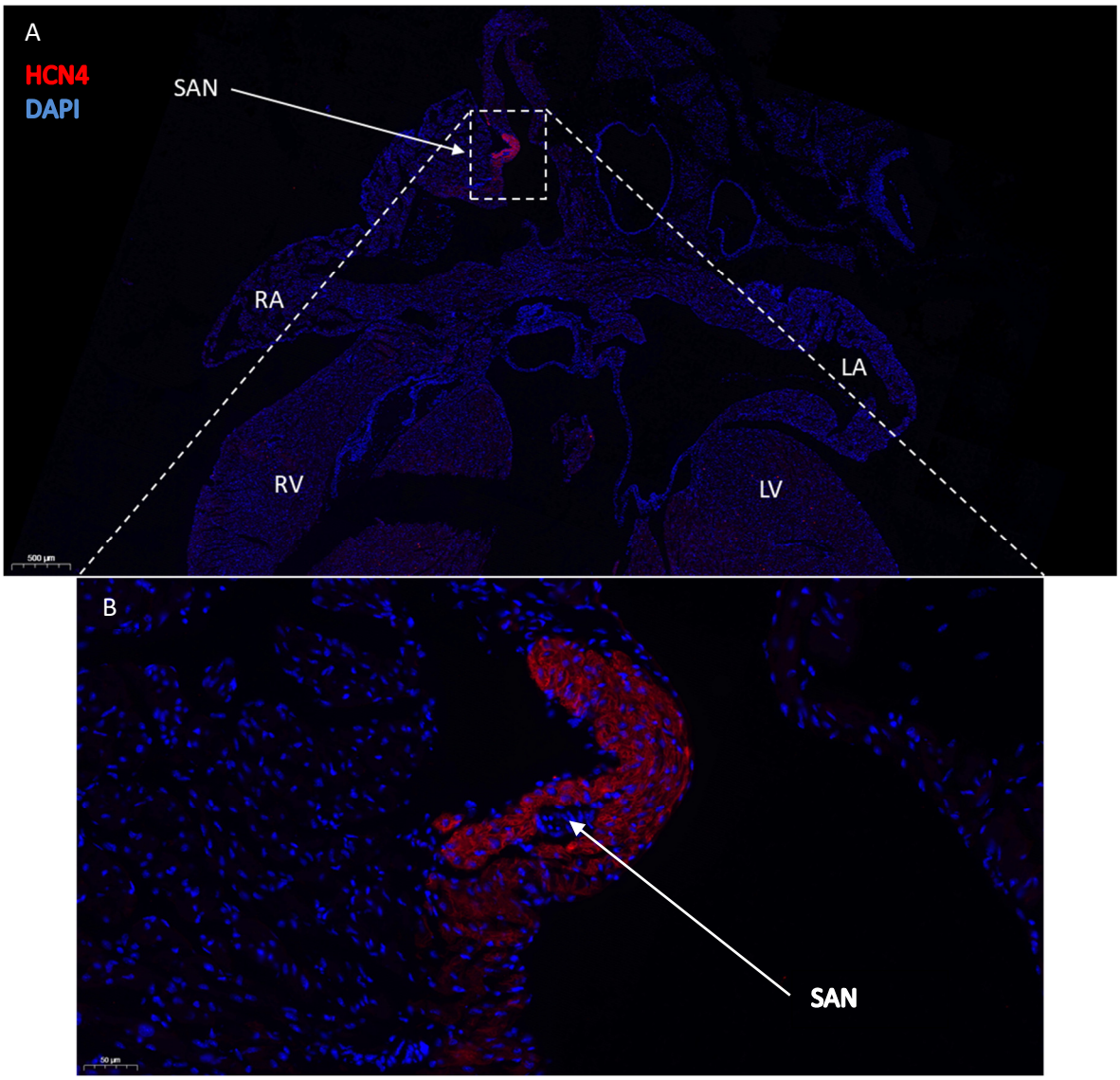

Figure 5.1: visualisation of the SAN in 4 chamber heart sections. A) Low magnification image of the heart, cut in the sagittal plane. HCN4 pseudocoloured red demarcates the SAN, DAPI (blue) demarcates cell nuclei. Scale bar denotes 500 µm. B) High magnification image of the SAN from panel A. The SAN is identified by intense HCN4 staining (red) and the SAN artery. Scale bar denotes 50 µm. RV- right ventricle; LV- left ventricle; RA- right atrium; LA- left atrium.

AAV9-CMV-GFP was used to determine optimal experimental conditions for gene delivery to the CCS. This vector has previously shown potent transgene expression in most tissues *in vivo* after systemic administration, including the heart, and so served as an effective positive control to assess efficiency of viral transduction and transgene delivery[412,200,206,410]. GFP expression was confirmed in all tissues harvested from AAV9-CMV-GFP injected animals, comprising the heart, liver, lung, skeletal muscle, kidney and brain (figure 5.2). GFP expression appeared highest in the heart (ventricle, atrium, SAN) and liver (figure 5.2).

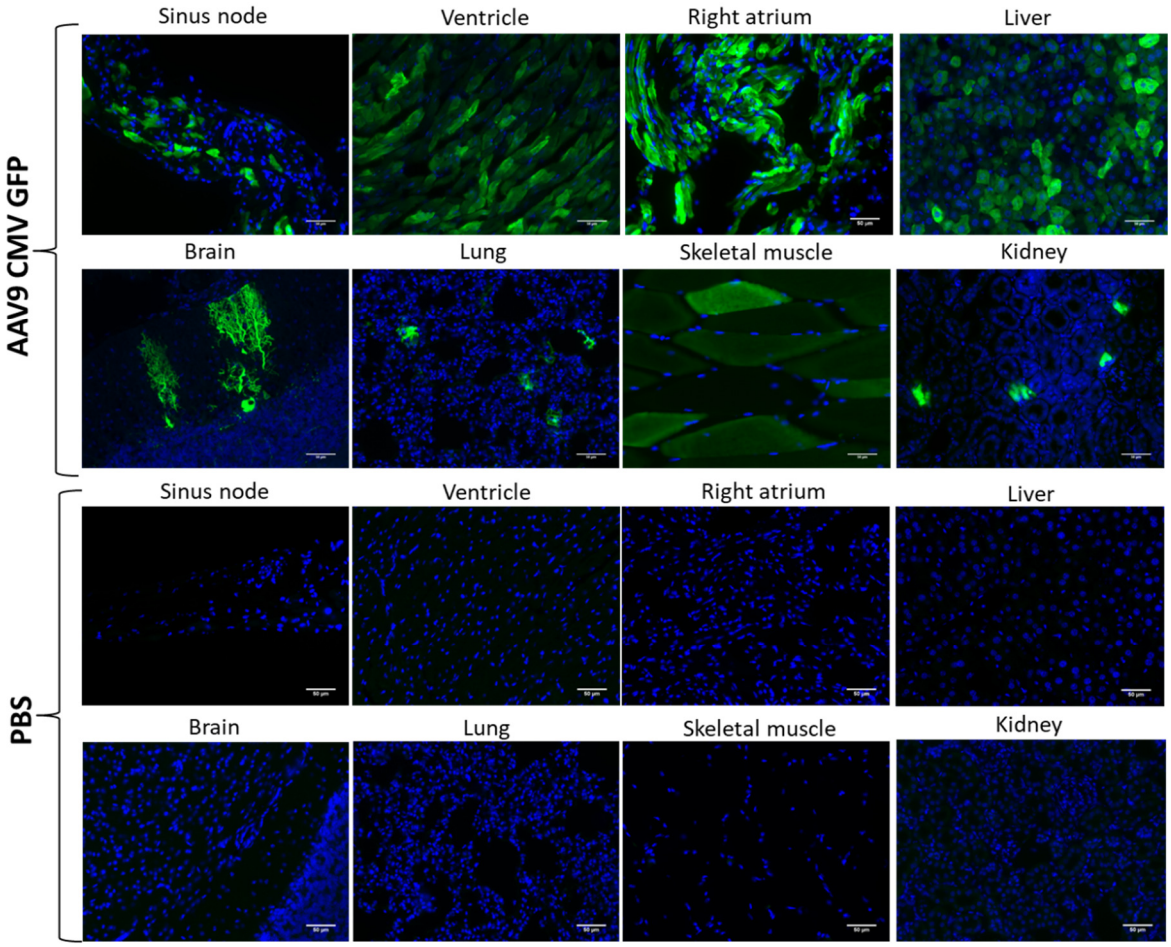

Figure 5.2: AAV9-CMV-GFP mediated transgene expression in multiple tissues visualised by immunohistochemistry. Green represents GFP, DAPI cell nuclei. Comparable images from a negative control (PBS) injected mouse are shown for comparison (lower panels), where no GFP positive cells are evident.

In some sagittal 4 chamber heart sections, the entire CCS could be observed (SAN, AVN and Purkinje fibres). Initial examination revealed apparent differences in transduction efficiency between components of the CCS. The AVN was seemingly less efficiently transduced compared to the SAN (figure 5.3), with only a few GFP positive cells, and GFP expression was virtually absent from the Purkinje fibres examined (figure 5.4). It is important to bear in mind that these findings from the AVN and Purkinje fibres are representative from only a very small sample size (1 heart) and thus conclusive evaluation of AVN and Purkinje fibre transduction by AAV9 requires further investigation. This information was merely used to guide further experiments, and thus detailed subsequent analyses on CCs transgene expression focussed on the SAN in light of severe time restrictions imposed by the Covid-19 pandemic.

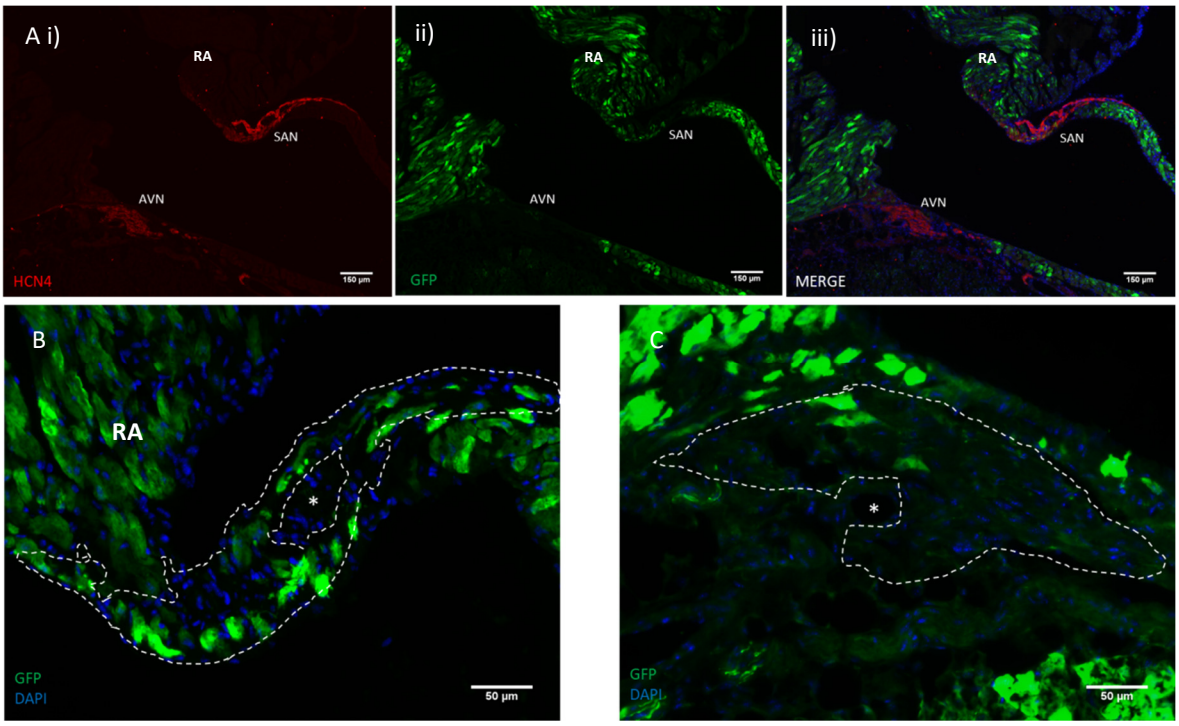

Figure 5.3: Regional transduction efficiency in the CCS after administration of AAV9 CMV GFP. A) Sagittal view of the SAN and AVN at low magnification. i) The SAN and AVN are identified by positive HCN4 staining (pseudocoloured red), whereas the working myocardium is devoid of HCN4 signal. ii) GFP fluorescence (green) in the same field as in panel A i. iii) HCN4 and GFP signals merged and combined with DAPI signal (blue) demarcating cell nuclei, showing distribution of GFP expression in the working myocardium and conduction tissues of the SAN and AVN. GFP appears to be lowly expressed in the AVN in particular. B) High magnification image showing GFP expression (green) in the SAN in adjacent tissue section to that shown in panel A. Dotted lines demarcate the SAN, asterisk identifies the SAN artery. C) High magnification image showing GFP expression (green) in the AVN in adjacent tissue section to that that shown in panel A. Dotted line demarcates the AVN. Asterisk identifies the AVN artery. Representative of 1 heart, 2 individual sections. RA- right atrium. SAN- sinoatrial node. AVN- atrioventricular node.

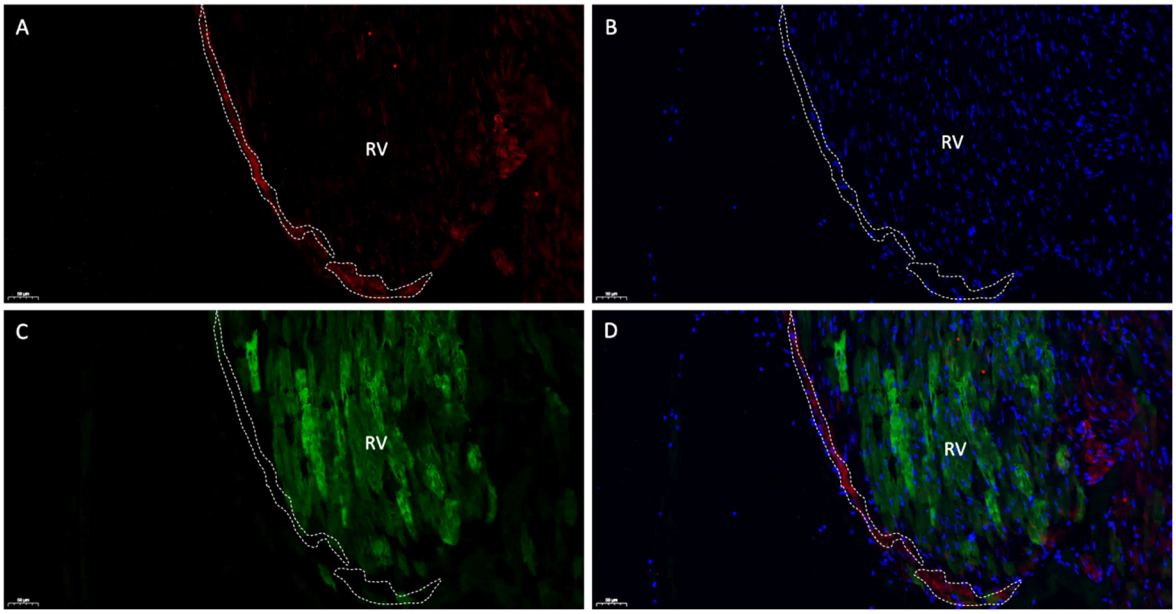

Figure 5.4: Transduction of the Purkinje fibres after administration of AAV9-CMV-GFP. A) HCN4 staining (red), identifying Purkinje fibres as thin streaks of HCN4 positive tissue adjacent to the ventricle. Purkinje fibres are demarcated by the dotted line in this panel and throughout. The right ventricular working myocardium (RV) is devoid of HCN4 signal as expected. B) DAPI staining in the same field as in A, showing distribution of cell nuclei. C) GFP staining (green) in the same field as in A and B, showing high GFP expression in the RV, and low/ absent expression in the Purkinje fibre demarcated by dotted line. D) merge of panels A, B, and C. HCN4, GFP, and DAPI are represented by red, green and blue staining respectively. Representative of 1 heart, 2 individual sections.

5.4 AAV9 cTnT GFP

A minimal cardiac troponin T (cTnT) promoter in combination with the cardiotropism of the AAV9 capsid is capable of providing high level cardiac specific transgene expression after systemic administration[12] and direct intracardiac injection in mice[363]. Recent proteomic and transcriptomic studies have also demonstrated high expression of contractile proteins, including cTnT in the mouse SAN[261]. With this in mind, I next set out to evaluate the potential of AAV9-cTnT-GFP in directing transgene expression to the SAN in a cardiac specific context. As expected, the cTnT promoter drove expression of GFP in both the atrial and ventricular myocardium, although expression in the right atrium appeared higher compared to the ventricle (figure 5.5). Some GFP expression was also observed in the liver (figure 5.5). The SAN showed some GFP expression, albeit significantly lower than that in the atria and ventricles (figure 5.5).

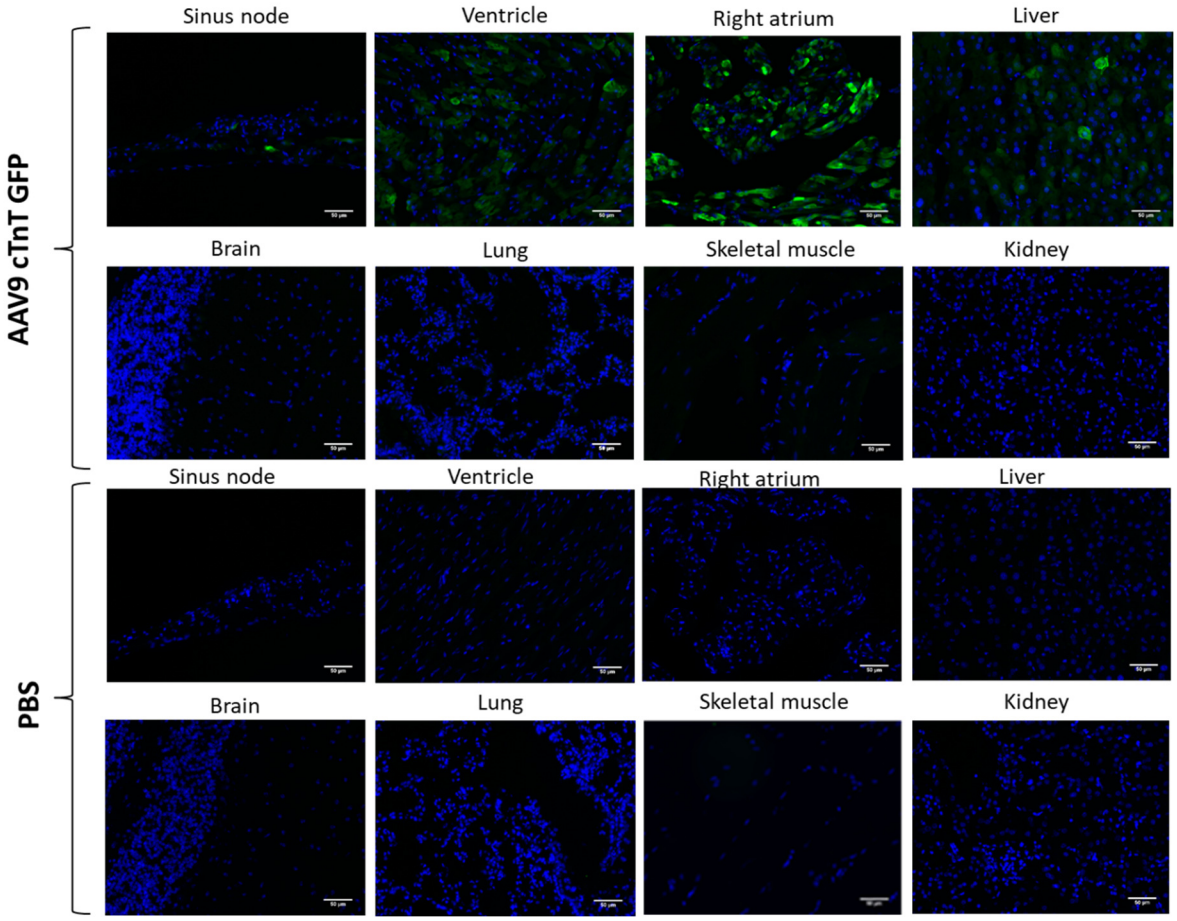

Figure 5.5: AAV9 cTnT GFP mediated transgene expression (green signal) in multiple tissues visualised by immunohistochemistry. Comparable images from a negative control (PBS) injected mouse are shown for comparison, where no GFP positive cells are evident. Cell nuclei are demarcated by DAPI staining (blue signal).

Next, GFP expression in the SAN was examined in detail using cTnT and CMV promoters. AAV9-CMV proved effective for SAN gene delivery, with 65% of SAN myocytes expressing the GFP transgene (figure 5.6 A i, figure 5.6 B). Notably, the proportion of GFP positive cells appeared lower than that of working myocardial cells of the juxtaposed atrial tissue, where almost 100% of cells were GFP positive (figure 5.6 C).

Next, activity of the AAV9-cTnT-GFP construct was assessed in the SAN. The cTnT promoter proved less effective compared to CMV, with 7.23% of SAN tissue GFP positive ($p \leq 0.01$) (figure 5.6 A i, figure 5.6 B). Although the proportion of SAN tissue expressing GFP was low using the cTnT promoter, GFP positive cells appeared relatively bright, albeit significantly less so compared with CMV. Average GFP fluorescence intensity using cTnT and CMV promoters was quantified at 1833.96 and 4052.04 arbitrary units in the SAN respectively, representing a 75.4% difference ($p \leq 0.05$) (figure 5.6 B ii). In order to give a more complete measure of promoter performance for comparison, percentage GFP positive tissue was multiplied by the average fluorescence intensity, to give total GFP fluorescence. Total fluorescence from the CMV promoter was approximately 20 fold higher than cTnT, quantified at 2633.8 and 132.6 arbitrary units respectively ($p \leq 0.05$) (figure 5.6 B iii).

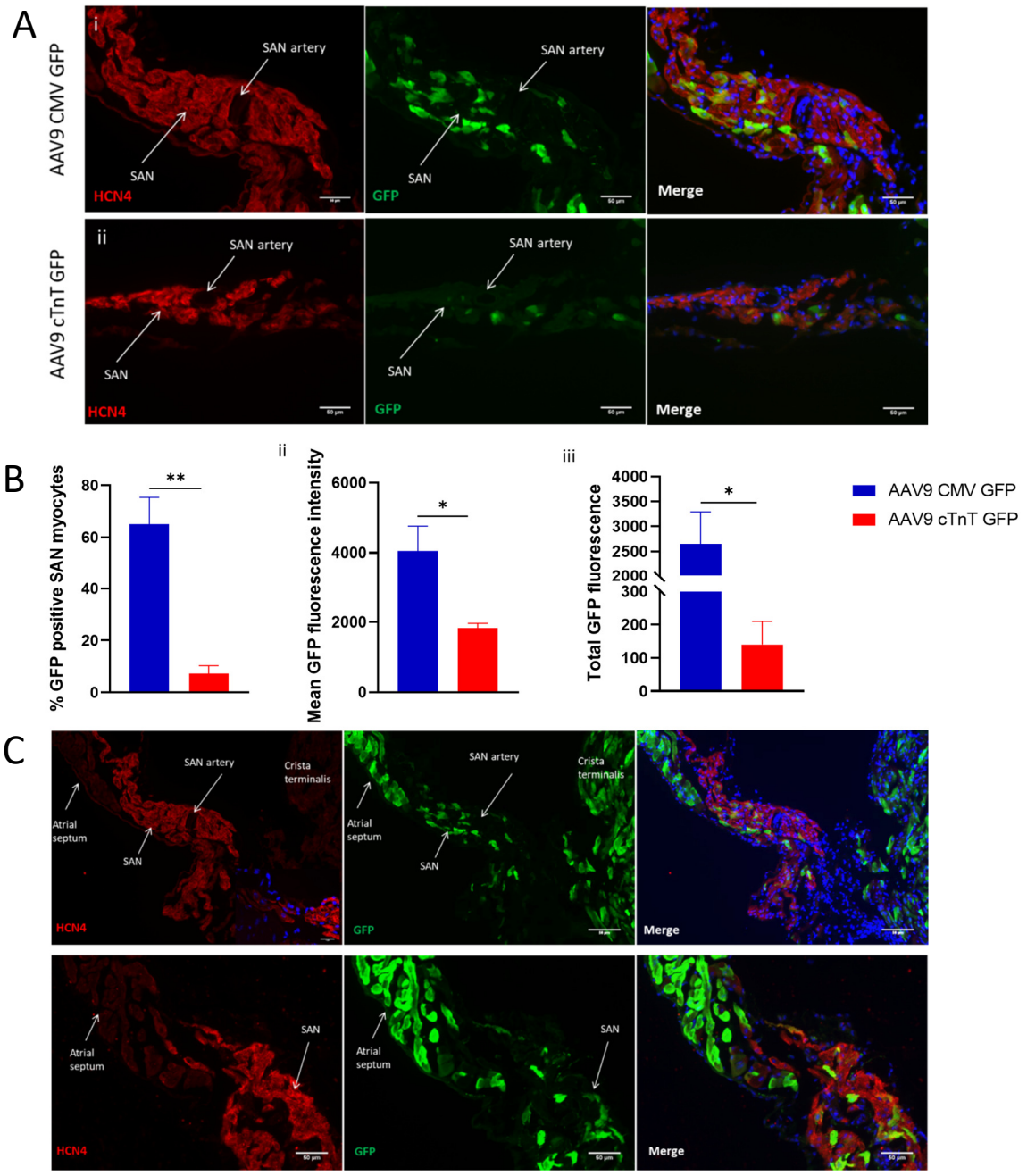
A
AAV9 CMV GFP
AAV9 cTnT GFP
i
ii
SAN artery
SAN
HCN4
GFP
Merge
B
% GFP positive SAN myocytes
Mean GFP fluorescence intensity
Total GFP fluorescence
**
*
AAV9 CMV GFP
AAV9 cTnT GFP
C
Crista terminalis
Atrial septum

Figure 5.6: GFP transgene expression in the SAN from AAV9 vectors. A) Representative GFP expression in the SAN from i) AAV9 CMV GFP and ii) AAV9 cTnT GFP vectors. B) Quantification of GFP expression in the SAN from AAV9 CMV GFP and AAV9 cTnT GFP. i) percentage GFP positive cells, ii) mean fluorescence intensity of GFP positive tissue, iii) total fluorescence, calculated as mean fluorescence intensity multiplied by the percentage GFP positive area. C) direct comparison of GFP expression driven by AAV9-CMV in SAN tissue and adjacent atrial tissue comprising the crista terminalis and atrial septum (representative images). Scale bars denote 50 µm. Data and representative images derived from 3 hearts per construct, from which at least 3 central SAN sections were quantified. Error bars denote SEM. *p ≤ 0.05, **p ≤ 0.01. Significance assessed using unpaired T-test

SAN sections were examined in detail to assess distribution of GFP positive cells. Using the cTnT promoter, it appeared that GFP was more highly present in SAN myocytes that border the region between the crista terminalis (CT) and the SAN (figure 5.7 A, B). This suggests that the cTnT promoter is capable of driving higher levels of transgene expression in a select population of SAN myocytes.

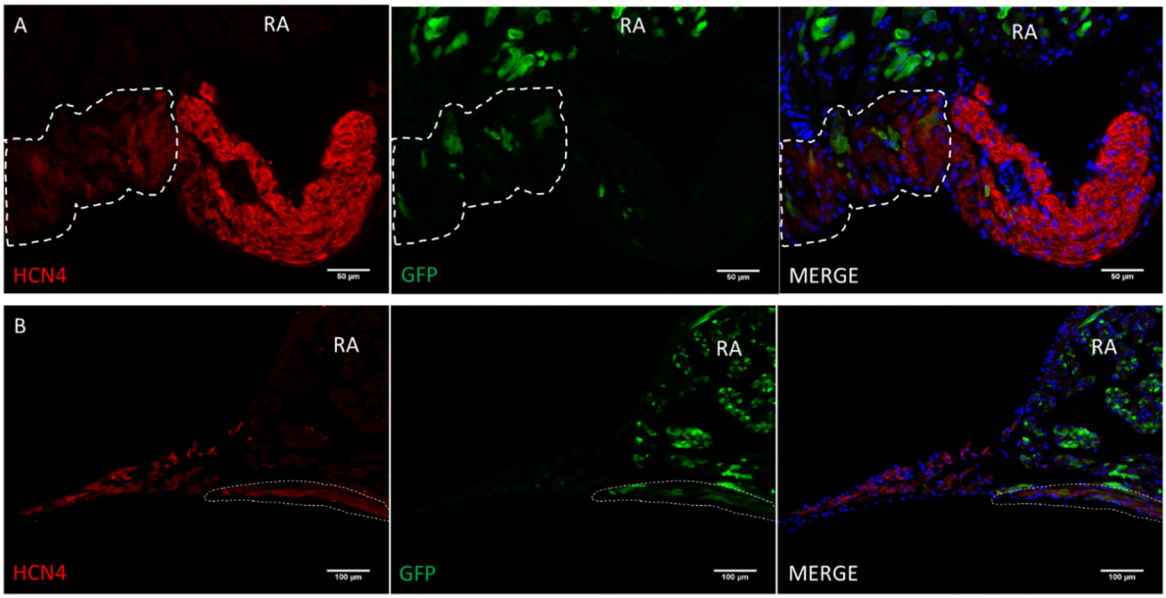

Figure 5.7: Distribution of GFP transgene expression driven by AAV9-cTnT-GFP in the mouse SAN in 4 chamber view (A) and in isolated SAN preparations (B). Peripheral SAN zone corresponds to area enclosed by dotted white line, in which GFP expression appears higher compared to central SAN region. RA- right atrium. A- scale bar denotes 50 µm, B- scale bar denotes 100 µm. Representative images from 3 hearts, from which at least 3 SAN tissue sections were examined.

5.5 AAV9 0.8 kb HCN4/ 1.2 kb HCN4/ 1.6 kb KCNE1

Next, CCS tissue specific promoter constructs 0.8 kb HCN4, 1.2 kb HCN4, and 1.6 kb KCNE1 were tested. As shown in chapter 4, these promoters showed a favourable transcriptional profile in ESC derived sinoatrial node-like myocytes (Shox2 cell line). Due to time constraints and the impact of the COVID-19 pandemic, the 0.8 kb KCNE1 promoter and all constructs carrying CMV enhancer could not be packaged into AAV9 and tested *in vivo*. Contrary to the *in vitro* results, neither the 0.8 kb or 1.2 kb HCN4 variants, nor the 1.6 kb KCNE1 promoter conferred any measurable GFP expression in the CCS tissues examined, evidenced by lack of GFP signal above background levels (figures 5.8 – 5.10).

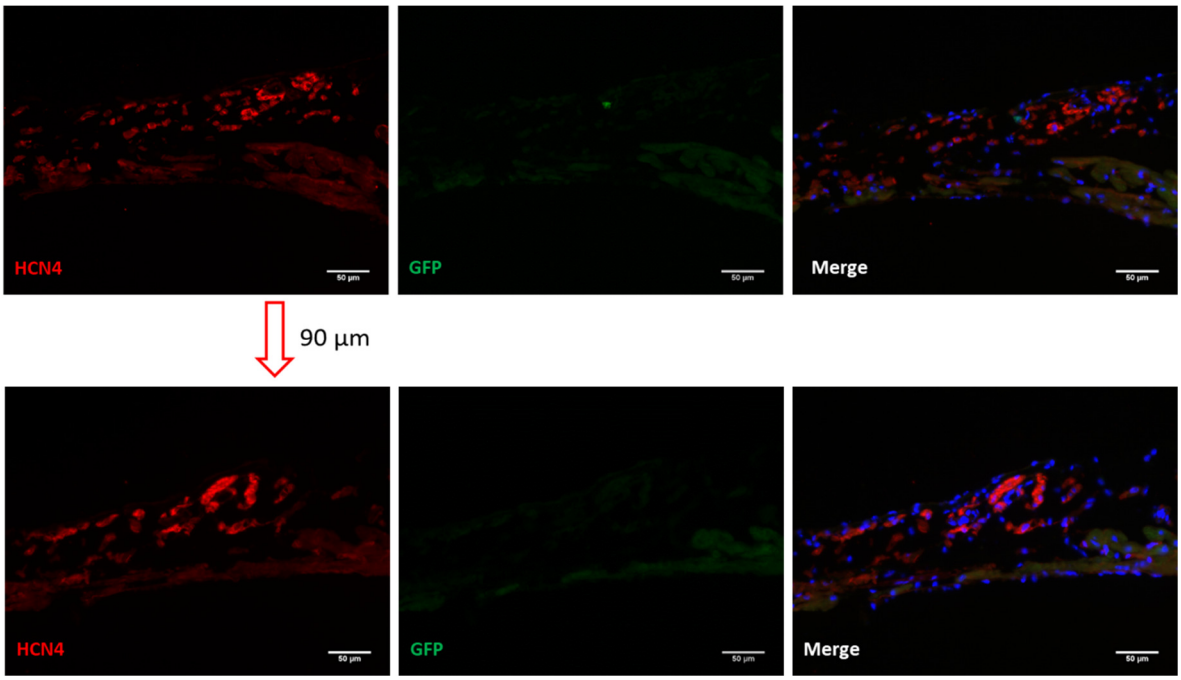

Figure 5.8: 0.8 kb HCN4 promoter activity in the SAN *in vivo*, conferred by intravenously administered AAV9-0.8 kb HCN4 GFP. Sections at various planes over a total z axis distance of 90 um (6 sections) were examined to verify lack of observable transgene expression. Representative from 3 hearts.

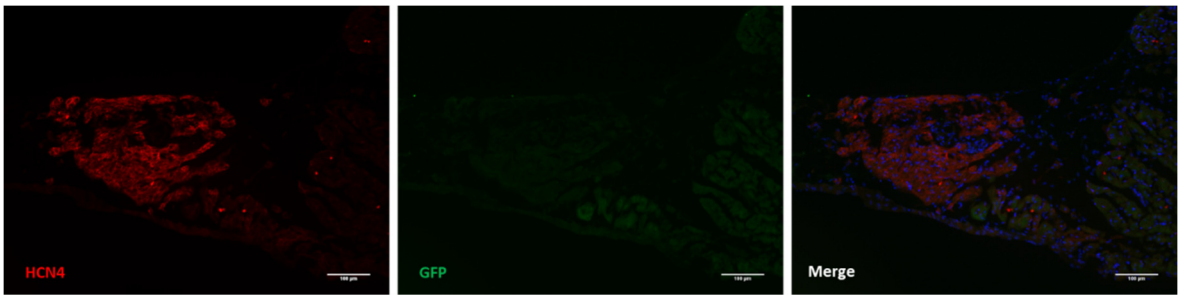

Figure 5.9: 1.2 kb HCN4 promoter activity in the SAN *in vivo*, conferred by intravenously administered AAV9-1.2 kb HCN4 GFP. The SAN is demarcated by HCN4 positive labelling (left panel), whilst GFP expression is absent above background levels (middle panel). Right panel shows HCN4 and GFP channels merged. Representative from 3 hearts. Scale bar denotes 100 µm.

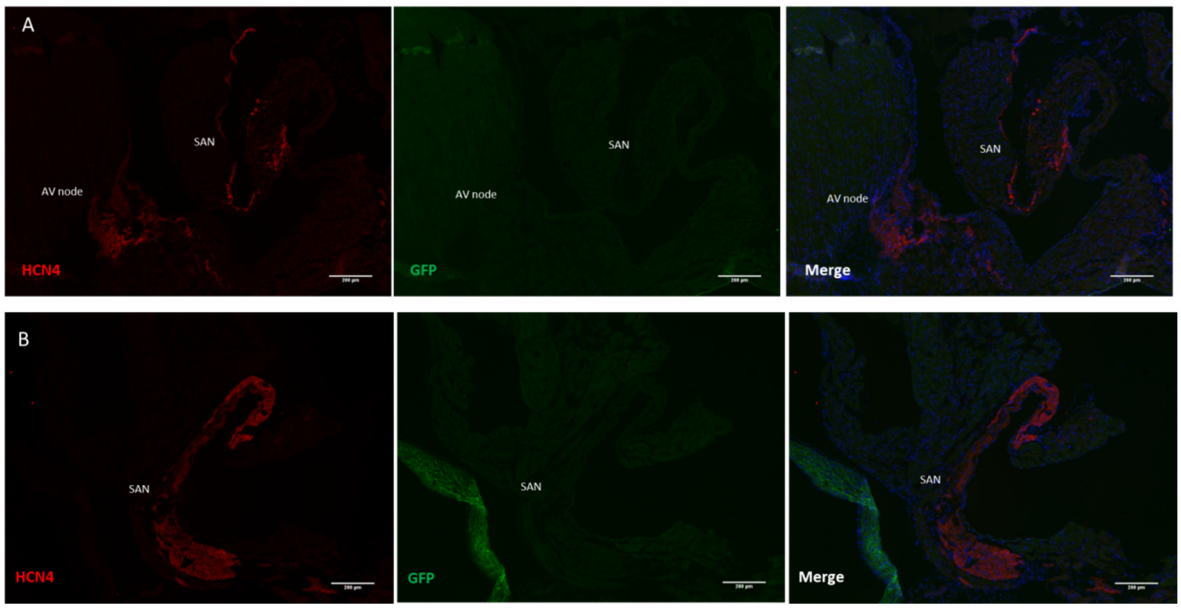

Figure 5.10: 1.6 kb KCNE1 promoter activity in the SAN and AVN in vivo, conferred by intravenously administered AAV9-1.6 kb KCNE1 GFP. CCS tissues are demarcated by HCN4 positive labelling. A) low magnification view of the SAN and AVN regions in a 4 chamber heart section. B) detailed view of the SAN, demarcated by HCN4 positive immunolabelling. Scale bars denote 200 µm.

5.6 Discussion

A number of variables must be considered when considering testing a gene therapy vector *in vivo*. Variables in a multitude of experimental conditions in the literature make direct comparison and determination of optimal experimental conditions challenging. Firstly, the age of the animals used is important. Older and thus larger animals will have differing biodistribution of systemically administered vectors and larger organs may be more difficult to transduce with high efficiency- thus vectors are often dosed in terms of vector genomes per kilo of body weight. Beyond this, tissues have shown intrinsic variability in transduction profiles between adult and newborn mice, depending on their development stage- for example, the liver[413], kidney[414] and aorta[413] are more efficiently transduced in adult mice by AAV compared to neonatal. This is partially attributable to the vigorous cellular proliferation that occurs in many organs, such as the liver, in neonatal life, where non-integrating AAV vectors are gradually diluted and lost from progeny cells[415]. Cardiomyocytes have shown the capacity to proliferate up until around postnatal day 7[416].

The route of vector administration must also be considered. For clinical applications, a non-invasive route would be desirable. Intravenous injection is one of the most widely used and studied in animal models. Various studies have already shown that AAV9 facilitates extremely high and preferential cardiac transduction after systemic intravenous injection in adult mice[401,412,205]. Such studies often involve injection into the superficial veins of the tail or face. Other methods including intramyocardial injection[363,417,418] have proven capable of conferring high transduction of the heart with ameliorated expression in off target tissues, however the invasive nature of the associated procedure and limitation of the transduced region close to the injection site often limit the utility of this technique in practice. Furthermore, for targeting of minute tissues comprising the CCS, direct injection is not appropriate owing to poor access to the tissues via thoracotomy and their small size. To this end transmurally, the human SAN is only 1-2 mm thick and thus direct injection *in situ* would be exceptionally difficult, and in small mammals, virtually impossible[419]. Selective intracoronary perfusion with adenoviral vectors has previously been used to target the AVN in pigs, with a transduction of approximately 50% in AV nodal myocytes, although some transgene expression was also observed in the liver, kidney and ovaries[341]. This approach involved catheterisation of the AV nodal branch of the right coronary artery, with infusion of adenoviral vectors combined with VEGF and nitroglycerin to promote microvascular permeability and vasodilation respectively. Adenoviral vectors, whilst providing high transduction efficiency and rapid onset gene expression, are only capable of providing short term transgene expression due to high immunogenicity[420]. Furthermore, in small animal models such as mice, effective catheterisation of these minute vascular structures would be extremely challenging.

The time between vector administration and examining transgene expression also varies greatly within the literature, and it has been shown that transgene expression from AAV exhibits a lag phase after which maximal transgene expression is achieved[194]. One study administered 1 x 10^{12} AAV9 vector genomes containing a CMV promoter driven alkaline phosphatase reporter gene to 8 week old mice via the tail vein, and examined the expression 12 weeks after administration. Highly effective cardiac transduction was achieved using these conditions[413]. Another study administered 1 x 10^{11} vector genomes to 8 week old mice via tail vein injection, and examined the time course of luciferase expression driven by AAV9-CMV promoter. Transgene expression increased steadily from day 7 post injection, peaking at 100 days and declining modestly thereafter. AAV9 also had the highest total luciferase expression, and the highest cardiac expression of all serotypes tested[410]. Similarly, another study found that transgene expression from AAV9 increased steadily after day 7 post-injection, roughly doubling between days 7 and day 35[421]. Another similar study noted maximal GFP transgene expression from AAV9 after systemic IV administration at 5 weeks post vector administration in 8 week old mice, with modest decline at 8 weeks post-injection[206]. Using an IV dose of 1 x 10^{11} vg, the authors noted significant transgene expression only in the heart and liver driven by the CMV promoter, with over 80% cardiac transduction efficiency at 5 weeks post injection[206]. Another study demonstrated only 21% cardiac transduction with the same dose after 4 weeks in adult mice, significantly lower than that achieved in neonatal mice[412]. Similarly, only 2% of the left ventricle was successfully transduced after IV injection of AAV9 CMV GFP at 1 x 10^{11} dose, increasing significantly with an elevated dose of 1 x 10^{12} [160].

AAV transduction follows a dose dependent relationship, and thus higher numbers of vector genomes injected will give higher transduction rates and thus higher transgene expression[160,422]. AAV transduction of the heart after systemic administration follows a Poisson distribution, where on average, a transduction hit rate of 5 vector genomes per cell is required to achieve >99% transduction efficiency[205]. It is likely that even greater levels of transduction are necessary when dealing with weak promoters, where transcription of the transgene may be inefficient and at low levels compared to strong promoters such as CMV. For example, one study demonstrated atrial specific transgene expression after systemic delivery of AAV9 with a 653 bp segment of the atrial natriuretic factor (ANF) promoter[422]. AAV9 was injected IV through the retro-orbital route, showing a dose dependent increase in transduction efficiency, with maximal transduction of approximately 80% of atrial myocytes achieved with the highest dose used, 5 x 10^{12} vg[422]. The authors ultimately decided on a working dose of 1 x 10^{12}, which also provided highly efficient transduction. Of note, this is a significantly higher dose than necessary when using strong promoters such as CMV, where complete cardiac transduction has been achieved in adult mice via the systemic venous route using

much lower doses. Indeed, in the current study, a dose of 1.5 x 10^{12} vg was sufficient to achieve transduction of the atria approaching 100% using AAV9-CMV-GFP.

When considering the 'systemic intravenous' route, differences in transduction efficiencies of various organs have been noted depending on the precise IV route taken[423]- other common IV routes include the tail vein and jugular vein. Accessing the jugular vein requires invasive surgery, but injection is technically much easier compared to tail vein, as the jugular vein is much larger and fully exposed after access is gained surgically.

Given our tissue specific promoter candidates were expected to have significantly less transcriptional strength as compared to CMV, and that targeting the minute tissues of the CCS could be more challenging than the well perfused working myocardium, I used a high dose of 1.5 x 10^{12} vg/ mouse and incubated for 5 weeks. Preliminary dose escalation studies also showed inefficient cardiac transduction with a dose of 1 x 10^{11} vg/ mouse (data not shown). Indeed, the combination of 1.5 x 10^{12} vg with 5 week incubation time proved highly effective in driving transgene expression from both CMV and cTnT promoters.

The reporter gene used, as well as the methods used to detect it are also critical. Many studies utilise luciferase, which can generate quantitative data from examining bioluminescence emitted from whole body scans of mice, and/ or organs. However, when examining minute and discreet regions of the heart that comprise CCS tissues, sectioning of the organs in particular planes accompanied with microscopic analysis is the preferred method of analysing reporter gene expression. GFP also has the advantage of being a relatively small gene (approximately 700 bp) and so does not take up too much of the limited capacity for AAV vectors, a maximum of 4.7 kb. Studies have also validated GFP as a fully quantitative reporter gene, where GFP fluorescence increases in direct proportion with the GFP copy number delivered to eukaryotic cells, and fluorescence intensity is directly proportional to GFP mRNA levels within cells[424]. GFP however, is prone to high autofluorescence and so promoters must be relatively strong in order to drive fluorescence above background levels[425]. Furthermore, native GFP fluorescence is quenched by common fixation methods including immersion in paraformaldehyde, and thus the precise fixation protocol used (duration, temperature) has the potential to produce significant variability in the reported signal. Fixation prior to freezing and/ or sectioning of GFP containing tissues is essential, as GFP is a soluble protein and will rapidly leak from damaged cells causing significant loss of signal.[425] One study found that GFP could not be detected in frozen sections prepared from unfixed tissues, even after IHC, whereas robust fluorescence was evident in tissues that had been fixed prior to processing[426]. Fixation is necessary in order to immobilise the GFP, for example by cross linking to other cellular

proteins. GFP detection by IHC can overcome issues associated with signal quenching during fixation, and the use of a fluorophore corresponding to spectra less susceptible to autofluorescence can ameliorate background fluorescence. For this reason, I chose an Alexa Fluor 647 conjugated secondary antibody for GFP detection. Using a channel different to the native GFP fluorescence also allowed accurate assessment of endogenous background fluorescence in the GFP detection channel in adjacent tissue sections and thus facilitated setting fluorescence positive thresholds with high fidelity.

Limitations in *in vivo* studies primarily relate to time restrictions. Firstly, detailed analysis of the SAN, Purkinje fibres and AVN were not feasible within the given timeframe. It appeared that the AVN and Purkinje fibres were less effectively transduced by AAV9 compared to the SAN, although detailed analyses could not be carried out to confirm this finding. Instead, I focussed on the SAN in light of its apparently superior transduction profile. Thus, particularly for the 1.6 kb KCNE1 construct that was expected to be highly active in the AVN and Purkinje fibres, it is not clear if it's inactivity could be attributed to lack of effective gene delivery by the AAV9 vector, or inactivity of the promoter. Since the structural and molecular makeup of each CCS component is distinct, promoter activity could be expected to vary across the SAN, AVN and Purkinje fibres. Thus, although it appears that the CCS specific caididate promoters are inactive in the SAN *in vivo*, further characterisation in the AVN and Purkinje fibres may be warranted. Analysing data from the 1.6 kb KCNE1 construct is also challenging in light of the lower dose used compared with the rest of the vectors (2.5×10^{11} vs 1.5×10^{12}). This was attributable to the lower viral titer of AAV9 1.6 kb KCNE1 GFP. It would have been beneficial to carry out injections with AAV9-CMV-GFP at this lower dose to provide a positive control, and examine if the SAN was effectively transduced. Given the linear relationship between dose administered and AAV9 mediated transduction efficiency (up to a point of saturation), it could be expected that transduction of the SAN would be less efficient at this lower dose. Again, this experiment would shed further light on the role of viral transduction efficiency vs promoter activity/ inactivity in the absence of transgene expression from AAV9 1.6 kb KCNE1 GFP.

5.7 Summary and conclusions

In conclusion, conditions optimal for the delivery and detection of transgenes delivered to the CCS were determined. Due to a multitude of variables within published literature, these conditions must always be determined through experimental means, requiring significant optimisation for the precise application. It appears that systemic administration of AAV9 is an efficient means of targeting the SAN, at a dose of 1.5×10^{12} vg. The CMV promoter was capable of providing high levels

of SAN transgene expression, and expression was also high in the working myocardium, liver and skeletal muscle. AAV9 cTnT GFP performed well in cardiac tissues, with some expression also in the liver. The cTnT promoter had limited activity in the SAN, particularly in central nodal myocytes. However, overall SAN transduction efficiency approaching 10% was achieved, with relatively high levels of transgene expression in the transduced cells. Thus, depending upon the particular application, i.e. upon the level of transgene expression required, AAV9 cTnT GFP may be suitable for delivering therapeutic transgenes to the SAN with limited off target expression confined to the atria and ventricles, and to some extent the liver. Tissue specific promoter candidates of HCN4 and KCNE1 failed to illicit any measurable transcriptional activity *in vivo*. This is perhaps attributable to the more complex transcriptional control and regulatory mechanisms elicited *in vivo* compared to *in vitro* conditions. To this end, caution must be used when interpreting data collected in 'surrogate' cell lines as a representation of native tissue.

6.0 Chapter 6: General discussion

6.1 Introduction

The current study has proven the capability of targeting the SAN via a single systemic intravenous dose of AAV9, and provides proof of concept for genetic modulation of the SAN in a cardiac specific context. The potent ubiquitous CMV promoter conferred high level transgene expression in the SAN in a non-tissue specific context, with high levels expression also conferred in the working myocardium, skeletal muscle, and liver. The cardiac specific cTnT promoter conferred low level transgene expression in the SAN, and high levels in the working myocardium. CCS specific promoter candidates were generated and showed promising performance in an *in vitro* ESC derived SAN cell model. Coupling these promoters to the strong CMV enhancer element resulted in elevated promoter strength concurrent with some loss of tissue specificity *in vitro,* particularly for the CMVe 0.8 kb KCNE1 construct which had highest overall transcriptional strength among the CCS candidates. Although native CCS promoters 1.2 kb HCN4, 0.8 kb HCN4 and 1.6 kb KCNE1 appeared inactive *in vivo*, further testing of hybrid promoter/ CMV enhancer constructs, in addition to the more potent 0.8 kb KCNE1 promoter variant, may be warranted. Further work is necessary to investigate the reasons for the apparent lack of transduction efficiency in the AVN and Purkinje fibres. The implications of these findings in the context of current knowledge and future directions are discussed in the following sections.

6.2 CCS promoter candidates are active *in vitro* in ESC derived SAN cells

As discussed, Shox2 cells were used to represent SAN/ CCS tissue *in vitro*. These cells were generated via overexpression of a neomycin resistance gene by the Shox2 promoter in mouse ESCs, followed by antibiotic selection, thus facilitating selection of a pure Shox2 expressing cell population[402]. Shox2 cells express a transcriptional profile similar to bona fide SAN cells, including HCN4, Cx45, Cx30.2, Tbx2, and Tbx3[402]. However, these cells also express some cardiac genes including Tbx5, GATA4, alpha-skeletal actin, and MLC2V. To this end, the native SAN is also known to express some working myocardial associated genes including cardiac troponin I (cTnI) and MLC2V[403]. Of note, critical repressors of the SAN gene expression profile such as Nkx2.5, and atrial specific ANF were only expressed at very low levels in Shox2 cells[402]. Shox2 cells also express HCN4 at levels significantly higher than other characterised HCN4 expressing cell lines, such as HL-1[402]. Furthermore, HL-1 cells are atrial derived, and thus the overall transcriptional profile is not suspected to resemble that of CCS cells. To this end, abundant ANF, desmin and connexin 43 are

expressed in HL-1 cells, similar to native atrial cardiomyocytes[427]. Vast differences in gene[403,302], protein[261], TF[428,259,429] and miR[429] expression levels have been demonstrated between SAN and RA tissues, and so specialised SAN cells are required to accurately assess candidate promoter performance. Despite abundant HCN4 expression at protein level, Shox2 are quiescent under standard culture conditions. It would be interesting to perform patch clamp analysis to demonstrate if functional I_f is expressed in these cells. Thus abundant evidence suggests that Shox2 cells are an adequate *in vitro* model for assessing the transcriptional activity of CCS specific gene promoters.

All CCS specific promoter candidates exhibited promising activity in Shox2 cells, effectively inducing expression of the GFP reporter gene. In addition, all minimal promoter candidates showed high specificity, with minimal activity in non SAN-like cells including NIH-3T3 and HEK293A. Achieving significant cell specific transgene expression from minimal constructs <=1.6 kb validated their potential utility for CCS specific gene expression in an AAV vector system, and thus necessitated further validation *in vivo*. Although it is not known whether Shox2 cells express cTnT and KCNE1, it seems likely given the high activity of the respective gene promoters and SAN-like gene expression profiles of the cells.

Although the minimal gallus cTnT promoter proved active in both Shox2 cells and native SAN tissue *in vivo*, the same could not be said for CCS specific candidates. The performance of the 1.6 kb and 0.8 kb KCNE1 promoters was on par with that of cTnT in Shox2 cells, indicating that the transcriptional landscape *in vivo* controlling the expression of CCS restricted genes is complex, and additional regulatory elements are required to activate, or relieve repression upon, the KCNE1 and HCN4 promoters in their native context.

These results urge caution when using *in vitro* conditions to predict *in vivo* function, especially when not using primary cells directly derived from the tissue in question. SAN myocytes can be isolated and cultured *ex vivo*, and adenovirus is capable of conferring transgene expression to these primary cells *in vitro*[430]. This may represent a more effective test bed for future use. I was also successful in isolating and culturing SAN cells from rats and mice (data not shown). Adenoviruses containing each promoter driven by GFP were generated, however as discussed it was later found that the constructs lacked polyadenylation signals due to aberrant restriction site placement, and thus it is likely that high levels of mRNA degradation occurred, confounding analysis of promoter activity as measured by GFP protein expression. Transfecting primary SAN cells with lipofectamine was not possible due to the combination of low cell yield from the tissue, low survival in culture, and high toxicity of transfection reagents. Thus, I opted to use the HCN4 expressing Shox2 cell line as a SAN

cell representative[402]. AdVs were also used to assess promoter performance in primary NRCMs, where little activity was shown by HCN4 and KCNE1 promoters (data not shown). However, the same confounding factors with the AdV use exist, and thus it is not clear whether the promoters were inactive in these cells, or if high mRNA degradation precluded GFP protein production.

It is also possible to isolate and culture SAN tissue *ex vivo*, where intrinsic rates of above 400 bpm are achievable for at least 24 hours from the mouse SAN. Injection of genetic constructs into the explanted SAN could also prove to be an effective test bed before progressing to *in vivo* studies in future. This technique has already proven effective in examining molecular mechanisms regulating intrinsic SAN rate via miR overexpression[429].

6.3 Effect of the CMV enhancer on promoter activity *in vitro*

In order to enhance CCS specific promoter strength, the 380 bp human CMV immediate-early enhancer (CMV enhancer) was appended upstream of 0.8 kb HCN4, 1.2 kb HCN4 and 0.8 kb KCNE1 promoters. In its native context, the CMV enhancer activates expression of CMV immediate early genes which are critical regulators of viral replication, infection and latency/ reactivation of human CMV[431]. In ESC derived Shox2 cells, the effect of the CMV enhancer on promoter strength was in general modest, with only the CMVe 0.8 kb KCNE1 construct resulting in significantly enhanced transcriptional activity. This is surprising, as the CMV enhancer is a well characterised strong enhancer element that has provided markedly increased activity of other promoters including cardiac specific ANF, MLC2V, and alveolar specific SP-C[262]. Activity of the ANF promoter was increased 45 fold by the addition of the CMV enhancer[262]. Importantly, the promoters mostly retained tissue specificity with minimal activity in off target cells. In these studies, the MLC2v promoter was tested in primary cardiomyoyctes, which may provide a better surrogate for native tissue as compared with immortalised cell lines. Furthermore, addition of the 380 bp CMV enhancer upstream of the neuron specific PDGF-beta promoter significantly elevated neuronal transgene expression with minimal effect on specificity both *in vitro* and *in vivo*[266]. Addition of the CMV enhancer to the 1.5 kb MLC2V cardiac specific promoter in a separate study resulted in 50 fold greater cardiac expression compared to the CMV promoter after tail vein injection of AAV2 vectors, and 50 fold greater expression compared to the next highest transduced organ, the liver[375]. Notably, some ectopic liver expression was demonstrated with a similar MLC2V promoter *in vivo* without the enhancer[375].

It appears that the effect of the CMV enhancer is promoter dependent. Addition of the CMV enhancer to the cardiac specific alpha MHC promoter resulted in increased transcriptional activity,

however tissue specificity was drastically compromised in vitro[262]. Furthermore, the CMV enhancer also significantly compromised the specificity of tumor specific promoters in light of an up to 1096 fold enhancing effect[265]. Thus, trialling CMVe constructs *ex vivo* in isolated SAN tissue may be an appropriate next step in determining their ability to drive expression in the native SAN. Constructs could also be injected into the adjacent right atrial muscle to assess specificity.

It is not entirely clear how the CMV enhancer acts synergistically with certain promoters, but to a lesser degree with others. Different TF binding motifs may act synergistically or antagonistically to promote or impair transcription in a context specific manner[432]. Differing TF synergy possibly reflects the promoter specific effects elicited the CMV enhancer described previously. To this end, it has been suggested that control of tissue specific genes is only minimally attributable to differential expression of TFs across tissues. Binding sites for the ubiquitous TF SP1 showed little enrichment in ubiquitous promoters vs tissue specific promoters[432]. Furthermore, TFs are less likely to be expressed in a tissue specific manner compared to other genes, and even apparently tissue specific factors are usually expressed in multiple tissues[433]. These data suggest that differential TF expression is unlikely to be the primary driver of tissue specific gene expression. Instead, it is likely that tissue specific gene expression is related to temporal changes in the non-canonical binding activity and behaviour of TFs in a context/ tissue specific manner. Such non-canonical interactions are thought to include binding between multiple TFs to form different complexes[432,433]. For example, STAT3 and NR2C2 TFs change binding partners in a tissue specific manner[434]. Such shifts in TF function and behaviour across different tissues may enable a relatively small subset of TFs to illicit diverse functions, including control of tissue specific restricted genes.

With regards to the CMV enhancer, recruitment of ubiquitous and possibly tissue restricted TFs to the promoter region may facilitate formation of complexes to promote transcription. It is perhaps the unique interactions between different ubiquitous and tissue specific TFs that determines whether tissue specificity is maintained in light of potentiation, and to what extent. This principle has been demonstrated in the erythroid-lineage specific transcriptional activity elicited by GATA-1. GATA-1 synergises with ubiquitous SP1 to activate erythroid restricted genes *in vivo*, where SP1 recruits GATA-1 to such promoters even in the absence of discrete GATA-1 binding sites[435]. GATA6 sites in the human CMV enhancer also participated in transactivation of the hybrid cardiac specific CMVe-MLC2v promoter during cardiac differentiation *in vitro* via GATA6 binding[436]. Thus, TFBS in the CMV enhancer may act synergistically or independently of other elements present in core promoters, in a mechanism that is likely promoter specific. Given the importance of ubiquitous TFs such as SP1 in activation of the HCN4 and KCNE1 promoters *in vitro*[377], it is possible that a diverse array of interactions with SP1 and other associated TFs may act to activate or indeed repress

promoter activity *in vivo*. To this end, CMVe contains multiple consensus SP1 TFBS which could act to potentiate HCN4 and KCNE1 promoters *in vitro*[437].

Large scale TF mapping studies have provided key insights into the transcriptional regulatory landscape in mammalian tissues. Most large scale TF mapping studies including the landmark mouse TF atlas study[438], only examine the left ventricle and right atrial appendage when considering the heart. Sampling details suggest little or no nodal tissue would have been included in biopsies from the right atrial appendage. In order to promote further understanding of the complex regulation of CCS gene expression, it would be useful to study the CCS tissues in the context of large comparative studies. To this end, whilst there was significant convergence of TF expression and regulation activities across related tissues, such as sub-compartments of the brain and digestive system[438], the CCS is known to have a highly divergent TF and gene expression compared to the working myocardium[397]. This reflects the highly specialised function of the CCS, and necessitates further understanding of its specific gene regulatory network in future studies. Such information would aid in the rational design of CCS specific promoter/ enhancer constructs for gene therapy. As alluded to previously, identification of minimal CCS specific elements from the HCN4 promoter has proved challenging, and fine patterning of CCS gene expression is highly complex[439].

Limiting factors in gene expression likely includes recruitment of RNA polymerase, chromatin modification, and rates of RNA polymerase transcription after initiation[440]. To this end, recruitment of RNA polymerase may be potentiated by repeat TFBS in the CMVe, facilitating transcription of the downstream gene. It is likely that at least some synergistic activity occurred with our CCS specific promoters given the varying transcriptional activities of each promoter when coupled with CMVe. If the CMVe element masked transcription from the respective promoters, roughly uniform GFP transgene expression would be seen regardless of the downstream promoter. To this end, the 0.8 kb KCNE1 promoter was most highly active without CMVe, and of all CMVe coupled promoters, it maintained the highest activity. Furthermore, promoters maintained a degree of cell type specificity upon addition of CMVe in light of modest potentiation. Since the ubiquitous CMVe has little tissue or cell specific preference in isolation, it seems reasonable to suggest that the enhancer potentiated promoter activity whilst maintaining some tissue specificity. Thus, we speculate that the CMVe acted in synergy with the respective prompter elements, albeit the enhancing effect was generally modest and some transcriptional specificity was lost. The effect of the CMV enhancer on tissue specificity and transcriptional activation *in vivo* remains to be seen, and is an interesting avenue for further work.

The relatively modest effect of the CMV enhancer in Shox2 cells may be partially attributable to intrinsic properties of the cell line. The CMV promoter (compositing immediate early enhancer and promoter) used for positive control was less active in Shox2 cells compared with the other cells used, particularly HEK293A, highlighted by the lower illumination power used between Shox2 cells and the others for flow cytometry. One study observed no enhancement of the CMV promoter from the CMV enhancer in the mouse pre-B cell line FL5.12, where activity of the promoter was also low[376]. Another study using adenoviral gene delivery noted the absence of CMV driven reporter gene expression in undifferentiated ESCs. Transgene expression gradually increased during differentiation, and was achieved in 27% of differentiated ESC derived cardiomyocytes[441]. Due to differences in MOI and other variables, it is difficult to compare to the current study. However, we achieved CMV- driven GFP expression in up to 100% of primary rat cardiomyocytes using adenoviral vectors- whether these disparities are due to varying transduction efficiency of the virus or inactivity of the CMV promoter in ESC derived cells compared to primary cardiomyocytes is not clear. Interestingly, human CMV cannot effectively replicate in poorly differentiated cells, such as progenitor cells, and the virus remains latent. In this context, the CMV enhancer/ promoter is inactive[431]. Thus, the ESC derived Shox2 cell line may not truly reflect the potential effect of the CMV enhancer on tissue specific promoter candidates in native tissue. In native SAN tissue *in vivo*, the positive control CMV enhancer/ promoter was highly active, evidenced by high number of GFP expressing SAN myocytes with signal intensity that appeared on par with that of the working cardiomyocytes. Thus, *in vivo*, it is possible that CMVe HCN4 or KCNE1 promoters may be active in CCS tissues. Unfortunately due to the coronavirus pandemic and global laboratory shutdowns, we were unable to package any of the CMVe constructs into AAV9 for *in vivo* testing.

Some promoter activity increases in off target cell lines were observed when combined with CMVe in HEK293A and NIH 3T3 cells. Activity of CMVe HCN4/KCNE1 appeared elevated in HEK 293 cells, with higher numbers of GFP positive cells visible in photomicrographs and via flow cytometry. HEK 293A cells were established from human kidney cells and transformed with adenoviral type 5 DNA[442]. Adenoviral sequences comprise E1 genes (E1A and E1B) which participate in transactivation of viral promoters including CMV[443], conferring high activity. Thus, the viral CMV enhancer/ promoter may be expected to be high in this cell line, as demonstrated via flow cytometry. Another systematic study examined CMV promoter performance in many cell lines, and concluded that activity in HEK 293 cells was highest[400]. The high propensity of CMV enhancer/ promoter activation may partially account for increased activation of the CCS tissue specific promoter constructs which were highly specific for Shox2 cells without the enhancer. *In vivo* studies are essential to understand if this modest increase in promoter promiscuity applies *in vivo* in native kidney cells and others. The

importance of any residual off target expression may also depend upon the intended application. For example, high expression of miR inhibitor transgenes such as miR sponges or decoys are necessary to illicit the desired effect and effectively sequester the miR target[399]. Thus, low level off target expression may not meaningfully decrease the amount of free miR available for target binding. Also, since miRs are expressed in a tissue specific manner, these concerns would only exist assuming the miR is expressed in tissues where off target transgene expression occurs. The case may be of greater concern if expressing a therapeutic gene such as HCN4 using the proposed vector system, since it is thought that ectopic expression of HCN4 in the working myocardium contributes to arrhythmogenesis in heart failure[444]. It follows that ectopic expression of HCN4 in other organs could be detrimental, and thus transgene expression must be restricted stringently to the target tissue (SAN) for such applications.

6.4 CCS specific promoters are inactive *in vivo*

Regulation of HCN4 expression is clearly complex in nature, and additional elements to the core promoter are likely necessary to recapitulate HCN4 expression *in vivo*. Although both 1.2 kb and 0.8 kb mHCN4 promoter constructs elicited favourable transcriptional profiles *in vitro*, neither proved capable of inducing transcription *in vivo*. Although key roles for specific TFs such as ISL-1[259] and MEF2[370] have been elucidated, little is known about the nature of cis acting elements responsible for fine patterning of cardiac HCN4 expression. Subsequent studies have probed further into HCN4 expression in the SAN by examining non coding cis regulatory elements (CREs). Examination of deeply conserved regions in the HCN4 locus identified a 5.7 kb region within intron 1 of HCN4 that was capable of directing transgene expression to the AV bundle in postnatal hearts, and developing CCS aside from the SAN in embryonic hearts[439]. TF MEF2C was a critical regulator of enhancer activity. Kuratomi and colleagues[370] identified an intronic enhancer region (+14,090 / +14,247 bp relative to the mHCN4 TSS) capable of significantly inducing HCN4 core promoter activity *in vitro* by a magnitude of 30 fold, also dependent on the same MEF2 site[370]. This region was also implicated in ectopic expression of HCN4 associated with hypertrophy *in vivo*, where stress induced nuclear export and consequent inhibition of histone deacetylases (HDACs) potentiated the enhancer, leading to promiscuous activity and ectopic expression of enhancer driven transgene in the working myocardium in TAC[439]. Notably, the HCN4 core promoter combined with the +14,090 / +14,247 enhancer was not capable of recapitulating HCN4 expression *in vivo*, indicating that multiple enhancer and repressor elements act in concert to facilitate fine patterning of cardiac HCN4 expression.

Evidence suggests that CCS specific epigenetic modifications contribute to CCS transcriptional activation, and/ or repression in the working myocardium. Differential activity of GATA4 induced H3K27 acetylation or deacetylation in the AV canal and working myocardium respectively, resulting in transcriptional induction in the AV canal and repression in the working myocardium[445]. Interestingly, GATA elements were also responsible for repressing activity of the cardiac specific cTnI promoter in skeletal muscle, thus contributing to cardiac specificity[446]. In addition, a minimal GATA6 enhancer induced AV canal restricted gene expression during development[447]. Coupling this enhancer to the pan-cardiac cTnT promoter restricted transgene expression to the AV canal during development, indicating the this element represses promoter activity in the working myocardium[445]. Further characterisation of such CCS specific regulatory switches may facilitate the fine tuning of promoter activity in efforts to achieve CCS specificity. Such insights could permit fine tuning of cardiac specific promoters to activate selectively in the CCS. To this end, we have demonstrated some activation of the cTnT promoter in the SAN in the current study, and other working myocardial genes are known the be expressed in components of the CCS, such as MLC2V[403], as previously discussed. Perhaps application of such CCS specific switch elements could turn off transgene expression in the working myocardium, whilst maintaining expression in compartments of the CCS.

ISL1 is a TF expressed highly in the SAN in adult hearts, but absent from the working myocardium[448]. ISL1 deficient mice suffer severe cardiac malformations, and ISL1+ progenitors are thought to contribute more than two-thirds of the cells in the embryonic heart, highlighting a key role in development[449]. Importantly, ISL1 deletion results in depletion of SAN associated genes, and enrichment of RA associated genes in the SAN, establishing a role in maintaining the SAN transcriptional programme[259]. A recent study provided further insight regulation of CCS specific gene expression using ATAC-seq, contrasting regions of chromatin accessibility between SAN myocytes and right atrial myocytes. The study identified a 2.9 kb ISL1 enhancer capable of directing transgene expression to the SAN both along its developmental axis and in the postnatal heart[450]. In the adult heart, the enhancer directed strong reporter gene expression in the SAN, with some expression also observed in the coronary sinus and ventricular conduction system, and only very low levels in the working ventricular myocardium[450]. Interestingly, genome wide association (GWAS) analysis on the UK biobank cohort revealed associations between polymorphisms corresponding to this enhancer region in humans and heart rate, and CRISPR mediated deletion of the enhancer in mice resulted in impaired SAN development and arrhythmia[450]. It would be of great interest to trial this enhancer with an AAV9 vector in order to assess its ability to exogenously induce transgene expression in the adult CCS. Critically, this 2.9 kb enhancer could be used in

applications where the intended transgene is small, e.g. miR inhibitor transgenes and miR overexpression cassettes. For wider application, identification of minimal enhancer regions will be of particular interest for AAV gene therapy. Critically, how the activity of this enhancer reacts to pathological stimuli remains to be seen. This is of great importance, as the proposed gene therapy vector is intended for regulating SAN gene expression primarily in pathological settings, including HF. As mentioned, previously identified HCN4 regulatory elements have shown promiscuous activity in the working myocardium in response to TAC induced hypertrophy[439]. However, whilst ectopic ventricular expression of HCN4 has been demonstrated in response to pathological stimuli[451], there is limited evidence to suggest that the same occurs for Isl1. Lack of Isl1 induction was seen in response to myocardial infarction[448,452], whilst ischemia reperfusion stimulated some Isl1 expression mainly confined to the outflow tract[452]. Regardless, Isl1 positive cells were virtually undetectable in tissue sections from hearts under all multiple pathological stimuli (myocardial infarction and ischemia reperfusion), indicating that Isl1 expression is not significantly elevated in the working myocardium in response to injury.

Given the critical role of the SAN to generate the heartbeat, and the conduction tissue to co-ordinate efficient pump action via precise action potential propagation, it stands to sense that patterning of cardiac HCN4 and other CCS gene expression is under extremely tight regulation. To this end, ectopic or altered expression of cardiac HCN4 in response to pathological stimuli such as HF[453], high intensity exercise training[101,135], and ageing[97] is a an established pathological mechanism. To this end, the HDAC mediated repression of MEF2 in the regulation of HCN4 expression has been implicated in ectopic expression of HCN4 in HF, as discussed[439]. Indeed, identification of mechanisms regulating gene expression in specialised cardiomyocytes of the CCS has proven difficult, particularly in the SAN. Prior to the discovery of the aforementioned ISL1 SAN enhancer, attempts to elucidate functional cis regulatory elements capable of specific SAN expression had been relatively fruitless. Of 4 CCS marker mouse strains, precise histological analysis of hearts showed that none exhibited transgene expression in the SAN in a CCS specific context. Only transcription factor homeodomain only protein (HOP)-LACz mice showed beta galactosidase reporter expression in the SAN, however strong expression was also present in the atria[454]. Curiously, the authors also demonstrated absence of beta galactosidase reporter expression in the SAN of KCNE1-LacZ mice, but strong expression in the AVN, at odds with a previous report of strong LacZ expression in the SAN region[258]. However, a later study demonstrated clear beta galactosidase expression in the SAN of KCNE1 LacZ mice, visualised in isolated SAN tissue preparations[374]. The reasons for disparity between these studies is unclear, but may relate to different methods used to detect the transgene.

Although vital insights into CCS developmental gene regulatory networks have been gained through transgenic studies, the picture is less clear in the adult. A 660 bp minimal Cx30.2 enhancer was capable of directing reporter gene expression specifically to the AVN throughout embryonic development in a Gata4 and Tbx5 dependent manner[455]. Cx30.2 is expressed in the SAN and AVN of adult hearts, but is absent from the working myocardium. This is the lowest conductance connexion isoform, and is critical for fine tuning of electrical impulse propagation, particularly mediating conduction delay at the AVN[456]. Given the distinct behaviour of the Isl1 enhancer from embryonic to adult stages, it remains to be seen whether other minimal elements maintain specificity in the transcriptional landscape of the fully developed heart, and indeed in disease contexts.

Although less is known about the KCNE1 promoter and regulation of KCNE1 expression in the CCS, our results suggest a similar complex regulatory landscape in the same vein as with HCN4. I aligned the characterised human KCNE1 core promoter to the mouse genome and selected a highly conserved 1.6 kb region for further studies, incorporating a truncated 0.8 kb variant via restriction site placement. *In vitro*, the KCNE1 promoters appeared superior in transcriptional strength compared to HCN4. As previously mentioned, the rationale for KCNE1 promoter trial was based upon a homologous recombination study, where KCNE1-LacZ expressed the reporter specifically in the CCS of the adult mouse heart[258]. Of course, reporter gene was under control of the entire KCNE1 regulatory region, far too large to incorporate into an AAV vector. In light of the impressive findings by Vedantham et al. (2020)[450] in identifying a minimal CCS specific Isl1 enhancer, it may be of great interest to utilise ATAC-seq to reveal tissue specific enhancer elements responsible for CCS KCNE1 expression in the adult heart. Although the core promoter region undoubtedly plays key roles in the regulation and initiation of transcription, further characterisation of other cis regulatory elements may facilitate transgene recapitulation of endogenous cardiac KCNE1 expression from minimal elements.

The cTnT promoter was moderately active in the SAN *in vivo*, along with being highly active in all regions of the working myocardium, as expected. The promoter contains two copies of the MCAT motif (CATTCCT), which is critical for promoter activation in cardiac muscle[457]. Divergent transcriptional enhancer factor-1 (DTEF-1) trans-activates the gallus cTnT promoter in a cardiac specific manner via interactions with MCAT, both independently of and synergistically with MEF2[458]. DTEF-1 expression is specifically enriched in cardiac muscle, and does not activate the cTnT promoter in skeletal muscle, thus contributing to cardiac specific promoter activation[458]. Activity of the cTnT promoter in the SAN may occur via a similar mechanism, although It is not clear whether DTEF-1 is expressed in the SAN. MEF2 is expressed highly in the SAN, and interestingly, it was shown

that core cardiac TFs Gata4, Mef2c, and Tbx5 were expressed at similar levels in the SAN and RA[259]. Perhaps DTEF-1 and other cardiac specific factors are expressed mainly in the paranodal/ transitional region of the SAN / CT border and poorly in the central SAN, which could explain why the cTnT promoter appeared more active in the paranodal region. Transitional SAN cells are implicated in propagation of action potentials to the surrounding atrial muscle, whereas central nodal cells are thought to primarily contribute to spontaneous action potential generation and pacemaking, and thus the leading pacemaker site of the SAN is usually in the SAN centre under physiological conditions[10]. Thus, the central and peripheral zones likely differ in molecular makeup. Indeed, a paranodal region was identified in the human heart, with a transitional gene expression profile resembling both SAN and RA[302]. Another study identified and characterised a peripheral pacemaker site in the rat heart located near the inferior vena cava, revealing differential expression of cardiac receptors in the central SAN vs peripheral site[459]. It would be interesting to probe the SAN for cTnT mRNA expression via in situ hybridization and protein via IHC to examine its distribution. Perhaps this could shed further light on the low activity of the promoter and apparent preference for peripheral nodal myocytes over central. To this end, proteomic studies have already shown that cTnT is robustly expressed in the SAN, but cannot offer spatial information on it's distribution within the tissue[261].

Perhaps one of the most impressive CCS marker genes is contactin 2 (Cntn2). Cntn2 is a cell adhesion molecule with key roles in neuronal patterning and regulation of ion channel expression in myelinated axons[460]. Adult Cntn2-GFP mice express GFP throughout the CCS, with very strong expression in the AVN, His bundle and Purkinje fibres[461]. The Cntn2 promoter has not yet been characterised in detail, and thus identification of minimal elements capable of recapitulating ctnt2-GFP expression in the heart requires further work. This may represent a promising future candidate for CCS transgene expression, particularly in the ventricular conduction system. Utilisation of techniques such as comparative ATAC-seq may provide insight into tissue specific enhancers and other cis regulatory elements responsible for directing cntn2 expression to the various components of the CCS.

Thus, the primary challenge in the realisation of the proposed AAV based CCS specific gene therapy likely lies in recapitulating CCS specific gene expression from minimal promoter/ enhancer elements. Large regulatory regions of HCN4[259], KCNE1[258], Cntn2[461] among others can achieve CCS specific gene expression. To this end, HCN4 GFP mice are generated using a ~237 kb BAC clone that encompasses the entire HCN4 gene and regulatory sequences[462]. For our purposes, identification of minimal elements and motifs is critical in the context of the 4.7 kb total packaging capacity limit of AAV vectors. Regardless, in the current study it has been verified that systemically delivered AAV

vectors at a dose of 1.5 x 10^{12} vg target the SAN effectively in adult mice, with high transduction rate of SAN myocytes and high levels of transgene expression using a strong promoter. This proof of concept validates further development of tissue specific approaches using tissue specific promoter and/ or enhancer elements in future. Identification of minimal elements that are activated only in the CCS and to a sufficient level is a primary barrier to the realisation of this concept.

6.5 cTnT (or other cardiac specific promoters) for CCS gene delivery in a cardiac specific context

Interestingly, the cTnT promoter appeared more highly active in the peripheral zones of the SAN as opposed to the SAN centre. The region bordering the SAN/ CT may represent a transitional zone, where cell characteristics resemble both SAN myocytes and atrial myocytes. In humans, dogs and rabbits, there is evidence that cells gradually transition in morphology from the central SAN to the adjoining atrial muscle[10,11,419]. Peripheral SAN myocytes may have more organised myofilaments and more mitochondria compared to those in the SAN centre[463]. Transitional cells have also been observed in the mouse SAN, distributed in the SAN periphery. These cells are smaller than central or typical pacemaker cells, with positive expression of NF-160 and HCN4 (similarly to central SAN cells).[464] Furthermore, a rare population of cells at the CT/ SAN boundary were found to express both Cx43 and HCN4, thus showing hallmarks of both trial and SAN cells[347]. To this end, the peripheral cells that also exhibited stronger cTnT driven GFP expression appeared to have lower HCN4 expression, suggesting a transitional morphology (figure 5.8 A, B).

Achieving high level gene expression in the SAN in a cardiac specific context may be desirable in certain circumstances, for example when negatively regulating miRs expressed only in the SAN. miR decoy sequences specific to the miR of interest would thus have no effect in the working myocardium in such circumstances. To this end, as discussed, miR expression is chamber specific in the heart[465]. A recent study profiled miR expression profiles in the SAN and RA, finding significantly differential expression of 66 miRs[429]. miR-426-3p was capable of modulating extrinsic SAN rate via targeting HCN4[429]. A key SAN HCN4 regulating miR of interest, miR-370-3p, is also expressed in the ventricle, where it was found to ameliorate post MI fibrosis via interactions with TBF-beta[466]. The miR-370 TGF beta interaction was also demonstrated in gastric carcinoma, where elevated miR-370 contributed to carcinoma progression[467]. Conversely, miR-370-3p was shown to possess tumor suppressor properties in the context of pituitary adenoma, and it's reduced expression results in drug resistance in glioblastoma[468,469]. We detected relatively strong transgene expression in the

brain using AAV9-CMV-GFP, consistent with previous reports of this vector's ability to effectively cross the blood brain barrier[470]. Thus, due to tissue and pathology specific effects of miRs such as miR-370, SAN specific modulation would be key for harnessing it's therapeutic potential shown in SAN dysfunction in HF[107].

Alpha myosin heavy chain (alpha MHC) is robustly expressed in the SAN, AVN, His bundle and Purkinje fibres[471,472] as well as the working myocardium, being the most abundant protein constituent of the cardiac sarcomere[473]. A 363 bp alpha MHC promoter has been successfully utilised for cardiac specific transgene expression from AAV9, albeit significantly less potent than CMV[247]. Another study utilising lentiviral vectors demonstrated that the cTnT promoter conferred higher cardiac transgene expression compared to alpha MHC, although the alpha MHC promoter was more cardiac specific[474]. Significant ectopic expression from the cTnT promoter was observed in the liver, agreeing with the current study[474]. The alpha MHC promoter has also proven capable of driving transgene expression in the SAN and AVN[472,475]. Interestingly, transgenic overexpression of GFP tagged Kir2.1 and Kir6.2 using the alpha MHC promoter was limited in the SAN, AVN and His bundle, but robust in the working myocardium. In this case, the expression of transgene followed the endogenous expression of the respective ion channels, rather than the endogenous expression of alpha MHC, which was shown to be robustly expressed in SAN and AVN[472]. Notably, Alpha MHC-driven Kir6.2-GFP was robustly expressed in the SAN. Since these studies were carried out in transgenic mice, entire regulatory regions of alpha MHC were used to drive transgene expression, and thus it remains to be seen whether minimal promoter elements are capable of recapitulating these results. It is also interesting that alpha MHC driven Kir2.1-GFP was expressed in the SAN periphery but not central nodal myocytes. This implies different transcriptional regulatory mechanisms at play between these regions of the SAN, which may also explain the apparently higher cTnT promoter activity in peripheral SAN tissue compared to central in the current study. Thus, the alpha MHC promoter may be another promising candidate for CCS gene delivery in a cardiac specific context. Perhaps the first test in this context would be the ability of minimal promoters, as used in viral vector systems, to express transgenes in the CCS as well as working myocardium.

As stated previously, the level of transgene expression and transduction efficiency of target cells required to illicit a therapeutic effect varies depending upon the application. Interestingly, studies have demonstrated that transduction efficiency of only around 40-66% of ventricular myocytes was sufficient for suppression of CPVT precipitated by delayed after depolarisations (DADs) through AAV mediated delivery of the calsequestrin 2 gene[476]. This is thought to be due to the source-sink relationship that governs conduction of cardiac impulses- for example, a single or small group of

myocytes exhibiting DADs will not be capable of propagating this signal to surrounding myocytes, as the surrounding myocytes act as current sinks, effectively attenuating voltage gradients between the DAD source cells and those surrounding. Thus, interspersion of DAD cells with transduced stabiliser cells results in attenuation of DAD amplitude and reduces its probability of successful propagation via reaching threshold voltage. To this end, elegant *in silico* studies have suggested that transduction of only 15-25% of cells may be necessary to suppress arrhythmia propagation in CPVT in some cases[477]. However, in applications for miR modulation including overexpression and inhibition, it is likely that strong promoters will be required to illicit a the desired effect. This was partially the rationale for attempting to enhance CCS promoters via the addition of the CMV enhancer. miR sponge/ decoy technology relies upon competitive inhibition of miR activity, acting to sequester miRs from endogenous binding sites. Due to the very nature of this technique, high miR decoy sequence expression is required to significantly reduce the amount of free miRs within cells available for gene repression[399,478].

6.6 Improved CCS gene delivery may enable use of weaker promoters

Although high levels of transgene expression were achieved in the SAN using AAV9-CMV-GFP, the percentage of transgene positive cells was lower than the juxtaposed atrial working myocardium, and ventricular myocardium. The AVN and Purkinje fibres appeared to be inefficiently transduced by AAV9. This could be attributable to 2 primary factors. Perhaps SAN tissue is not quite as effectively transduced by the AAV9 vector, and thus the number of vector genomes introduced per cell is insufficient so as to guarantee high transgene expression. To this end, it has been estimated that a mean transduction rate of one vector genome per cell is only adequate to ensure that 63% of target cells will express at least one genome, and approximately 5 vector genomes per cell is necessary to effectively target > 99% of cells[205]. The ability of AAV to enter cells depends upon the expression of primary and secondary receptors. Galactose and the laminin receptor are important mediators of AAV9 transduction[479]. Expression of these receptors in the SAN and other CCS tissues is unknown, and may provide insight into limiting factors of transduction when compared to the working myocardium. Alternatively, SAN myocytes may possess a lower ability to convert AAV ssDNA to transcriptionally active dsDNA and thus confer transgene expression. This principle was shown in trabecular meshwork cells of the eye, which are considered non-permissible to AAV transduction[214,480]. The use of scAAV, thus bypassing host second strand DNA synthesis, achieved highly efficient transduction with AAV2[214]. AAV entry into trabecular meshwork cells induced downregulation of genes involved in DNA replication and synthesis, likely inhibiting conversion of

AAV ssDNA to dsDNA[214]. Even in the absence of second strand synthesis, conversion to dsDNA is possible by annealing of complementary sense and antisense strands. Cells would need to be infected with high numbers of both sense and antisense ssAAV genomes in order to confer efficient expression in this context. If DNA synthesis is the limiting factor in SAN AAV transduction, higher efficiency could be achieved using scAAV vectors as demonstrated in the ocular trabecular meshwork cells. However as discussed, these vectors have only half the transgene capacity of ssAAV vectors, presenting further challenges for even minimal promoter/ enhancer constructs. AAV transduction of fibroblasts is also inefficient, attributed to inefficient intracellular viral trafficking to the nucleus[481]. Circumvention of ubiquitination, and thus proteasome mediated degradation of virions significantly enhanced AAV transduction of fibroblasts[481]. To address the reason for the apparently lower transduction of the SAN vs adjacent RA , another cohort of mice were injected with 1.5 x 10^{12} vg AAV9. Mice were sacrificed and the SAN, right atrium, ventricle and liver removed and snap frozen for qPCR to investigate the number of distribution of vector genomes, giving an insight into regional variation in cardiac transduction efficiency with AAV9. These studies are ongoing. It is possible that with further improved transduction efficiency, perhaps by elevated viral dose or viral capsid pseudotyping, transgenes driven by weaker promoters may achieve more therapeutically relevant levels of expression. In light of the apparently inefficient gene delivery to the AVN and Purkinje fibres, unravelling this mechanism may be of even greater efficiency to develop strategies to effectively target the entire CCS.

6.7 Future directions for CCS specific gene delivery

Currently, most efforts in biopacemaking aim to generate a *de novo* pacemaker, rather than restoring function to the native SAN. However this approach has proven challenging (reviewed by[482]). As studies from animal models of disease further elucidate the mechanisms underlying SAN dysfunction, therapeutic targets for restoration of function are emerging. For example, elevated miR-370-3p has been identified as a driver of reduced HCN4 expression and bradycardia in HF, and miR 423-5p acts in a similar manner in driving sinus bradycardia in athletic training via aberrant HCN4 regulation[107,128]. Interestingly in both cases, silencing the respective miRs using oligonucleotide antagomiRs rescued SAN function. Age related remodelling of Cav1.2 and Cav1.3, which contributed to decreased intrinsic rate and depressed pacemaker activity, was related to increased expression of miR-1976 is the sinus node[96]. Thus, miRs may represent ideal targets for restoration of CCS function in disease. Thioredoxin 2 (Trx2), a molecule involved in counteraction of oxidative stress and ROS scavenging, also mediates SAN HCN4 expression[117]. Induction of oxidative stress via CCS specific knockout of Trx2 resulted in drastically reduced HCN4 expression

in the SAN, with severe sinus bradycardia and AV block[117]. Indeed, increased oxidative stress is a hallmark of many disorders strongly associated with SND, including ageing[119], AF[120,121], HF and hypertension[122]. Thus, targeting the ROS/Trx2/HCN4 axis may represent an attractive therapeutic approach for the treatment of multiple disease states where SND is implicated.

Although the discussion of the proposed gene therapy focusses on ion channel and electrical remodelling as the primary target and proposed mechanism underlying CCS dysfunction, the potential role of other processes should not be ignored. Elevated fibrosis and SAN myocyte loss have been linked to SND particularly in ageing, in both humans and animal models. The SAN naturally has a high fibrotic content which provides electrical insulation from the hyperpolarising influence of the surrounding atrial myocardium, and provide defined exit pathways for electrical impulses[86]. Histological studies on the ageing human SAN revealed decreased overall SAN volume, loss of peripheral SAN regions and replacement by fatty tissue, and elevated proportion of connective tissue relative to total SAN volume[483]. Interestingly, disparities existed between fibrotic content and various pathologies- severe chronic SAN exit block and tachy-brady syndrome were strongly associated with severe fibrosis of the SAN, whereas there was no significant association with fibrosis and atrial fibrillation. Nevertheless, the amount of nodal cells in the SAN was found to decrease with age, whilst those remaining underwent hypertrophy perhaps as a compensatory mechanism[87,484]. These findings were corroborated in a study of aged mice which developed SND in the presence of increased interstitial fibrosis[485]. Since increasing age is an established independent risk factor for SND, SAN cell loss and/ or elevated fibrosis may be an contributing mechanism of SND in this context[87]. Remarkably however, a stark paucity of SAN cells (only 10% of SAN myocytes remaining) was also found to be capable of maintaining sinus rhythm in some patients, and thus the link between SAN cells loss remains somewhat unclear[87]. Although the mechanisms surrounding these structural changes are not well established, recent findings in mice may point towards a potential role for Popdc1 and/ or Popdc2 proteins in the modulation of pacemaking, and in age related decline in pacemaker function. Knockout of Popdc1 or Popdc2 in mice caused SND in an age and stress dependent manner[486]. Notably, regions of the SAN in aged and stressed (physical or psychological) knockout mice were hypoplastic, and a reduction in nodal extensions into the surrounding atrial muscle was observed[486]. Although the precise roles Popdc proteins play in maintaining SAN function are not yet clearly defined, they may represent an attractive therapeutic target for maintaining or enhancing SAN function in ageing via reversing or preventing SAN cell loss. Further studies may elucidate the precise role of these proteins, and whether their genetic mutation or remodelling in ageing or other pathological states contributes to SAN dysfunction. Our proposed gene therapy could potentially be utilised to harness such targets,

and thus also be used to address structural SAN remodelling. Further research may identify other potential targets for preserving SAN function through modulation of structural remodelling.

Thus despite the emergence of many potential therapeutic targets for CCS repair and corrective modulation in disease, effective methods for targeting the CCS and harnessing these targets remain understudied. Methods such as antogomiR injection have systemic effects, and thus affect miR expression globally, and require repeat dosing. Furthermore, there are no studies that directly examine the effectiveness of such gene delivery methods to the minute tissues comprising the CCS. To this end, AAV mediated modulation of miR expression has already shown therapeutic potential in the working myocardium. As well as overexpression, miRs could also be downregulated using AAV vectors. Such approaches could involve miR decoys or sponges, which contain multiple repeat binding sites complementary to the miR(s) of interest[399,478]. When expressed at high levels, the decoy sequences bind free miRs and thus sequester them from their endogenous gene targets, relieving miR based repression of gene expression[478]. *In vivo*, AAV9-miR-25 decoy sequences selectively decreased miR-25 expression, increased levels of target SERCA2a protein, and attenuated cardiac dysfunction and fibrosis in HF[340]. Decoy sequence expression was driven by the ubiquitous U6 promoter. The ability to drive decoy transgenes with tissue specific promoters raises the possibility of tissue specific miR modulation. Importantly, in post mitotic tissues such as the heart, long term transgene expression can be conferred using AAV vectors, whereas antagomiRs and other oligonucleotide techniques require repeat dosing, limiting their translational potential.

Systemic gene delivery has the advantages of being minimally invasive, without the requirement for surgical procedures. Often the ability to target all tissues of the body is considered advantageous, however in the case of tissue specific gene delivery, limiting transgene to the target tissue specific can be challenging. This, and many other studies, has shown that systemic delivery of AAV9 effectively transduces many tissues. Thus, restricting transgene expression can be achieved at two primary levels; 1) limiting the exposure of the vector primarily to the target cells (e.g. intramyocardial injection, intracoronary perfusion) and 2) spatially limiting the expression of the transgene by placing under the regulation of tissue specific promoters. In an effort to modify gene expression of the AVN with minimal off target expression, one group used intracoronary perfusion of the AV nodal artery with adenoviral vectors, as discussed previously. Using this approach, the authors achieved a transduction efficiency of 45%, when the vector was combined with vasodilator and microvascular permeability enhancing agents[341]. Of note, this approach achieved successful modification of AV nodal electrophysiology via overexpression of $G\alpha_{i2}$[341]. This approach, demonstrated here in pigs, may not be suitable for small animal models of disease where catherterisation of miniscule coronary arterial branches would be extremely challenging. Thus, this

technique would be limited in most animal models of disease and transgenic studies, the majority of which are carried out in small mammals such as mice. In addition, adenoviral vectors are limited by their short duration of transgene expression, partially attributed to high immunogenicity[487]. Here we achieved a higher transduction efficiency of 65% in the SAN using systemic IV administration of AAV9. Given the successful alteration of AVN electrophysiology with only 45% transduction efficiency, it seems reasonable that the 65% achieved by our systemic method would be sufficient for therapeutic modulation of gene expression. As previously mentioned, future challenges involve identification of minimal regulatory elements capable of driving gene expression in the CCS specifically, rather than from ubiquitous promoters. To this end, the development of constructs such as the aforementioned CCS specific ISL1 enhancer may pave the way for such efforts, with a focus on identifying minimal elements capable of recapitulating CCS specific expression[450].

6.7.1 Fine tuning AAV transgene expression using miR binding sites

Tissue specific miR expression also presents the opportunity to provide further restriction of transgene expression. miR binding sites can be introduced into AAV vector transgene cassettes in order to attenuate transgene expression in certain tissues where expression of that particular miR is high. Assuming low expression of the candidate miR in the target tissue, mRNA degradation and translational repression occurs only in off target tissues where miR expression is high (mechanism shown in figure 6.1). To this end, miR mediated repression of gene expression mainly occurs via decreasing target mRNA levels[488].

Aside from the heart, AAV9 mediated transgene expression is usually highest in the liver, especially when vectors are administered systemically[206,401]. Thus, detargeting transgene expression from the liver has received particular interest. One study inserted 5 copies of the liver specific miR-122 target sequence into the 3' UTR of an AAV expression construct, and after intravenous injection of the vectors, a 50 fold reduction in hepatic luciferase reporter expression was observed, without any reduction in the heart[489]. This approach has also been successfully used to achieve cell type specific transgene expression within whole organs, such as to astrocytes in the brain via neuronal detargeting using miR-124[490]. Another example used a combination of miR target sites to achieve cell specific transgene expression in the liver. Effective detargeting of GFP transgene expression in Kuppfer cells and hepatocytes was achieved via inclusion of miR-142-3p and miR-122a sites respectively, and transgene expression was restricted to liver endothelial cells i*n vivo*[491]. Thus, using multiple miR target sites can be used to effectively fine tune transgene expression *in vivo*. This technique could be particularly useful in directing transgene expression in the CCS via detargeting

from the working myocardial cells. To this end, HCN4 and KCNE1 are both expressed in multiple components of the CCS, and so the respective promoters may not be capable of restricting transgene expression to the SAN, AVN or Purkinje fibres specifically. Here, SAN/ AVN/ His-Purkinje specific or enriched miRs could facilitate true compartment specific transgene expression.

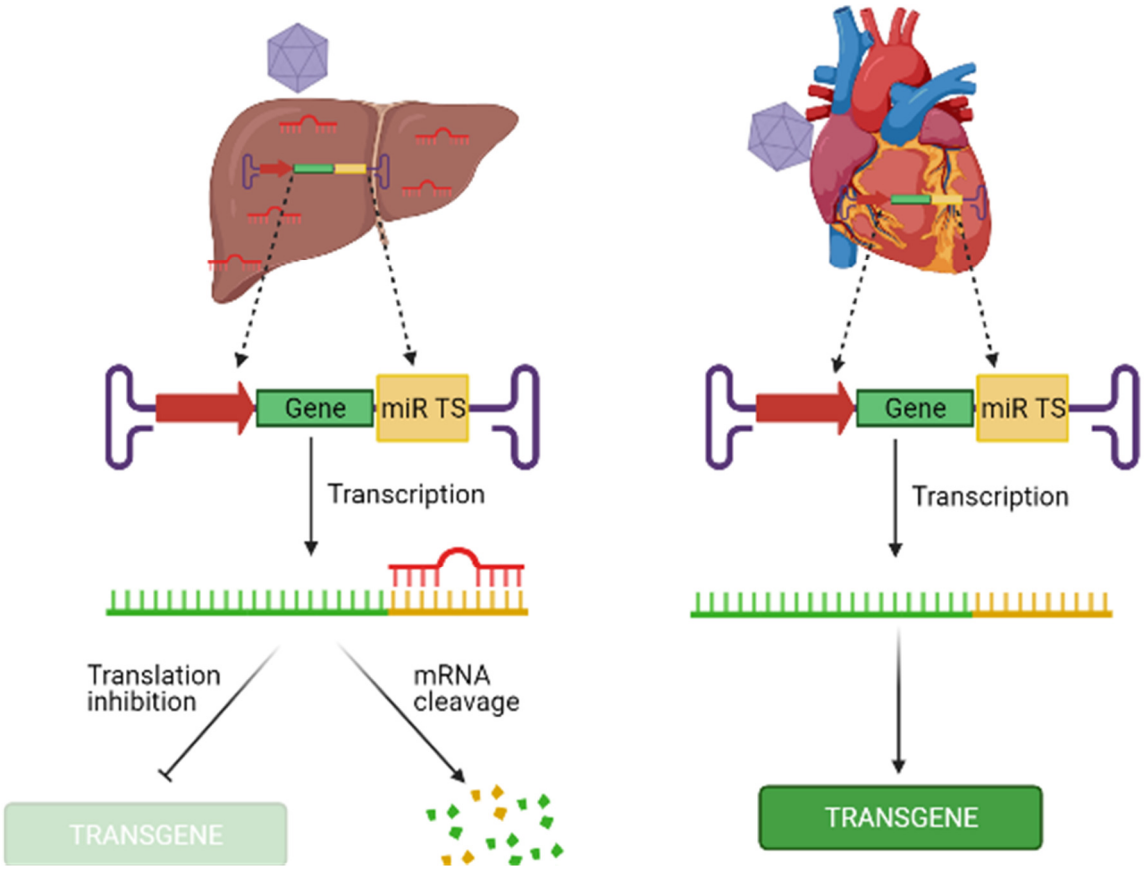

Figure 6.1: mechanism of miR detargeting of AAV vectors. In this example, transgene expression is detargeted from the liver. AAV delivers it's transgene cargo to both heart and liver effectively, resulting in high vector genome copy numbers. AAV expression constructs have been designed to include multiple copies of a miR binding site, where the miR is expressed highly in the liver, but minimally in the heart. In the liver, endogenous miRs bind to the transgene at the engineered complimentary binding sites, inducing repression of the encoded transgene by mRNA degradation and/ or translational repression. In the heart, there is little or endogenous miR expressed, and thus the transgene is free to be expressed without repression. This results in high expression of the transgene in the heart, and reduced off target expression in the liver. miR TS- microRNA target sequence. Figure generated using BioRender.

However, it must also be considered that miR expression changes in response to disease[492]. Thus, miRs used for detargeting would need to be also absent or expressed only at very low levels in the target tissue also in disease in order to avoid interfering with transgene expression. To this end, one study demonstrated that miR-122, previously considered to be liver specific, was also expressed in the heart of certain transgenic mouse strains, and this expression significantly attenuated cardiac transgene expression from AAV9-miR-122 liver detargeted vectors[493]. Furthermore, miR-122 was also found in the hearts of humans suffering from dilated cardiomyopathy[493]. Thus, it would be important to validate any proposed de-targeting miR in the species and disease model of choice before proceeding to therapeutic trial using AAV vectors.

As previously mentioned, miR expression profiles have been examined between SAN tissue and RA in human tissue[429]. 18 miRs showed significantly higher expression in the SAN, whereas 48 were significantly higher in RA[429]. The largest difference was seen with miR-1233, which was high in RA but very low in SAN. This miR could represent a candidate for atrial detargeting of transgene expression from AAV9-cTnT-GFP for example. However, it is unclear whether this expression gradient is also evident in mouse tissue, and if expression of miR-1233 is also high in the ventricles, so as to provide ventricular detargeting also. Studies have documented increased circulating levels of miR-1233 in both heart failure[494] and cases of congenital heart disease[495], however it is unclear if the tissue expression is high, or heightened in disease. Further profiling of the unique transcriptional profile of CCS tissue in comparison to the working myocardium will elucidate other potential candidates for enhancing AAV mediated transgene specificity**.**

6.8 Concluding remarks

The work presented herein provides proof of concept for a systemic gene therapy to target the SAN from a single intravenous dose of AAV9. Although we were unable to achieve specific gene expression in the SAN or other components of the CCS using tissue specific promoters, the feasibility of our approach has been validated on a proof of concept level. Now that the gene delivery vehicle is validated, future studies must focus on understanding the transcriptional mechanisms that govern CCS specific gene expression. It is clear that these mechanisms are complex, given the lack of intrinsic transcriptional activity conferred by CCS specific promoter candidates of KCNE1 and HCN4 *in vivo*. However, it is important to bear in mind that time constraints precluded detailed analysis of AAV9 mediated transgene delivery and promoter performance in the AVN and Purkinje fibres. Thus, further studies are required to confirm if the findings for the SAN hold for the wider CCS.

Most studies examining transcriptional control of the CCS examine this in the context of development, and thus the identification of discrete minimal promoter and/ or enhancer elements capable of driving transgene expression in the adult heart requires further work. The recent discovery of a 2.9 kb CCS specific ISL1 enhancer active in the adult heart is a promising development, and warrants the further use of methods such as ATAC-seq to provide further insights into other promoter/ enhancer elements important for CCS specific gene expression[450].

A key issue confounding the current study was the scarcity of suitable *in vitro* test beds for studying promoter activity in SAN and other CCS cells. Primary SAN cells are difficult to isolate and suffer from low cell yield, contamination with adjacent working myocardial cells, and low survival, particularly when exposed to transfection reagents. We were successful in isolating and conferring transgene expression from adenoviral vectors in rat SAN cells using AdV-CMV-GFP(data not shown). However further analysis of CCS specific promoters was confounded by errors in vector generation, as previously discussed.

Stem cell derived Shox2 cells were an appropriate candidate for this purpose, although ultimately the performance of promoters *in vitro* was not a reflection of their characteristics *in vivo*. This issue is also prevalent in the wider study of promoters/ enhancers predicted via conservation analysis, where in vivo validation rate is generally very low at ~2%[439]. This low *in vivo* success rate highlights the necessity for reliable *in vitro* model systems for validation studies. Neonatal rat ventricular cardiomyocytes may also be appropriate since they express low levels of HCN channels and I_f, albeit If is mainly carried by HCN2 in these cells[496]. However, in the postnatal phase, HCN4 is strongly downregulated in the ventricles[371]. This is essential for coordinated electrical function of the heart, and ectopic ventricular HCN expression has been associated with arrhythmia development in heart failure[451]. Thus, studying HCN4 promoter activity in cells in which the downstream gene is under active repression may not be ideal, and most likely will not reflect the native SAN tissue. Another potential test bed is the isolated SAN tissue explant, where tissue may be maintained viable at intrinsic rates of above 400 bpm for at least 48 hours in culture. This system has the advantage of circumventing lengthy cell isolation procedures and concomitant low cell yield. In future, this may be the best *in vitro* model for promoter validation before progressing to *in vivo* studies using expensive AAV vectors.

In the absence of CCS specific promoters, it may also be possible to re-purpose existing cardiac specific promoters that are also active in the CCS. We have shown in the current study that the cTnT promoter, as well as conferring high transgene expression in the working myocardium, is also active in the SAN. Other cardiac genes are also prominently expressed in the CCS, including MLC2V and

alpha MHC[403]. This strategy has been previously discussed, but could be achieved in 2 primary methods: i) utilising cardiac compartment specific miR binding sites to selectively repress transgene expression, or ii) utilising so called CCS specific 'switches' such as the GATA dependent elements discussed previously. The latter perhaps requires the most development, as such elements have been primarily studied in the developing, rather than the postnatal heart, and were mostly specific to the AV canal[445]. miR expression profiling has already been carried out in the SAN, and some highly SAN- enriched miRs have been identified, paving the way for the generation of miR detargeted AAV vectors for CCS specific gene expression[429].

In conclusion, it appears that CCS specific systemic gene therapy is an achievable goal. Future studies should aim to generate further understanding of CCS specific gene regulatory mechanisms, and trial promising minimal promoter/ enhancer elements *in vivo* in combination with AAV vectors, as used in the current study. Given the increasingly appreciated role of gene expression (particularly ion channel) remodelling in multiple disease states contributing to CCS dysfunction, development of the tools to harness these potential therapeutic targets should be of key importance.

7.0 References

1. Dobrzynski, H. *et al.* Structure, function and clinical relevance of the cardiac conduction system, including the atrioventricular ring and outflow tract tissues. *Pharmacol. Ther.* **139**, 260–288 (2013).
2. Sanders, P., Kistler, P. M., Morton, J. B., Spence, S. J. & Kalman, J. M. Remodeling of sinus node function in patients with congestive heart failure: reduction in sinus node reserve. *Circulation* **110**, 897–903 (2004).
3. Lip, G. Y. H. *et al.* Hypertension and cardiac arrhythmias: a consensus document from the European Heart Rhythm Association (EHRA) and ESC Council on Hypertension, endorsed by the Heart Rhythm Society (HRS), Asia-Pacific Heart Rhythm Society (APHRS) and Sociedad Latinoamericana de Estimulaci on Card ıaca y Electrofisiolog ıa (SOLEACE). doi:10.1093/europace/eux091.
4. Grisanti, L. A. Diabetes and Arrhythmias: Pathophysiology, Mechanisms and Therapeutic Outcomes. *Front. Physiol.* **9**, (2018).
5. Keith, A. & Flack, M. The Form and Nature of the Muscular Connections between the Primary Divisions of the Vertebrate Heart. *J. Anat. Physiol.* **41**, 172–89 (1907).
6. Anderson, K. R., Ho, S. Y. & Anderson, R. H. Location and vascular supply of sinus node in human heart. *Br. Heart J.* **41**, 28–32 (1979).
7. Chandler, N. *et al.* Computer Three-Dimensional Anatomical Reconstruction of the Human Sinus Node and a Novel Paranodal Area. *Anat. Rec. Adv. Integr. Anat. Evol. Biol.* **294**, 970–979 (2011).
8. Gomes, J. A. & Winters, S. L. The origins of the sinus node pacemaker complex in man: demonstration of dominant and subsidiary foci. *J. Am. Coll. Cardiol.* **9**, 45–52 (1987).
9. Schuessler, R. B., Boineau, J. P. & Bromberg, B. I. Origin of the sinus impulse. *J. Cardiovasc. Electrophysiol.* **7**, 263–74 (1996).
10. Choudhury, M., Boyett, M. R. & Morris, G. M. Biology of the Sinus Node and its Disease. *Arrhythmia Electrophysiol. Rev.* **4**, 28–34 (2015).
11. Boyett, M. R., Honjo, H. & Kodama, I. The sinoatrial node, a heterogeneous pacemaker structure. *Cardiovasc. Res.* **47**, 658–87 (2000).
12. JAMES, T. N., SHERF, L., FINE, G. & MORALES, A. R. Comparative Ultrastructure of the Sinus Node in Man and Dog. *Circulation* **34**, (1966).
13. Verheijck, E. E. *et al.* Distribution of Atrial and Nodal Cells Within the Rabbit Sinoatrial Node Models of Sinoatrial Transition.
14. Bleeker, W. K., Mackaay, A. J., Masson-Pévet, M., Bouman, L. N. & Becker, A. E. Functional

and morphological organization of the rabbit sinus node. *Circ. Res.* **46**, 11–22 (1980).

15. Monfredi, O., Dobrzynski, H., Mondal, T., Boyett, M. R. & Morris, G. M. The Anatomy and Physiology of the Sinoatrial Node—A Contemporary Review. doi:10.1111/j.1540-8159.2010.02838.x.
16. Severs, N. *et al.* Gap junction alterations in human cardiac disease. *Cardiovasc. Res.* **62**, 368–377 (2004).
17. Weisbrod, D., Khun, S. H., Bueno, H., Peretz, A. & Attali, B. Mechanisms underlying the cardiac pacemaker: the role of SK4 calcium-activated potassium channels. *Acta Pharmacol. Sin.* **37**, 82–97 (2016).
18. Baruscotti, M., Barbuti, A. & Bucchi, A. The cardiac pacemaker current. *J. Mol. Cell. Cardiol.* **48**, 55–64 (2010).
19. Michels, G. *et al.* Direct evidence for calcium conductance of hyperpolarization-activated cyclic nucleotide-gated channels and human native If at physiological calcium concentrations. *Cardiovasc. Res.* **78**, 466–475 (2008).
20. DiFrancesco, D. The Role of the Funny Current in Pacemaker Activity. *Circ. Res.* **106**, 434–446 (2010).
21. Alig, J. *et al.* Control of heart rate by cAMP sensitivity of HCN channels. *Proc. Natl. Acad. Sci. U. S. A.* **106**, 12189–94 (2009).
22. Baruscotti, M., Bucchi, A. & DiFrancesco, D. Physiology and pharmacology of the cardiac pacemaker ("funny") current. *Pharmacol. Ther.* **107**, 59–79 (2005).
23. DiFrancesco, D. & Tortora, P. Direct activation of cardiac pacemaker channels by intracellular cyclic AMP. *Nature* **351**, 145–147 (1991).
24. Yaniv, Y., Maltsev, V. A., Ziman, B. D., Spurgeon, H. A. & Lakatta, E. G. The "Funny" Current (If) Inhibition by Ivabradine at Membrane Potentials Encompassing Spontaneous Depolarization in Pacemaker Cells. *Molecules* **17**, 8241–8254 (2012).
25. Bucchi, A., Barbuti, A., Difrancesco, D. & Baruscotti, M. Funny Current and Cardiac Rhythm: Insights from HCN Knockout and Transgenic Mouse Models. *Front. Physiol.* **3**, 240 (2012).
26. Mesirca, P. *et al.* Cardiac arrhythmia induced by genetic silencing of 'funny' (f) channels is rescued by GIRK4 inactivation. *Nat. Commun.* **5**, 4664 (2014).
27. Milano, A. *et al.* HCN4 mutations in multiple families with bradycardia and left ventricular noncompaction cardiomyopathy. *J. Am. Coll. Cardiol.* **64**, 745–756 (2014).
28. LAISH-FARKASH, A. *et al.* A Novel Mutation in the HCN4 Gene Causes Symptomatic Sinus Bradycardia in Moroccan Jews. *J. Cardiovasc. Electrophysiol.* **21**, 1365–1372 (2010).
29. M, B. *et al.* A gain-of-function mutation in the cardiac pacemaker HCN4 channel increasing

cAMP sensitivity is associated with familial Inappropriate Sinus Tachycardia. *Eur. Heart J.* **38**, 280–288 (2017).

30. Hagiwara, N., Irisawa, H. & Kameyama, M. Contribution of two types of calcium currents to the pacemaker potentials of rabbit sino-atrial node cells. *J. Physiol.* **395**, 233–53 (1988).
31. Bogdanov, K. Y., Vinogradova, T. M. & Lakatta, E. G. Sinoatrial Nodal Cell Ryanodine Receptor and Na+-Ca2+ Exchanger. *Circ. Res.* **88**, (2001).
32. Lei, M., Cooper, P. J., Camelliti, P. & Kohl, P. Role of the 293b-sensitive, slowly activating delayed rectifier potassium current, iKs, in pacemaker activity of rabbit isolated sino-atrial node cells. *Cardiovasc. Res.* **53**, 68–79 (2002).
33. Lei, M. & Brown, H. Two components of the delayed rectifier potassium current, IK, in rabbit sino-atrial node cells. *Exp. Physiol.* **81**, 725–741 (1996).
34. Joung, B., Ogawa, M., Lin, S.-F. & Chen, P.-S. The calcium and voltage clocks in sinoatrial node automaticity. *Korean Circ. J.* **39**, 217–22 (2009).
35. Kapoor, N. *et al.* Regulation of calcium clock-mediated pacemaking by inositol-1,4,5-trisphosphate receptors in mouse sinoatrial nodal cells. *J. Physiol.* **593**, 2649–63 (2015).
36. Hüser, J., Blatter, L. A. & Lipsius, S. L. Intracellular Ca2+ release contributes to automaticity in cat atrial pacemaker cells. *J. Physiol.* **524 Pt 2**, 415–22 (2000).
37. Yaniv, Y., Lakatta, E. G. & Maltsev, V. A. From two competing oscillators to one coupled-clock pacemaker cell system. *Front. Physiol.* **6**, 28 (2015).
38. Vinogradova, T. M. *et al.* Sinoatrial Node Pacemaker Activity Requires Ca 2⁒ /Calmodulin-Dependent Protein Kinase II Activation.
39. Baudot, M. *et al.* Concomitant genetic ablation of L-type Ca v 1.3 (α 1D) and T-type Ca v 3.1 (α 1G) Ca 2+ channels disrupts heart automaticity. (2020) doi:10.1038/s41598-020-76049-7.
40. Irisawa, H., Brown, H. F. & Giles, W. Cardiac pacemaking in the sinoatrial node. *Physiol. Rev.* **73**, 197–227 (1993).
41. Boyett, M. R. *et al.* Downward gradient in action potential duration along conduction path in and around the sinoatrial node. *Am. J. Physiol.* **276**, H686-98 (1999).
42. Dobrzynski, H. *et al.* Site of Origin and Molecular Substrate of Atrioventricular Junctional Rhythm in the Rabbit Heart. *Circ. Res.* **93**, 1102–1110 (2003).
43. Mani, B. C. & Pavri, B. B. Dual Atrioventricular Nodal Pathways Physiology: A Review of Relevant Anatomy, Electrophysiology, and Electrocardiographic Manifestations. *Indian Pacing Electrophysiol. J.* **14**, 12 (2014).
44. Mazgalev, T. & Tchou, P. Atrioventricular Nodal Conduction Gap and Dual Pathway

Electrophysiology. *Circulation* **92**, (1995).

45. Nikolski, V. P., Jones, S. A., Lancaster, M. K., Boyett, M. R. & Efimov, I. R. Cx43 and Dual-Pathway Electrophysiology of the Atrioventricular Node and Atrioventricular Nodal Reentry. *Circ. Res.* **92**, 469–475 (2003).
46. Greener, I. D. *et al.* Ion Channel Transcript Expression at the Rabbit Atrioventricular Conduction Axis. *Circ. Arrhythmia Electrophysiol.* **2**, 305–315 (2009).
47. Nikmaram, M. R. *et al.* Characterization of the effects of Ryanodine, TTX, E-4031 and 4-AP on the sinoatrial and atrioventricular nodes. *Prog. Biophys. Mol. Biol.* **96**, 452–464 (2008).
48. Munk, A. A., Adjemian, R. A., Zhao, J., Ogbaghebriel, A. & Shrier, A. Electrophysiological properties of morphologically distinct cells isolated from the rabbit atrioventricular node. *J. Physiol.* **493**, 801–818 (1996).
49. Peters, N. S. & Wit, A. L. Myocardial Architecture and Ventricular Arrhythmogenesis.
50. Greener, I. D. *et al.* Molecular architecture of the human specialised atrioventricular conduction axis. *J. Mol. Cell. Cardiol.* **50**, 642–651 (2011).
51. Temple, I. P., Inada, S., Dobrzynski, H. & Boyett, M. R. Connexins and the atrioventricular node. *Hear. Rhythm* **10**, 297–304 (2013).
52. Temple, I. P., Inada, S., Dobrzynski, H. & Boyett, M. R. Connexins and the atrioventricular node. *Hear. Rhythm* **10**, 297–304 (2013).
53. Ansari, A., Ho, S. Y. & Anderson, R. H. Distribution of the Purkinje fibres in the sheep heart. *Anat. Rec.* **254**, 92–7 (1999).
54. Tranum-Jensen, J., Wilde, A. A., Vermeulen, J. T. & Janse, M. J. Morphology of electrophysiologically identified junctions between Purkinje fibers and ventricular muscle in rabbit and pig hearts. *Circ. Res.* **69**, 429–37 (1991).
55. IDEKER, R. E., KONG, W. & POGWIZD, S. Purkinje Fibers and Arrhythmias. *Pacing Clin. Electrophysiol.* **32**, 283–285 (2009).
56. Haissaguerre, M., Vigmond, E., Stuyvers, B., Hocini, M. & Bernus, O. Ventricular arrhythmias and the His–Purkinje system. *Nat. Rev. Cardiol.* **13**, 155–166 (2016).
57. Scheinman, M. M., Verma, A., Wazni, O. & al., et. Role of the His-Purkinje system in the genesis of cardiac arrhythmia. *Hear. Rhythm* **6**, 1050–1058 (2009).
58. Dun, W. & Boyden, P. A. The Purkinje cell; 2008 style. *J. Mol. Cell. Cardiol.* **45**, 617–24 (2008).
59. Persson, F., Andersson, B., Duker, G., Jacobson, I. & Carlsson, L. Functional effects of the late sodium current inhibition by AZD7009 and lidocaine in rabbit isolated atrial and ventricular tissue and Purkinje fibre. *Eur. J. Pharmacol.* **558**, 133–143 (2007).

60. Atkinson, A. *et al.* Anatomical and molecular mapping of the left and right ventricular His–Purkinje conduction networks. *J. Mol. Cell. Cardiol.* **51**, 689–701 (2011).
61. Schram, G., Pourrier, M., Melnyk, P. & Nattel, S. Differential Distribution of Cardiac Ion Channel Expression as a Basis for Regional Specialization in Electrical Function Overview of Regional Functional Specificity. doi:10.1161/01.RES.0000018627.89528.6F.
62. Nerbonne, J. M. & Kass, R. S. Molecular Physiology of Cardiac Repolarization. *Physiol. Rev.* **85**, 1205–1253 (2005).
63. Brugada, R., Campuzano, O., Sarquella-Brugada, G., Brugada, J. & Brugada, P. Brugada syndrome. *Methodist DeBakey cardiovascular journal* vol. 10 25–28 (2014).
64. D'Souza, A., Sharma, S. & Boyett, M. R. CrossTalk opposing view: Bradycardia in the trained athlete is attributable to a downregulation of a pacemaker channel in the sinus node. *Journal of Physiology* vol. 593 1749–1751 (2015).
65. Chang, H.-Y. *et al.* Sinus node dysfunction in atrial fibrillation patients: the evidence of regional atrial substrate remodelling. doi:10.1093/europace/eus219.
66. Yeh, Y.-H. *et al.* Funny Current Downregulation and Sinus Node Dysfunction Associated With Atrial Tachyarrhythmia: A Molecular Basis for Tachycardia-Bradycardia Syndrome. *Circulation* **119**, 1576–1585 (2009).
67. Chen, Z., Sun, B., Tse, G., Jiang, J. & Xu, W. *Original Article Reversibility of both sinus node dysfunction and reduced HCN4 mRNA expression level in an atrial tachycardia pacing model of tachycardia-bradycardia syndrome in rabbit hearts*. *Int J Clin Exp Pathol* vol. 9 www.ijcep.com/ (2016).
68. STOCKBURGER, M. *et al.* Pacemaker-Based Analysis of Atrioventricular Conduction and Atrial Tachyarrhythmias in Patients with Primary Sinus Node Dysfunction. *Pacing Clin. Electrophysiol.* **32**, 604–613 (2009).
69. Gervais, R. *et al.* Surface electrocardiogram to predict outcome in candidates for cardiac resynchronization therapy: a sub-analysis of the CARE-HF trial. *Eur. J. Heart Fail.* **11**, 699–705 (2009).
70. Olshansky, B. *et al.* Does cardiac resynchronization therapy provide unrecognized benefit in patients with prolonged PR intervals? The impact of restoring atrioventricular synchrony: An analysis from the COMPANION Trial. *Hear. Rhythm* **9**, 34–39 (2012).
71. Park, S.-J. *et al.* Short- and long-term outcomes depending on electrical dyssynchrony markers in patients presenting with acute heart failure: clinical implication of the first-degree atrioventricular block and QRS prolongation from the Korean Heart Failure registry. *Am. Heart J.* **165**, 57-64.e2 (2013).

72. Kashou, A. H., Goyal, A., Nguyen, T. & Chhabra, L. Atrioventricular Block. *StatPearls* (2021).
73. Feigl, D., Ashkenazy, J. & Kishon, Y. Early and late atrioventricular block in acute inferior myocardial infarction. *J. Am. Coll. Cardiol.* **4**, 35–8 (1984).
74. Knabben, V., Chhabra, L. & Slane, M. *Third-Degree Atrioventricular Block*. *StatPearls* (StatPearls Publishing, 2021).
75. Forrester, J. D. & Mead, P. Third-degree heart block associated with lyme carditis: Review of published cases. *Clinical Infectious Diseases* vol. 59 996–1000 (2014).
76. Kashani, A. & Barold, S. S. Significance of QRS Complex Duration in Patients With Heart Failure. *J. Am. Coll. Cardiol.* **46**, 2183–2192 (2005).
77. Parmley, W. W. Factors causing arrhythmias in chronic congestive heart failure. *Am. Heart J.* **114**, 1267–1272 (1987).
78. Zipes, D. P. & Wellens, H. J. Sudden cardiac death. *Circulation* **98**, 2334–51 (1998).
79. Freudenberger, R., Sikora, J. A., Fisher, M., Wilson, A. & Gold, M. Electrocardiogram and clinical characteristics of patients referred for cardiac transplantation: Implications for pacing in heart failure. *Clin. Cardiol.* **27**, 151–153 (2004).
80. Kalra, P. R. *et al.* Clinical characteristics and survival of patients with chronic heart failure and prolonged QRS duration. *Int. J. Cardiol.* **86**, 225–31 (2002).
81. Iuliano, S. *et al.* QRS duration and mortality in patients with congestive heart failure. *Am. Heart J.* **143**, 1085–91 (2002).
82. Xiao, H. B., Roy, C., Fujimoto, S. & Gibson, D. G. Natural history of abnormal conduction and its relation to prognosis in patients with dilated cardiomyopathy. *Int. J. Cardiol.* **53**, 163–70 (1996).
83. Ariyaratnam J, Yanni J, Nikolaidou T, Wang Y, Morris GM, Hart G, Monfredi OJ and Boyett, M. Control of heart rate in heart failure - treading a fine line. *J. Am. Coll. Cardiol.* **Invited re**, (2017).
84. Dunn, M. Left bundle branch block: variations on a theme. *J. Am. Coll. Cardiol.* **10**, 81–2 (1987).
85. Shamim, W. *et al.* Intraventricular conduction delay: a prognostic marker in chronic heart failure. *Int. J. Cardiol.* **70**, 171–8 (1999).
86. Csepe, T. A., Kalyanasundaram, A., Hansen, B. J., Zhao, J. & Fedorov, V. V. Fibrosis: a structural modulator of sinoatrial node physiology and dysfunction. *Front. Physiol.* **6**, 37 (2015).
87. Thery, C., Gosselin, B., Lekieffre, J. & Warembourg, H. Pathology of sinoatrial node. Correlations with electrocardiographic findings in 111 patients. *Am. Heart J.* **93**, 735–40

(1977).

88. Brignole, M. Sick sinus syndrome. *Clin. Geriatr. Med.* **18**, 211–27 (2002).

89. Biernacka, A. & Frangogiannis, N. G. Aging and Cardiac Fibrosis. *Aging Dis.* **2**, 158–173 (2011).

90. Morris, G. M. *et al.* Characterization of a right atrial subsidiary pacemaker and acceleration of the pacing rate by HCN over-expression. *Cardiovasc. Res.* **100**, 160–169 (2013).

91. Alings, A. M., Abbas, R. F. & Bouman, L. N. Age-related changes in structure and relative collagen content of the human and feline sinoatrial node. A comparative study. *Eur. Heart J.* **16**, 1655–67 (1995).

92. Evans, R. & Shaw, D. B. Pathological studies in sinoatrial disorder (sick sinus syndrome). *Br. Heart J.* **39**, 778–786 (1077).

93. Glukhov, A. V. *et al.* Calsequestrin 2 deletion causes sinoatrial node dysfunction and atrial arrhythmias associated with altered sarcoplasmic reticulum calcium cycling and degenerative fibrosis within the mouse atrial pacemaker complex. *Eur. Heart J.* **36**, 686-697a (2015).

94. Yanni, J., Tellez, J. O., Sutyagin, P. V., Boyett, M. R. & Dobrzynski, H. Structural remodelling of the sinoatrial node in obese old rats. *J. Mol. Cell. Cardiol.* **48**, 653–662 (2010).

95. Gui, J. *et al.* Multiple Loss-of-Function Mechanisms Contribute to SCN5A-Related Familial Sick Sinus Syndrome. *PLoS One* **5**, e10985 (2010).

96. Zhang, J. *et al.* MicroRNA-1976 regulates degeneration of the sinoatrial node by targeting Cav1.2 and Cav1.3 ion channels. *J. Mol. Cell. Cardiol.* **134**, 74–85 (2019).

97. Tellez, J. O. *et al.* Ageing-dependent remodelling of ion channel and Ca $^{2+}$ clock genes underlying sino-atrial node pacemaking. *Exp. Physiol.* **96**, 1163–1178 (2011).

98. Baldesberger, S. *et al.* Sinus node disease and arrhythmias in the long-term follow-up of former professional cyclists. *Eur. Heart J.* **29**, 71–78 (2007).

99. Northcote, R. J., Canning, G. P. & Ballantyne, D. Electrocardiographic findings in male veteran endurance athletes. *Br. Heart J.* **61**, 155–160 (1989).

100. Northcote, R. J., Rankin, A. C., Scullion, R. & Logan, W. Is severe bradycardia in veteran atheletes an indication for a permanent pacemaker? *Br. Med. J.* **298**, 231–232 (1989).

101. D'Souza, A. *et al.* Exercise training reduces resting heart rate via downregulation of the funny channel HCN4. *Nat. Commun.* **5**, 3775 (2014).

102. Boyett, M. R. *et al.* Viewpoint: Is the resting bradycardia in athletes the result of remodeling of the sinoatrial node rather than high vagal tone? *Journal of Applied Physiology* vol. 114 1351–1355 (2013).

103. Hall, M. E., George, E. M. & Granger, J. P. The Heart During Pregnancy CARDIOVASCULAR ADAPTATIONS DURING NORMAL PREGNANCY. *Rev Esp Cardiol* **64**, 1045–1050 (2011).
104. El Khoury, N. *et al.* Upregulation of the hyperpolarization-activated current increases pacemaker activity of the sinoatrial node and heart rate during pregnancy in mice. *Circulation* **127**, 2009–20 (2013).
105. ZICHA, S. *et al.* Sinus node dysfunction and hyperpolarization-activated (HCN) channel subunit remodeling in a canine heart failure model. *Cardiovasc. Res.* **66**, 472–481 (2005).
106. Yanni, J. *et al.* Changes in ion channel gene expression underlying heart failure-induced sinoatrial node dysfunction. *Circ. Heart Fail.* **4**, 496–508 (2011).
107. Yanni J, Wang Y, Zeef L, Choudhury M, Zi M, Cai X, Logantha SJRJ, Nakao S, Atkinson A, Petkova M, Doris U, Ariyaratnam J, Cartwright E, Hart G, D. H. and B. M., Yanni J, Wang Y, Zeef L, Choudhury M, Zi M, Cai X, Logantha SJRJ, Nakao S, Atkinson A, Petkova M, Doris U, A. & J, Cartwright E, Hart G, D. H. and B. M. Silencing miR-370 rescues funny current and sinus node function and improves survival in heart failure. *Nat. Commun.* **Full paper**, (2017).
108. Yanni, J. *et al.* Silencing miR-370-3p rescues funny current and sinus node function in heart failure. *Sci. Rep.* **10**, 11279 (2020).
109. Milanesi, R., Baruscotti, M., Gnecchi-Ruscone, T. & DiFrancesco, D. Familial Sinus Bradycardia Associated with a Mutation in the Cardiac Pacemaker Channel. *N. Engl. J. Med.* **354**, 151–157 (2006).
110. Ishikawa, T. *et al.* Sick sinus syndrome with HCN4 mutations shows early onset and frequent association with atrial fibrillation and left ventricular noncompaction. *Hear. Rhythm* **14**, 717–724 (2017).
111. Opthof, T. *et al.* Changes in sinus node function in a rabbit model of heart failure with ventricular arrhythmias and sudden death. *Circulation* **101**, 2975–80 (2000).
112. Verkerk, A. O., Wilders, R., Coronel, R., Ravesloot, J. H. & Verheijck, E. E. Ionic Remodeling of Sinoatrial Node Cells by Heart Failure. *Circulation* **108**, 760–766 (2003).
113. Howarth, F. C., Nowotny, N., Zilahi, E., El Haj, M. A. & Lei, M. Altered expression of gap junction connexin proteins may partly underlie heart rhythm disturbances in the streptozotocin-induced diabetic rat heart. *Mol. Cell. Biochem.* **305**, 145–151 (2007).
114. Zhang, Y. *et al.* Electrical Conduction System Remodeling in Streptozotocin-Induced Diabetes Mellitus Rat Heart. *Front. Physiol.* **10**, 826 (2019).
115. Boyett, M. R. *et al.* Connexins in the sinoatrial and atrioventricular nodes. *Advances in Cardiology* vol. 42 175–197 (2006).

116. Qiao, Y. *et al.* Transient Notch Activation Induces Long-Term Gene Expression Changes Leading to Sick Sinus Syndrome in Mice. *Circ. Res.* (2017).
117. Yang, B. *et al.* Mitochondrial thioredoxin-2 maintains HCN4 expression and prevents oxidative stress-mediated sick sinus syndrome. *J. Mol. Cell. Cardiol.* (2020) doi:10.1016/j.yjmcc.2019.10.009.
118. Kuratomi, S. *et al.* NRSF regulates the developmental and hypertrophic changes of HCN4 transcription in rat cardiac myocytes. *Biochem. Biophys. Res. Commun.* **353**, 67–73 (2007).
119. Liguori, I. *et al.* Oxidative stress, aging, and diseases. *Clin. Interv. Aging* **13**, 757–772 (2018).
120. Samman Tahhan, A. *et al.* Association between oxidative stress and atrial fibrillation. *Hear. Rhythm* **14**, 1849–1855 (2017).
121. Yang, K.-C. & Dudley, S. C. Oxidative stress and atrial fibrillation: finding a missing piece to the puzzle. *Circulation* **128**, 1724–6 (2013).
122. Giordano, F. J. Oxygen, oxidative stress, hypoxia, and heart failure. *J. Clin. Invest.* **115**, 500–508 (2005).
123. Beckendorf, J., van den Hoogenhof, M. M. G. & Backs, J. Physiological and unappreciated roles of CaMKII in the heart. *Basic Research in Cardiology* vol. 113 29 (2018).
124. Swaminathan, P. D. *et al.* Oxidized CaMKII causes cardiac sinus node dysfunction in mice. *J. Clin. Invest.* **121**, 3277–88 (2011).
125. Backs, J., Song, K., Bezprozvannaya, S., Chang, S. & Olson, E. N. CaM kinase II selectively signals to histone deacetylase 4 during cardiomyocyte hypertrophy. *J. Clin. Invest.* **116**, 1853–1864 (2006).
126. An, M. & Kim, M. Protective effects of kaempferol against cardiac sinus node dysfunction via CaMKII deoxidization. *Anat. Cell Biol.* **48**, 235–43 (2015).
127. Hao, X. *et al.* TGF- 1-Mediated Fibrosis and Ion Channel Remodeling Are Key Mechanisms in Producing the Sinus Node Dysfunction Associated With SCN5A Deficiency and Aging. *Circ. Arrhythmia Electrophysiol.* **4**, 397–406 (2011).
128. D'Souza, A. *et al.* Targeting miR-423-5p Reverses Exercise Training-Induced HCN4 Channel Remodeling and Sinus Bradycardia. *Circ. Res.* **121**, 1058–1068 (2017).
129. Jones, S. A., Boyett, M. R. & Lancaster, M. K. Declining into failure: The age-dependent loss of the L-type calcium channel within the sinoatrial node. *Circulation* **115**, 1183–1190 (2007).
130. Larson, E. D., Clair, J. R. S., Sumner, W. A., Bannister, R. A. & Proenza, C. Depressed pacemaker activity of sinoatrial node myocytes contributes to the age-dependent decline in maximum heart rate. *Proc. Natl. Acad. Sci. U. S. A.* **110**, 18011–18016 (2013).

131. Nikolaidou, T. *et al.* Congestive Heart Failure Leads to Prolongation of the PR Interval and Atrioventricular Junction Enlargement and Ion Channel Remodelling in the Rabbit. *PLoS One* **10**, e0141452 (2015).
132. Yanni, J. *et al.* Structural and functional alterations in the atrioventricular node and atrioventricular ring tissue in ischaemia-induced heart failure. *Histol. Histopathol.* **29**, 891–902 (2014).
133. Temple, I. P. *et al.* Atrioventricular Node Dysfunction and Ion Channel Transcriptome in Pulmonary Hypertension. *Circ. Arrhythmia Electrophysiol.* **9**, (2016).
134. Mangoni, M. E. *et al.* Functional role of L-type Cav1.3 Ca2+ channels in cardiac pacemaker activity. *Proc. Natl. Acad. Sci.* **100**, 5543–5548 (2003).
135. Mesirca, P. *et al.* Intrinsic Electrical Remodeling Underlies Atrioventricular Block in Athletes. *Circ. Res.* CIRCRESAHA.119.316386 (2021) doi:10.1161/CIRCRESAHA.119.316386.
136. Maguy, A. *et al.* Ion Channel Subunit Expression Changes in Cardiac Purkinje Fibers: A Potential Role in Conduction Abnormalities Associated With Congestive Heart Failure. *Circ. Res.* **104**, 1113–1122 (2009).
137. Han, W., Chartier, D., Li, D. & Nattel, S. Ionic remodeling of cardiac Purkinje cells by congestive heart failure. *Circulation* **104**, 2095–100 (2001).
138. Harris, B. S. *et al.* Remodeling of the peripheral cardiac conduction system in response to pressure overload. *Am. J. Physiol. Heart Circ. Physiol.* **302**, H1712-25 (2012).
139. BANAI, S. & TZIVONI, D. Drug Therapy For Torsade de Pointes. *J. Cardiovasc. Electrophysiol.* **4**, 206–210 (1993).
140. Logantha, S. *et al.* Remodelling of the Purkinje network in congestive heart failure in the rabbit. *Circ. Hear. Fail.* (2021).
141. Jones, S. A., Lancaster, M. K. & Boyett, M. R. Ageing-related changes of connexins and conduction within the sinoatrial node. *J. Physiol.* **560**, 429–437 (2004).
142. Saeed, Y. *et al.* Structural and functional remodeling of the atrioventricular node with aging in rats: The role of hyperpolarization-activated cyclic nucleotide-gated and ryanodine 2 channels. (2018) doi:10.1016/j.hrthm.2017.12.027.
143. BASKERVILLE, S. & BARTEL, D. P. Microarray profiling of microRNAs reveals frequent coexpression with neighboring miRNAs and host genes. *RNA* **11**, 241 (2005).
144. Liu, J., Wang, H. & Li, J. Inflammation and Inflammatory Cells in Myocardial Infarction and Reperfusion Injury: A Double-Edged Sword. *Clin. Med. Insights. Cardiol.* **10**, 79 (2016).
145. Y, S. *et al.* Specific activation of microRNA-127 with downregulation of the proto-oncogene BCL6 by chromatin-modifying drugs in human cancer cells. *Cancer Cell* **9**, 435–443 (2006).

146. Vorburger, S. A. & Hunt, K. K. Adenoviral Gene Therapy. *Oncologist* **7**, 46–59 (2002).

147. Friedmann, T. & Roblin, R. Gene therapy for human genetic disease? *Science (80-.).* **175**, 949–955 (1972).

148. Dunbar, C. E. *et al.* Gene therapy comes of age. *Science* vol. 359 (2018).

149. Zhao, Y. & Huang, L. Lipid nanoparticles for gene delivery. in *Advances in Genetics* vol. 88 13–36 (Academic Press Inc., 2014).

150. A. Holgado, M., Martin-Banderas, L., Alvarez-Fuentes, J., Fernandez-Arevalo, M. & L. Arias, J. Drug Targeting to Cancer by Nanoparticles Surface Functionalized with Special Biomolecules. *Curr. Med. Chem.* **19**, 3188–3195 (2012).

151. Djurovic, S., Iversen, N., Jeansson, S., Hoover, F. & Christensen, G. Comparison of nonviral transfection and adeno-associated viral transduction on cardiomyocytes. *Appl. Biochem. Biotechnol. - Part B Mol. Biotechnol.* **28**, 21–31 (2004).

152. Cannatà, A., Ali, H., Sinagra, G. & Giacca, M. Gene Therapy for the Heart Lessons Learned and Future Perspectives. *Circulation Research* 1394–1414 (2020) doi:10.1161/CIRCRESAHA.120.315855.

153. Tian, Y. *et al.* A microRNA-Hippo pathway that promotes cardiomyocyte proliferation and cardiac regeneration in mice. *Sci. Transl. Med.* **7**, 279ra38 LP-279ra38 (2015).

154. Grunebaum, E. *et al.* Bone marrow transplantation for severe combined immune deficiency. *J. Am. Med. Assoc.* **295**, 508–518 (2006).

155. Howe, S. J. *et al.* Insertional mutagenesis combined with acquired somatic mutations causes leukemogenesis following gene therapy of SCID-X1 patients. *J. Clin. Invest.* **118**, 3143–3150 (2008).

156. Hacein-Bey-Abina, S. *et al.* Insertional oncogenesis in 4 patients after retrovirus-mediated gene therapy of SCID-X1. *J. Clin. Invest.* **118**, 3132–3142 (2008).

157. Wu, X., Li, Y., Crise, B. & Burgess, S. M. Transcription start regions in the human genome are favored targets for MLV integration. *Science (80-.).* **300**, 1749–1751 (2003).

158. Kang, Y. *et al.* In Vivo Gene Transfer Using a Nonprimate Lentiviral Vector Pseudotyped with Ross River Virus Glycoproteins. *J. Virol.* **76**, 9378–9388 (2002).

159. Brown, B. D. *et al.* In vivo administration of lentiviral vectors triggers a type I interferon response that restricts hepatocyte gene transfer and promotes vector clearance. *Blood* **109**, 2797–2805 (2007).

160. Merentie, M. *et al.* Efficacy and safety of myocardial gene transfer of adenovirus, adeno-associated virus and lentivirus vectors in the mouse heart. *Gene Ther.* **23**, 296–305 (2016).

161. Fleury, S. *et al.* Multiply attenuated, self-inactivating lentiviral vectors efficiently deliver

and express genes for extended periods of time in adult rat cardiomyocytes in vivo. *Circulation* **107**, 2375–82 (2003).

162. VandenDriessche, T. *et al.* Lentiviral vectors containing the human immunodeficiency virus type-1 central polypurine tract can efficiently transduce nondividing hepatocytes and antigen-presenting cells in vivo. *Blood* **100**, 813–822 (2002).
163. DePolo, N. J. *et al.* VSV-G pseudotyped lentiviral vector particles produced in human cells are inactivated by human serum. *Mol. Ther.* **2**, 218–222 (2000).
164. Fausther-Bovendo, H. & Kobinger, G. P. Pre-existing immunity against Ad vectors: Humoral, cellular, and innate response, what's important? *Human Vaccines and Immunotherapeutics* vol. 10 2875–2884 (2014).
165. Wilson, J. M. Lessons learned from the gene therapy trial for ornithine transcarbamylase deficiency. in *Getting to Good: Research Integrity in the Biomedical Sciences* vol. 96 490–497 (Springer International Publishing, 2018).
166. Lee, C. S. *et al.* Adenovirus-mediated gene delivery: Potential applications for gene and cell-based therapies in the new era of personalized medicine. *Genes and Diseases* vol. 4 43–63 (2017).
167. Crystal, R. G. Adenovirus: The first effective in vivo gene delivery vector. *Human Gene Therapy* vol. 25 3–11 (2014).
168. Alba, R., Bosch, A. & Chillon, M. Gutless adenovirus: Last-generation adenovirus for gene therapy. *Gene Ther.* **12**, S18–S27 (2005).
169. Chen, H. H. *et al.* Applied biological sciences persistence in muscle of an adenoviral vector that lacks all viral genes. *Proc. Natl. Acad. Sci. U. S. A.* **94**, 1645–1650 (1997).
170. Morral, N. *et al.* Administration of helper-dependent adenoviral vectors and sequential delivery of different vector serotype for long-term liver-directed gene transfer in baboons. *Proc. Natl. Acad. Sci. U. S. A.* **96**, 12816–12821 (1999).
171. Brunetti-Pierri, N. *et al.* Acute Toxicity after High-Dose Systemic Injection of Helper-Dependent Adenoviral Vectors into Nonhuman Primates. *Hum. Gene Ther.* **15**, 35–46 (2004).
172. Lee, D. *et al.* No more helper adenovirus: production of gutless adenovirus (GLAd) free of adenovirus and replication-competent adenovirus (RCA) contaminants. *Exp. Mol. Med.* **51**, 1–18 (2019).
173. Hüser, D. *et al.* High Prevalence of Infectious Adeno-associated Virus (AAV) in Human Peripheral Blood Mononuclear Cells Indicative of T Lymphocytes as Sites of AAV Persistence. *J. Virol.* **91**, (2017).

174. Daya, S. & Berns, K. I. Gene therapy using adeno-associated virus vectors. *Clinical Microbiology Reviews* vol. 21 583–593 (2008).
175. Sonntag, F., Schmidt, K. & Kleinschmidt, J. A. A viral assembly factor promotes AAV2 capsid formation in the nucleolus. *Proc. Natl. Acad. Sci. U. S. A.* **107**, 10220–10225 (2010).
176. Kotin, R. M. *et al.* Site-specific integration by adeno-associated virus. *Proc. Natl. Acad. Sci. U. S. A.* **87**, 2211–2215 (1990).
177. Linden, R. M., Ward, P., Giraud, C., Winocour, E. & Berns, K. I. Site-specific integration by adeno-associated virus. *Proc. Natl. Acad. Sci. U. S. A.* **93**, 11288–11294 (1996).
178. Kotin, R. M., Menninger, J. C., Ward, D. C. & Berns, K. I. Mapping and direct visualization of a region-specific viral DNA integration site on chromosome 19q13-qter. *Genomics* **10**, 831–834 (1991).
179. Inagaki, K., Piao, C., Kotchey, N. M., Wu, X. & Nakai, H. Frequency and Spectrum of Genomic Integration of Recombinant Adeno-Associated Virus Serotype 8 Vector in Neonatal Mouse Liver. *J. Virol.* **82**, 9513–9524 (2008).
180. Nowrouzi, A. *et al.* Integration frequency and intermolecular recombination of rAAV vectors in non-human primate skeletal muscle and liver. *Mol. Ther.* **20**, 1177–1186 (2012).
181. Nault, J. C. *et al.* Recurrent AAV2-related insertional mutagenesis in human hepatocellular carcinomas. *Nat. Genet.* **47**, 1187–1193 (2015).
182. Gil-Farina, I. *et al.* Recombinant AAV Integration Is Not Associated with Hepatic Genotoxicity in Nonhuman Primates and Patients. *Mol. Ther.* **24**, 1100–1105 (2016).
183. Srivastava, A. & Carter, B. J. AAV Infection: Protection from Cancer. *Hum. Gene Ther.* **28**, 323–327 (2017).
184. Duan, D. *et al.* Circular Intermediates of Recombinant Adeno-Associated Virus Have Defined Structural Characteristics Responsible for Long-Term Episomal Persistence in Muscle Tissue. *J. Virol.* **72**, 8568–8577 (1998).
185. Nakai, H. *et al.* Extrachromosomal recombinant adeno-associated virus vector genomes are primarily responsible for stable liver transduction in vivo. *J. Virol.* **75**, 6969–76 (2001).
186. Ylä-Herttuala, S. Endgame: Glybera finally recommended for approval as the first gene therapy drug in the European union. *Molecular Therapy* vol. 20 1831–1832 (2012).
187. Ameri, H. Prospect of retinal gene therapy following commercialization of voretigene neparvovec-rzyl for retinal dystrophy mediated by RPE65 mutation. *Journal of Current Ophthalmology* vol. 30 1–2 (2018).
188. Trapani, I. Adeno-associated viral vectors as a tool for large gene delivery to the retina. *Genes (Basel).* **10**, (2019).

189. Zhou, R. & Caspi, R. R. Ocular immune privilege. *F1000 Biology Reports* vol. 2 (2010).
190. Lisowski, L., Tay, S. S. & Alexander, I. E. Adeno-associated virus serotypes for gene therapeutics. *Current Opinion in Pharmacology* vol. 24 59–67 (2015).
191. Bell, C. L. *et al.* The AAV9 receptor and its modification to improve in vivo lung gene transfer in mice. *J. Clin. Invest.* **121**, 2427–2435 (2011).
192. Akache, B. *et al.* The 37/67-Kilodalton Laminin Receptor Is a Receptor for Adeno-Associated Virus Serotypes 8, 2, 3, and 9. *J. Virol.* **80**, 9831–9836 (2006).
193. Kotchey, N. M. *et al.* A potential role of distinctively delayed blood clearance of recombinant adeno-associated virus serotype 9 in robust cardiac transduction. *Mol. Ther.* **19**, 1079–1089 (2011).
194. Zincarelli, C., Soltys, S., Rengo, G. & Rabinowitz, J. E. Analysis of AAV Serotypes 1–9 Mediated Gene Expression and Tropism in Mice After Systemic Injection. *Mol. Ther.* **16**, 1073–1080 (2008).
195. GN, N. *et al.* A long-term study of AAV gene therapy in dogs with hemophilia A identifies clonal expansions of transduced liver cells. *Nat. Biotechnol.* **39**, 47–55 (2021).
196. DA, K. *et al.* The clinical landscape for AAV gene therapies. *Nat. Rev. Drug Discov.* **20**, 173–174 (2021).
197. Prinzen, F. W., Vernooy, K. & Auricchio, A. Cardiac Resynchronization Therapy: State-of-the-Art of Current Applications, Guidelines, Ongoing Trials, and Areas of Controversy. *Circulation* **128**, 2407–2418 (2013).
198. Poole, J. E. *et al.* Complication Rates Associated With Pacemaker or Implantable Cardioverter-Defibrillator Generator Replacements and Upgrade Procedures. *Circulation* **122**, 1553–1561 (2010).
199. Bish, L. T. *et al.* Adeno-Associated Virus (AAV) Serotype 9 Provides Global Cardiac Gene Transfer Superior to AAV1, AAV6, AAV7, and AAV8 in the Mouse and Rat. *Hum. Gene Ther.* **19**, 1359–1368 (2008).
200. Inagaki, K. *et al.* Robust systemic transduction with AAV9 vectors in mice: efficient global cardiac gene transfer superior to that of AAV8. *Mol. Ther.* **14**, 45–53 (2006).
201. Colella, P., Ronzitti, G. & Mingozzi, F. Emerging Issues in AAV-Mediated In Vivo Gene Therapy. *Molecular Therapy - Methods and Clinical Development* vol. 8 87–104 (2018).
202. Simonatto, M., Latella, L. & Puri, P. L. DNA damage and cellular differentiation: More questions than responses. *Journal of Cellular Physiology* vol. 213 642–648 (2007).
203. Lovric, J. *et al.* Terminal differentiation of cardiac and skeletal myocytes induces permissivity to AAV transduction by relieving inhibition imposed by DNA damage response

proteins. *Mol. Ther.* **20**, 2087–2097 (2012).

204. Cervelli, T. *et al.* Processing of recombinant AAV genomes occurs in specific nuclear structures that overlap with foci of DNA-damage-response proteins. *J. Cell Sci.* **121**, 349–357 (2008).
205. Prasad, K. M. R., Xu, Y., Yang, Z., Acton, S. T. & French, B. A. Robust cardiomyocyte-specific gene expression following systemic injection of AAV: In vivo gene delivery follows a Poisson distribution. *Gene Ther.* **18**, 43–52 (2011).
206. Chen, B.-D. *et al.* Targeting transgene to the heart and liver with AAV9 by different promoters. *Clin. Exp. Pharmacol. Physiol.* **42**, 1108–1117 (2015).
207. Fang, H. *et al.* Comparison of adeno-associated virus serotypes and delivery methods for cardiac gene transfer. *Hum. Gene Ther. Methods* **23**, 234–241 (2012).
208. DiMattia, M. A. *et al.* Structural Insight into the Unique Properties of Adeno-Associated Virus Serotype 9. *J. Virol.* **86**, 6947–6958 (2012).
209. Gabisonia, K. *et al.* MicroRNA therapy stimulates uncontrolled cardiac repair after myocardial infarction in pigs. *Nature* vol. 569 418–422 (2019).
210. Ferrari, F. K., Samulski, T., Shenk, T. & Samulski, R. J. Second-strand synthesis is a rate-limiting step for efficient transduction by recombinant adeno-associated virus vectors. *J. Virol.* **70**, 3227–3234 (1996).
211. Fisher, K. J. *et al.* Transduction with recombinant adeno-associated virus for gene therapy is limited by leading-strand synthesis. *J. Virol.* **70**, 520–532 (1996).
212. Nakai, H., Storm, T. A. & Kay, M. A. Recruitment of Single-Stranded Recombinant Adeno-Associated Virus Vector Genomes and Intermolecular Recombination Are Responsible for Stable Transduction of Liver In Vivo. *J. Virol.* **74**, 9451–9463 (2000).
213. Jayandharan, G. R., Zhong, L., Li, B., Kachniarz, B. & Srivastava, A. Strategies for improving the transduction efficiency of single-stranded adeno-associated virus vectors in vitro and in vivo. *Gene Ther.* **15**, 1287–1293 (2008).
214. Borrás, T. *et al.* Mechanisms of AAV transduction in glaucoma-associated human trabecular meshwork cells. *J. Gene Med.* **8**, 589–602 (2006).
215. McCarty, D. M., Monahan, P. E. & Samulski, R. J. Self-complementary recombinant adeno-associated virus (scAAV) vectors promote efficient transduction independently of DNA synthesis. *Gene Ther.* **8**, 1248–1254 (2001).
216. Andino, L. M. *et al.* Rapid, widespread transduction of the murine myocardium using self-complementary Adeno-associated virus. *Genet. Vaccines Ther.* **5**, (2007).
217. McCarty, D. M. Self-complementary AAV vectors; advances and applications. *Molecular*

Therapy vol. 16 1648–1656 (2008).

218. Dong, B., Nakai, H. & Xiao, W. Characterization of genome integrity for oversized recombinant AAV vector. *Mol. Ther.* **18**, 87–92 (2010).
219. Wu, Z., Yang, H. & Colosi, P. Effect of genome size on AAV vector packaging. *Mol. Ther.* **18**, 80–86 (2010).
220. Lai, Y., Yue, Y., Bostick, B. & Duan, D. Delivering large therapeutic genes for muscle gene therapy. in *Muscle Gene Therapy* 205–218 (Springer New York, 2010). doi:10.1007/978-1-4419-1207-7_12.
221. Duan, D., Yue, Y. & Engelhardt, J. F. Expanding AAV packaging capacity with Trans-splicing or overlapping vectors: A quantitative comparison. *Mol. Ther.* **4**, 383–391 (2001).
222. Lai, Y. *et al.* Efficient in vivo gene expression by trans-splicing adeno-associated viral vectors. *Nat. Biotechnol.* **23**, 1435–1439 (2005).
223. Koo, T., Popplewell, L., Athanasopoulos, T. & Dickson, G. Triple trans-splicing adeno-associated virus vectors capable of transferring the coding sequence for full-length dystrophin protein into dystrophic mice. *Hum. Gene Ther.* **25**, 98–108 (2014).
224. Maddalena, A. *et al.* Triple Vectors Expand AAV Transfer Capacity in the Retina. *Mol. Ther.* **26**, 524–541 (2018).
225. Patel, A., Zhao, J., Duan, D. & Lai, Y. Design of AAV vectors for delivery of large or multiple transgenes. in *Methods in Molecular Biology* vol. 1950 19–33 (Humana Press Inc., 2019).
226. Jun-ichi, M. *et al.* Expression vector system based on the chicken β-actin promoter directs efficient production of interleukin-5. *Gene* **79**, 269–277 (1989).
227. Vandamme, C., Adjali, O. & Mingozzi, F. Unraveling the Complex Story of Immune Responses to AAV Vectors Trial After Trial. *Human Gene Therapy* vol. 28 1061–1074 (2017).
228. Calcedo, R. *et al.* Adeno-associated virus antibody profiles in newborns, children, and adolescents. *Clin. Vaccine Immunol.* **18**, 1586–1588 (2011).
229. Tobiasch, E., Burguete, T., Klein-Bauernschmitt, P., Heilbronn, R. & Schlehofer, J. R. Discrimination between different types of human adeno-associated viruses in clinical samples by PCR. *J. Virol. Methods* **71**, 17–25 (1998).
230. Boutin, S. *et al.* Prevalence of serum IgG and neutralizing factors against adeno-associated virus (AAV) types 1, 2, 5, 6, 8, and 9 in the healthy population: Implications for gene therapy using AAV vectors. *Hum. Gene Ther.* **21**, 704–712 (2010).
231. Scallan, C. D. *et al.* Human immunoglobulin inhibits liver transduction byAAV vectors at low AAV2 neutralizing titers in SCID mice. *Blood* **107**, 1810–1817 (2006).
232. Fitzpatrick, Z. *et al.* Influence of Pre-existing Anti-capsid Neutralizing and Binding

Antibodies on AAV Vector Transduction. *Mol. Ther. - Methods Clin. Dev.* **9**, 119–129 (2018).

233. Wang, L. *et al.* The pleiotropic effects of natural AAV infections on liver-directed gene transfer in macaques. *Mol. Ther.* **18**, 126–134 (2010).
234. Manno, C. S. *et al.* Successful transduction of liver in hemophilia by AAV-Factor IX and limitations imposed by the host immune response. *Nat. Med.* **12**, 342–347 (2006).
235. Raupp, C. *et al.* The Threefold Protrusions of Adeno-Associated Virus Type 8 Are Involved in Cell Surface Targeting as Well as Postattachment Processing. *J. Virol.* **86**, 9396–9408 (2012).
236. Tse, L. V. *et al.* Structure-guided evolution of antigenically distinct adeno-associated virus variants for immune evasion. *Proc. Natl. Acad. Sci. U. S. A.* **114**, E4812–E4821 (2017).
237. Wang, D., Tai, P. W. L. & Gao, G. Adeno-associated virus vector as a platform for gene therapy delivery. *Nature Reviews Drug Discovery* vol. 18 358–378 (2019).
238. Maheshri, N., Koerber, J. T., Kaspar, B. K. & Schaffer, D. V. Directed evolution of adeno-associated virus yields enhanced gene delivery vectors. *Nat. Biotechnol.* **24**, 198–204 (2006).
239. Shen, S. *et al.* Glycan Binding Avidity Determines the Systemic Fate of Adeno-Associated Virus Type 9. *J. Virol.* **86**, 10408–10417 (2012).
240. Adachi, K., Enoki, T., Kawano, Y., Veraz, M. & Nakai, H. Drawing a high-resolution functional map of adeno-associated virus capsid by massively parallel sequencing. *Nat. Commun.* **5**, (2014).
241. Yang, L. *et al.* A myocardium tropic adeno-associated virus (AAV) evolved by DNA shuffling and in vivo selection. *Proc. Natl. Acad. Sci. U. S. A.* **106**, 3946–3951 (2009).
242. Weinmann, J. & Grimm, D. Next-generation AAV vectors for clinical use: an ever-accelerating race. *Virus Genes* **53**,.
243. Pulicherla, N. *et al.* Engineering liver-detargeted AAV9 vectors for cardiac and musculoskeletal gene transfer. *Mol. Ther.* **19**, 1070–1078 (2011).
244. Büning, H., Huber, A., Zhang, L., Meumann, N. & Hacker, U. Engineering the AAV capsid to optimize vector-host-interactions. *Curr. Opin. Pharmacol.* **24**, 94–104 (2015).
245. Boshart, M. *et al.* A very strong enhancer is located upstream of an immediate early gene of human cytomegalovirus. *Cell* **41**, 521–30 (1985).
246. Cheng, L., Ziegelhoffer, P. R. & Yang, N.-S. *In vivo promoter activity and transgene expression in mammalian somatic tissues evaluated by using particle bombardment*. *Proc. Natl. Acad. Sci. USA* vol. 90 (1993).
247. Pacak, C. A., Sakai, Y., Thattaliyath, B. D., Mah, C. S. & Byrne, B. J. Tissue specific promoters

improve specificity of AAV9 mediated transgene expression following intra-vascular gene delivery in neonatal mice. *Genet. Vaccines Ther.* **6**, 13 (2008).

248. Hsu, C. C. *et al.* Targeted methylation of CMV and E1A viral promoters. *Biochem. Biophys. Res. Commun.* **402**, 228–234 (2010).
249. Brooks, A. R. *et al.* Transcriptional silencing is associated with extensive methylation of the CMV promoter following adenoviral gene delivery to muscle. **6**, 395–404 (2004).
250. Gray, S. J. *et al.* Optimizing promoters for recombinant adeno-associated virus-mediated gene expression in the peripheral and central nervous system using self-complementary vectors. *Hum. Gene Ther.* **22**, 1143–1153 (2011).
251. Löser, P., Jennings, G. S., Strauss, M. & Sandig, V. Reactivation of the previously silenced cytomegalovirus major immediate-early promoter in the mouse liver: involvement of NFkappaB. *J. Virol.* **72**, 180–90 (1998).
252. Grassi, G. *et al.* Inhibitors of DNA methylation and histone deacetylation activate cytomegalovirus promoter-controlled reporter gene expression in human glioblastoma cell line U87. doi:10.1093/carcin/bgg118.
253. Moore, L. D., Le, T. & Fan, G. DNA methylation and its basic function. *Neuropsychopharmacology* vol. 38 23–38 (2013).
254. Lange, A. M., Altynova, E. S., Nguyen, G. N. & Sabatino, D. E. Overexpression of factor VIII after AAV delivery is transiently associated with cellular stress in hemophilia A mice. *Mol. Ther. - Methods Clin. Dev.* **3**, 16064 (2016).
255. Kornegay, J. N. *et al.* Widespread muscle expression of an AAV9 human mini-dystrophin vector after intravenous injection in neonatal dystrophin-deficient dogs. *Mol. Ther.* **18**, 1501–1508 (2010).
256. Kim, S. J. *et al.* An α-cardiac myosin heavy chain gene mutation impairs contraction and relaxation function of cardiac myocytes. *Am. J. Physiol. - Hear. Circ. Physiol.* **276**, (1999).
257. James, J. *et al.* Transgenic over-expression of a motor protein at high levels results in severe cardiac pathology. *Transgenic Res.* **8**, 9–22 (1999).
258. Kupershmidt, S. *et al.* Replacement by Homologous Recombination of the minK Gene With lacZ Reveals Restriction of minK Expression to the Mouse Cardiac Conduction System. *Circ. Res.* **84**, (1999).
259. Vedantham, V., Galang, G., Evangelista, M., Deo, R. C. & Srivastava, D. RNA sequencing of mouse sinoatrial node reveals an upstream regulatory role for Islet-1 in cardiac pacemaker cells. *Circ. Res.* **116**, 797–803 (2015).
260. Ramakers, C. *et al.* Coordinated down-regulation of KCNQ1 and KCNE1 expression

contributes to reduction of IKs in canine hypertrophied hearts. *Cardiovasc. Res.* **57**, 486–496 (2003).

261. Linscheid, N. *et al.* Quantitative proteomics and single-nucleus transcriptomics of the sinus node elucidates the foundation of cardiac pacemaking. *Nat. Commun.* **10**, 1–19 (2019).
262. Gruh, I. *et al.* Human CMV immediate-early enhancer: a useful tool to enhance cell-type-specific expression from lentiviral vectors. *J. Gene Med.* **10**, 21–32 (2008).
263. Müller, O. J. *et al.* Improved cardiac gene transfer by transcriptional and transductional targeting of adeno-associated viral vectors. *Cardiovasc. Res.* **70**, 70–78 (2006).
264. Pleger, S. T. *et al.* Cardiac AAV9-S100A1 gene therapy rescues post-ischemic heart failure in a preclinical large animal model. *Sci. Transl. Med.* **3**, 92ra64 (2011).
265. Jia, Z., Jia, J., Zhang, S. & Cao, J. CMV enhancer may not be suitable for tissue-specific enhancement of promoters in cancer gene therapy. *Cancer Gene Therapy* 1–4 (2019) doi:10.1038/s41417-019-0106-x.
266. Liu, B. H., Wang, X., Ma, Y. X. & Wang, S. CMV enhancer/human PDGF-β promoter for neuron-specific transgene expression. *Gene Ther.* **11**, 52–60 (2004).
267. Zareba, W. *et al.* Effectiveness of Cardiac Resynchronization Therapy by QRS Morphology in the Multicenter Automatic Defibrillator Implantation Trial–Cardiac Resynchronization Therapy (MADIT-CRT). doi:10.1161/CIRCULATIONAHA.110.960898.
268. MOND, H. G. & PROCLEMER, A. The 11th World Survey of Cardiac Pacing and Implantable Cardioverter-Defibrillators: Calendar Year 2009-A World Society of Arrhythmia's Project. *Pacing Clin. Electrophysiol.* **34**, 1013–1027 (2011).
269. Dobrzynski, H., Boyett, M. R. & Anderson, R. H. New Insights Into Pacemaker Activity: Promoting Understanding of Sick Sinus Syndrome. *Circulation* **115**, 1921–1932 (2007).
270. RASMUSSEN, K. Chronic sinus node disease: natural course and indications for pacing. *Eur. Heart J.* **2**, 455–459 (1981).
271. Gregoratos, G. Indications and recommendations for pacemaker therapy. *Am. Fam. Physician* **71**, 1563–70 (2005).
272. Camm, A. J. & Griffin, J. C. VVIR or DDD(R): Does it matter? *Clin. Cardiol.* **14**, 257–260 (1991).
273. Connolly, S. J. *et al.* Effects of Physiologic Pacing versus Ventricular Pacing on the Risk of Stroke and Death Due to Cardiovascular Causes. *N. Engl. J. Med.* **342**, 1385–1391 (2000).
274. Morgan, J. M. Basics of cardiac pacing: selection and mode choice. *Heart* **92**, 850–4 (2006).
275. Linde, C. *et al.* Randomized Trial of Cardiac Resynchronization in Mildly Symptomatic Heart Failure Patients and in Asymptomatic Patients With Left Ventricular Dysfunction and

Previous Heart Failure Symptoms. *J. Am. Coll. Cardiol.* **52**, 1834–1843 (2008).

276. Moss, A. J. *et al.* Cardiac-Resynchronization Therapy for the Prevention of Heart-Failure Events. *N. Engl. J. Med.* **361**, 1329–1338 (2009).

277. Tang, A. S. L. *et al.* Cardiac-Resynchronization Therapy for Mild-to-Moderate Heart Failure. *N. Engl. J. Med.* **363**, 2385–2395 (2010).

278. Lin, G. *et al.* Severe Symptomatic Tricuspid Valve Regurgitation Due to Permanent Pacemaker or Implantable Cardioverter-Defibrillator Leads. *J. Am. Coll. Cardiol.* **45**, 1672–1675 (2005).

279. Kapa, S., Bruce, C. J., Friedman, P. A. & Asirvatham, S. J. Advances in Cardiac Pacing: Beyond the Transvenous Right Ventricular Apical Lead. *Cardiovasc. Ther.* **28**, 369–379 (2010).

280. Kodama, I., Kamiya, K. & Toyama, J. Effect of Chronic Right Ventricular Apical Pacing on Left Ventricular Function. *Expert Opin Pharmacother Cardiovasc Res* **2**, 1877–1890 (2001).

281. van Oosterhout, M. F. *et al.* Asynchronous electrical activation induces asymmetrical hypertrophy of the left ventricular wall. *Circulation* **98**, 588–95 (1998).

282. O'Keefe, J. H. *et al.* Effect of chronic right ventricular apical pacing on left ventricular function. *Am. J. Cardiol.* **95**, 771–773 (2005).

283. Kaye, G. The desire for physiological pacing: Are we there yet? *J. Cardiovasc. Electrophysiol.* **30**, 3025–3038 (2019).

284. Vijayaraman, P. *et al.* Permanent His-bundle pacing: Long-term lead performance and clinical outcomes. *Hear. Rhythm* **15**, 696–702 (2018).

285. Sharma, P. S. *et al.* Permanent His-bundle pacing is feasible, safe, and superior to right ventricular pacing in routine clinical practice. *Hear. Rhythm* **12**, 305–312 (2015).

286. Lewis, A. J. M., Foley, P., Whinnett, Z., Keene, D. & Chandrasekaran, B. His Bundle Pacing: A New Strategy for Physiological Ventricular Activation. *J. Am. Heart Assoc.* **8**, 10972 (2019).

287. Echt, D. S. *et al.* Feasibility and safety of a novel technology for pacing without leads. *Hear. Rhythm* **3**, 1202–1206 (2006).

288. Reynolds, D. *et al.* A Leadless Intracardiac Transcatheter Pacing System. *N. Engl. J. Med.* **374**, 533–541 (2016).

289. Reddy, V. Y. *et al.* Percutaneous Implantation of an Entirely Intracardiac Leadless Pacemaker. *N. Engl. J. Med.* **373**, 1125–1135 (2015).

290. Eberhardt, F. *et al.* Long term complications in single and dual chamber pacing are influenced by surgical experience and patient morbidity. *Heart* **91**, 500–6 (2005).

291. Xiao, Y.-F., Sigg, D. C. & 萧永福用生物学方法重建心脏起搏点的研究进展. Biological

approaches to generating cardiac biopacemaker for bradycardia. *Acta Physiol. Sin.* **59**, 562–570 (2007).

292. Chan, Y.-C. *et al.* Synergistic effects of inward rectifier (I) and pacemaker (I) currents on the induction of bioengineered cardiac automaticity. *J. Cardiovasc. Electrophysiol.* **20**, 1048–54 (2009).
293. Miake, J., Marbán, E. & Nuss, H. B. Gene therapy: Biological pacemaker created by gene transfer. *Nature* **419**, 132–133 (2002).
294. Cingolani, E. *et al.* Biological pacemaker created by percutaneous gene delivery via venous catheters in a porcine model of complete heart block. *Hear. Rhythm* **9**, 1310–1318 (2012).
295. Tan, H. L., Hou, C. J., Lauer, M. R. & Sung, R. J. Electrophysiologic mechanisms of the long QT interval syndromes and torsade de pointes. *Ann. Intern. Med.* **122**, 701–14 (1995).
296. Boink, G. J. J. & Robinson, R. B. Gene Therapy for Restoring Heart Rhythm. *J. Cardiovasc. Pharmacol. Ther.* **19**, 426–438 (2014).
297. Qu, J. *et al.* Expression and Function of a Biological Pacemaker in Canine Heart. *Circulation* **107**, (2003).
298. Plotnikov, A. N. *et al.* Biological Pacemaker Implanted in Canine Left Bundle Branch Provides Ventricular Escape Rhythms That Have Physiologically Acceptable Rates. *Circulation* **109**, (2004).
299. Bucchi, A. *et al.* Wild-Type and Mutant HCN Channels in a Tandem Biological-Electronic Cardiac Pacemaker. *Circulation* **114**, (2006).
300. Plotnikov, A. N. *et al.* HCN212-channel biological pacemakers manifesting ventricular tachyarrhythmias are responsive to treatment with I(f) blockade. *Hear. Rhythm* **5**, 282–8 (2008).
301. Soattin, L. *et al.* Structural and Functional Properties of Subsidiary Atrial Pacemakers in a Goat Model of Sinus Node Disease. *Front. Physiol.* **12**, (2021).
302. Chandler, N. J. *et al.* Molecular architecture of the human sinus node insights into the function of the cardiac pacemaker. *Circulation* **119**, 1562–1575 (2009).
303. Soattin, L. *et al.* Structural and Functional Properties of Subsidiary Atrial Pacemakers in a Goat Model of Sinus Node Disease. *Front. Physiol.* **12**, 82 (2021).
304. Zhang, H. *et al.* Implantation of sinoatrial node cells into canine right ventricle: Biological pacing appears limited by the substrate. *Cell Transplant.* **20**, 1907–1914 (2011).
305. Joyner, R. W. & van Capelle, F. J. Propagation through electrically coupled cells. How a small SA node drives a large atrium. *Biophys. J.* **50**, 1157–1164 (1986).
306. Mattick, P. *et al.* Ca2+-stimulated adenylyl cyclase isoform AC1 is preferentially expressed

in guinea-pig sino-atrial node cells and modulates the I(f) pacemaker current. *J. Physiol.* **582**, 1195–203 (2007).

307. Boink, G. J. J. *et al.* Ca(2+)-stimulated adenylyl cyclase AC1 generates efficient biological pacing as single gene therapy and in combination with HCN2. *Circulation* **126**, 528–36 (2012).
308. Lou, Q., Janardhan, A. & Efimov, I. R. Remodeling of calcium handling in human heart failure. *Adv. Exp. Med. Biol.* **740**, 1145–1174 (2012).
309. Boink, G. J. J. *et al.* HCN2/SkM1 Gene Transfer Into Canine Left Bundle Branch Induces Stable, Autonomically Responsive Biological Pacing at Physiological Heart Rates. *J. Am. Coll. Cardiol.* **61**, 1192–1201 (2013).
310. Végh, A. M. D. *et al.* Toward Biological Pacing by Cellular Delivery of Hcn2/SkM1. *Front. Physiol.* **11**, (2021).
311. Takahashi, K. & Yamanaka, S. Induction of Pluripotent Stem Cells from Mouse Embryonic and Adult Fibroblast Cultures by Defined Factors. *Cell* **126**, 663–676 (2006).
312. Ieda, M. *et al.* Direct Reprogramming of Fibroblasts into Functional Cardiomyocytes by Defined Factors. *Cell* **142**, 375–386 (2010).
313. Qian, L. *et al.* In vivo reprogramming of murine cardiac fibroblasts into induced cardiomyocytes. *Nature* **485**, 593–598 (2012).
314. Hoogaars, W. M. H. *et al.* The transcriptional repressor Tbx3 delineates the developing central conduction system of the heart. *Cardiovasc. Res.* **62**, 489–499 (2004).
315. Bakker, M. L. *et al.* T-box transcription factor TBX3 reprogrammes mature cardiac myocytes into pacemaker-like cells. doi:10.1093/cvr/cvs120.
316. Zhao, H. *et al. HCN2* and *TBX3* Reprogram Human-Induced Pluripotent Stem Cells-Derived Cardiomyocytes into Pacemaker-Like Cells. *DNA Cell Biol.* **39**, 289–298 (2020).
317. Wiese, C. *et al.* Formation of the Sinus Node Head and Differentiation of Sinus Node Myocardium Are Independently Regulated by Tbx18 and Tbx3. *Circ. Res.* **104**, 388–397 (2009).
318. Kapoor, N., Galang, G., Marbán, E. & Cho, H. C. Transcriptional suppression of connexin43 by TBX18 undermines cell-cell electrical coupling in postnatal cardiomyocytes. *J. Biol. Chem.* **286**, 14073–9 (2011).
319. Kapoor, N., Liang, W., Marbán, E. & Cho, H. C. Direct conversion of quiescent cardiomyocytes to pacemaker cells by expression of Tbx18. *Nat. Biotechnol.* **31**, 54–62 (2013).
320. Hu, Y. F., Dawkins, J. F., Cho, H. C., Marbán, E. & Cingolani, E. Biological pacemaker created

by minimally invasive somatic reprogramming in pigs with complete heart block. *Sci. Transl. Med.* **6**, (2014).

321. Segers, V. F. M. & Lee, R. T. Stem-cell therapy for cardiac disease. *Nature* **451**, 937–942 (2008).
322. Potapova, I. *et al.* Human Mesenchymal Stem Cells as a Gene Delivery System to Create Cardiac Pacemakers. *Circ. Res.* **94**, 952–959 (2004).
323. Plotnikov, A. N. *et al.* Xenografted Adult Human Mesenchymal Stem Cells Provide a Platform for Sustained Biological Pacemaker Function in Canine Heart. *Circulation* **116**, 706–713 (2007).
324. Zhang, H. *et al.* Autologous biological pacing function with adrenergic-responsiveness in porcine of complete heart block. *Int. J. Cardiol.* **168**, 3747–3751 (2013).
325. Freeman, B. T., Kouris, N. A. & Ogle, B. M. Tracking fusion of human mesenchymal stem cells after transplantation to the heart. *Stem Cells Transl. Med.* **4**, 685–94 (2015).
326. Bruzauskaite, I. *et al.* Relevance of HCN2-expressing human mesenchymal stem cells for the generation of biological pacemakers. *Stem Cell Res. Ther.* **7**, 67 (2016).
327. Végh, A. M. D. *et al.* Cardiomyocyte progenitor cells as a functional gene delivery vehicle for long-term biological pacing. *Molecules* **24**, (2019).
328. Végh, A. M. D. *et al.* Toward Biological Pacing by Cellular Delivery of Hcn2/SkM1. *Front. Physiol.* **11**, (2021).
329. Sartiani, L. *et al.* Developmental Changes in Cardiomyocytes Differentiated from Human Embryonic Stem Cells: A Molecular and Electrophysiological Approach. *Stem Cells* **25**, 1136–1144 (2007).
330. Ionta, V. *et al.* SHOX2 Overexpression Favors Differentiation of Embryonic Stem Cells into Cardiac Pacemaker Cells, Improving Biological Pacing Ability. *Stem Cell Reports* **4**, 129–142 (2015).
331. Kehat, I., Gepstein, A., Spira, A., Itskovitz-Eldor, J. & Gepstein, L. High-resolution electrophysiological assessment of human embryonic stem cell-derived cardiomyocytes: a novel in vitro model for the study of conduction. *Circ. Res.* **91**, 659–61 (2002).
332. Kehat, I. *et al.* Electromechanical integration of cardiomyocytes derived from human embryonic stem cells. *Nat. Biotechnol.* **22**, 1282–1289 (2004).
333. Protze, S. I. *et al.* Sinoatrial node cardiomyocytes derived from human pluripotent cells function as a biological pacemaker. *Nat. Biotechnol.* **35**, 56–68 (2017).
334. Medvedev, S. P., Shevchenko, A. I. & Zakian, S. M. Induced Pluripotent Stem Cells: Problems and Advantages when Applying them in Regenerative Medicine. *Acta Naturae* **2**,

18–28 (2010).

335. Chauveau, S. *et al.* Induced Pluripotent Stem Cell–Derived Cardiomyocytes Provide In Vivo Biological Pacemaker Function. *Circ. Arrhythmia Electrophysiol.* **10**, (2017).
336. Efimov, V. P. *et al.* No Title. **92**, 469–475 (2003).
337. Cheng, S. *et al.* Long-term Outcomes in Individuals With Prolonged PR Interval or First-Degree Atrioventricular Block. *JAMA* **301**, 2571–2577 (2009).
338. Zhang, H. *et al.* Implantation of sinoatrial node cells into canine right ventricle: biological pacing appears limited by the substrate. *Cell Transplant.* **20**, 1907–14 (2011).
339. Raso, A. *et al.* Therapeutic Delivery of miR-148a Suppresses Ventricular Dilation in Heart Failure. *Mol. Ther.* **27**, 584–599 (2019).
340. Jeong, D. *et al.* miR-25 Tough Decoy Enhances Cardiac Function in Heart Failure. *Mol. Ther.* **26**, 718–729 (2018).
341. Donahue, J. K. *et al. Focal modification of electrical conduction in the heart by viral gene transfer*. *NATURE MEDICINE • VOLUME* vol. 6 http://medicine.nature.com (2000).
342. Böhm, M. *et al.* Heart rate as a risk factor in chronic heart failure (SHIFT): The association between heart rate and outcomes in a randomised placebo-controlled trial. *Lancet* **376**, 886–894 (2010).
343. Fox, K. *et al.* Ivabradine for patients with stable coronary artery disease and left-ventricular systolic dysfunction (BEAUTIFUL): a randomised, double-blind, placebo-controlled trial. *Lancet* **372**, 807–816 (2008).
344. Lugenbiel, P. *et al.* Biological Heart Rate Reduction Through Genetic Suppression of Gα s Protein in the Sinoatrial Node . *J. Am. Heart Assoc.* **1**, (2012).
345. Kikuchi, K., McDonald, A. D., Sasano, T. & Donahue, J. K. Targeted modification of atrial electrophysiology by homogeneous transmural atrial gene transfer. *Circulation* **111**, 264–270 (2005).
346. Verkerk, A. O. & Wilders, R. Pacemaker activity of the human sinoatrial node: an update on the effects of mutations in HCN4 on the hyperpolarization-activated current. *Int. J. Mol. Sci.* **16**, 3071–94 (2015).
347. Liu, J., Dobrzynski, H., Yanni, J., Boyett, M. R. & Lei, M. Organisation of the mouse sinoatrial node: structure and expression of HCN channels. *Cardiovasc. Res.* **73**, 729–738 (2007).
348. Shi, W. *et al.* Distribution and prevalence of hyperpolarization-activated cation channel (HCN) mRNA expression in cardiac tissues. *Circ. Res.* **85**, e1-6 (1999).
349. Tellez, J. O. *et al.* Differential Expression of Ion Channel Transcripts in Atrial Muscle and Sinoatrial Node in Rabbit. *Circ. Res.* **99**, 1384–1393 (2006).

350. Huang, X., Yang, P., Du, Y., Zhang, J. & Ma, A. Age-related down-regulation of HCN channels in rat sinoatrial node. *Basic Res. Cardiol.* **102**, 429–435 (2007).

351. Stieber, J. *et al.* The hyperpolarization-activated channel HCN4 is required for the generation of pacemaker action potentials in the embryonic heart. (2003).

352. Lesage, F., Attali, B., Lazdunski, M. & Barhanin, J. ISK, a slowly activating voltage-sensitive K+ channel Characterization of multiple cDNAs and gene organization in the mouse. *FEBS Lett.* **301**, 168–172 (1992).

353. Ohno, S. *et al.* N- and C-terminal KCNE1 mutations cause distinct phenotypes of long QT syndrome. *Hear. Rhythm* **4**, 332–340 (2007).

354. Caref, E. B., Boutjdir, M., Himel, H. D. & El-Sherif, N. Role of subendocardial Purkinje network in triggering torsade de pointes arrhythmia in experimental long QT syndrome. *Europace* **10**, 1218–1223 (2008).

355. Warth, R. & Barhanin, J. The multifaceted phenotype of the knockout mouse for the KCNE1 potassium channel gene. (2002).

356. Vetter, D. E. *et al.* Inner ear defects induced by null mutation of the isk gene. *Neuron* **17**, 1251–64 (1996).

357. Han, W., Bao, W., Wang, Z. & Nattel, S. Comparison of ion-channel subunit expression in canine cardiac Purkinje fibers and ventricular muscle. *Circ. Res.* **91**, 790–7 (2002).

358. MIQUEROL, L. *et al.* Architectural and functional asymmetry of the His–Purkinje system of the murine heart. *Cardiovasc. Res.* **63**, 77–86 (2004).

359. Gros, D. B. & Jongsma, H. J. Connexins in mammalian heart function. *BioEssays* **18**, 719–730 (1996).

360. Gearing, L. J. *et al.* CiiiDER: A tool for predicting and analysing transcription factor binding sites. *PLoS One* **14**, e0215495 (2019).

361. Kel, A. E. *et al.* MATCH^{TM}: A tool for searching transcription factor binding sites in DNA sequences. *Nucleic Acids Res.* **31**, 3576–3579 (2003).

362. Mathelier, A. *et al.* JASPAR 2016: A major expansion and update of the open-access database of transcription factor binding profiles. *Nucleic Acids Res.* **44**, D110–D115 (2016).

363. Lin, Z. *et al.* Cardiac-Specific YAP Activation Improves Cardiac Function and Survival in an Experimental Murine MI Model. *Circ. Res.* **115**, 354–363 (2014).

364. Sanger, F., Nicklen, S. & Coulson, A. R. DNA sequencing with chain-terminating inhibitors. *Proc. Natl. Acad. Sci. U. S. A.* **74**, 5463–7 (1977).

365. Hartley, J. L., Temple, G. F. & Brasch, M. A. DNA cloning using in vitro site-specific recombination. *Genome Res.* **10**, 1788–1795 (2000).

366. Arsic, N. *et al.* Induction of functional neovascularization by combined VEGF and angiopoietin-1 gene transfer using AAV vectors. *Mol. Ther.* **7**, 450–459 (2003).
367. Turner, P. V., Brabb, T., Pekow, C. & Vasbinder, M. A. Administration of substances to laboratory animals: Routes of administration and factors to consider. *Journal of the American Association for Laboratory Animal Science* vol. 50 600–613 (2011).
368. Edelstein, A. D. *et al.* Advanced methods of microscope control using μManager software. *J. Biol. Methods* **1**, 10 (2014).
369. W, X., AE, M. G., Y, L., LI, B. & CL, C. NRF2 promotes neuronal survival in neurodegeneration and acute nerve damage. *J. Clin. Invest.* **125**, 1433–1445 (2015).
370. Kuratomi, S. *et al.* The cardiac pacemaker-specific channel Hcn4 is a direct transcriptional target of MEF2. *Cardiovasc. Res.* **83**, 682–687 (2009).
371. Schweizer, P. A. *et al.* Transcription profiling of HCN-channel isotypes throughout mouse cardiac development. *Basic Res. Cardiol.* **104**, 621–629 (2009).
372. Lundquist, A. L., Turner, C. L., Ballester, L. Y. & George, A. L. Expression and transcriptional control of human KCNE genes. *Genomics* **87**, 119–128 (2006).
373. Mustapha, Z., Pang, L. & Nattel, S. Characterization of the cardiac KCNE1 gene promoter. *Cardiovasc. Res.* **73**, 82–91 (2007).
374. Temple, J. *et al.* Atrial fibrillation in KCNE1-null mice. *Circ. Res.* **97**, 62–69 (2005).
375. Müller, O. J. *et al.* Improved cardiac gene transfer by transcriptional and transductional targeting of adeno-associated viral vectors. *Cardiovasc. Res.* **70**, 70–78 (2006).
376. Schlabach, M. R., Hu, J. K., Li, M. & Elledge, S. J. Synthetic design of strong promoters. doi:10.1073/pnas.0914803107.
377. Lin, H., Xiao, J., Luo, X., Chen, G. & Wang, Z. Transcriptional control of pacemaker channel genes HCN2 and HCN4 by Sp1 and implications in re-expression of these genes in hypertrophied myocytes. *Cell. Physiol. Biochem.* **23**, 317–326 (2009).
378. Hoogaars, W. M. H. *et al.* Tbx3 controls the sinoatrial node gene program and imposes pacemaker function on the atria. *Genes Dev.* **21**, 1098–1112 (2007).
379. Espinoza-Lewis, R. A. *et al.* Ectopic expression of Nkx2.5 suppresses the formation of the sinoatrial node in mice. *Dev. Biol.* **356**, 359–369 (2011).
380. Fernandez-Perez, A., Sathe, A., Bhakta, M., Leggett, K. & Xing, C. Hand2 Selectively Reorganizes Chromatin Accessibility to Induce Pacemaker-like Transcriptional Reprogramming The Hand2 N terminus diversifies cardiomyocyte subtype formation. *CellReports* **27**, 2354-2369.e7 (2019).
381. Wymore, R. S. *et al.* Characterization of the transcription unit of mouse Kv1.4, a voltage-

gated potassium channel gene. *J. Biol. Chem.* **271**, 15629–15634 (1996).

382. Luo, X. *et al.* Retracted: Transcriptional activation by stimulating protein 1 and post-transcriptional repression by muscle-specific microRNAs of IKs-encoding genes and potential implications in regional heterogeneity of their expressions. *J. Cell. Physiol.* **212**, 358–367 (2007).

383. Luo, X. *et al.* Retraction: Transcriptional activation by stimulating protein 1 and post-transcriptional repression by muscle-specific microRNAs of IKs-encoding genes and potential implications in regional heterogeneity of their expressions. *J. Cell. Physiol.* **227**, 877–877 (2012).

384. Shekhar, A. *et al.* Transcription factor ETV1 is essential for rapid conduction in the heart. *J. Clin. Invest.* **126**, 4444–4459 (2016).

385. Azzoni, A. R., Ribeiro, S. C., Monteiro, G. A. & Prazeres, D. M. F. The impact of polyadenylation signals on plasmid nuclease-resistance and transgene expression. *J. Gene Med.* **9**, 392–402 (2007).

386. Briggs, M. R., Kadonaga, J. T., Bell, S. P. & Tjin, R. *Purification and Biochemical Characterization Of the Promoter-Specific Transcription Factor, Spi Downloaded from*. http://science.sciencemag.org/.

387. Saffer, J. D., Jackson, S. P. & Annarella, M. B. Developmental expression of Sp1 in the mouse. *Mol. Cell. Biol.* **11**, 2189–2199 (1991).

388. Brady, M. *et al.* Sp1 and Sp3 transcription factors are required for trans-activation of the human SERCA2 promoter in cardiomyocytes. *Cardiovasc. Res.* **60**, 347–354 (2003).

389. O'Connor, L., Gilmour, J. & Bonifer, C. The role of the ubiquitously expressed transcription factor Sp1 in tissue-specific transcriptional regulation and in disease. *Yale Journal of Biology and Medicine* vol. 89 513–525 (2016).

390. Liu, A., Hoffman#, P. W., Lu, W. & Bai, G. *NF-κB site interacts with Sp factors and upregulates the NR1 promoter during neuronal differentiation. Downloaded from*. http://www.jbc.org/ (2020).

391. Liang, X. *et al.* Transcription factor ISL1 is essential for pacemaker development and function. *J. Clin. Invest.* **125**, 3256–3268 (2015).

392. Liu, H. *et al.* Functional redundancy between human SHOX and mouse Shox2 genes in the regulation of sinoatrial node formation and pacemaking function. *J. Biol. Chem.* **286**, 17029–17038 (2011).

393. Espinoza-Lewis, R. A. *et al.* Shox2 is essential for the differentiation of cardiac pacemaker cells by repressing Nkx2-5. *Dev. Biol.* **327**, 376–385 (2009).

394. Caballero, R. *et al.* Tbx20 controls the expression of the KCNH2 gene and of hERG channels. *Proc. Natl. Acad. Sci. U. S. A.* **114**, E416–E425 (2017).
395. Shekhar, A. *et al.* ETV1 activates a rapid conduction transcriptional program in rodent and human cardiomyocytes. *Sci. Rep.* **8**, 1–16 (2018).
396. Zhou, B. *et al.* Fog2 is critical for cardiac function and maintenance of coronary vasculature in the adult mouse heart. *J. Clin. Invest.* **119**, 1462–1476 (2009).
397. van Eif, V. W. W., Devalla, H. D., Boink, G. J. J. & Christoffels, V. M. Transcriptional regulation of the cardiac conduction system. *Nature Reviews Cardiology* vol. 15 617–630 (2018).
398. GEO Accession viewer. https://www.ncbi.nlm.nih.gov/geo/query/acc.cgi?acc=GSE121464.
399. Ebert, M. S. & Sharp, P. A. MicroRNA sponges: progress and possibilities. *RNA* **16**, 2043–50 (2010).
400. Qin, J. Y. *et al.* Systematic Comparison of Constitutive Promoters and the Doxycycline-Inducible Promoter. *PLoS One* **5**, e10611 (2010).
401. Zincarelli, C., Soltys, S., Rengo, G. & Rabinowitz, J. E. Analysis of AAV serotypes 1-9 mediated gene expression and tropism in mice after systemic injection. *Mol. Ther.* **16**, 1073–1080 (2008).
402. Hashem, S. I. & Claycomb, W. C. Genetic isolation of stem cell-derived pacemaker-nodal cardiac myocytes. *Mol. Cell. Biochem.* **383**, 161–171 (2013).
403. Marionneau, C. *et al.* Specific pattern of ionic channel gene expression associated with pacemaker activity in the mouse heart. *J. Physiol.* **562**, 223–234 (2005).
404. McConnell, B. B. & Yang, V. W. Mammalian Krüppel-Like factors in health and diseases. *Physiological Reviews* vol. 90 1337–1381 (2010).
405. Cowley, S. M. *et al.* The mSin3A Chromatin-Modifying Complex Is Essential for Embryogenesis and T-Cell Development. *Mol. Cell. Biol.* **25**, 6990–7004 (2005).
406. Lomberk, G. & Urrutia, R. The family feud: Turning off Sp1 by Sp1-like KLF proteins. *Biochemical Journal* vol. 392 1–11 (2005).
407. Cao, S. *et al.* KLF11-mediated repression antagonizes Sp1/sterol-responsive element-binding protein-induced transcriptional activation of caveolin-1 in response to cholesterol signaling. *J. Biol. Chem.* **280**, 1901–1910 (2005).
408. Prosdocimo, D. A., Sabeh, M. K. & Jain, M. K. Kruppel-like factors in muscle health and disease. *Trends in Cardiovascular Medicine* vol. 25 278–287 (2015).
409. Chen, I. Y. *et al.* Indirect imaging of cardiac-specific transgene expression using a bidirectional two-step transcriptional amplification strategy. *Gene Ther.* **17**, 827–838

(2010).

410. Zincarelli, C., Soltys, S., Rengo, G. & Rabinowitz, J. E. Analysis of AAV Serotypes 1–9 Mediated Gene Expression and Tropism in Mice After Systemic Injection. *Mol. Ther.* **16**, 1073–1080 (2008).

411. Atkinson, A. J. *et al.* Functional, anatomical, and molecular investigation of the cardiac conduction system and arrhythmogenic atrioventricular ring tissue in the rat heart. *J. Am. Heart Assoc.* **2**, e000246 (2013).

412. Pacak, C. A. *et al.* Recombinant Adeno-Associated Virus Serotype 9 Leads to Preferential Cardiac Transduction In Vivo. *Circ. Res.* **99**, (2006).

413. Bostick, B., Ghosh, A., Yue, Y., Long, C. & Duan, D. Systemic AAV-9 transduction in mice is influenced by animal age but not by the route of administration. *Gene Ther.* **14**, 1605–1609 (2007).

414. Ghosh, A., Yue, Y., Long, C., Bostick, B. & Duan, D. Efficient whole-body transduction with trans-splicing adeno-associated viral vectors. *Mol. Ther.* **15**, 750–755 (2007).

415. Wang, L., Wang, H., Bell, P., McMenamin, D. & Wilson, J. M. Hepatic gene transfer in Neonatal mice by Adeno-associated virus serotype 8 vector. *Hum. Gene Ther.* **23**, 533–539 (2012).

416. Soonpaa, M. H., Rubart, M. & Field, L. J. Challenges measuring cardiomyocyte renewal. *Biochim. Biophys. Acta* **1833**, 799 (2013).

417. Svensson, E. C. *et al.* Efficient and Stable Transduction of Cardiomyocytes After Intramyocardial Injection or Intracoronary Perfusion With Recombinant Adeno-Associated Virus Vectors. *Circulation* **99**, 201–205 (1999).

418. Prasad, K. M. R., Smith, R. S., Xu, Y. & French, B. A. A single direct injection into the left ventricular wall of an adeno-associated virus 9 (AAV9) vector expressing extracellular superoxide dismutase from the cardiac troponin-T promoter protects mice against myocardial infarction. *J. Gene Med.* **13**, 333–341 (2011).

419. Csepe, T. A. *et al.* Human sinoatrial node structure: 3D microanatomy of sinoatrial conduction pathways. *Prog. Biophys. Mol. Biol.* **120**, 164–178 (2016).

420. Kotterman, M. A., Chalberg, T. W. & Schaffer, D. V. Viral Vectors for Gene Therapy: Translational and Clinical Outlook. (2015) doi:10.1146/annurev-bioeng-071813-104938.

421. Moulay, G., Scherman, D. & Kichler, A. Fasting increases the in vivo gene delivery of AAV vectors. *Clin. Transl. Sci.* **3**, 333–6 (2010).

422. Ni, L. *et al.* Atrial-Specific Gene Delivery Using an Adeno-Associated Viral Vector. *Circ. Res.* **124**, 256–262 (2019).

423. Gruntman, A. M., Su, L. & Flotte, T. R. Retro-Orbital Venous Sinus Delivery of rAAV9 Mediates High-Level Transduction of Brain and Retina Compared with Temporal Vein Delivery in Neonatal Mouse Pups. *Hum. Gene Ther.* **28**, 228–230 (2017).
424. Soboleski, M. R., Oaks, J. & Halford, W. P. Green fluorescent protein is a quantitative reporter of gene expression in individual eukaryotic cells. *FASEB J.* **19**, 1–20 (2005).
425. Swenson, E. S., Price, J. G., Brazelton, T. & Krause, D. S. Limitations of Green Fluorescent Protein as a Cell Lineage Marker. *Stem Cells* **25**, 2593–2600 (2007).
426. Kusser, K. L. & Randall, T. D. Simultaneous detection of EGFP and cell surface markers by fluorescence microscopy in lymphoid tissues. *J. Histochem. Cytochem.* **51**, 5–14 (2003).
427. Claycomb, W. C. *et al.* HL-1 cells: A cardiac muscle cell line that contracts and retains phenotypic characteristics of the adult cardiomyocyte. *Proc. Natl. Acad. Sci. U. S. A.* **95**, 2979–2984 (1998).
428. van Eif, V. W. W. *et al.* Transcriptome analysis of mouse and human sinoatrial node cells reveals a conserved genetic program. *Dev.* **146**, (2019).
429. Petkova, M. *et al.* Identification of Key Small Non-Coding MicroRNAs Controlling Pacemaker Mechanisms in the Human Sinus Node. *J. Am. Heart Assoc.* **9**, e016590 (2020).
430. Clair, J. R. S., Sharpe, E. J. & Proenza, C. Culture and adenoviral infection of sinoatrial node myocytes from adult mice. *Am. J. Physiol. - Hear. Circ. Physiol.* **309**, H490–H498 (2015).
431. Stinski, M. F. & Isomura, H. Role of the cytomegalovirus major immediate early enhancer in acute infection and reactivation from latency. *Medical Microbiology and Immunology* vol. 197 223–231 (2008).
432. Schug, J. *et al.* Promoter features related to tissue specificity as measured by Shannon entropy. *Genome Biol.* **6**, R33 (2005).
433. Abhijeet Rajendra Sonawane, A. *et al.* Understanding Tissue-Specific Gene Regulation. *Cell Rep.* **21**, (2017).
434. Steuernagel, L. *et al.* Computational identification of tissue-specific transcription factor cooperation in ten cattle tissues. *PLoS One* **14**, e0216475 (2019).
435. Merika, M. & Orkin, S. H. Functional synergy and physical interactions of the erythroid transcription factor GATA-1 with the Krüppel family proteins Sp1 and EKLF. *Mol. Cell. Biol.* **15**, 2437–2447 (1995).
436. Wakayama, T., Ohashi, K., Fujimoto, Y. & Maeda, M. The Cytomegalovirus Enhancer Induces an Immediate Response to the Myosin Light Chain 2v Promoter during P19CL6 Cell Differentiation. *Am. J. Mol. Biol.* **07**, 1068–1081 (2017).
437. Isomura, H. & Stinski, M. F. The Human Cytomegalovirus Major Immediate-Early Enhancer

Determines the Efficiency of Immediate-Early Gene Transcription and Viral Replication in Permissive Cells at Low Multiplicity of Infection. *J. Virol.* **77**, 3602–3614 (2003).

438. Zhou, Q. *et al.* A mouse tissue transcription factor atlas. *Nat. Commun.* **8**, 1–15 (2017).
439. Vedantham, V., Evangelista, M., Huang, Y. & Srivastava, D. Spatiotemporal regulation of an Hcn4 enhancer defines a role for Mef2c and HDACs in cardiac electrical patterning. *Dev. Biol.* **373**, 149–62 (2013).
440. Fuda, N. J., Ardehali, M. B. & Lis, J. T. Defining mechanisms that regulate RNA polymerase II transcription in vivo. *Nature* vol. 461 186–192 (2009).
441. Rust, E. M., Westfall, M. V., Samuelson, L. C. & Metzger, J. M. Gene transfer into mouse embryonic stem cell-derived cardiac myocytes mediated by recombinant adenovirus. *Vitr. Cell. Dev. Biol. - Anim.* **33**, 270–276 (1997).
442. Graham, F. L., Smiley, J., Russell, W. C. & Nairn, R. Characteristics of a human cell line transformed by DNA from human adenovirus type 5. *J. Gen. Virol.* **36**, 59–72 (1977).
443. Gorman, C. M., Gies, D., McCray, G. & Huang, M. The human cytomegalovirus major immediate early promoter can be trans-activated by adenovirus early proteins. *Virology* **171**, 377–385 (1989).
444. Stillitano, F. *et al.* Molecular basis of funny current (If) in normal and failing human heart. *J. Mol. Cell. Cardiol.* **45**, 289–299 (2008).
445. Stefanovic, S. *et al.* GATA-dependent regulatory switches establish atrioventricular canal specificity during heart development. *Nat. Commun.* **5**, 1–11 (2014).
446. Di Lisi, R., Picard, A., Ausoni, S. & Schiaffino, S. GATA elements control repression of cardiac troponin I promoter activity in skeletal muscle cells. *BMC Mol. Biol.* **8**, 78 (2007).
447. Adamo, R. F., Guay, C. L., Edwards, A. V., Wessels, A. & Burch, J. B. E. GATA-6 gene enhancer contains nested regulatory modules for primary myocardium and the embedded nascent atrioventricular conduction system. in *Anatomical Record - Part A Discoveries in Molecular, Cellular, and Evolutionary Biology* vol. 280 1062–1071 (2004).
448. Weinberger, F. *et al.* Localization of islet-1-positive cells in the healthy and infarcted adult murine heart. *Circ. Res.* **110**, 1303–1310 (2012).
449. Gao, R. *et al.* Pioneering function of Isl1 in the epigenetic control of cardiomyocyte cell fate. *Cell Res.* **29**, 486–501 (2019).
450. Galang, G. *et al.* ATAC-seq Reveals an Isl1 Enhancer that Regulates Sinoatrial Node Development and Function . *Circ. Res.* (2020) doi:10.1161/circresaha.120.317145.
451. Kuwabara, Y. *et al.* Increased expression of HCN channels in the ventricular myocardium contributes to enhanced arrhythmicity in mouse failing hearts. *J. Am. Heart Assoc.* **2**,

(2013).

452. Genead, R. *et al.* Ischemia-Reperfusion Injury and Pregnancy Initiate Time-Dependent and Robust Signs of Up-Regulation of Cardiac Progenitor Cells. *PLoS One* **7**, e36804 (2012).

453. Yanni J, Wang Y, Zeef L, Choudhury M, Zi M, Cai X, Logantha SJRJ, Nakao S, Atkinson A, Petkova M, Doris U, A. & J, Cartwright E, Hart G, D. H. and B. M. Silencing miR-370 rescues funny current and sinus node function and improves survival in heart failure. *Nat. Commun.* **Full paper**, (2017).

454. Viswanathan, S., Burch, J. B. E., Fishman, G. I., Moskowitz, I. P. & Benson, D. W. Characterization of sinoatrial node in four conduction system marker mice. *J. Mol. Cell. Cardiol.* **42**, 946–53 (2007).

455. Munshi, N. V. *et al.* Cx30.2 enhancer analysis identifies Gata4 as a novel regulator of atrioventricular delay. *Development* **136**, 2665–2674 (2009).

456. Kreuzberg, M. M. *et al.* Connexin30.2 containing gap junction channels decelerate impulse propagation through the atrioventricular node. *Proc. Natl. Acad. Sci. U. S. A.* **103**, 5959–5964 (2006).

457. Tidyman, W. E. *et al.* In vivo regulation of the chicken cardiac troponin T gene promoter in zebrafish embryos. *Dev. Dyn.* **227**, 484–496 (2003).

458. Azakie, A., Lamont, L., Fineman, J. R. & He, Y. Divergent transcriptional enhancer factor-1 regulates the cardiac troponin T promoter. *Am J Physiol Cell Physiol* **289**, 1522–1534 (2005).

459. Brennan, J. A. *et al.* Evidence of Superior and Inferior Sinoatrial Nodes in the Mammalian Heart. *JACC Clin. Electrophysiol.* **6**, 1827–1840 (2020).

460. Poliak, S. *et al.* Juxtaparanodal clustering of Shaker-like K+ channels in myelinated axons depends on Caspr2 and TAG-1. *J. Cell Biol.* **162**, 1149–1160 (2003).

461. Pallante, B. A. *et al.* Contactin-2 Expression in the Cardiac Purkinje Fiber NetworkCLINICAL PERSPECTIVE. *Circ. Arrhythmia Electrophysiol.* **3**, (2010).

462. Nam, Y. J. *et al.* Induction of diverse cardiac cell types by reprogramming fibroblasts with cardiac transcription factors. *Dev.* **141**, 4267–4278 (2014).

463. Boyett, M. R., Honjo, H. & Kodama, I. No Title. **47**, (2000).

464. Wen, Y. & Li, B. *Morphology of mouse sinoatrial node and its expression of NF-160 and HCN4*. *Int J Clin Exp Med* vol. 8 www.ijcem.com/ (2015).

465. Kakimoto, Y. *et al.* MicroRNA deep sequencing reveals chamber-specific miR-208 family expression patterns in the human heart. *Int. J. Cardiol.* **211**, 43–48 (2016).

466. Yuan, H. & Gao, J. The role of miR-370 in fibrosis after myocardial infarction. *Mol. Med.*

Rep. **15**, 3041–3047 (2017).

467. Lo, S. S. *et al.* Overexpression of miR-370 and downregulation of its novel target TGFB-RII contribute to the progression of gastric carcinoma. *Oncogene* **31**, 226–237 (2012).

468. Cai, F. *et al.* CXCL12-regulated miR-370–3p functions as a tumor suppressor gene by targeting HMGA2 in nonfunctional pituitary adenomas. *Mol. Cell. Endocrinol.* **488**, 25–35 (2019).

469. Gao, Y. T., Chen, X. B. & Liu, H. L. Up-regulation of miR-370-3p restores glioblastoma multiforme sensitivity to temozolomide by influencing MGMT expression. *Sci. Rep.* **6**, (2016).

470. Dayton, R. D., Wang, D. B. & Klein, R. L. The advent of AAV9 expands applications for brain and spinal cord gene delivery. *Expert Opinion on Biological Therapy* vol. 12 757–766 (2012).

471. Kuro-o, M., Tsuchimochi, H., Ueda, S., Takaku, F. & Yazaki, Y. Distribution of cardiac myosin isozymes in human conduction system. Immunohistochemical study using monoclonal antibodies. *J. Clin. Invest.* **77**, 340–347 (1986).

472. Dobrzynski, H. *et al.* Expression of Kir2.1 and Kir6.2 transgenes under the control of the α-MHC promoter in the sinoatrial and atrioventricular nodes in transgenic mice. *J. Mol. Cell. Cardiol.* **41**, 855–867 (2006).

473. Gupta, M., Zak, R., Libermann, T. A. & Gupta, M. P. Tissue-Restricted Expression of the Cardiac α-Myosin Heavy Chain Gene Is Controlled by a Downstream Repressor Element Containing a Palindrome of Two Ets-Binding Sites. *Mol. Cell. Biol.* **18**, 7243–7258 (1998).

474. Lee, C. J., Fan, X., Guo, X. X. & Medin, J. A. Promoter-specific lentivectors for long-term, cardiac-directed therapy of Fabry disease. *J. Cardiol.* **57**, 115–122 (2011).

475. Sah, V. P. *et al.* Cardiac-specific overexpression of RhoA results in sinus and atrioventricular nodal dysfunction and contractile failure. *J. Clin. Invest.* **103**, 1627–1634 (1999).

476. Denegri, M. *et al.* Single delivery of an adeno-associated viral construct to transfer the CASQ2 gene to knock-in mice affected by catecholaminergic polymorphic ventricular tachycardia is able to cure the disease from birth to advanced age. *Circulation* **129**, 2673–2681 (2014).

477. Liu, M. B., Priori, S. G., Qu, Z. & Weiss, J. N. Stabilizer Cell Gene Therapy: A Less-Is-More Strategy to Prevent Cardiac Arrhythmias. *Circ. Arrhythmia Electrophysiol.* **13**, 982–994 (2020).

478. Ebert, M. S., Neilson, J. R. & Sharp, P. A. MicroRNA sponges: competitive inhibitors of small RNAs in mammalian cells. *Nat. Methods* **4**, 721–726 (2007).

479. Ambrosi, C. M., Sadananda, G., Han, J. L. & Entcheva, E. Adeno-associated virus mediated gene delivery: Implications for Scalable in vitro and in vivo Cardiac Optogenetic Models. *Front. Physiol.* **10**, 168 (2019).

480. Buie, L. K. K. *et al.* Self-complementary AAV virus (scAAV) safe and long-term gene transfer in the trabecular meshwork of living rats and monkeys. *Investig. Ophthalmol. Vis. Sci.* **51**, 236–248 (2010).

481. Li, M. *et al.* High-efficiency transduction of fibroblasts and mesenchymal stem cells by tyrosine-mutant AAV2 vectors for their potential use in cellular therapy. *Hum. Gene Ther.* **21**, 1527–1543 (2010).

482. de Bakker, J. M. T. & Zaza, A. Biopacemaking: Clinically Attractive, Scientifically a Challenge. in 1–5 (Springer, Berlin, Heidelberg, 2007). doi:10.1007/978-3-540-72110-9_1.

483. I, S., T, T., T, M., Z, O. & S, F. Quantitative histological analysis of the human sinoatrial node during growth and aging. *Circulation* **85**, 2176–2184 (1992).

484. S, I., F, S., H, N. & K, G. A new method for the histological study of aging changes in the sinoatrial node. *Jpn. Heart J.* **27**, 653–660 (1986).

485. Moghtadaei, M. *et al.* The impacts of age and frailty on heart rate and sinoatrial node function. *J. Physiol.* **594**, 7105 (2016).

486. Froese, A. *et al.* Popeye domain containing proteins are essential for stress-mediated modulation of cardiac pacemaking in mice. *J. Clin. Invest.* **122**, 1119–1130 (2012).

487. Lai, C. M., Lai, Y. K. Y. & Rakoczy, P. E. Adenovirus and Adeno-Associated Virus Vectors. *DNA Cell Biol.* **21**, 895–913 (2002).

488. Guo, H., Ingolia, N. T., Weissman, J. S. & Bartel, D. P. Mammalian microRNAs predominantly act to decrease target mRNA levels. *Nature* **466**, 835–840 (2010).

489. Qiao, C. *et al.* Liver-specific microRNA-122 target sequences incorporated in AAV vectors efficiently inhibits transgene expression in the liver. *Gene Ther.* **18**, 403–410 (2011).

490. Colin, A. *et al.* Engineered lentiviral vector targeting astrocytes in vivo. *Glia* **57**, 667–679 (2009).

491. Brown, B. D. *et al.* Endogenous microRNA can be broadly exploited to regulate transgene expression according to tissue, lineage and differentiation state. *Nat. Biotechnol.* **25**, 1457–1467 (2007).

492. Colpaert, R. M. W. & Calore, M. MicroRNAs in Cardiac Diseases. *Cells* **8**, 737 (2019).

493. Kraszewska, I. *et al.* Variability in Cardiac miRNA-122 Level Determines Therapeutic Potential of miRNA-Regulated AAV Vectors. *Mol. Ther. - Methods Clin. Dev.* **17**, 1190–1201 (2020).

494. Wong, L. L. *et al.* Circulating microRNAs in heart failure with reduced and preserved left ventricular ejection fraction. *Eur. J. Heart Fail.* **17**, 393–404 (2015).
495. Nagy, O., Baráth, S. & Ujfalusi, A. *The role of microRNAs in congenital heart disease*.
496. Campostrini, G. *et al.* A loss-of-function HCN4 mutation associated with familial benign myoclonic epilepsy in infancy causes increased neuronal excitability. *Front. Mol. Neurosci.* **11**, 269 (2018).
497. Stephenson, R. S. *et al.* High resolution 3-Dimensional imaging of the human cardiac conduction system from microanatomy to mathematical modeling. *Sci. Rep.* **7**, 1–13 (2017).
498. Seisenberger, G. *et al.* Real-time single-molecule imaging of the infection pathway of anadeno-associated virus. *Science (80-.).* **294**, 1929–1932 (2001).
499. Mitchell, A. M. & Samulski, R. J. Mechanistic Insights into the Enhancement of Adeno-Associated Virus Transduction by Proteasome Inhibitors. *J. Virol.* **87**, 13035–13041 (2013).